

8	GEOTHERMAL ENERGY.....	1
8.1	THE EARTH'S THERMAL REGIME	1
8.1.1	<i>The Structure of the Earth</i>	1
8.1.2	<i>Energy Budget of the Earth</i>	4
8.1.2.1	Heat Income	5
8.1.2.1.1	External Heat Sources	5
8.1.2.1.2	Internal Heat Sources	6
8.1.2.2	Heat Expenditure.....	8
8.1.2.3	Heat Budget.....	9
8.1.3	<i>The Thermal Regime of the Earth's Crust</i>	9
8.1.4	<i>Heat Storage</i>	10
8.1.4.1	Measuring Techniques	12
8.1.4.2	Calculated Heat Capacity	12
8.1.5	<i>Heat Transport</i>	23
8.1.5.1	Heat Conduction.....	23
8.1.5.1.1	Measuring Techniques	23
8.1.5.1.2	Indirect Methods.....	24
8.1.5.1.3	Thermal Conductivity of Minerals	28
8.1.5.2	Thermal Conductivity of Rocks	35
8.1.5.2.1	Thermal Conductivity of Sedimentary, Volcanic, Plutonic, and Metamorphic Rocks	36
8.1.5.2.2	Influence of Various Factors on Thermal Conductivity	46
8.1.5.3	Heat Advection.....	52
8.1.5.4	Heat Radiation and Thermal Conductivity in the Earth's Mantle.....	56
8.2	GEOTHERMAL ENERGY RESOURCES.....	58
8.3	TYPES OF GEOTHERMAL ENERGY USE	60
8.3.1	<i>Direct Use</i>	60
8.3.1.1	Space Heating.....	63
8.3.1.1.1	Earth Coupled Heat Extraction Systems.....	64
8.3.1.1.2	Hydrothermal Heating Systems.....	67
8.3.1.2	Commercial and Industrial Applications	68
8.3.2	<i>Power Generation</i>	70
8.4	TECHNOLOGICAL AND ECONOMICAL ASPECTS OF GEOTHERMAL ENERGY	74
8.4.1	<i>Direct Use</i>	75
8.4.1.1	Earth Coupled Heat Extraction Systems.....	75
8.4.1.2	Hydrothermal Heating Systems.....	81
8.4.2	<i>Power Generation</i>	83
8.4.2.1	Natural Steam Power Plants	83
8.4.2.2	Binary Power Plants	87
8.4.2.3	Power Plants for Hot Dry Rock or Enhanced Geothermal Systems	90
8.4.2.4	Technical, Economic, and Ecological Aspects of Geothermal Power Production.....	93
8.4.2.4.1	Efficiency	93
8.4.2.4.2	Cost and Life Time	95
8.4.2.4.3	Pollution	98
8.5	SUMMARY	103
	REFERENCES	105

8 Geothermal Energy

Geothermal energy is the heat contained in the solid Earth and its internal fluids. This sets it apart from other terrestrial energy sources such as

- fossil or fissionable fuels in the subsurface;
- biomass, solar energy, and hydropower on the surface of the solid Earth and in its rivers and seas;
- wind energy in the atmosphere.

Geothermal energy is stored as sensible or latent heat. Supplied by both internal and external sources, it represents a vast supply which is only started to be tapped by mankind for space heating, process heat, and generation of electric power. The options and challenges involved in turning this promising potential into operational, efficient, and economic technologies are the topic of this assessment.

The major topics associated with an enhanced future use of geothermal energy are reviewed in four main chapters: (1) *The Earth's thermal regime*: where on Earth is heat, how much is there, where does it come from, and how is it transferred? (2) *Geothermal energy resources*: what kinds of resources are available in which reservoirs and how big are they? (3) *Types of geothermal energy use*: how can geothermal heat be used directly or converted into electricity and what is the present use of geothermal energy?; (4) *Technological and economical aspects of geothermal energy use*: which technologies are available to produce geothermal energy, and how much does it cost? A summary and outlook concludes this review.

8.1 The Earth's Thermal Regime

Since the conditions under which geothermal energy can be exploited strongly depend on both the origin of geothermal heat and the environment in which it is stored, we first need to examine briefly the internal structure of the Earth. Next we analyze the energy budget of the Earth and quantify the contributions of the various external and internal sources and sinks of heat. Then we examine the thermal regime of the Earth' crust and the magnitudes of heat storage and transport and the associated physical properties specific heat capacity, thermal conductivity, and diffusivity.

8.1.1 The Structure of the Earth

Our information on the internal structure of the Earth and the variation of its physical properties (pressure, temperature, density, seismic velocities) and chemical composition are derived from seismology, i.e. the interpretation of travel time curves of earthquakes which passed through the Earth. The variation with depth of the observed seismic velocities and elastic constants combined with Maxwell's four thermodynamic relations between pressure P, volume V, entropy S ($\Delta S = \Delta Q/T$; Q: heat), and temperature T yield the predominantly radial structure of the Earth.

From Maxwell's relation $(\partial T/\partial P)_S = (\partial V/\partial S)_P$ one obtains an expression for the adiabatic temperature gradient in terms of temperature, the volume coefficient of thermal expansion $\alpha = (\partial V/\partial T)_P/V$, and the isobaric specific heat capacity c_p (at constant pressure):

$$\left(\frac{\partial T}{\partial z}\right)_S = T \frac{\alpha g}{c_p}, \quad (8.1)$$

where g is gravity and subscripts P and S refer to isobaric and adiabatic conditions, respectively, i.e. constant pressure and constant entropy.

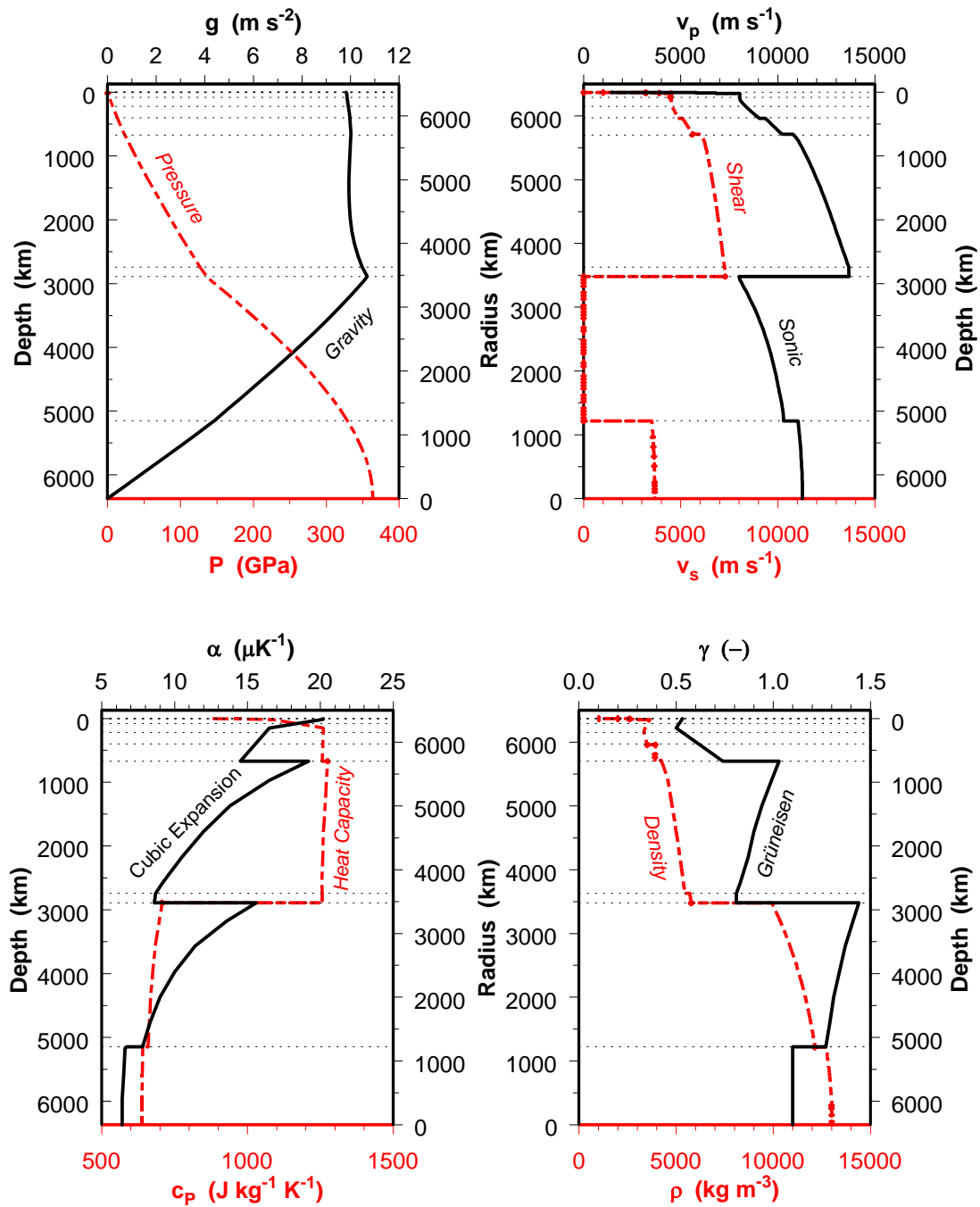


Fig. 8.1 Variation of selected properties versus depth in the Earth according to the Earth models PREM (gravity g , pressure P , coefficient of thermal volume expansion α and isobaric specific heat capacity c_p ; Grüneisen parameter γ) [1981Dzi; data: 1992Sta] and AK135-f (sonic and shear wave velocities v_p and v_s ; density ρ) [1995Ken; 1995Mon].

Assuming lower mantle values (at about 1500 km depth) of $T=2400$ K, $g=9.9$ m s⁻², $c_p=1200$ J kg⁻¹ K⁻¹, and $\alpha=14$ μ K⁻¹, yields an adiabatic temperature gradient of about 0.3 K km⁻¹; the corresponding values for the outer core (at about 3500 km depth) of $T=4000$ K, $g=10.1$ m s⁻², $c_p=700$ J kg⁻¹ K⁻¹, and $\alpha=14$ μ K⁻¹ (Fig. 8.1), yield an adiabatic temperature gradient of about 0.8 K km⁻¹ [1992Sta; 1997Low].

Approximate estimates for the adiabatic temperature inside the Earth can be obtained with the aid of the dimensionless Grüneisen parameter $\gamma = \alpha K_S / (\rho c_p)$, where K_S is the adiabatic incompressibility or bulk modulus and ρ is density (Fig. 8.1):

$$\frac{\partial T}{T} = \gamma \frac{d\rho}{\rho}, \text{ or: } T = T_0 \left(\frac{\rho}{\rho_0} \right)^\gamma. \quad (8.2)$$

From a known temperature T_0 and density ρ_0 at a given depth, eq. (8.2) allows computing the adiabatic temperature from the density profile in a region where the Grüneisen parameter is known. Fortunately, the Grüneisen parameter does not vary too much within large regions of the Earth's interior (Fig. 8.1). However, eq. (8.2) cannot be applied across the boundaries between these domains, where γ is discontinuous. But if T_0 and ρ_0 are known at calibration points, the adiabatic temperature profile can be computed in an iterative fashion within these depth intervals. The currently accepted estimate of the temperature profile is characterized by steep gradients in the lithosphere, asthenosphere and in the lower mantle D'' layer (immediately above the core-mantle boundary). Neglecting large lateral variations in the crust and lithosphere it indicates, on average, temperatures of less than 1000 K in the lithosphere, close to 3750 K at the core-mantle boundary, and around 5100 K at the center of the Earth (Fig. 8.2) [1992Sta; 1997Low;].

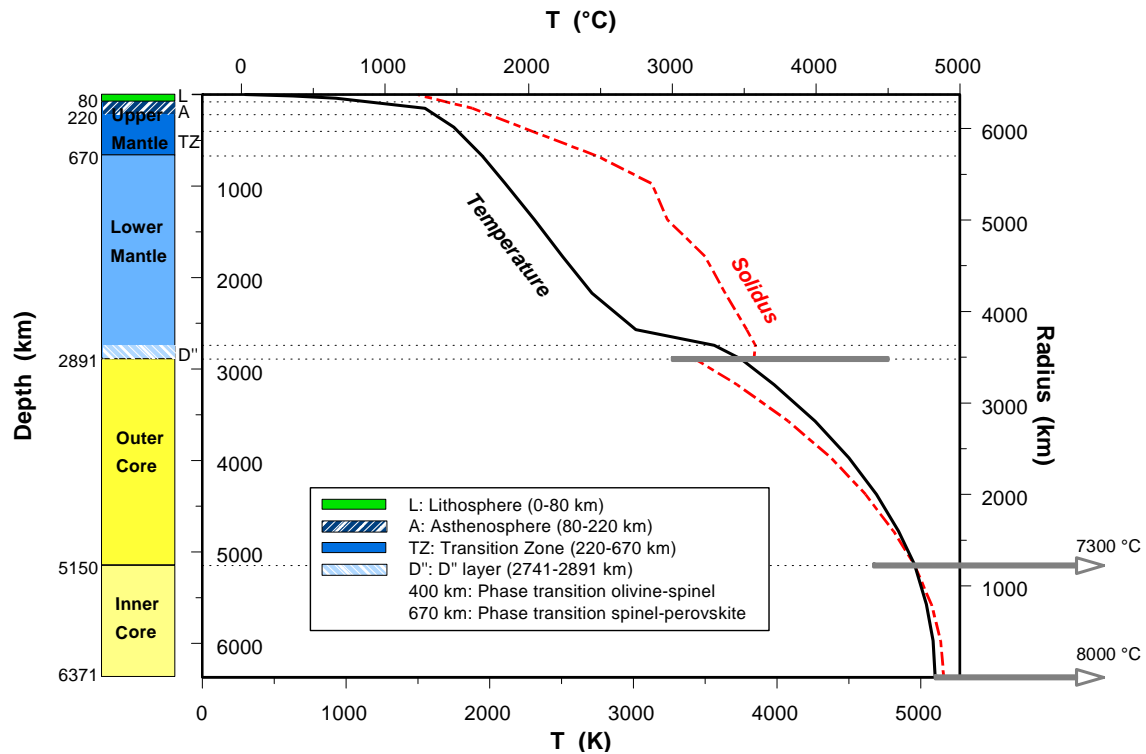


Fig. 8.2. Variation of estimated temperature and melting point in the Earth with depth; Data according to Stacey [1992Sta] selected to be representative and consistent with the Preliminary Reference Earth Model (PREM) [1981Dzi]. Temperature is poorly constrained in the deeper sections, indicated by large error bars; data: [1993Bro].

However, there are large uncertainties, particularly in the mantle and core [1993Bro; 2001Bea], indicating ranges for conceivable minimum and maximum temperatures of 3000 °C – 4500 °C at the core-mantle boundary, 4400 °C – 7300 °C at the transition between outer and inner core, and a maximum temperature at the center of the Earth of less than 8000 °C (Fig. 8.2).

From another one of Maxwell's thermodynamic relations, $(\partial S/\partial P)_T = -(\partial V/\partial T)_P$, one can derive the fractional variation of the melting point temperature T_{mp} with depth within the Earth:

$$\frac{1}{T_{mp}} \frac{dT_{mp}}{dz} = \frac{g}{L} \frac{(\rho_{solid} - \rho_{liquid})}{\rho_{liquid}}, \quad (8.3)$$

where L is the latent heat of fusion, and ρ_{solid} and ρ_{liquid} are the densities of the solid and liquid phases, respectively. With the information on the variation of gravity and density with depth derived from seismic travel times (Fig. 8.1) one may obtain a profile of the melting point temperature with depth. Assuming outer core values (at about 3300 km depth) of $T=4000$ K, $g=10.1$ m s⁻², $\rho_{solid}=13000$ kg m⁻³, $\rho_{liquid}=11000$ kg m⁻³, and $L=7$ MJ kg⁻¹ for iron yields a melting point temperature gradient of about 1 K km⁻¹ (Fig. 8.2) [1997Low]. Thus, the melting point temperature increases more rapidly with depth than the adiabatic temperature. However, the variation of the properties (e.g. L , g , c_p) in the Earth is known only with large uncertainty, and an accordingly large uncertainty is associated with the temperature profiles based on eqs. (8.2) and (8.3).

8.1.2 Energy Budget of the Earth

In order to avoid numbers with too many digits energy budgets are usually quantified in multiples of 1000 of the base units Joule and Kilowatt-hour (Table 8.1; Table 8.2).

Table 8.1 Abbreviations, prefixes, and names for various powers of ten in different systems.

American	system British/French/German	prefix	abbreviation	factor
thousand	thousand	Kilo	k	10 ³
million	million	Mega	M	10 ⁶
billion	milliard	Giga	G	10 ⁹
trillion	billion	Tera	T	10 ¹²
quadrillion	–	Peta	P	10 ¹⁵
quintillion	trillion	Exa	E	10 ¹⁸
sextillion	–	Zetta	Z	10 ²¹
septillion	quadrillion	Yotta	Y	10 ²⁴

The Earth's energy budget is determined by its thermal income and expenditure. The Earth receives remarkable amounts of energy from both external and internal sources. Their enormous size can be best illustrated by comparison with the global production of primary energy in the year 2001, about 420 EJ [2003IEA¹] or the annual primary energy requirements predicted for the current century, estimated to 600 EJ – 1800 EJ depending on various assumptions [1997Edw; 1997Nak; 2000Nak; 2002IEA] (Fig. 8.3).

Table 8.2 Units and conversion factors for energy and power.

quantity	unit	abbreviation	conversion
Energy (e.g. heat)	Joule	J	1 GJ = (1000/3.6) MJ ≈ 278 kW h
	Kilowatt-hours	kW h	1 kW h = 3.6 MJ
Power	Watt	W	1 W = 1 J s ⁻¹

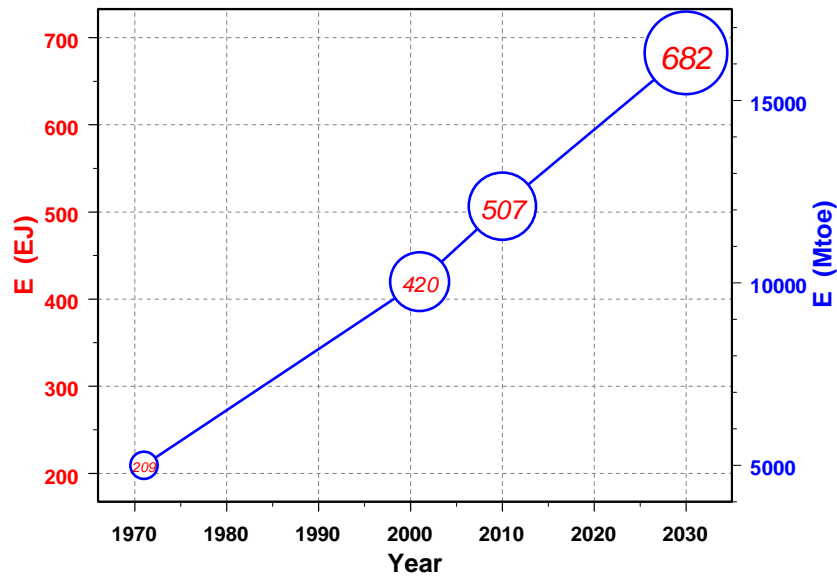


Fig. 8.3. Global primary energy consumption in 1971 and 2001 and expected primary energy demand in 2010 and 2030 in EJ (left axis) or Megatonnes of oil equivalent (Mtoe, right axis) [2002IEA; 2003IEA]; 1 Mtoe = 41.868 PJ.

8.1.2.1 Heat Income

The largest *external* energy source of the Earth is the solar irradiation. The incident energy of the Sun's rays falling on the Earth for just one day, 1.5×10^{22} J (computed from the solar irradiance given below), correspond to about 35 years worth of the global production of primary energy in the year 2001 (Fig. 8.3). In other terms, 4–12 days of solar irradiation corresponds to the expected cumulative primary energy requirements for the entire current century. However, only regrettably small amounts of the irradiated solar energy are converted into forms of energy which can be stored relatively permanently by the Earth, mainly as fossil fuels, as will be seen below. The conversion of solar energy reaching the Earth's surface into heat and electricity is the topic of Chap. 4 of this book.

The largest *internal* energy source of the Earth is provided by the decay of radiogenic isotopes in the rocks of the Earth's crust. The heat thus produced within one year, 8.6×10^{20} J (computed from the average terrestrial heat generation rate given below), corresponds to more than twice the global production of primary energy in the year 2000 (Fig. 8.3). This huge energy source by itself clearly exceeds the world's energy demands expected for the period 2000–2030 [2002IEA]. If it could be harnessed, it would suffice alone to satisfy the primary energy demand of the entire 21st century.

8.1.2.1.1 External Heat Sources

The Earth receives energy from two major external sources: electromagnetic energy from the *solar radiation* and *gravitational energy* due to forces of the Sun and Moon exerted on the rotating Earth.

Solar Radiation: The solar constant $S = 1373 \text{ W m}^{-2}$ [2000Lid] is the solar irradiance (or incident solar radiation flux) on a plane normal to the Sun's rays, just outside the Earth's atmosphere, when the Earth is at a distance of one astronomical unit (1 AU = 1.496×10^8 km) from the Sun. Long-term observations of the solar irradiation from satellites [1999Kyl; 2002NGD] indicate a variability of the solar "constant" on the order of fractions of a percent due to changes in the solar activity. With its cross section of $\pi (R_E)^2$ the

Earth intercepts from the total solar radiation a radiation power $P=S \pi (R_E)^2 \approx 1.75 \times 10^{17} \text{ W}$, where $R_E=6371 \text{ km}$ is the radius of the best-fitting sphere for the Earth. Of this solar energy flux, about 35 % ($6.1 \times 10^{16} \text{ W}$) are directly reflected as short wavelength radiation, and 65 % ($1.14 \times 10^{17} \text{ W}$) are scattered and absorbed in atmosphere, hydrosphere, and lithosphere, and finally re-emitted as long-wavelength radiation. Of this absorbed fraction of the total incident solar energy, 31 % ($3.53 \times 10^{16} \text{ W}$) are absorbed in the atmosphere, while 69 % (**$7.87 \times 10^{16} \text{ W}$**) reach the surface of the Earth. Thus less than half of the total solar irradiation of the Earth, just about 45 % can be considered an external source to the terrestrial heat budget. But most of this energy is directly re-emitted as long-wavelength radiation (see Sect.). Only a tiny fraction of less than 1 ppm ($3.2 \times 10^9 \text{ W} - 3.2 \times 10^{10} \text{ W}$) of this absorbed energy flux is converted into biomass by photosynthesis and finally stored in the Earth's crust as fossil fuels, such as coal and hydrocarbons [1981Bro]. A small fraction of the solar energy incident on the Earth's surface is used to heat up the surface, but it penetrates only to very shallow depth, some decimeters for the daily cycle and some tens of meters for the annual seasonal changes. As a result, large as it may be, solar energy has negligible influence on the Earth's thermal regime. However, the solar heating of the very surface of the Earth contributes to some extent to the heat that can be extracted from the shallow subsurface with Earth coupled heat exchangers (see section 8.3.1.1.1).

Gravitational Energy: Exchange of gravitational energy between the Earth and the Moon and Sun is the source of tidal energy both in the oceans and the body of the solid Earth. Among the Earth's celestial neighbors only the Sun and the Moon are sufficiently massive or close to cause significant tides on the Earth. This is owing to the fact that tidal accelerations and the associated torques are linearly and inversely proportional to the mass and the cube of the distance between the two bodies, respectively. Tidal deceleration of the Earth results in a decrease of rotational kinetic energy at a rate of about $3 \times 10^{12} \text{ W} - 6 \times 10^{12} \text{ W}$ [1980Ver]. This energy is dissipated by tidal friction and finally converted into heat. Most of this heat, at least 80 %, is dissipated in the oceans, and only a fraction of less than 20 % in the Earth's mantle. Thus, heat derived from gravitational energy is accumulated in the solid Earth at a rate of about **$6 \times 10^{11} \text{ W} - 12 \times 10^{11} \text{ W}$** [1980Ver; 1981Bro]. Clearly, there is considerable uncertainty attached to these numbers, and it should be realized that they are probably correct only with respect to the order of magnitude. They indicate, however, that the heat delivered to the Earth by conversion of gravitational energy into heat is 1–2 orders of magnitude less than that which is produced by the decay of radioactive isotopes in the rocks of the Earth (see below). However, the relative importance of gravitational and radioactive heating might have changed during the Earth's life time.

8.1.2.1.2 Internal Heat Sources

The interior of the Earth is gaining heat from four main sources: *radiogenic heat* from the decay of unstable, radioactive isotopes; *original heat*, i.e. the heat content of the infant Earth immediately after formation; *potential energy* released as heat during the creation of new crust, the enrichment of heavy metals in the Earth's mantle or the formation iron core of the Earth; *frictional heat* from elastic energy released in earthquakes.

Radiogenic Heat: When radioactive isotopes decay, they emit energetic particles (α - and β -particles; neutrinos and antineutrinos without mass or charge) and γ -rays. Matter is almost transparent to neutrinos and antineutrinos and most of the energy carried by them is transmitted into space. In contrast, α - and β -particles (helium nuclei and electrons) do interact with the surrounding rock which absorbs their kinetic energy thus generating heat. In order to be a significant source of heat to the Earth, a radioactive isotope must be sufficiently abundant, have a half-life comparable to the age of the Earth, and most of its decay energy must be converted into heat. Mainly uranium, thorium, and potassium isotopes fulfill these conditions: ^{238}U and ^{235}U (natural uranium: 99.28 % ^{238}U + 0.71 % ^{235}U + 0.01% ^{234}U), ^{232}Th , and ^{40}K (natural Potassium: 0.01167 % ^{40}K). The low concentration of the ^{40}K isotope is made up for by the abundance of potassium in rocks. Therefore the heat production of ^{40}K is not negligible. The ratios of the initial concentrations of uranium, thorium and potassium in the infant bulk Earth are believed to be: $c_{\text{K}}/c_{\text{U}}=1.1 \times 10^4 - 1.3 \times 10^4$; $c_{\text{Th}}/c_{\text{U}}=3.7-4.0$; $c_{\text{K}}/c_{\text{U}}=1.1 \times 10^4$. By comparison, the potassium-uranium ratio in

chondrites, believed to be remnants of the early universe, is $c_K/c_U=7 \times 10^4$ [1995Van]. The heat production of a bulk rock can be determined from its concentrations in uranium, thorium and potassium. The current heat generation rate of average Earth A_{av} determined from estimated concentrations of the radiogenic isotopes ^{238}U , ^{235}U , ^{232}Th and ^{40}K equals about $A_{av} = 2.75 \times 10^{13} \text{ W}$ [1995Van]. In the geological past, when less radioactive isotopes had yet decayed, heat generation was considerably larger. The total heat production E accumulated over a period of 4.6×10^9 years can be computed from the current value and the different half-lives of uranium, thorium, and potassium to $E \sim 8.9 \times 10^{30} \text{ J}$ [1995Van]. This is equivalent to several millions of years of solar irradiation received by the Earth. The Earth loses heat by conduction (see Heat Expenditure below) at a rate of $Q_{\text{global}} = 4.42 \times 10^{13} \text{ W}$ [1993Pol]. Combined with the total accumulated heat production this global heat loss yields a typical cooling time τ for the Earth of

$$\tau = E / Q_{\text{global}} = 8.9 \times 10^{30} \text{ J} / 4.42 \times 10^{13} \text{ W} = 2.0 \times 10^{17} \text{ s} \approx 6.4 \times 10^9 \text{ a} .$$

In view of the age of the Earth (4.6×10^9 a) this means that the current terrestrial heat flow could be sustained by radioactive heat alone at least for another 1.8×10^9 years. This period is more than doubled if the original heat and the latent heat which would be liberated during a further solidification of the Earth's core are also considered. The ratio of radiogenic heat generation to global heat loss is $2.75 \times 10^{13} \text{ W} / 4.42 \times 10^{13} \text{ W} = 0.62$. This means that slightly less than $\frac{2}{3}$ of the Earth's heat output can be accounted for by radioactivity.

Original Heat: It is generally accepted that the cooling of the Earth since its early history, when internal temperatures were much higher than they are now, contributes a significant amount to the present terrestrial heat flow comparable to that from radiogenic heat. Assuming an average specific heat capacity of $1088 \text{ J kg}^{-1} \text{ K}^{-1}$ and a temperature drop of 650 K over a cooling time of 4.6×10^9 years yields $2.9 \times 10^{13} \text{ W}$ as the average rate for the loss of original heat [1991Vac; 1992Vac]. As the heat loss was much larger for the hotter and not yet solidified young Earth than today, this contribution is certainly lower at present (see below). Original heat is believed to derive (1) from gravitational contraction of the interstellar material, and (2) in part from the Moon-forming collision of a proto-planet the size of Mars and the proto-Earth providing an enormous energy on the order of 10^{31} J [1990Mel; 2000Can].

Potential Energy: Potential energy is liberated by the formation of

- the iron core of the Earth at an average rate of: $\sim 3.2 \times 10^{11} \text{ W}$ [1981Bro] – $4.5 \times 10^{13} \text{ W}$ [1992Vac] over the past 4.6×10^9 years;
- new crust or the enrichment of heavy metals in the Earth's mantle at rates of $\sim 3.2 \times 10^{10}$ – $3.2 \times 10^{12} \text{ W}$ [1981Bro].

In summary, $3.5 \times 10^{10} \text{ W}$ – $4.8 \times 10^{13} \text{ W}$ is released by the conversion of potential energy into heat.

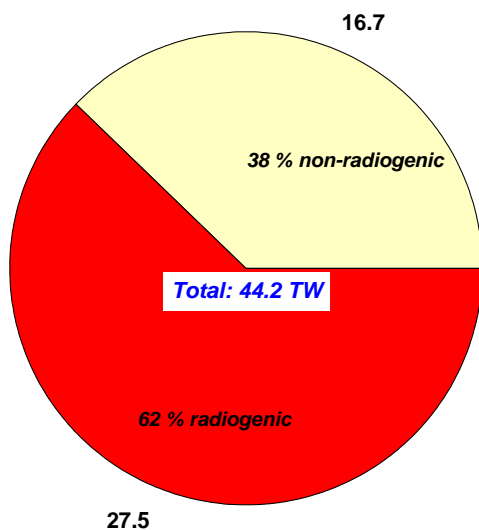


Fig. 8.4. Thermal power (TW) received by the Earth from different sources.

Frictional Heat: Heat due to release of elastic energy in earthquakes (for 10–40 earthquakes per year of surface wave magnitudes $M_s > 7$) is dissipated at a rate of $1.6 \times 10^{10} \text{ W} - 1.3 \times 10^{12} \text{ W}$ [1997Low].

Thus the maximum estimate for the non-radiogenic heat generation rate from original heat, potential energy, and frictional heat amounts to $7.8 \times 10^{13} \text{ W}$. The true value, however, is certainly much lower. The rate at which non-radiogenic heat is actually generated in the Earth today can be estimated by subtracting the current average radiogenic heat production rate of $2.75 \times 10^{13} \text{ W}$ [1995Ste] from the Earth's total heat loss of $4.42 \times 10^{13} \text{ W}$ [1993Pol] (see Heat Expenditure below). This calculation yields $1.67 \times 10^{13} \text{ W}$ for the current rate of non-radiogenic heat generation in the Earth. Thus radiogenic exceeds non-radiogenic heat generation by a factor of 5/3 (Fig. 8.4).

8.1.2.2 Heat Expenditure

The Earth is losing heat owing mainly to three processes: *Long-wavelength heat radiation, volcanism, and global heat flow.* By far the largest heat loss is due to global heat flow. As a process contributing to global heat flow, thermal and compositional convection in the Earth's fluid outer core provide the energy which drives the geomagnetic dynamo. However, this comprises no heat sink since this electromagnetic energy is finally dissipated again as heat (Fig. 8.5).

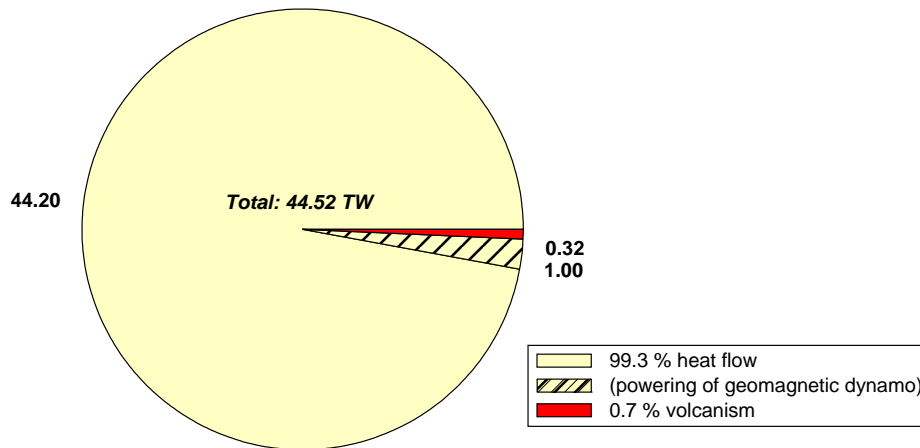


Fig. 8.5. Thermal power (TW) spent by the Earth via different processes (disregarding long-wavelength heat radiation).

Long-Wavelength Heat Radiation: Of the Sun's irradiation power of $3.53 \times 10^{16} \text{ W}$ which are absorbed in the atmosphere, 73 % are directly heating the atmosphere, while about 27 % are converted into kinetic wind energy. These transmit about 10 % of their energy to waves on the Earth's water surface [1981Bro]. Ultimately, all wind and wave energy is again converted into heat and re-emitted as long-wavelength radiation. Because rocks and soil are poor heat conductors, most of the energy flux of $7.87 \times 10^{16} \text{ W}$ incident at the Earth's surface does not penetrate to any depth greater than one meter and must be re-emitted as long-wavelength radiation, particularly at night. Since only small amounts of solar energy are converted into energy forms that can be permanently stored in the Earth, any disturbance of the delicate balance between solar income and terrestrial radiation will lead to a heating of the Earth's surface.

Global Heat Flow: The global rate of heat loss across the surface of the Earth is: $Q_{\text{global}} = Q_{\text{oceans}} + Q_{\text{continents}} = 3.1 \times 10^{13} \text{ W} + 1.32 \times 10^{13} \text{ W} = (4.42 \pm 1.0) \times 10^{13} \text{ W}$ [1993Pol]. Of the heat loss to the oceans, $34 \pm 12 \%$ or $(1.1 \pm 0.4) \times 10^{13} \text{ W}$ are associated with hydrothermal flow [1995Ste]. The average global specific heat flow $\bar{q} = 87 \text{ mW m}^{-2}$ was determined in a global compilation [1993Pol] of 24774 observations at 20201 locations (10337 continental; 9864 marine). The average on the continents $\bar{q}_{\text{continents}} = 67 \text{ mW m}^{-2}$ is

lower than in the oceans $\bar{q}_{\text{oceans}} = 101 \text{ mW m}^{-2}$. Fig. 8.5 summarizes the contributions of heat flow, energy supply to the geomagnetic dynamo, and volcanism to the energy expenditure of the Earth. The contribution by emission of long-wavelength heat radiation is disregarded since it is almost totally canceled by the corresponding contribution to the energy income.

Depending on various assumptions the powering of the geomagnetic dynamo consumes electromagnetic energy at a rate of $3.2 \times 10^9 \text{ W} - 1 \times 10^{12} \text{ W}$ [80Ver; 81Bro; 03Buf]. A recent combined analysis of laboratory dynamo experiments and numerical simulations indicates a more constrained range of $2 \times 10^{11} \text{ W} - 5 \times 10^{11} \text{ W}$ [04Chr]. This is two orders of magnitude less than the conductive heat loss. With Carnot-style efficiencies of 5% - 15% for the conversion of thermal and compositional convection into magnetic field energy [02Buf; 03Buf; 03Rob], this yields a heat flow on the order of 10^{12} W required to drive the geomagnetic dynamo. Due to the very low frequencies in which the Earth's magnetic field varies virtually none of its electromagnetic energy is radiated.

8.1.2.3 Heat Budget

The budget of the heat income and heat expenditure of the Earth based on the numbers discussed above and shown in Fig. 8.4 and Fig. 8.5 is negative. It shows that the Earth is cooling at a rate of approximately **1.4 TW**. This number is based on the balance calculated between the Earth's global heat loss by heat flow and the estimated radiogenic heat generation rate. Its uncertainty is largely dominated by the uncertainty of this estimate and future estimates may modify this number to a certain extent. However, there is no doubt that the Earth has been losing heat since its formation and still continues to do so at a rate equivalent to roughly 2 ppm of the total solar irradiation intercepted by the Earth.

8.1.3 The Thermal Regime of the Earth's Crust

In the Earth's crust, the variation of temperature with depth is more irregular than in the mantle and core and shows large lateral variations. It depends strongly on the content of radioactive isotopes in the rocks (see below) and on the tectonic and hydrological regime. Typically, average values vary from $10 \text{ K km}^{-1} - 60 \text{ K km}^{-1}$ for the continental crust of 25 km - 45 km thickness. In the 5 km - 8 km thin oceanic crust these values may be much exceeded due to hydrothermal activity. The temperature regime has been compiled from observations in boreholes and mapped for several regions in the continental crust [e.g. 1980Hän; 1988Hän; 1991Gho; 1992Bla; 1992Hur; 1995Gup; 1996Ham; 1996Wan; 1998Ano; 2002Hur]. These maps and atlases provide reasonable general information on the regional variability of temperature at drilling depth in the crust. More specific local information on the temperature field requires, as a rule, additional analyses of the thermal regime. In particular, this involves some sort of analytical or numerical modeling based on measured thermal properties, such as thermal conductivity, thermal diffusivity, specific heat capacity, density, radiogenic heat generation rate, of the dominating local rocks.

Studies of the specific heat flow, the loss of heat across the surface of the Earth per unit time and area, based on observations at 20201 sites worldwide reveal remarkable variability and characteristic trends [1993Pol]. In general, there is a decrease of specific heat flow with age: Specific heat flow is lower in old stable platforms than in young, tectonically active crust, on average by a factor of $1 \frac{1}{2}$ (Fig. 8.6). As a consequence, the mean specific heat flow is larger in the generally young oceans (101 mW m^{-2}) than on the continents (67 mW m^{-2}).

Surprising as this may appear, the earth has been drilled to a maximum depth of only 12.262 km, less than 1 % of its diameter. In contrast, our universe has been explored by spacecraft beyond the limits of our solar system. Unfortunately, data from existing commercial boreholes of several kilometers depth, drilled for hydrocarbons, is rarely available for geothermal research. Therefore, the vast majority of marine and continental data is derived from measurements with heat flow probes penetrating only a few meters into

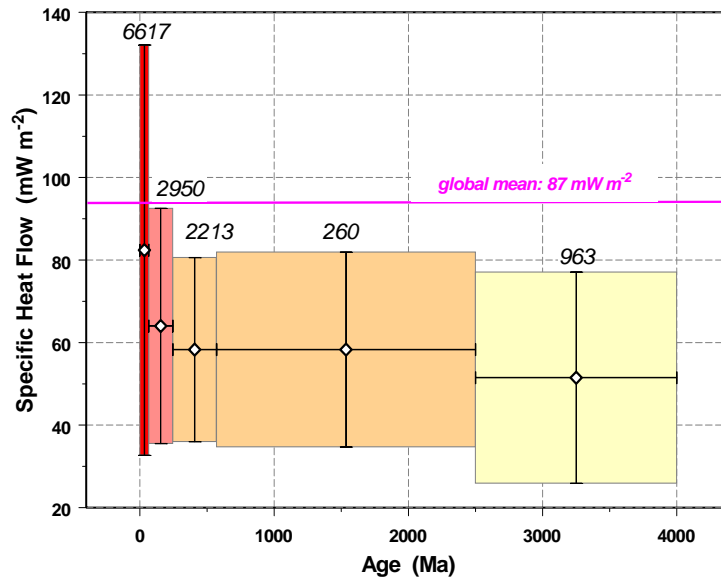


Fig. 8.6. Variation of specific heat flow with age based on 13003 observations in the continental crust. Diamonds show mean values for specific heat flow. The number of observations in each geologic era is shown above the corresponding box. Width and height of each box represents the duration of the different eras (from left to right: Cenozoic, Mesozoic, Paleozoic, Proterozoic, Archean) and one standard deviation above and below the mean specific heat flow, respectively; data: [1993Pol].

deep-sea sediments and in shallow boreholes of a few hundred meters depth, respectively. Therefore, specific heat flow derived from this data comprises signatures from a variety of factors and processes, both steady-state and transient, such as topography, contrasts in thermal properties in a heterogeneous subsurface, groundwater flow, paleoclimatic variations of the Earth's mean surface temperature, and others. This has to be considered when using heat flow data for thermal regime analyses, in particular for temperature predictions beyond the drilled depth.

Large anomalies occur both in the oceans and on the continents where heat is not only diffused to the surface but also advected by moving fluids. This occurs in particular near mid-ocean ridges, where upwelling magma maintains large lateral temperature gradients in the high-porosity sediments, but also in volcanic regions and many sedimentary basins on the continents where heat is redistributed by regional or focused groundwater flow [see e.g. 2002Cla for a summary of the literature].

Economic production of geothermal energy is facilitated, but not restricted to, regions of elevated heat flow. Various types of geothermal energy extraction schemes are available, suitable for both power production and direct thermal use (see section 8.3), which can be implemented in high and low temperature regimes, respectively.

8.1.4 Heat Storage

Heat is stored in the Earth by virtue of the heat capacity of its rocks and fluids. In comparison, the amount of heat stored in gas in the Earth is negligible. Heat capacity C is defined as the ratio of heat ΔQ required to raise the temperature of a body by ΔT . For each molecule this temperature increase requires an energy of $(f/2) k \Delta T$, where f is the number of degrees of freedom of the molecules and $k=1.3806503 \times 10^{-23} \text{ J K}^{-1}$ the Boltzmann constant. For a body of mass $M=m N_A$ (where m is the mass of the molecules and N_A is the

Avogadro's number $N_A = M/m = 6.022\,141\,99 \times 10^{23} \text{ mol}^{-1}$) a temperature increase by ΔT requires an energy of $\Delta Q = (M/m) (f/2) k \Delta T$. Thus the heat capacity of the body is:

$$C = \frac{\Delta Q}{\Delta T} = \frac{M}{m} k \frac{f}{2} = N_A k \frac{f}{2}. \quad (8.4)$$

Specific heat capacity c of a substance is defined as heat capacity C related to unit mass:

$$c = \frac{\Delta Q}{M \Delta T} = \frac{f}{2} \frac{k}{m} = \frac{f k}{2 \mu m_H}, \quad (8.5)$$

where μ is atomic mass relative to the mass of the hydrogen atom $m_H = 1.67 \times 10^{-27} \text{ kg}$.

For single gas molecules $f=3$, corresponding to the three degrees of freedom of translation along each direction in space. For solids, $f=6$, corresponding to the three degrees of freedom of potential and kinetic lattice vibration energy in each space direction. Isobaric specific heat capacity c_p (at constant pressure) is larger than isochoric specific heat capacity c_v (at constant volume) because additional work is required for volume expansion. Their ratio, the adiabatic exponent, is:

$$\frac{c_p}{c_v} = \frac{f+2}{f}, \quad (8.6)$$

Alternatively, isobaric specific heat capacity c_p can be expressed by means of enthalpy $H(T,P) = E + P V$, a state function of temperature and pressure, where E is internal energy, P pressure and V volume [e.g. 1989Hem]. In a closed system, the change in internal energy (dE) is the sum of the change in heat (dQ) and the work delivered (dW): $dE = dQ + dW$. If we only consider volume expansion work: $dW = -P dV$, the change in enthalpy dH becomes:

$$dH(T, P) = dE + P dV + V dP = dQ + V dP = \left(\frac{\partial H}{\partial T} \right)_P dT + \left(\frac{\partial H}{\partial P} \right)_T dP. \quad (8.7)$$

Comparing coefficients, we obtain:

$$\frac{dQ}{dT} = \left(\frac{\partial H}{\partial T} \right)_P \doteq c_p. \quad (8.8)$$

Thus, eq. (8.8) defines isobaric specific heat capacity c_p as the first derivative of enthalpy with respect to temperature. Comparing eqs. (8.5) and (8.8) we see that both expressions are equivalent for $dQ = \Delta Q/M$, and the isobaric enthalpy change is equal to the specific heat content $\Delta H = \Delta Q/M$.

Isobaric and isochoric specific heat capacity are related to compressibility $\beta = \Delta V / (V \Delta P)$ and its inverse, incompressibility or bulk modulus $K = V \Delta P / (\Delta V)$, by $c_p/c_v = \beta_T / \beta_S = K_S / K_T$ [e.g. 1992Sta]. Subscripts T and S refer to isothermal and adiabatic conditions, respectively, i.e. constant temperature and constant entropy. Inserting the thermodynamic relation $\beta_T = \beta_S + \alpha^2 T / (\rho c_p)$ [e.g. 1966Bir] between isothermal and adiabatic compressibility yields the relative difference between isobaric and isochoric specific heat capacity:

$$c_p/c_v = 1 + \alpha \gamma T, \quad (8.9)$$

where ρ is density, $\alpha = \Delta V / (V \Delta T)$ the volume expansion coefficient, and

$$\gamma = \frac{\alpha K_S}{\rho c_p} = \frac{\alpha K_T}{\rho c_v}, \quad (8.10)$$

the dimensionless Grüneisen parameter. Inserting the expressions for α and K in eq. (8.10) yields:

$$\gamma = \frac{1}{\rho c_p} \frac{\Delta V}{V \Delta T} \frac{V \Delta P}{\Delta V} = \frac{\Delta P}{\rho c_p \Delta T}, \quad (8.11)$$

Thus the Grüneisen parameter γ is the relative pressure change in a material heated at constant volume.

The absolute difference between isobaric and isochoric specific heat capacity follows from eqs. (8.9) and (8.6), assuming $f = 6$:

$$c_p - c_v = \frac{K_T \alpha^2 T}{\rho} = \frac{3 K_S \alpha^2 T}{4 \rho}. \quad (8.12)$$

For crustal rocks ($\gamma = 0.5$; $\alpha = 20 \mu\text{K}^{-1}$; $T < 10^3 \text{ K}$; $\rho = 2600 \text{ kg m}^{-3}$; $K_S < 75 \text{ GPa}$ [1981Dzi; 1992Sta]), the difference between isobaric and isochoric specific heat capacity is less than 1 % or $9 \text{ J kg}^{-1} \text{ K}^{-1}$ according to eqs. (8.9) and (8.12), respectively. Thus, the distinction between isobaric and isochoric specific heat capacity is negligible for crustal rocks at temperatures below 1000 K. Therefore, from here on, “specific heat capacity” will always refer to isobaric specific heat capacity, denoted simply by the letter c without the subscript “P”.

For temperatures above the Debye temperature this classical treatment of heat capacity is sufficient. In the Earth, the actual temperature exceeds the Debye temperature everywhere, except in the crust [1992Sta]. Therefore we observe deviations from the classical Dulong-Petit values (eqs. (8.5)–(8.12)) in experiments at room temperature and atmospheric pressure – the lower the temperature, lighter the element, and stronger the lattice bonding the larger the deviations are. An adequate treatment of specific heat capacity under these conditions requires quantum mechanics. This is, however, beyond the scope of this text and interested readers are referred to standard physics textbooks [e.g. 1991Tip; 2002Mes].

8.1.4.1 Measuring Techniques

Specific heat capacity c can be measured directly or derived as the isobaric derivative of enthalpy H with respect to temperature. Specific heat capacity of rocks varies with temperature, pressure, porosity, and saturants. Accordingly, in situ values deviate from laboratory data according to temperature, pressure, and type and content of pore fluid.

There are numerous steady-state and transient calorimetric methods available for direct measurement of specific heat capacity. The most popular are mixing or drop calorimeters and heat flux differential scanning (DSC) calorimeters. The first method yields an absolute value, the second one is a comparative method. All of these methods are discussed in detail in the literature [1984Hem; 1989Hem; 1997Höh; 1998Gal; 2001Bro; 2001Sch; 2002Hai]. They are therefore not addressed here and readers are referred to the literature for details on measurements.

The isobaric enthalpy change (or specific heat content) ΔH of solids may be determined by the method of mixtures using a Bunsen-type calorimeter in which the unknown isobaric enthalpy change of a sample relative to a base temperature, for instance $25 \text{ }^\circ\text{C}$, is compared to the corresponding known isobaric enthalpy change of platinum [1960Kel; 1992Som].

8.1.4.2 Calculated Heat Capacity

When no direct measurements can be performed, isobaric enthalpy change and specific heat capacity of rocks can be calculated as the arithmetic mean from the contributions of the individual mineralogical constituents and saturating fluids of the rock weighted by the volume fractions n_i of the N individual phases relative to total rock volume, where $1 = \sum n_i$:

$$\Delta H = \sum_{i=1}^N n_i \Delta H_i ; \quad c = \sum_{i=1}^N n_i c_i . \quad (8.13)$$

This is frequently referred to as Kopp’s law. As specific heat capacity is a scalar quantity, we need not be concerned with a loss of information on anisotropy in this case, unlike in the case of thermal conductivity (see section 8.1.5.1.2 below). From eq. (8.13) and based on the data in Table 8.3, the isobaric enthalpy change ΔH can be computed for rocks such as sandstones, shales, and limestones which consist of complex mineral assemblages of a combination of various oxides [1992 Som].

By suitable combinations of the data for different oxides in Table 8.3 enthalpy changes can be computed for various other mineral components; the enthalpy change for CaCO_3 , for instance, is computed as the sum of the enthalpy changes for CaO and CO_2 . For temperatures above $100\text{ }^\circ\text{C}$, the loss of combined water needs to be accounted for in the calculations. It is considered to be linear between the drying temperature ($105\text{ }^\circ\text{C}$) and the ignition loss temperature ($800\text{ }^\circ\text{C}$); Somerton [1992Som] discusses further details of the calculations.

Table 8.3. Isobaric enthalpy change ΔH of common rock forming oxides relative to the corresponding enthalpies at $25\text{ }^\circ\text{C}$ for various temperatures; for water, subscripts “c” and “f” refer to combined and free water [1992Som; data: 1960Kel].

Oxide	Enthalpy change: $\Delta H = H(T) - H_{25\text{ }^\circ\text{C}}$ (kJ kg^{-1})									
	$50\text{ }^\circ\text{C}$	$75\text{ }^\circ\text{C}$	$100\text{ }^\circ\text{C}$	$150\text{ }^\circ\text{C}$	$200\text{ }^\circ\text{C}$	$300\text{ }^\circ\text{C}$	$400\text{ }^\circ\text{C}$	$500\text{ }^\circ\text{C}$	$600\text{ }^\circ\text{C}$	$700\text{ }^\circ\text{C}$
SiO_2	20.93	41.87	61.96	103.41	149.47	251.21	362.58	478.97	619.65	734.78
Al_2O_3	20.93	43.96	66.99	115.14	162.03	267.12	378.86	494.04	615.46	736.88
Fe_2O_3	16.71	33.41	50.33	85.91	125.60	210.43	301.53	392.72	492.79	592.43
CaO	20.93	39.90	58.87	100.73	140.01	228.98	314.01	405.70	497.39	595.36
K_2O	31.40	58.62	87.92	150.72	211.43	337.58	463.06	596.62	732.69	879.23
Na_2O	31.40	58.62	88.00	150.81	211.48	336.91	462.64	597.04	737.71	880.07
CO_2	24.87	50.37	75.24	132.81	190.37	320.54	458.04	608.34	765.35	929.05
$(\text{H}_2\text{O})_c$	50.66	102.16	154.91	264.23	379.07	628.86	907.70	1216.68	1558.75	1932.21
$(\text{H}_2\text{O})_f$	104.67	209.34	314.01	-	-	-	-	-	-	-

Based on the variation with temperature of isobaric enthalpy change ΔH measured for various oxides, Kelley [1960Kel] suggested a second order polynomial as fitting function for ΔH [1992Som]; according to eq. (8.8) this yields a corresponding polynomial for specific heat capacity c :

$$\Delta H = A_1 T + A_2 T^2 + \frac{A_3}{T} + A_4 ; \quad c = A_1 + 2 A_2 T - \frac{A_3}{T^2} \quad (T \text{ in K}). \quad (8.14)$$

The coefficients A_1 – A_4 shown in Table 8.4 are obtained from a least-squares fit of the polynomial (eq. (8.14)) for isobaric enthalpy change ΔH on the data in Table 8.3. Based on these coefficients ΔH and c can be computed from eq. (8.14) in kJ kg^{-1} and in $\text{kJ kg}^{-1} \text{K}^{-1}$, respectively. For ΔH , Fig. 8.7 compares the corresponding curves with the data in Table 8.3.

Table 8.4. Coefficients A_1 – A_4 for computing isobaric enthalpy change ΔH in kJ kg^{-1} relative to the corresponding enthalpies at $25\text{ }^\circ\text{C}$ and specific heat capacity c in $\text{kJ kg}^{-1} \text{K}^{-1}$ from eq. (8.14) (where temperature is in K) for common rock forming oxides and temperatures between $50\text{ }^\circ\text{C}$ – $700\text{ }^\circ\text{C}$; subscript “c” indicates that water and carbon dioxide are combined into the crystal lattice.

Oxide	A_1	$10^4 \times A_2$	A_3	A_4
SiO_2	1.0174	1.8785	50032	-479.87
Al_2O_3	0.95893	1.6540	22674	-375.39
Fe_2O_3	0.86410	0.97545	33080	-374.74
CaO	0.74142	1.2062	4493.2	-245.74
K_2O	0.87153	2.9471	-16396	-232.29
$(\text{CO}_2)_c$	1.0468	3.4676	33043	-451.55
$(\text{H}_2\text{O})_c$	0.59822	16.747	-39591	-195.23

Using the coefficients A_1 – A_4 in Table 8.4 the enthalpy changes ΔH_i and specific heat capacities c_i of individual mineral phases of a rock can be computed from eq. (8.14); Table 8.5 lists specific heat capaci-

ties of various minerals measured at different temperatures and coefficients A_1 – A_3 for calculating the specific heat capacities of a rock's mineral phases from eq. (8.14). According to eq. (8.13), these values combined with the specific heat capacity of the pore space and weighted by their volume fractions yield the specific heat capacity of the bulk rock. Rosen and Hashin [1970Ros] derived an exact expression for a two component medium which subtracts a temperature dependent, negative correction term from the empirical law in eq. (8.13) [1995Ber, p. 218].

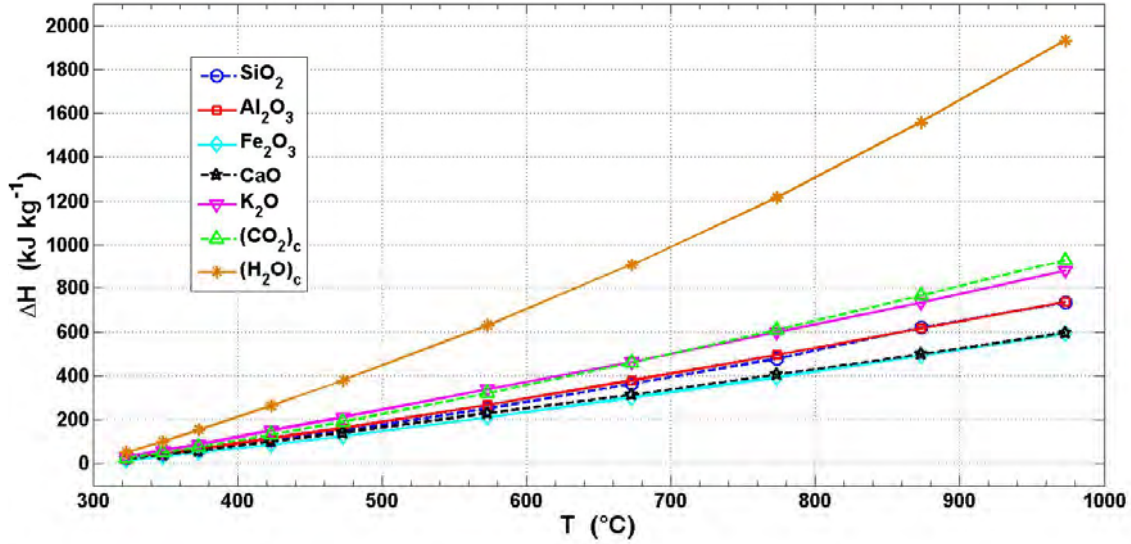


Fig. 8.7. Variation of isobaric enthalpy change ΔH with temperature T for common rock forming oxides: data (symbols; Table 8.3) and computed from eq. (8.14) (lines) with coefficients A_1 – A_4 in Table 8.4; data: [1960Kel; 1992Som]; subscript “c” indicates that water and carbon dioxide are combined into the crystal lattice.

For temperatures on the order of 300 K, however, this correction remains small: Assuming reasonable values for the quantities in eq. (58) of [1995Ber], it remains below -10 %. This is confirmed by a comparison of isobaric enthalpy changes measured over the temperature range of 127 °C – 527 °C on various clean to silty sandstones, siltstones, shale, and limestone with values calculated according to eq. (8.13) [1992Som]: Data and calculated values agree within a maximum deviation of less than 4.5 %, in most cases of better than 2 % (Fig. 8.8). Thus it appears acceptable to omit this correction for upper crustal conditions.

The heat capacity of the fraction of the rock volume occupied by pores and fractures is determined by the properties of its fluids: air, water, gas or oil. Table 8.6 and Table 8.7 list values for the specific heat capacity of air, water, and some gas and liquid hydrocarbons. However, because of the large density contrasts between different fluid and solid phases the heat capacity of saturated rocks is best calculated on a volumetric basis from thermal capacity.

Thermal capacity, also referred to as volumetric heat capacity, i.e. the product of specific heat capacity c and density ρ , is related to thermal conductivity λ and diffusivity κ :

$$\rho c = \lambda / \kappa . \quad (8.15)$$

In analogy to eq. (8.13) for specific heat capacity, Kopp's law yields rock bulk thermal capacity $(\rho c)_b$ as:

$$(\rho c)_b = (1 - \phi) (\rho c)_s + \phi \sum_1^N S_i (\rho c)_i , \quad (8.16)$$

where ϕ is porosity, $(\rho c)_s$ thermal capacity of the rock skeleton, S_i fractional saturation, and $(\rho c)_i$ thermal capacity of the i^{th} fluid phase in the pore space. Because of the low density of air and gas – about three

orders of magnitude lower than that of water and rock – the contribution of the gas phase to thermal capacity can often be ignored. In this case, N=2 for the fluid phases water and oil or N=1 for water only.

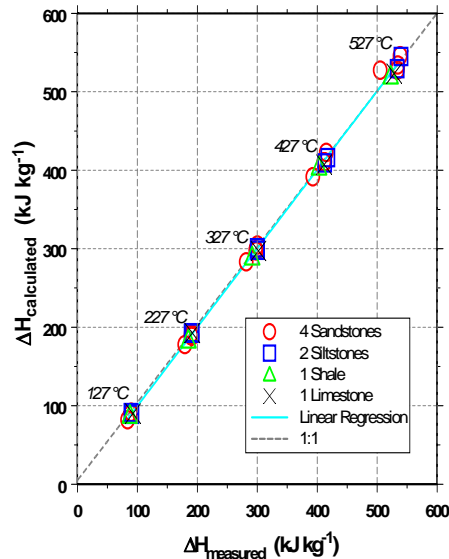


Fig. 8.8. Calculated versus measured isobaric enthalpy change ΔH relative to 25 °C at different temperatures for various sedimentary rocks. Linear regression (solid line): $y = (-0,4387 \pm 1.6236) + (1.0028 \pm 0.0048) x$, correlation coefficient: $R^2 = 0.9991$; broken line: $y = x$; data: [1992Som].

Table 8.5. Specific heat capacity c measured at different temperatures T and coefficients A_1 – A_3 for computing specific heat capacity c in $\text{kJ kg}^{-1} \text{K}^{-1}$ from eq. (8.14) (where temperature is in K) for different minerals (Ab: albite $\text{NaAlSi}_3\text{O}_8$; An: anorthite $\text{CaAl}_2\text{Si}_2\text{O}_8$). The last column shows the error Δc in % between specific heat capacity measured and calculated from eq. (8.14) and the temperature range for the coefficients (after [1942Gor]).

Compound	Mineral	c ($\text{kJ kg}^{-1} \text{K}^{-1}$) at T in °C						A_1	$2A_2 \times 10^4$	A_3	Δc (%); T-range (°C)
		-200	0	200	400	800	1200				
2Ab-3An	labradorite	0.82 at 60 °C									
3Ab-2An	andesine	0.7	0.97	1.07	1.18		0.991	2.0	25500	1; 0-900	
	glass	0.7	0.99	1.09	1.21		1.016	2.06	27800	1; 0-900	
4Ab-1An	oligoclase	0.85 at 60 °C									
	Ag native silver	0.146	0.233	0.24	0.26	0.28	0.217	0.58	0	0	1; 0-961
	Ag liquid						0.32	0.318	0	0	3; 961-1300
	AgCl cerargyrite	0.251	0.354	0.41	0.46		0.280	2.71	0	0	2; 0-453
Ag_3AsS_3	proustite	0.34 at 50 °C									5; 453-533
	Ag_2S acanthite	0.32					0.317	0	0	0	5; 0-175
	argentite		0.37				0.368	0	0	0	5; 175-325
Ag_3SbS_3	pyrargyrite	0.32 at 50 °C									

Pre-Print from:
 Clauser, C., 2006. Geothermal Energy, In: K. Heinloth (ed), *Landolt-Börnstein, Group VIII: Advanced Materials and Technologies, Vol. 3: Energy Technologies, Subvol. C: Renewable Energies*, Springer Verlag, Heidelberg-Berlin, 493-604.

Compound	Mineral	c (kJ kg ⁻¹ K ⁻¹) at T in °C						A_1	$2A_2 \times 10^4$	A_3	Δc (%); T-range (°C)
		-200	0	200	400	800	1200				
	Al ₂ O ₃ <i>corundum</i>	0.069	0.72	1	1.1	1.19	1.26	1.067	1.40	28900	4; 0-1700
	Al ₂ SiO ₅ <i>andalusite</i>	0.152	0.77	1.03	1.11	1.17	1.2	1.136	0.50	28100	3; 0-1300
	<i>cyanite</i>	0.077	0.7	1	1.1	1.2	1.27	1.080	1.36	31300	2; 0-1400
	<i>sillimanite</i>	0.133	0.743	1	1.08	1.16	1.22	1.054	1.23	25700	3; 0-1200
	Al ₆ Si ₂ O ₁₃ <i>mullite</i>		0.77	0.97	1.03	1.09	1.13	1.030	0.75	21000	3; 0-1100
	Al ₆ Si ₃ O ₁₈ <i>kaolinite</i>		0.93	1.02				0.806	4.63	0	4; 0-300
	Al ₂ Si ₂ O ₇ ·2H ₂ O <i>kaolin</i>		0.99	1.17	1.35			0.641	9.04	0	3; 0-500
	Al ₂ Si ₂ O ₇ <i>metakaolin</i>		0.71	1	1.1	1.2	1.27	1.062	1.51	28900	2; 0-1300
	2(AlF)O·SiO ₂ <i>topaz</i>	0.83 at 50 °C									
	Au <i>native gold</i>		0.127	0.13	0.14	0.15		0.119	0.306	0	2; 0-1063
	<i>liquid</i>						0.15				5; 1063-1300
	BaCO ₃ <i>α-witherite</i>	0.197	0.44	0.5	0.55	0.66		0.366	2.78	0	5; 0-810
	<i>β-witherite</i>					0.64		0.640	0	0	30; 810-950
	BaSO ₄ <i>barite</i>	0.197	0.45	0.5	0.55	0.65		0.383	2.53	0	5; 0-1050
	BeAl ₂ O ₄ <i>chrysoberyl</i>	0.84 at 50 °C									
	Be ₃ Al ₂ Si ₆ O ₁₈ <i>beryl</i>	0.84 at 50 °C									
	C <i>diamond</i>		0.435	1.06	1.37	1.86		0.754	10.67	45440	4; 0-1040
	<i>β-graphite</i>		0.635	1.18	1.45	1.88		0.932	9.13	40700	3; 0-1040
	Ca ₂ Al ₂ H ₂ (SiO ₄) ₃ <i>prehnite</i>	0.84 at 50 °C									
	Ca ₂ Al ₂ SiO ₇ <i>gehlenite</i>		0.75	0.97	1.03	1.09	1.12	1.042	0.6	22840	2; 0-1300
	CaAl ₂ Si ₂ O ₈ <i>anorthite</i>		0.7	0.95	1.05	1.17	1.27	0.950	2.26	23130	1; 0-1400
	<i>glass</i>		0.68	0.96	1.06			1.014	1.58	28200	1; 0-700
	CaCO ₃ <i>aragonite</i>	0.26	0.78	1	1.13			0.823	4.97	12860	3; 0-750
	<i>calcite</i>	0.28	0.79	1	1.13			0.823	4.97	12860	5; 0-1200
	CaF ₂ <i>fluorite</i>	0.22	0.85	0.89	0.93	1.01	1.1	0.798	2.04	0	
	CaMg(CO) ₃ <i>dolomite</i>	0.93 at 60 °C									
	CaMgSi ₂ O ₆ <i>diopside</i>		0.69	0.98	1.06	1.15	1.2	1.053	1.11	29000	1; 0-1300
	<i>glass</i>		0.71	0.98	1.07			0.999	1.88	25300	1; 0-700
	CaSiO ₃ <i>pseudo-wollastonite</i>	0.174	0.73	0.92	0.99	1.07	1.14	0.926	1.50	17700	2; 0-1400
	<i>(β) wollastonite</i>	0.172	0.67	0.92	1	1.06	1.1	1.007	0.74	26900	2; 0-1300
	<i>glass</i>		0.69	0.92	1.03			0.834	3.48	17500	2; 0-700
	CaSO ₄ <i>anhydrite</i>		0.52	0.58	0.6	0.64		0.569	6.75	4800	5; 0-1100
	CaSO ₄ ·2H ₂ O <i>gypsum</i>	0.322	1.03								
	CaWO ₄ <i>scheelite</i>	0.40 at 50 °C									
	CdS <i>greenockite</i>		0.445	0.5	0.55	0.65		0.374	2.605	0	?; 0-1000
	Cu <i>native copper</i>	0.161	0.384	0.4	0.42	0.46		0.358	0.96	0	2; 0-1084
	<i>liquid</i>							0.493	0	0	3; 1084-1300
	Cu ₂ O <i>cuprite</i>		0.47	0.51	0.54	0.61		0.419	1.81	0	5; 0-950
	CuO <i>tenorite</i>		0.52	0.63	0.68			0.572	1.88	7900	2; 0-537
	2CuO·CO ₂ ·H ₂ O <i>malachite</i>	0.74 at 57 °C									
	CuFeS ₂ <i>chalcopyrite</i>	0.54 at 50 °C									
	CuPbSbS ₃ <i>bournonite</i>	0.31 at 50 °C									

Compound	Mineral	c (kJ kg ⁻¹ K ⁻¹) at T in °C						A_1	$2A_2 \times 10^4$	A_3	Δc (%); T-range (°C)
		-200	0	200	400	800	1200				
Cu ₂ Se	<i>α</i> -berzelianite	0.42						0.420	0	0	5; 0-100
	<i>β</i> -berzelianite	0.41						0.410	0	0	5; 100-200
Cu ₂ S	<i>α</i> -chalcocite	0.255	0.47					0.247	8.2	0	3; 0-103
	<i>β</i> -chalcocite	0.55		0.55	0.55			0.550	0	0	10; 103-900
CuS	<i>covellite</i>	0.228	0.49	0.52	0.54	0.59	0.464	1.15	0	?; 0-1000	
CuSiO ₃ ·H ₂ O	<i>diopside</i>	0.77 at 34 °C									
Fe	<i>α</i> -iron	0.44	0.52	0.6			0.330	4	0	3; 0-755	
	<i>β</i> -iron					0.73	0.460	2.5	0	3; 755-903	
	<i>γ</i> -iron						0.63	0.630	0	0	5; 903-1401
	<i>δ</i> -iron						0.750	0	0	5; 1401-1530	
	<i>liquid</i>						0.610	0	0	5; 1530-1600	
FeAsS	<i>arsenopyrite</i>	0.43 at 55 °C									
FeCO ₃	<i>siderite</i>	0.234	0.68								
Fe ₂ O ₃	<i>hematite</i>	0.61	0.79	0.9	1.08			0.640	4.2	11100	3; 0-800
Fe ₃ O ₄	<i>α</i> -magnetite	0.6	0.83	0.93			0.744	3.4	17700	3; 0-576	
	<i>β</i> -magnetite					1.03	0.640	3.62	0	5; 576-800	
2Fe ₂ O ₃ ·3H ₂ O	<i>limonite</i>	0.94 at 60 °C									
Fe ₂ SiO ₄	<i>fayalite</i>	0.55	0.79	0.91	1.1			0.690	3.92	18100	3; 0-900
Fe ₂ Si ₂ O ₆	<i>hypersthene</i>	0.80 at 60 °C									
FeS	<i>α</i> -troilite	0.238	0.606					1.000	18.5	0	7; 0-138
	<i>β</i> -troilite	0.64		0.66	0.71	0.574	0.574	1.3	0	3; 138-1195	
FeS ₂	<i>pyrite</i>	0.075	0.5	0.59	0.69			0.373	4.66	0	7; 0-500
Fe ₇ S ₈	<i>pyrrhotite</i>	0.594	0.77					0.406	28.1	43100	3; 0-350
H ₂ O	<i>ice</i>	0.653	2.06								
Hg	<i>native mercury</i>	0.138	0.14					0.138	0	0	1; 0-347
	<i>α</i> -cinnabar	0.214	0.23	0.24					0.196	0.66	0
KAISi ₂ O ₆	<i>leucite</i>	0.74 at 80 °C									
	<i>glass</i>	0.73 at 60 °C									
KAISi ₂ O ₈	<i>adularia</i>	0.732	0.84	1							
	<i>microcline</i>	0.68	0.95	1.04	1.14			0.988	1.66	26300	1; 0-1100
	<i>orthoclase</i>	0.61	0.94	1.05	1.15			1.043	1.24	35100	1; 0-1100
	<i>glass</i>	0.7	0.97	1.07	1.19			0.976	0.216	24700	2; 0-1100
KCl	<i>sylvite</i>	0.418	0.682	0.72	0.75			0.682	1.68	0	2; 0-770
KNO ₃	<i>α</i> -niter	0.326						0.266	2.19	0	10; 0-128
	<i>β</i> -niter	1.19						1.190	0	0	5; 128-338
	<i>liquid</i>	1.22						1.220	0	0	10; 338-410
LiAlSi ₂ O ₅	<i>petalite</i>	0.85 at 58 °C									
LiAlSi ₂ O ₆	<i>spodumene</i>	0.90 at 60 °C									
	<i>glass</i>	0.91 at 60 °C									
Mg ₃ Al ₂ Si ₃ O ₁₂	<i>garnet</i>	0.74 at 58 °C									
Mg ₇ B ₁₆ Cl ₂ O ₂₅	<i>α</i> -boracite	0.796	1.18					0.275	19.09	0	5; 0-265
	<i>β</i> -boracite					1.41	0.502	13.46	0	5; 265-100	

Pre-Print from:

Clauser, C., 2006. Geothermal Energy, In: K. Heinloth (ed), *Landolt-Börnstein, Group VIII: Advanced Materials and Technologies, Vol. 3: Energy Technologies, Subvol. C: Renewable Energies*, Springer Verlag, Heidelberg-Berlin, 493-604.

Compound	Mineral	c (kJ kg ⁻¹ K ⁻¹) at T in °C						A ₁	2A ₂ × 10 ⁴	A ₃	Δc (%); T-range (°C)	
		-200	0	200	400	800	1200					
MgCl ₂	<i>chloromagnesite</i>	0.805	0.84	0.87				0.760	1.66	0	?; 0-718	
MgCO ₃	<i>magnesite</i>	0.161	0.864									
MgF ₂	<i>sellaite</i>	0.906	1.08	1.21	1.43			0.857	5.42	7360	3; 0-1000	
Mg(OH) ₂	<i>brucite</i>	1.30 at 35 °C										
MgO	<i>periclase</i>	0.066	0.87	1.09	1.16	1.24	1.3	1.127	1.24	21700	2; 0-1800	
MgSiO ₃	<i>pyroxene</i>	0.752	1.03	1.15				0.973	3.36	23300	1; 0-500	
	<i>amphibole</i>	0.74	1.03	1.13	1.24			1.067	1.83	28100	1; 0-1100	
	<i>glass</i>	0.756	1.02	1.14				0.971	3.22	22600	1; 0-700	
MgSO ₄ ·H ₂ O	<i>kieserite</i>	1.00 at 9 °C										
MgSO ₄ ·7H ₂ O	<i>epsomite</i>	1.51 at 32 °C										
Mg ₂ Fe ₂ SiO ₄	<i>olivine</i>	0.79 at 36 °C										
Mg ₃ H ₂ Si ₄ O ₁₂	<i>talc</i>	0.87 at 59 °C										
MnCO ₃	<i>rhodochrosite</i>	0.203	0.7	1.08	1.46			0.283	15.32	$0.33 \times 10^{-4} T^4$	4; 0-500	
MnO ₂	<i>pyrolusite</i>	0.975	1	1.01				0.924	2.27	$0.14 \times 10^{-11} T^4$?; 0-500	
Mn ₂ O ₃ ·H ₂ O	<i>manganite</i>	0.74 at 36 °C										
MnS	<i>alabandite</i>	0.322	0.569									
MoS ₂	<i>molybdenite</i>	0.537	0.55	0.57				0.515	0.82	0	5; 0-456	
NaAlSi ₃ O ₈	<i>albite</i>	0.709	0.99	1.09	1.2			1.018	1.87	26800	1; 0-1100	
	<i>glass</i>	0.724	1	1.11	1.26			0.978	2.82	24700	1; 0-900	
NaCl	<i>halite</i>	0.466	0.855	0.92	0.98	1.1		0.773	3	0	2; 0-800	
	<i>liquid</i>					1.14		1.140	0	0	3; 800-950	
NaF	<i>villiaumite</i>	1.034	1.1	1.29				0.473	11.51	-18400	2; 0-700	
Na ₂ B ₄ O ₇ ·10H ₂ O	<i>borax</i>	0.161 at 35 °C										
Na ₃ AlF ₆	<i>cryolite</i>	0.909	1.18	1.39	1.78			0.770	9.49	8950	2; 0-1000	
NiS	<i>millerite</i>	0.506	0.57					0.426	2.95	0	3; 0-324	
PbCO ₄	<i>cerussite</i>	0.177	0.318									
PbS	<i>galena</i>	0.142	0.207	0.22	0.24			0.188	0.7	0	5; 0-600	
PbSO ₄	<i>anglesite</i>	0.364 at 60 °C										
Pd	<i>palladium</i>	0.232	0.25	0.26	0.29	0.318		0.212	0.72	0	2; 0-1549	
Pt	<i>platinum</i>	0.134	0.14	0.14	0.15	0.164		0.127	0.249	0	1; 0-1600	
S ₈	<i>sulfur rhombic</i>							0.482	8.35	0	3; 0-95.6	
	"							0.572	5.76	0	3; 95.6-119	
	<i>monoclinic</i>							0.656	6.58	0	?; 119-160	
	" <i>liquid</i>							1.220	0	0	?; 160-270	
	" <i>viscous</i>											
Sb ₂ S ₃	<i>stibnite</i>	0.342	0.38	0.41				0.298	1.63	0	?; 0-548	
SiO ₂	<i>α-quartz</i>	0.173	0.698	0.97	1.13			0.757	6.07	16800	1; 0-575	
	<i>β-quartz</i>					1.17	1.327	0.763	3.83	0	4; 575-1600	
	<i>α-cristobalite</i>	0.186	0.69	1.01				0.254	16	0	4; 0-250	
	<i>β-cristobalite</i>				1.07	1.17	1.21	1.191	0.32	6250	2; 250-1700	
	<i>glass</i>	0.184	0.7	0.95	1.06	1.21	1.34	0.892	3.11	2100	5; 0-1700	
SnO ₃	<i>cassiterite</i>	0.34	0.43	0.48	0.55			0.387	1.57	7000	4; 0-1100	

Compound	Mineral	c (kJ kg ⁻¹ K ⁻¹) at T in °C						A_1	$2A_2 \times 10^4$	A_3	Δc (%); T-range (°C)
		-200	0	200	400	800	1200				
SrCO ₃	<i>strontianite</i>	0.211	0.536								
TiO ₂	<i>rutile, brookite</i>		0.7	0.8	0.88		0.619	3.95	2200		3; 0-450
WO ₃	<i>tungstite</i>		0.33	0.36	0.38	0.44	0.49	0.289	1.4	0	5; 0-1300
ZnCO ₃	<i>smithsonite</i>	0.238	0.632								
ZnO	<i>zincite</i>		0.48	0.58	0.62	0.66	0.69	0.586	0.75	9400	2; 0-1300
ZnS	<i>α-wurtzite, β-sphalerite</i>	0.43	0.45	0.53	0.56	0.59		0.550	0.41	8400	6; 0-900
ZrSiO ₄	<i>zircon</i>	0.61 at 60 °C									

Table 8.6. (a) Variation of specific heat capacity c of oil with oil gravity (in units of specific gravity G_o and °API) and temperature T according to eq. (8.20); (b) Variation of thermal conductivity λ of atmospheric air and light oil with temperature T ; data: [1992Som].

Oil gravity		c (kJ kg ⁻¹ K ⁻¹) at T in C°				(a)	(b)	λ (W m ⁻¹ K ⁻¹)	
G_o (-)	°API	20	50	100	150			air	oil
0.966	15	1.73	1.83	1.98	2.18	20		0.026	0.139
0.934	20	1.75	1.86	2.04	2.21	50		0.027	0.131
0.904	25	1.78	1.89	2.07	2.25	100		0.030	0.128
0.876	30	1.81	1.92	2.10	2.28	150		0.033	0.126
						200		0.037	0.124

Calculating the thermal capacity (ρc) of the solid and fluid phases requires expressions for density. Based on previous work by different researchers Somerton [1992Som] suggests the following relation between density $\rho_x(T)$ in kg m⁻³, density $\rho_{x,20}$ at 20 °C, temperature T in °C, and volume expansion coefficient α_x in K⁻¹, where the subscript x stands for fluid water, oil or solid rock, respectively:

$$\rho_x(T) = \frac{\rho_{x,20}}{1 + (T - 20) \alpha_x}, \quad x = f, o, s. \quad (8.17)$$

The volumetric thermal expansion coefficient of rocks and minerals ranges roughly from 10 μ K – 70 μ K⁻¹ [1966Ski; 1992Som; 1995Fei], and the following expressions may be used to obtain values for the thermal expansion coefficients of fluid water and oil, respectively:

$$\left. \begin{array}{l} \alpha_f \\ \alpha_o \\ \alpha_s \end{array} \right\} = \left\{ \begin{array}{l} 2.115 \times 10^{-4} + 1.32 \times 10^{-6} T + 1.09 \times 10^{-8} T^2 \\ 4.42 \times 10^{-4} + 1.03 \times 10^{-5} \times \text{°API} \\ (2\dots5) \times 10^{-5} \end{array} \right. . \quad (8.18)$$

Here, °API characterizes oils of different density, which is expressed relative to water density by means of specific gravity G_o at 20 °C [1992Som]:

$$\text{°API} = (141.5/G_o) - 131.5. \quad (8.19)$$

Heat capacity of oil varies with temperature and oil specific gravity G_o [1992Som] (cf. Table 8.6):

$$c_o = (0.389 + 0.00081 T) / \sqrt{G_o}. \quad (8.20)$$

Table 8.6 lists values for specific heat capacity c and thermal conductivity λ of oil and atmospheric air.

The thermal capacity of fluid water can be calculated most easily and accurately using either public domain FORTRAN software or an Excel™ spreadsheet add-in based on the most recent industry standard for the thermodynamic and transport properties of water and steam [1998Wag]. Table 8.8 displays a list of selected values at atmospheric pressure and Fig. 8.9 shows the variation of fluid water thermal capacity with pressure and temperature.

Table 8.7 Specific heat capacity c , thermal conductivity λ , and thermal diffusivity κ of different potential pore space fluids at various temperatures T .

Substance	T (°C)	c (kJ kg ⁻¹ K ⁻¹)	λ (W m ⁻¹ K ⁻¹)	κ (10 ⁻⁶ m ² s ⁻¹)	ρc (kJ m ⁻³ K ⁻¹)
air (dry) [1992Som;1996Sch]	0	1.005	0.024	18.7	1.283
	20	1.005	0.026	21.2	1.226
	40	1.009	0.027	24.9	1.084
	100	1.013	0.030	33.8	0.979
methane gas (CH₄) at 0.1 MPa [2000Lid]	1.85	2.182	0.031	20.1	1.540
	26.85	2.238	0.034	23.7	1.436
	76.85	2.369	0.041	31.7	1.292
	126.85	2.537	0.049	40.1	1.221
	176.85	2.712	0.057	48.5	1.175
	226.85	2.892	0.067	60.2	1.113
fluid water (at 0.1 MPa) [1998Wag]	326.85	3.198	0.084	81.9	1.026
	0	4,219	0,561	0,133	4218,8
	10	4,195	0,580	0,138	4194,2
	30	4,180	0,616	0,148	4161,8
	50	4,180	0,644	0,156	4129,6
	70	4,188	0,663	0,162	4095,0
water steam (at 0.1 MPa) [1998Wag]	90	4,205	0,675	0,166	4059,2
	100	2,074	0,025	20,5	1,223
	120	2,019	0,026	23,5	1,126
	140	1,993	0,028	26,6	1,055
	160	1,980	0,030	29,8	0,998
	180	1,976	0,031	33,1	0,950
	200	1,976	0,033	36,6	0,909
	250	1,989	0,038	46,2	0,827
water ice (hexagonal I_h) [1982Mil; 2000Lid]	300	2,012	0,043	57,0	0,762
	350	2,040	0,049	68,9	0,710
	0	2.11	2.14	1.18	1934.2
	-10	2.03	2.32	1.24	1865.0
	-20	1.96	2.4	1.33	1803.8
crude oil [1996Sch]	-30	1.88	2.5	1.43	1732.6
	-40	1.80	2.6	1.54	1661.0
crude oil [1996Sch]	20	1.88–2.76	0.13–0.14	0.05–0.11	1300–2350

™ registered trademark of Microsoft

Table 8.8 Variation of fluid water thermal capacity ρc_p with pressure P and temperature T; data: [1998Wag].

T (K)	P (MPa)	ρc_p (kJ m ⁻³ K ⁻¹)	T (K)	P (MPa)	ρc_p (kJ m ⁻³ K ⁻¹)	T (K)	P (MPa)	ρc_p (kJ m ⁻³ K ⁻¹)
273	0.1	4218.777	273	30	4149.336	273	70	4097.503
283	0.1	4194.196	283	30	4151.243	283	70	4120.714
303	0.1	4161.846	303	30	4142.055	303	70	4129.628
323	0.1	4129.598	323	30	4118.927	323	70	4113.534
343	0.1	4095.033	343	30	4088.580	343	70	4086.521
363	0.1	4059.186	363	30	4054.410	363	70	4053.775
373	0.1	1.222	373	30	4036.378	373	70	4035.909
393	0.1	1.125	393	30	3999.021	393	70	3997.876
413	0.1	1.055	413	30	3960.717	413	70	3957.526
433	0.1	0.998	433	30	3922.571	433	70	3915.792
453	0.1	0.950	453	30	3885.909	453	70	3873.683
473	0.1	0.909	473	30	3852.277	473	70	3832.217
523	0.1	0.826	523	30	3794.174	523	70	3737.215
573	0.1	0.762	573	30	3814.319	573	70	3660.831
623	0.1	0.710	623	30	4117.114	623	70	3590.696
273	1	4216.230	273	40	4132.426	273	80	4090.498
283	1	4192.600	283	40	4141.040	283	80	4116.918
303	1	4161.093	303	40	4137.604	303	80	4128.528
323	1	4129.178	323	40	4116.722	323	80	4113.480
343	1	4094.765	343	40	4087.432	343	80	4086.966
363	1	4058.975	363	40	4053.708	363	80	4054.432
373	1	4040.831	373	40	4035.725	373	80	4036.587
393	1	4004.547	393	40	3998.144	393	80	3998.441
413	1	3969.170	413	40	3959.176	413	80	3957.767
433	1	3936.203	433	40	3919.856	433	80	3915.485
453	1	13.948	453	40	3881.387	453	80	3872.571
473	1	11.790	473	40	3845.103	473	80	3829.994
523	1	9.502	523	40	3773.778	523	80	3730.281
573	1	8.298	573	40	3754.486	573	80	3644.226
623	1	7.515	623	40	3858.081	623	80	3554.707
273	10	4192.400	273	50	4118.286	273	90	4085.546
283	10	4177.733	283	50	4132.647	283	90	4114.422
303	10	4154.127	303	50	4134.099	303	90	4128.108
323	10	4125.334	323	50	4115.117	323	90	4113.873
343	10	4092.353	343	50	4086.727	343	90	4087.748
363	10	4057.114	363	50	4053.388	363	90	4055.371
373	10	4038.994	373	50	4035.451	373	90	4037.537
393	10	4002.287	393	50	3997.692	393	90	3999.285
413	10	3965.802	413	50	3958.176	413	90	3958.334
433	10	3930.870	433	50	3917.894	433	90	3915.592
453	10	3899.260	453	50	3877.959	453	90	3872.015
473	10	3873.290	473	50	3839.561	473	90	3828.535
523	10	3857.910	523	50	3758.236	523	90	3725.089
573	10	4064.012	573	50	3712.957	573	90	3631.687

Pre-Print from:

Clauser, C., 2006. Geothermal Energy, In: K. Heinloth (ed), *Landolt-Börnstein, Group VIII: Advanced Materials and Technologies, Vol. 3: Energy Technologies, Subvol. C: Renewable Energies*, Springer Verlag, Heidelberg-Berlin, 493-604.

T (K)	P (MPa)	ρc_p (kJ m ⁻³ K ⁻¹)	T (K)	P (MPa)	ρc_p (kJ m ⁻³ K ⁻¹)	T (K)	P (MPa)	ρc_p (kJ m ⁻³ K ⁻¹)
623	10	178.759	623	50	3722.856	623	90	3529.047
273	20	4169.245	273	60	4106.709	273	100	4082.519
283	20	4163.417	283	60	4125.916	283	100	4113.132
303	20	4147.533	303	60	4131.463	303	100	4128.318
323	20	4121.780	323	60	4114.067	323	100	4114.686
343	20	4090.207	343	60	4086.433	343	100	4088.848
363	20	4055.531	363	60	4053.420	363	100	4056.580
373	20	4037.452	373	60	4035.522	373	100	4038.745
393	20	4000.378	393	60	3997.616	393	100	4000.389
413	20	3962.889	413	60	3957.646	413	100	3959.196
433	20	3926.182	433	60	3916.570	433	100	3916.069
453	20	3891.763	453	60	3875.440	453	100	3871.945
473	20	3861.490	473	60	3835.345	473	100	3827.731
523	20	3821.248	523	60	3746.332	523	100	3721.322
573	20	3906.276	573	60	3682.980	573	100	3622.249
623	20	4868.968	623	60	3642.885	623	100	3510.407

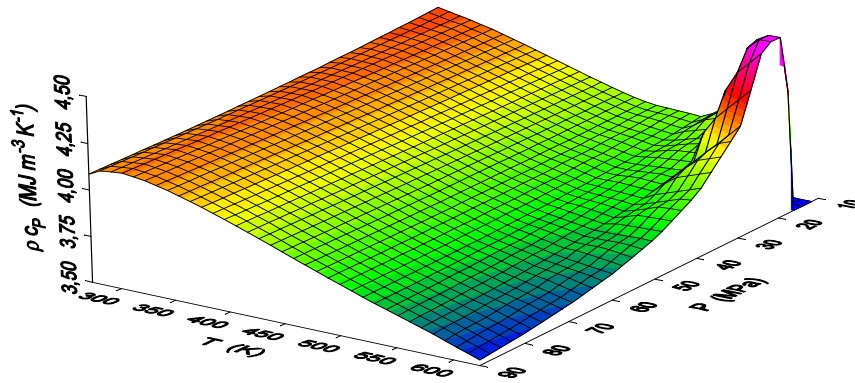


Fig. 8.9 Variation of fluid water thermal capacity ρc_p with pressure P and temperature T data: [1998Wag], see also Table 8.8.

Freezing and thawing of water in soils or rocks liberates or consumes heat, respectively. The latent heat L which corresponds to these additional heat sources and sinks can be elegantly combined with the specific heat capacities of water and ice, c_f and c_{ice} respectively, into an effective specific heat capacity c_{eff} of the pore space. This effective specific water heat capacity then accounts for the entire enthalpy change, including latent heat. In this approach, the latent heat effects are assumed to occur between the solidus and liquidus temperatures T_1 and T_2 , respectively. Weighting by the volume fractions of unfrozen fluid water ϕ_f and ice ϕ_{ice} , the enthalpy change of the water volume becomes $dH = (\phi_f c_f + \phi_{ice} c_{ice}) dT + L d\phi_f$, and the effective water heat capacity c_{eff} is:

$$c_{eff} = \frac{dH}{dT} = \phi_f c_f + \phi_{ice} c_{ice} + L \frac{d\phi_f}{dT}. \quad (8.21)$$

8.1.5 Heat Transport

Heat transport in the Earth is governed mainly by three mechanisms: radiation, advection, and transient diffusion or steady-state conduction. Generally, heat conduction or diffusion dominate within the lithosphere of the Earth. However, there are two exceptions:

- If rock hydraulic permeability is sufficiently large, convection driven heat advection can be equally or even more efficient, provided the associated driving forces are available for the corresponding forced or free convection systems. This is often the case in sedimentary basins [see e.g. 2002Cla for a summary of the literature]. However, fluid driven heat advection can be important also in crystalline rocks and on a crustal scale [e.g. 1983Eth; 1990Tor; 1992Cla; 1999Man; 2000Rat; 2001Cla];
- At ambient temperatures above 600 °C radiation of heat begins to contribute sizably to the overall heat transfer in most polycrystalline materials, but is really efficient only above 1200 °C. However, with single crystals and glasses (e.g. obsidian) radiation becomes important from temperatures as low as 200 °C – 400 °C. For the usual range of crustal temperatures and temperature gradients a linearization of the radiation law yields a "radiative thermal conductivity" which can be formally added to the coefficient of lattice or phonon thermal conductivity in Fourier's law of heat conduction (see below). Thermal conductivities determined at very high temperatures in the laboratory always include this radiative component. Radiative thermal conductivity will therefore not be treated separately here. Interested readers are referred to a review of heat radiation in the Earth [1988Cla].

8.1.5.1 Heat Conduction

Fourier's law of heat conduction defines specific heat flow q_i , i.e. heat flow normalized by area, as the product of the thermal conductivity tensor λ_{ij} and the temperature gradient vector $\partial T/\partial x_j$:

$$q_i = -\lambda_{ij} \frac{\partial T}{\partial x_j}. \quad (8.22)$$

Temperature measurements are usually performed along vertical profiles in boreholes. Therefore only the vertical component of the temperature gradient is generally known from measurements.

Thermal conductivity in some rocks is, to a good approximation, isotropic, particularly for volcanic and plutonic rocks. In these cases heat flow will be predominantly vertical, and it is sufficient to consider only the vertical component of (8.22). Thermal conductivity of many sedimentary and metamorphic rocks, in contrast, is strongly anisotropic, and lateral heat flow will be significant. Hence information on anisotropy is often required, demanding laboratory measurements in different directions. Anisotropy exists on several scales:

- On the microscopic scale many minerals are anisotropic (Table 8.9);
- On the laboratory scale the thermal conductivity of many rocks is also anisotropic. However, even if rocks are composed of anisotropic minerals, random orientation of the crystals within the rock may make the rock's thermal conductivity appear as isotropic on a macroscopic scale;
- On a still larger scale, if rocks are exposed to folding, orogenic or other tectonic processes, the thermal conductivity of the resulting rock formation may be either isotropic or anisotropic.

8.1.5.1.1 Measuring Techniques

Thermal conductivity can be measured in the laboratory on rock samples, i.e. cores or cuttings or in situ either in boreholes or with shallow penetration (3 m – 20 m) marine heat flow probes. There are numerous steady-state and transient techniques available for measuring thermal conductivity, the most prominent being the "divided bar", "needle probe", and "optical scanning". These methods are discussed

in detail in several textbook and review articles [1965Bec; 1969Tye; 1974Des; 1974Kap; 1981Roy; 1988Bec; 1988Dav; 1992Som; 1999Pop^a; 2001Bea]. Here they are therefore neither addressed again nor are the many details involved in performing the actual measurements discussed.

As is the case with most other petrophysical properties, in situ thermal conductivity may deviate significantly from laboratory values, even if the effects of temperature, pressure, and pore fluid are accounted for. The reason for this is a scale dependence in which different aspects are involved: in situ measurements, as a rule, represent an average over a much larger rock volume than laboratory measurements performed on small samples, and small-scale variations may be lost. Thus, the correct scale on which thermal conductivity should be determined depends on the specific question. This is analogous to the similar problem in hydrology of identifying a "representative elementary volume" for which reasonable averages for transport parameters (such as permeability and dispersion lengths) can be defined.

8.1.5.1.2 Indirect Methods

When no data are available or no direct measurements can be performed, thermal conductivity can be inferred indirectly, either from data on mineralogical composition and saturating fluids or from correlations with other physical properties. While some of these methods are based on well defined physical models, others are purely empirical.

Estimation From Mineralogical Composition and Saturating Fluids: Thermal conductivity of rocks may be estimated from their mineral content, as minerals, due to their well defined composition, exhibit a much smaller variance in thermal conductivity than rocks. Similarly, as the bulk thermal conductivity of porous rocks varies with different saturants, it may be of interest to know rock thermal conductivity for other saturants than those used in the laboratory measurement. Numerous models have been proposed for this, but all have their disadvantages: some overestimate while others underestimate systematically the true bulk thermal conductivity. Most of them are valid only for a specific range of volume ratios (or porosities), and yield unreasonable results outside this range.

The parallel and series model for thermal resistance of layered media are easy to understand, but have the disadvantage of being rather special cases, applicable mostly to bedded sediments. They correspond to the well known arithmetic and means harmonic λ_{ari} , and λ_{har} respectively, and define upper and lower limits for all other models. Thus they constrain the maximum variance of possible predictions. Quite successful in describing the data in many cases, but unfortunately without a clearly defined physical model, the geometric mean λ_{geo} falls in between these two extremes. So does the Hashin-Shtrikman mean λ_{HS} [1962Has], whose upper and lower bounds, $\lambda_{\text{HS}}^{\text{U}}$ and $\lambda_{\text{HS}}^{\text{L}}$, respectively, provide tighter constraints for the predictions of different models other than the arithmetic and harmonic means. Finally, effective medium theory [1935Bru; see also 1986Pal] provides a useful effective medium mean λ_{eff} for macroscopically homogeneous and isotropic rocks consisting of randomly distributed grains and pores. If λ_i is the thermal conductivity and n_i the volume fraction of the i -th phase relative to the total volume, where $1 = \sum n_i$, these five means are defined by:

$$\begin{aligned} \text{(a) } \lambda_{\text{max}} = \lambda_{\text{ari}} = \lambda_{\parallel} &= \sum_{i=1}^N n_i \lambda_i ; & \text{(b) } \lambda_{\text{min}} = \lambda_{\text{har}} = \lambda_{\perp} &= \left(\sum_{i=1}^N \frac{n_i}{\lambda_i} \right)^{-1} ; & \text{(c) } \lambda_{\text{mean}} &= \frac{1}{2} (\lambda_{\parallel} + \lambda_{\perp}) ; \\ \text{(d) } \lambda_{\text{geo}} &= \prod_{i=1}^N \lambda_i^{n_i} ; & \text{(e) } \lambda_{\text{eff}}^{-1} &= \sum_{i=1}^N \frac{3 n_i}{2 \lambda + \lambda_i} ; & \text{(f) } \lambda_{\text{HS}} &= \frac{1}{2} (\lambda_{\text{HS}}^{\text{U}} + \lambda_{\text{HS}}^{\text{L}}) ; \end{aligned} \quad (8.23)$$

where:

$$\begin{aligned} \lambda_{\text{HS}}^{\text{U}} &= \lambda_{\text{max}} + \frac{A_{\text{max}}}{1 - \alpha_{\text{max}} A_{\text{max}}} ; & A_{\text{max}} &= \sum_{i=1; \lambda_i \neq \lambda_{\text{max}}}^N \frac{n_i}{\alpha_{\text{max}} + 1/(\lambda_i - \lambda_{\text{max}})} ; & \lambda_{\text{max}} &= \max(\lambda_1, \dots, \lambda_N) ; & \alpha_{\text{max}} &= \frac{1}{3 \lambda_{\text{max}}} \\ \lambda_{\text{HS}}^{\text{L}} &= \lambda_{\text{min}} + \frac{A_{\text{min}}}{1 - \alpha_{\text{min}} A_{\text{min}}} ; & A_{\text{min}} &= \sum_{i=1; \lambda_i \neq \lambda_{\text{min}}}^N \frac{n_i}{\alpha_{\text{min}} + 1/(\lambda_i - \lambda_{\text{min}})} ; & \lambda_{\text{min}} &= \min(\lambda_1, \dots, \lambda_N) ; & \alpha_{\text{min}} &= \frac{1}{3 \lambda_{\text{min}}} . \end{aligned} \quad (8.24)$$

For a two-component system consisting of pore fluid and solid rock with thermal conductivities λ_f and λ_s , respectively, eq. 8.24 simplifies to [1962Has, 1971Hor]:

$$\lambda_{HS}^U = \lambda_s + \frac{\phi}{\frac{1}{\lambda_f - \lambda_s} + \frac{1-\phi}{3\lambda_s}}; \quad \lambda_{HS}^L = \lambda_f + \frac{1-\phi}{\frac{1}{\lambda_s - \lambda_f} + \frac{\phi}{3\lambda_f}}. \quad (8.25)$$

Generally, For a two-component system consisting of pore fluid and solid rock with thermal conductivities λ_f and λ_s , respectively, the implicit definition of λ_{eff} in (8.23e) can be resolved:

$$\lambda_{eff} = \frac{1}{4} \left\{ 3\phi(\lambda_f - \lambda_s) + 2\lambda_s - \lambda_f + \sqrt{9\phi^2\lambda_s^2 + 18\phi\lambda_s\lambda_f - 18\phi^2\lambda_s\lambda_f - 12\phi\lambda_s^2 + \lambda_f^2 - 6\phi\lambda_f^2 + 4\lambda_s\lambda_f + 9\phi^2\lambda_f^2 + 4\lambda_s^2} \right\}. \quad (8.26)$$

The different results obtained by the various methods in eq.(8.23) are illustrated in Fig. 8.10 for a two-phase rock with porosity ϕ consisting of solid rock and pore space. We see that in general:

$$\lambda_{\perp} = \lambda_{har} < \lambda_{HS}^L < \lambda_{mean} < \lambda_{geo} < \lambda_{HS} < \lambda_{eff} < \lambda_{HS}^U < \lambda_{ari} = \lambda_{\parallel}. \quad (8.27)$$

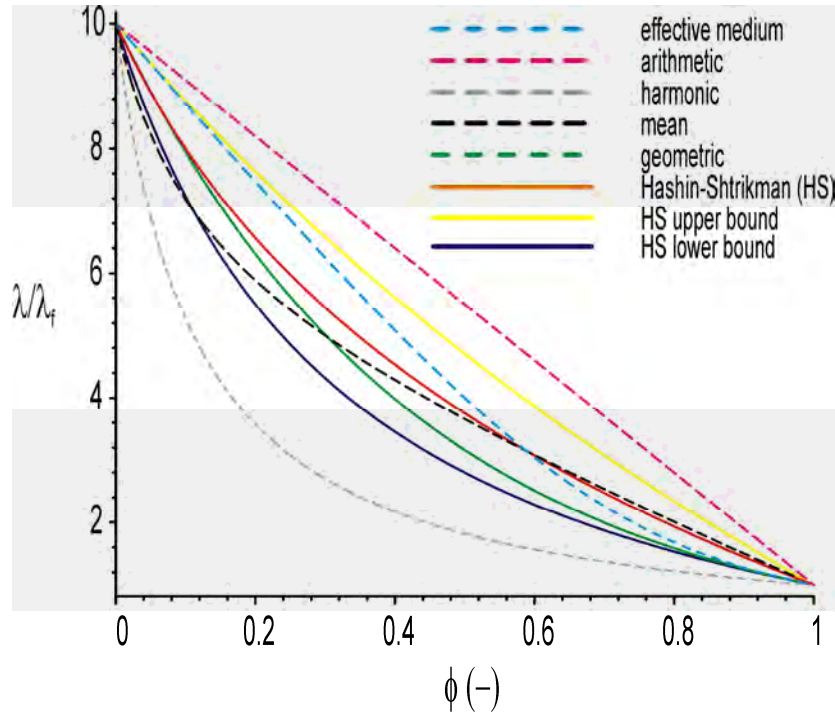


Fig. 8.10. Variation of thermal conductivity λ of a two-phase rock with porosity ϕ according to the five laws in (8.24) for solid and fluid thermal conductivities of $\lambda_s=6 \text{ W m}^{-1} \text{ K}^{-1}$ and $\lambda_f=0.6 \text{ W m}^{-1} \text{ K}^{-1}$, respectively (effective medium= λ_{eff} ; parallel= λ_{ari} ; series= λ_{har} ; mean= λ_{mean} ; geometric= λ_{geo} ; Hashin-Shtrikman= λ_{HS}).

While only these six models are presented and discussed here, various other mixing models are available which take into account additional factors, such as the shape of grains and voids [e.g. 1984Zim; 1989Zim]. Their specific advantages are discussed in considerable detail in the literature [e.g. 1988Bec; 1995Ber; 1996Sch]. Somerton [1992Som] discusses unconsolidated sands, effects of multi-fluid saturation, and provides many examples from hydrocarbon reservoir studies. Horai [1991Hor] tests the results of predictions from several different mixing-models on a remarkable data set in which porosity

virtually varies from 0 % – 100 %. As can be expected, most of the models tested were valid only for certain porosity ranges. Only two more recent two-phase models, assuming that pores can be treated as spheroidal inclusions in a homogeneous and isotropic material, are capable of explaining the complete data set. However, additional information on the spheroids' aspect ratio or orientation is required by these two models.

Given the typical ratios of conductivities we observe in nature, i.e. less than 10, most of the conductivity models work to within 10 % – 15 % accuracy. For larger ratios some break down more than others, and the geometric mean is one of them. The reason why it is still quite popular with many, even in extreme cases, is that it has often been found that errors introduced in the inverse problem (i.e. in predicting the matrix conductivity from measurements on samples saturated with one fluid) are automatically compensated for when using this incorrect matrix value in the subsequent forward calculation (i.e. in predicting the bulk conductivity of the matrix saturated with another fluid).

Correlations With Other Physical Properties: There are three different ways in which other physical properties, in particular those measured in well-logs, can be used to infer estimates for in situ thermal conductivity:

(1) One approach is to establish empirical relationships between thermal conductivity and other properties, such as porosity, bulk density, sonic (compressional elastic wave) velocity or travel times. This approach can be applied to data from both well logs and the laboratory. A useful summary of these different approaches is presented by Blackwell [1989Bla], who also illustrates their application to a specific case;

(2) In a second approach, Williams and Anderson [1990Wil] derive a phonon conduction model for thermal conductivity, which utilizes temperature, acoustic velocity, and bulk density measurements from well-logs. The method is claimed to be accurate to within 15 %, both in isotropic and anisotropic formations. Its application, however, is limited to unfractured rocks, since the effects of fracturing on compressional and shear velocities lead to inaccurate results. There are indications, however, that shear wave birefringence may pose a limit to the application of this method in foliated rocks as well [1993Prib].

(3) The third approach is basically an extension of the mixing-model approach to the borehole scale: The volume fractions V_i of the N different mineral (or fluid) phases are either taken directly from induced gamma ray spectroscopy logs [1990Wil] or determined from a joint analysis of a suitable number J of geophysical logs such as gamma ray (GR), sonic slowness (DT, the inverse of velocity), gamma density (DEN), and neutron porosity (NPHI) [1990Bri; 1991Dem; 2005Har]. If \mathbf{x} and \mathbf{b} are vectors consisting of the N volume fractions n_i and the J theoretical log responses R^j with respect to the N different rock constituents, then:

$$R^j = \sum_i^n n_i R_i^j, \text{ where: } \sum_i^n n_i = 1, \text{ and } \mathbf{x} = [n_1, \dots, n_N]^T, \mathbf{b} = [R^1, \dots, R^N]^T. \quad (8.28)$$

Arranging the specific responses of each log to the N rock constituents as rows of the matrix \mathbf{A} :

$$\mathbf{A} = \begin{bmatrix} R_1^1 & \dots & R_N^1 \\ \vdots & \ddots & \vdots \\ R_1^J & \dots & R_N^J \end{bmatrix}, \quad (8.29)$$

we can write the direct and inverse problems as:

$$\mathbf{A} \mathbf{x} = \mathbf{b} \text{ and } \mathbf{x} = \mathbf{A}^{-1} \mathbf{b}, \quad (8.30)$$

respectively. Thus in the direct problem, the log response vector \mathbf{b} is computed from the volume fraction vector \mathbf{x} and the specific log response matrix \mathbf{A} . Conversely in the inverse problem, the volume fractions \mathbf{x} are computed from the log responses \mathbf{b} and the inverse of the specific log response matrix, \mathbf{A}^{-1} . Thus,

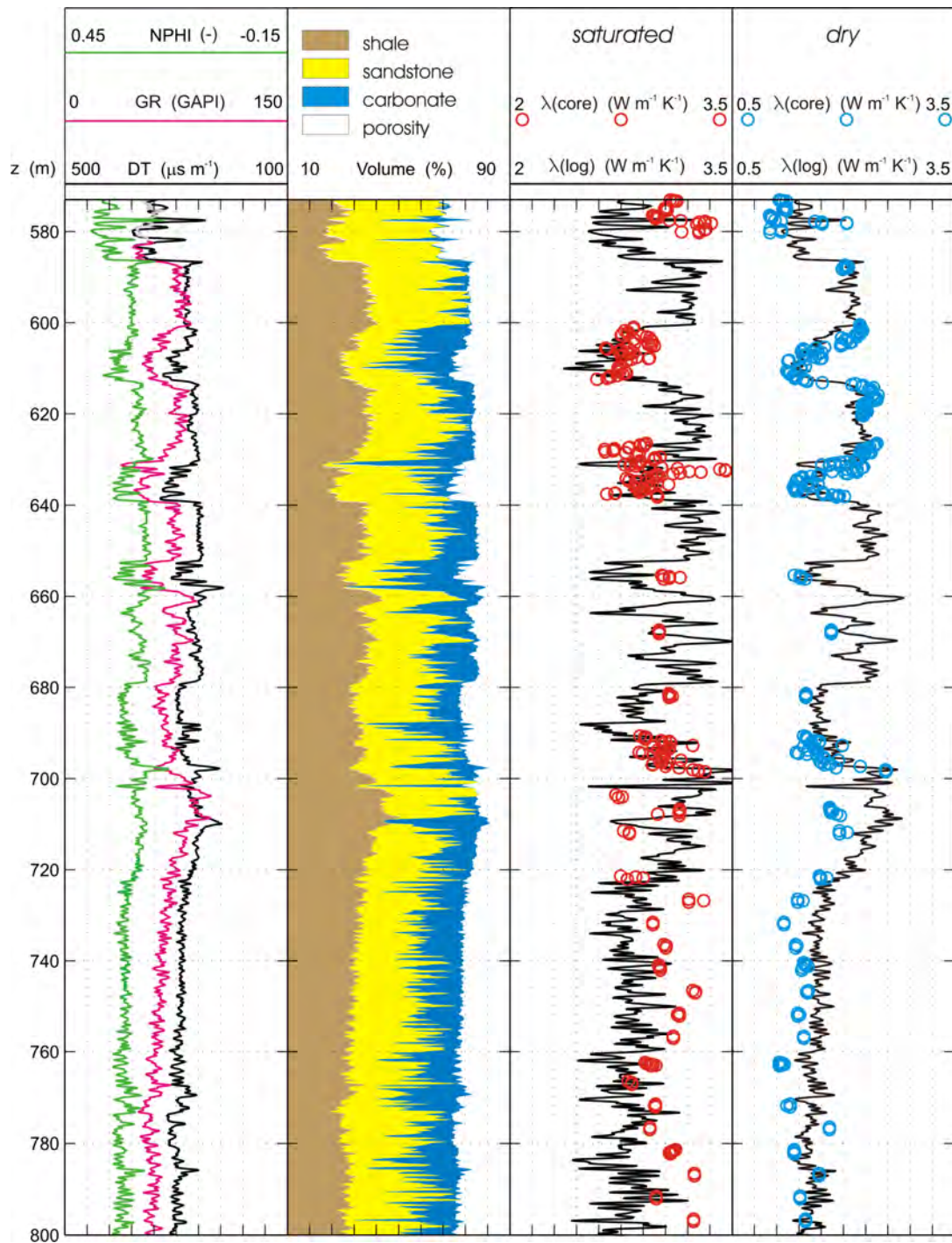


Fig. 8.11 Sand-Shale-Carbonate model for a borehole. Panels (from left to right): (1) Input data: NPHI - neutron porosity; GR - natural gamma radiation (GAPI: gamma ray API units); DT - acoustic slowness. (2) Composition computed from input logs. (3) Log of saturated thermal conductivity $\lambda(\log)$ computed from composition according to the geometric mean, eq. (8.23d). (4) Log of dry thermal conductivity $\lambda(\log)$ computed from composition according to the geometric mean, eq. (8.23d). In panels 3 and 4, thermal conductivity measured on saturated and dry core is shown as red and cyan circles, respectively (after [2005Har]).

solving the inverse requires at least as many logs as solid rock constituents. Porosity is not counted here, because it follows as the difference of one and the sum of the solid rock volume fractions. However, the inverse problem can also be solved in a least-squares sense, if more logs are available making the problem over-determined. Once the volume fractions are known and assigned appropriate thermal conductivities, an appropriate mixing model can be applied to compute rock thermal conductivity. Generally the geometric mean (eq. 8.23d) has turned out quite useful, but other mixing models may be appropriate in specific cases (cf. discussion above).

Assigning representative thermal conductivities to the solid rock constituents is not trivial. For reasons discussed in this text previously, tabulated values of rock thermal conductivity should be used only if they characterize specimens from the logged formations. In all other cases, these formations or their outcrops need to be sampled and these specimens tested in the laboratory. If measurements are performed at ambient conditions the values need to be corrected for the effect of temperature, and in some cases for pressure as well. In general the effect of temperature is more pronounced than that of pressure. However, for greater depth and little or less consolidated rocks it needs to be accounted for, too (for a more detailed discussion, see section 8.1.5.2.1 below).

If commercial log interpretation software is used to perform the inversion, the theoretical log responses R^j with respect to the different rock constituents are usually supplied. Alternatively, values for the log responses R^j can be obtained from the literature [e.g. 1986Cra].

8.1.5.1.3 Thermal Conductivity of Minerals

Data on thermal conductivity of minerals is not as abundant as for rocks. However, thermal conductivity of minerals is much better constrained than that of rocks, as there is a well defined specific crystal structure and chemical formula for each mineral. However there are two specific principal difficulties associated with the measurement of thermal conductivity on mineral samples: purity and sample size. Lattice imperfections in crystals significantly reduce the thermal conductivity of many minerals. Correction of alien mineral phases in samples is possible [1971Hor], but requires further microscopic and X-ray examination of the samples.

Measurements on single crystals or mono-mineral, polycrystalline aggregates require a minimum sample size. But large single crystals which can be machined to the desired size are relatively rare. When single-mineral aggregates are used instead, uncertainty is introduced by porosity. The same is true for needle-probe measurements on finely ground samples of minerals saturated with water [1969Hor; 1971Hor]. This way sample size poses no problem, but all information on anisotropy is lost. Moreover, the interpretation of measurements of thermal conductivity on fragments is not without ambiguity. In their comparison obtained for splits from Horai's and Simmons' [1969Hor] original mineral samples using the transient needle-probe method [1969Hor] and a steady-state divided-bar "cell" method Sass et al. [1971Sas] find that the results of measurements on fragments depend on both the technique and the model used for inferring the thermal conductivity of the solid constituents of the mixture (see e.g. eqs. 8.24a-e).

This review collates a summary of data from original contributions and previous compilations (Table 8.9) comprising data measured on both single crystals as well as natural single-mineral, polycrystalline aggregates, and artificial mono-mineral aggregates produced from a mixture of powdered mineral specimens and distilled water. Data are compiled from four main sources: (1) Diment and Pratt [1988Dim] who report their own measurements as well as those performed or reported previously [1940Bir^a; 1940Bir^b; 1942Bir; 1947Cos; 1954Bir; 1959Rat; 1965Sas; 1966Cla; 1988Rob]; (2) Dreyer [1974Dre], a compilation of data measured by a variety of researchers; (3) Horai [1971Hor, including 1969Hor; 1972Hor]; and finally (4) Popov [1999Pop^a, including 1987Pop].

Table 8.9 Thermal conductivity λ ($\text{W m}^{-1} \text{K}^{-1}$) of different rock-forming minerals. Minerals marked "iso" are isotropic; T: temperature ($^{\circ}\text{C}$: unspecified room temperature); (n): the number of data for mean and standard deviation (always calculated, even if n is statistically insignificant); "state" describes the directional dependence of λ : "x": measurements of unknown orientation on single crystals, "a": on single-mineral aggregates; anisotropy is specified either by (1) the mineral's optical a-, b- or c-axes (100, 010, 001); (2) the diagonal elements of the thermal conductivity tensor (λ_{11} , λ_{22} , λ_{33}), where λ_{33} is parallel to the crystal's optical c-axis, and the optical a-axis lies within the plane defined by λ_{11} and λ_{22} ; (3) the thermal conductivity components normal (\perp) or parallel (\parallel) to the direction of maximum thermal conductivity; Mean values λ_m are calculated as $\lambda_m = (\lambda_{100} + \lambda_{010} + \lambda_{001})/3$ [1987Pop]. Chemical formulas are given as by Ralph [2003Ral].

Mineral	T, state, λ , (n)	Source
MISCELLANEOUS		
diamond, C, (iso)	? $^{\circ}\text{C}$, λ_{11} : 545.3 (?)	[1974Dre]
diamond, C (Type I/IIa/IIb)	(T in K), $T/\lambda_{\text{type I}}/\lambda_{\text{type IIa}}/\lambda_{\text{type IIb}}$: 10/140/317/203, 50/3530/9210/5910, 100/3000/10000/5420, 150/1950/6020/3250, 200/1410/4030/2260, 250/1100/2970/1700, 300/895/2300/1350, 350/755/1850/1110, 400/650/1540/932	[2000Lid]
natural graphite, C	? $^{\circ}\text{C}$, a: 189.7 , λ_{11} : 355.0 , λ_{33} : 89.4 (?)	[1974Dre]
pyrolytic graphite, C (highly purified)	? $^{\circ}\text{C}$, a: 155.0 (?) (T in K), T/λ_{\parallel} : 10/81.1, 50/2310, 100/4970, 150/4510, 200/3230, 250/2440, 300/1950, 350/1620, 400/1390, 500/1080, 600/892, 800/676, 1000/534, 1200/448, 1400/384, 1600/333, 1800/293, 2000/262 (T in K), T/λ_{\perp} : 10/1.16, 50/15.2, 100/16.8, 150/12.5, 200/9.23, 250/7.11, 300/5.70, 350/4.77, 400/4.09, 500/3.22, 600/2.68, 800/2.01, 1000/1.60, 1200/1.34, 1400/1.16, 1600/1.00, 1800/0.895, 2000/0.807	[1990Gri] [2000Lid]
water ice, H_2O	0 $^{\circ}\text{C}$, λ_{11} : 1.9 (?), λ_{33} : 2.3 (?), a: 2.0 (?); -125 $^{\circ}\text{C}$, a: 4.0 (?) (T in $^{\circ}\text{C}$), T/λ_m : 0/2.14, -10/2.32, -20/2.4, -30/2.5, -40/2.6, -60/3.0, -80/3.3, -100/3.7, -120/4.2, -140/4.9, -160/5.7, -180/7.0, -200/8.7, -220/11.8, -240/20, -250/32	[1974Dre] [1982Mil] 2000Lid]
ORTHOSILICATES		
olivine group		
olivine (Fa_{xy} : xy % fayalite)	? $^{\circ}\text{C}$, a: Fa_0 – Fa_{10} /5.10, Fa_{10} – Fa_{30} /4.27, Fa_{30} – Fa_{60} /3.60, Fa_{60} – Fa_{90} /3.18, Fa_{70} – Fa_{90} /3.05, Fa_{90} – Fa_{100} /3.14	[1972Hor]
fayalite, Fe_2SiO_4	30 $^{\circ}\text{C}$, a: 3.85 \pm 0.08 (4) (dunite, mostly Fa) ? $^{\circ}\text{C}$, a: 3.16 ($\text{Fo}_4\text{Fa}_{96}$) (1) ? $^{\circ}\text{C}$, λ_m : 3.30 (1)	[1988Dim] [1971Hor] [1987Pop] 1999Pop ^a
forsterite, Mg_2SiO_4	30 $^{\circ}\text{C}$, a: 4.68 \pm 0.38 (3) (dunite, 97 % $\text{Fo}_{92}\text{Fa}_8$) ? $^{\circ}\text{C}$, a: 5.03 \pm 0.2 (5) ($\text{Fo}_{98}\text{Fa}_2$ – $\text{Fo}_{91}\text{Fa}_9$)	[1940Bir ^a] [1971Hor]
monticellite, CaMgSiO_4	35 $^{\circ}\text{C}$, a: 3.25 \pm 0.04 (3)	[1988Dim]
garnet group		
almandine, $\text{Fe}_3\text{Al}_2[\text{SiO}_4]_3$ iso (cubic)	(Mg, Fe, Mn, Ca) ₃ (Al, Fe) ₂ [SiO ₄] ₃ ? $^{\circ}\text{C}$, a: 3.56 (1) ? $^{\circ}\text{C}$, a: 3.31 (1) ? $^{\circ}\text{C}$, λ_{11} : 3.6 (?) 27 $^{\circ}\text{C}$ (100): 3.53 \pm 0.14 (3), (010): 3.53 \pm 0.14 (3), (001): 3.53 \pm 0.14 (3)	[1988Dim] [1971Hor] [1974Dre] [1987Pop] 1999Pop ^a
grossular, $\text{Ca}_3\text{Al}_2[\text{SiO}_4]_3$, iso (cubic)	? $^{\circ}\text{C}$, a: 5.32 (1) ? $^{\circ}\text{C}$, a: 5.48 \pm 0.24 (3) 27 $^{\circ}\text{C}$ (100): 5.90 (1), (010): 5.90 (1), (001): 5.90 (1)	[1988Dim] [1971Hor] [1987Pop]
hibschite (hydrogrossular), $\text{Ca}_3\text{Al}_2[\text{SiO}_4]_{3-x}[\text{OH}]_{4x}$? $^{\circ}\text{C}$, a: 6.53 (1)	1999Pop ^a
spessartine, $\text{Mn}_3\text{Al}_2[\text{SiO}_4]_3$ (cubic)	35 $^{\circ}\text{C}$, a: 3.06 \pm 0.10 (3) 27 $^{\circ}\text{C}$ (100): 3.66 (1), (010): 3.66 (1), (001): 3.66 (1)	[1988Dim] [1987Pop] 1999Pop ^a
zircon group		
zircon, ZrSiO_4	? $^{\circ}\text{C}$, λ_{11} : 3.9 (?), λ_{33} : 4.8 (?) ? $^{\circ}\text{C}$, a: 5.54	[1974Dre] [1971Hor]
titanite group (sphene)		

Pre-Print from:

Clauer, C., 2006. Geothermal Energy, In: K. Heinloth (ed), *Landolt-Börnstein, Group VIII: Advanced Materials and Technologies, Vol. 3: Energy Technologies, Subvol. C: Renewable Energies*, Springer Verlag, Heidelberg-Berlin, 493-604.

Mineral	<i>T</i> , state, λ , (n)	Source
titanite, CaTiSiO ₅	? °C, a: 2.34 (1)	[1971Hor]
Al₂SiO₅ group (disthene series)		
andalusite, Al ₂ SiO ₅	35 °C, a: 6.56 ± 0.45 (8) (<5 % quartz impurity) ? °C, a: 7.58 (1)	[1988Dim] [1971Hor]
kyanite, Al ₂ SiO ₅	35 °C, a: 7.15 ± 0.17 (4), a: 12.45 ± 0.71 (3) (< 5 % quartz impurity) ? °C, a: 14.16 (1)	[1988Dim] [1971Hor]
sillimanite, Al ₂ SiO ₅	35 °C, a: 10.73 ± 0.64 (3) ? °C, a: 9.10 (1)	[1988Dim] [1971Hor]
topaz, Al ₂ SiO ₄ (F,OH) ₂	? °C, λ_m : 20.9 (1)	[1987Pop, 1999Pop ^a]
SOROSILICATES		
allanite, (Y,Ce,Ca) ₂ (Al,Fe ³⁺) ₃ [SiO ₄] ₃ [OH]	? °C, λ_m : 1.44 (1)	[1987Pop, 1999Pop ^a]
epidote, Ca ₂ (Al,Fe) ₃ [SiO ₄] ₃ [OH]	32 °C, λ : 3.10 (1); 32 °C, \perp : 2.93 (1); 31 °C, a: 2.51 ± 0.03 (2) ? °C, a: 2.83 ± 0.3 (2)	[1988Dim] [1971Hor]
ilvaite, CaFe ₂ ²⁺ Fe ³⁺ [SiO ₄] ₂ [OH]	? °C, λ_m : 1.84 (1)	[1987Pop, 1999Pop ^a]
vesuvianite, (tetragonal) Ca ₁₀ Mg ₂ Al ₄ [SiO ₄] ₅ [Si ₂ O ₇] ₂ [OH] ₄	? °C, x: 2.31 ± 0.23 (2), a: 2.86 (1); 27 °C (100): 2.17 ± 0.22 (3), (010): 2.17 ± 0.22 (3), (001): 2.34 ± 0.18 (3)	[1987Pop, 1999Pop ^a]
CYCLOSILICATES		
beryl, Be ₃ Al ₂ Si ₆ O ₁₈ (hexagonal)	? °C, x: 3.93 ± 0.08 (2); λ_m : 4.16 (1), a: 3.87 (1); 27 °C (100): 3.81 ± 0.09 (2), (010): 3.81 ± 0.09 (2), (001): 4.31 ± 0.19 (2)	[1987Pop, 1999Pop ^a]
cordierite, (Mg,Fe) ₂ Al ₄ Si ₅ O ₁₈	35 °C, λ : 3.33 ± 0.04 (3); ? °C, \perp : 3.06 ± 0.03 (2) ? °C, λ_m : 2.41 (1)	[1988Dim] [1987Pop, 1999Pop ^a]
eudialyte, Na ₄ (Ca,Ce) ₂ (Fe ²⁺ ,Mn,Y) ZrSi ₆ O ₂₂ (OH,Cl) ₂	? °C, a: 1.14 (1)	[1987Pop, 1999Pop ^a]
schorl (tourmaline) (trigonal), NaFe ₃ ²⁺ Al ₆ [BO ₃] ₃ Si ₆ O ₁₈ [OH] ₄	? °C, x: 3.97 ± 0.47 (2); λ_m : 3.64 (1); 27 °C (100): 4.36 ± 0.40 (2), (010): 4.36 ± 0.40 (2), (001): 3.19 ± 0.59 (2)	[1987Pop, 1999Pop ^a]
CHAIN SILICATES		
pyroxene group		
augite, (Ca,Na)(Mg,Fe,Al,Ti)(Al,Si) ₂ O ₆	(Na,Ca)(Mg,Fe,Al)(Al,Si) ₂ O ₆ 35 °C, a: 4.20 ± 0.05 (3)	[1988Dim]
diallage (augite)	? °C, λ_m : 3.17 (1)	[1987Pop, 1999Pop ^a]
diopside, CaMgSi ₂ O ₆	35 °C, a: 4.40 ± 0.42 (2) ? °C, a: 4.66 ± 0.31 (4) ? °C, λ_m : 4.05 ± 0.03 (3)	[1988Dim] [1971Hor] [1987Pop, 1999Pop ^a]
enstatite, Mg ₂ Si ₂ O ₆	? °C, a: 4.47 ± 0.35 (4)	[1971Hor]
jadeite, Na(Al,Fe)Si ₂ O ₆	34 °C, a: 5.59 ± 1.22 (2) ? °C, a: 5.64 ± 1.44 (2)	[1988Dim] [1971Hor]
pyroxene (Fs _{xy} : xy % ferrosilite, Fs = Fe ₂ Si ₂ O ₆)	? °C, a: Fs ₀ -Fs ₁₀ /4.73, Fs ₁₀ -Fs ₃₀ /4.93, Fs ₃₀ -Fs ₅₀ /(3.43), Fs ₅₀ -Fs ₇₀ /(3.18), Fs ₇₀ -Fs ₉₀ /(3.14), Fs ₉₀ -Fs ₁₀₀ /(3.22)	[1972Hor]
spodumene, LiAlSi ₂ O ₆	? °C, λ_m : 5.28 ± 0.77 (2)	[1987Pop, 1999Pop ^a]
amphibole group		
actinolite, Ca ₂ (Mg,Fe ²⁺) ₅ [Si ₈ O ₂₂][OH] ₂	NaCa ₂ (Mg,Fe,Al)(Al,Si) ₈ O ₂₂ (OH) ₂ 31 °C, λ : 5.34 ± 0.12 (2); ? °C, \perp : 2.96 (1)	[1988Dim]
nephrite (actinolite)	? °C, a: 3.64 ± 0.50 (2)	[1987Pop, 1999Pop ^a]
hornblende, Ca ₂ (Mg,Fe ²⁺) ₄ (Al,Fe ³⁺) [Si ₇ Al]O ₂₂ [OH] ₂	? °C, λ : 2.75 ± 0.18 (2); 35 °C, \perp : 1.88 (1) 20 °C, a: 2.91 ± 0.09 (2) ? °C, a: 2.81 ± 0.27 (2) ? °C, λ_{11} : 3.0 , λ_{33} : 2.4 (?) ? °C, λ_m : 1.82 ± 0.01 (2)	[1988Dim] [1966Cla] [1971Hor] [1974Dre] [1987Pop, 1999Pop ^a]
pargasite, NaCa ₂ (Mg,Fe ²⁺) ₄ Al[Si ₆ Al ₂]O ₂₂ [OH] ₂	? °C, λ_m : 2.65 (1)	[1987Pop, 1999Pop ^a]
rhodonite, (Mn ²⁺ ,Fe ²⁺ ,Mg,Ca)SiO ₃	? °C, λ_m : 2.35 (1)	[1987Pop, 1999Pop ^a]
tremolite, [Ca ₂ Mg ₅][Si ₈ O ₂₂][OH] ₂	31 °C, λ : 5.79 ± 0.28 (2); 32 °C, \perp : 4.54 ± 0.14 (2)	[1988Dim]

Mineral	<i>T</i> , state, λ , (n)	Source
wollastonite, CaSiO ₃	? °C, a: 6.36 (1)	[1987Pop, 1999Pop ⁵]
PHYLLOSILICATES		
mica group		
biotite (monoclinic), K(Mg,Fe) ₃ (Al,Fe ³⁺)Si ₃ O ₁₀ (OH,F) ₂	33 °C, μ : 3.14 ; 32 °C, \perp : 0.52 ± 0.01 (2) ? °C, a: 2.02 ± 0.32 (2) ? °C, λ_m : 2.29 ± 0.26 (2), x: 2.10 (1); 27 °C (100): 2.61 (1), (010): 2.61 (1), (001): 1.30 (1)	[1988Dim] [1971Hor] [1987Pop, 1999Pop ⁵]
clinochlore, (Mg,Fe ²⁺) ₅ Al[Si ₃ Al]O ₁₀ [OH] ₈	29 °C, μ : 10.34 ± 0.57 (2), \perp : 1.97 ± 0.06 (2)	[1988Dim]
chlorite (monoclinic), (Mg,Fe) ₃ [(Si,Al) ₄ O ₁₀ [OH] ₂] · (Mg,Fe,Al) ₃ [OH] ₆	30 °C, a: 3.06 ± 1.32 (5) ? °C, a: 5.2 (?), λ_{11} : 5.5 (?), λ_{33} : 5.1 (?) ? °C, a: 5.15 ± 0.94 (3) ? °C, λ_m : 3.77 (1), x: 7.87 (1); 27 °C (100): 11.1 (1), (010): 11.1 (1), (001): 1.38 (1)	[1988Dim] [1974Dre] [1971Hor] [1987Pop, 1999Pop ⁵]
chrysotile, Mg ₃ Si ₂ O ₅ [OH] ₄	? °C, a: 1.95 (1)	[1987Pop, 1999Pop ⁵]
muscovite (monoclinic), KAl ₂ [Si ₃ Al]O ₁₀ [OH] ₂	30 °C, μ : 3.89 ± 0.0 (2); 32-45 °C, \perp : 0.62 ± 0.13 (4) ? °C, a: 2.28 ± 0.07 (3) ? °C, λ_m : 2.34 (1), x: 2.88 (1); ; 27 °C (100): 3.80 (1), (010): 3.80 (1), (001): 1.03 (1)	[1988Dim] [1971Hor] [1987Pop, 1999Pop ⁵]
phlogopite, KMg ₃ Si ₃ AlO ₁₀ (F,OH) ₂	30 °C, μ : 4.01 (3), \perp : 0.48 ± 0.02 (4) ? °C, λ_m : 1.57 (1)	[1988Dim] [1987Pop, 1999Pop ⁵]
prochlorite, (Mg,Fe ²⁺ ,Al) ₆ Al[Si _{2.5} Al _{1.5}]O ₁₀ [OH] ₈	29-34 °C, a: 2.61 ± 0.40 (10)	[1988Dim]
pyrophyllite, Al ₂ Si ₄ O ₁₀ [OH] ₂	30 °C, μ : 6.17 ± 0.73 (5), \perp : 1.12 ± 0.42 (2) 30-35 °C, a: 4.47 ± 0.47 (7) (<i>T</i> in °C), <i>T</i> / λ_{μ} : 0/4.98, 100/4.17, 200/3.59, 300/3.14, 400/2.81	[1988Dim] [1966Cla]
serpentine (antigorite), (Mg,Fe) ₃ [Si ₂ O ₅][OH] ₄	? °C, μ : 2.76 ± 0.03 (4); 32 °C, \perp : 2.41 ± 0.15 (2) 30-34 °C, a: 2.61 ± 0.40 (10) ? °C, a: 2.1 (?), λ_{11} : 2.6 (?), λ_{33} : 2.3 (?) ? °C, a: 3.53 ± 1.57 (3) ? °C, a: 2.80 ± 0.20 (4) ? °C, λ_m : 2.78 (1)	[1988Dim] [1988Dim] [1974Dre] [1971Hor] [1987Pop, 1999Pop ⁵]
talca, Mg ₃ Si ₄ O ₁₀ [OH] ₂	29-34 °C, μ : 10.69 ± 1.50 (5); 30 °C, \perp : 1.76 ± 0.0 (2) 30 °C, a: 2.97 (1) ? °C, a: 6.1 ± 1.27 (2) ? °C, λ_{11} : 3.1 (?), λ_{33} : 2.9 (?)	[1988Dim] [1954Bir] [1971Hor] [1974Dre]
Tectosilicates		
feldspar group		
albite, NaAlSi ₃ O ₈	25 °C, a: 2.34 (1) ? °C, a: 2.14 ± 0.22 (4) ? °C, λ_{11} : 2.1 (?), λ_{33} : 2.9 (?) ? °C, λ_m : 2.04 ± 0.25 (6)	[1965Sas] [1971Hor] [1974Dre] [1987Pop, 1999Pop ⁵]
anorthite, CaAl ₂ Si ₂ O ₈	25 °C, a: 2.72 (1) ? °C, a: 1.68 (1)	[1965Sas] [1971Hor]
cancrinite, Na ₆ Ca ₂ Al ₆ Si ₆ O ₂₄ [CO ₃] ₂	? °C, λ_m : 1.36 (1)	[1987Pop, 1999Pop ⁵]
labradorite, (Ca,Na)(Si,Al) ₄ O ₈	? °C, a: 1.71 (1)	[1987Pop, 1999Pop ⁵]
microcline, KAlSi ₃ O ₈	? °C, (001): 2.04 (1) ? °C, a: 2.49 ± 0.10 (3) ? °C, a: 2.41 ± 0.11 (3)	[1965Sas] [1971Hor] [1987Pop, 1999Pop ⁵]
natrolite, Na ₂ Al ₂ Si ₃ O ₁₀ · 2H ₂ O	? °C, λ_m : 1.73 (1)	[1987Pop, 1999Pop ⁵]
nepheline, (Na,K)AlSiO ₄	35 °C, a: 1.39 ± 0.15 (3) ? °C, a: 1.36 (1)	[1988Dim] [1987Pop, 1999Pop ⁵]
oligoclase, (Na,Ca)(Si,Al) ₄ O ₈	? °C, λ_m : 2.11 (1)	[1987Pop, 1999Pop ⁵]
orthoclase, KAlSi ₃ O ₈	30 °C, (100): 2.34 ± 0.11 (2), (010): 2.68 (1), (001): 2.30 ± 0.3 (2) ? °C, a: 2.31 (1)	[1965Sas] [1971Hor]

Pre-Print from:

Clauser, C., 2006. Geothermal Energy, In: K. Heinloth (ed), *Landolt-Börnstein, Group VIII: Advanced Materials and Technologies, Vol. 3: Energy Technologies, Subvol. C: Renewable Energies*, Springer Verlag, Heidelberg-Berlin, 493-604.

Mineral	T , state, λ , (n)	Source
	? °C, \perp : 2.9 , \parallel_1 : 4.2 , \parallel_2 : 4.6 , λ_{11} : 2.94 , λ_{22} : 4.2 , λ_{33} : 4.63 (1)	[1974Dre]
	? °C, a: 2.15 ± 0.05 (2)	[1987Pop, 1999Pop ^a]
plagioclase (An _{xy} : xy % anorthite)	? °C, a: An ₀ -An ₆ / 2.34 , An ₆ -An ₁₅ / 1.92 , An ₁₅ -An ₃₀ / 1.63 , An ₃₀ -An ₅₀ / 1.46 , An ₅₀ -An ₇₀ / 1.46 , An ₇₀ -An ₈₅ / 1.59 , An ₈₅ -An ₁₀₀ / 1.72	[1972Hor]
sanidine, (K,Na)(Si,Al) ₄ O ₈	? °C, λ_m : 1.73 (1)	[1987Pop, 1999Pop ^a]
scapolite (tetragonal)	35 °C, x ₁ : 1.76 ± 0.00 (3), x ₂ : 1.95 ± 0.04 (2)	[1988Dim]
(Na,Ca) ₄ (Si,Al) ₁₂ O ₂₄ (Cl,CO ₃ ,SO ₄)	? °C, x: 1.42 (1); 27 °C (100): 1.34 (1), (010): 1.34 (1), (001): 1.59 (1)	[1987Pop, 1999Pop ^a]
sodalite, Na ₄ Al ₃ Si ₃ O ₁₂ Cl	35 °C, a: 3.16 ± 0.12 (3)	[1988Dim]
silica group	SiO ₂	
α quartz, SiO ₂ (trigonal)	30 °C, \parallel : 10.17 (1)	[1940Bir ^a]
	30 °C, \perp : 6.15 (1)	[1959Rat]
	? °C, a: 8.1 , λ_{11} : 6.5 (?), λ_{33} : 11.3 (?)	[1974Dre]
	? °C, a: 7.69 (1)	[1971Hor]
	? °C, x: 7.60 ± 0.0 (4); 27 °C (100): 6.05 ± 0.0 (4), (010): 6.05 ± 0.0 (4), (001): 10.7 ± 0.0 (4)	[1987Pop, 1999Pop ^a]
α quartz \perp	(T in °C), T/λ , x: 0/ 6.82 , 50/ 5.65 , 100/ 4.94 , 150/ 4.44 , 200/ 4.06 , 250/ 3.73 , 300/ 3.52 , 350/ 3.31	[1940Bir ^a]
α quartz \parallel	(T in °C), T/λ , x: 0/ 11.43 , 50/ 9.38 , 100/ 7.95 , 150/ 7.03 , 200/ 6.32 , 250/ 5.69 , 300/ 5.15 , 350/ 4.73	[1940Bir ^a]
chalcedony, SiO ₂	? °C, a: 3.17 (1)	[1987Pop, 1999Pop ^a]
pyrex 774 glass	(T in °C), amorphous: T/λ : 0/ 1.21 , 50/ 1.26 , 100/ 1.32 , 150/ 1.38 , 200/ 1.44 , 250/ 1.49 , 300/ 1.55 , 350/ 1.61 , 400/ 1.66 , 450/ 1.72 , 500/ 1.83 (T in °C)	[1940Bir ^a]
silica glass	30 °C, amorphous: 1.38 (?)	[1959Rat]
	? °C, amorphous: 1.2 (?)	[1974Dre]
silica glass	(T in °C), amorphous: T/λ : 0/ 1.36 , 50/ 1.44 , 100/ 1.48 , 150/ 1.53 , 200/ 1.58 , 250/ 1.64 , 300/ 1.70 , 350/ 1.78 , 400/ 1.85 , 450/ 1.94 , 500/ 2.07	[1940Bir ^a]
NON-SILICATES		
oxides		
cassiterite, SnO ₂	? °C, λ_m : 12.3 (1)	[1987Pop, 1999Pop ^a]
chromite, iso, FeCr ₂ O ₄	35 °C, a: 2.20 ± 0.27 (3)	[1974Dre]
	? °C, a: 2.52 (1)	[1971Hor]
	? °C, a: 2.62 (1)	[1987Pop, 1999Pop ^a]
corundum, Al ₂ O ₃	26-70 °C, \parallel : 18.37 ± 3.86 (5); 23-77 °C, \perp : 17.70 ± 3.60 (4)	[1988Dim]
	? °C, λ_{11} : 31.2 (?), λ_{33} : 38.9 (?)	[1974Dre]
hematite, Fe ₂ O ₃	30 °C, a: 12.42 ± 1.74 (3)	[1954Bir, 1966Cla]
	? °C, λ_{11} : 14.7 (?), λ_{33} : 12.1 (?)	[1974Dre]
	? °C, a: 11.28 (1)	[1971Hor]
	? °C, λ_m : 18.25 ± 1.25 (2)	[1987Pop, 1999Pop ^a]
ilmenite, FeTiO ₃	35 °C, a: 2.50 ± 0.02 (3)	[1988Dim]
	? °C, a: 2.38 ± 0.25 (2)	[1971Hor]
	? °C, a: 2.92 (1)	[1987Pop, 1999Pop ^a]
magnetite, iso, Fe ²⁺ Fe ³⁺ ₂ O ₄	22-33 °C, a: 4.61 ± 0.39 (8)	[1988Dim]
	? °C, λ_{11} : 9.7 (?)	[1974Dre]
	? °C, a: 5.10 (1)	[1971Hor]
	? °C, λ_m : 4.34 ± 0.90 (2)	[1987Pop, 1999Pop ^a]
periclase, MgO, iso	? °C, λ_{11} : 33.5 (?)	[1974Dre]
artificial periclase	400 K, λ_{11} : 41.05 (1)	[1968Kan]
pyrochlore, (Na,Ca) ₂ Nb ₂ O ₆ (OH,F)	? °C, a: 1.52 (1)	[1987Pop, 1999Pop ^a]
rutile, TiO ₂ (tetragonal)	44-67 °C, \perp : 7.95 ± 1.198 (2)	[1988Dim, 1966Cla]
	36-67 °C, \perp : 13.19 ± 0.89 (2); ? °C, a: 4.90 ± 0.21 (3)	[1966Cla]
	? °C, λ_{11} : 9.3 (?), λ_{33} : 12.9 (?)	[1974Dre]

Mineral	T , state, λ , (n)	Source
scheelite, CaWO_4	? °C, a: 5.12 (1)	[1971Hor]
	? °C, x: 4.89 (1),	[1987Pop,
	27 °C (100): 4.38 (1), (010): 4.38 (1), (001): 5.92 (1)	1999Pop ^a]
	? °C, λ_m : 2.53 ± 0.20 (4)	[[1987Pop,
		1999Pop ^a]
spinel, iso, MgAl_2O_4	35-70 °C, a: 12.14 ± 1.51 (3)	[1966Cla]
	? °C, λ_{11} : 13.8 (?)	[1974Dre]
	? °C, a: 9.48 (1)	[1971Hor]
wolframite, (Fe,Mn) WO_4	? °C, λ_m : 2.81 ± 0.38 (5)	[1987Pop,
		1999Pop ^a]
wulfenite, PbMoO_4	? °C, λ_m : 1.82 (1)	[1987Pop,
		1999Pop ^a]
sulfides		
arsenopyrite, FeAsS	? °C, a: 7.24 (1)	[1987Pop,
		1999Pop ^a]
chalcopyrite, CuFeS_2	35 °C, a: 7.55 ± 0.33 (3)	[1988Dim]
	? °C, a: 10.7 (1)	[1987Pop,
		1999Pop ^a]
galena, PbS iso (cubic)	35 °C, a: 2.76 ± 0.22 (3)	[1988Dim]
	? °C, a: 2.28 (1)	[1971Hor]
	? °C, a: 1.99 (1), x: 2.02 (1),	[1987Pop,
	27 °C (100): 2.02 (1), (010): 2.02 (1), (001): 2.02 (1)	1999Pop ^a]
pyrite, FeS_2 , iso (cubic)	35 °C, a: 23.15 ± 2.45 (3)	[1988Dim]
	? °C, a: 19.21 (1)	[1971Hor]
	? °C, a: 23.7 (1)	[1987Pop,
	27 °C (100): 41.4 (1), (010): 41.4 (1), (001): 41.4 (1)	1999Pop ^a]
	? °C, x: 41.4 (1), λ_{11} : 37.9 (?)	[1974Dre]
pyrrhotite, FeS (hexagonal)	35 °C, a: 3.53 ± 0.06 (3)	[1988Dim]
	? °C, a: 4.60 (1)	[1971Hor]
	? °C, a: 3.52 (1),	[1987Pop,
	27 °C (100): 3.43 (1), (010): 3.43 (1), (001): 3.71 (1)	1999Pop ^a]
sphalerite, (Zn,Fe ²⁺)S	35 °C, a: 11.20 ± 0.02 (3)	[1988Dim]
sphalerite (marmatite), (Zn,Fe ²⁺)S	? °C, a: 18.9 (1)	[1987Pop,
sphalerite (cleiophane), ZnS	? °C, a: 4.67 (1)	1999Pop ^a]
wurtzite, (Zn,Fe)S	? °C, a: 4.19 (1)	[1987Pop,
		1999Pop ^a]
sulfates		
anhydrite, CaSO_4	25-35 °C, a: 5.36 ± 0.30 (6)	[1988Dim]
	? °C, a: 4.76 (1)	[1971Hor]
barite, BaSO_4	25-100 °C, μ : 2.92 ± 0.09 (4), \perp : 2.07 ± 0.03 (2)	[1988Dim]
	25-35 °C, a: 1.72 ± 0.05 (4)	
	? °C, a: 1.51 ± 0.12 (2)	[1987Pop,
		1999Pop ^a]
celestine, SrSO_4	35 °C, μ : 1.38 (1); 35 °C, \perp : 1.29 ± 0.11 (3)	[1988Dim]
	? °C, λ_m : 1.32 (1)	[1987Pop,
		1999Pop ^a]
gypsum, $\text{CaSO}_4 \cdot 2\text{H}_2\text{O}$? °C, a: 1.30 (1)	[1988Dim]
	? °C, a: 1.22 (1)	[1987Pop,
	? °C, \perp : 1.6 , μ_{11} : 2.5 , μ_{12} : 3.8 , λ_{11} : 2.6 , λ_{22} : 1.6 , λ_{33} : 3.7 (1)	1999Pop ^a]
		[1974Dre]
carbonates		
aragonite, CaCO_3	25-100 °C, a: 2.37 ± 0.23 (11)	[1988Dim]
	? °C, a: 2.24 (1)	[1971Hor]
calcite, CaCO_3 (trigonal)	? °C, λ_{11} : 4.2 (?), λ_{33} : 5.0 (?)	[1974Dre]
	? °C, x: 3.13 (1);	[1987Pop,
	27 °C (100): 3.21 (1), (010): 3.21 (1), (001): 3.50 (1)	1999Pop ^a]
	? °C, λ_m : 3.28 ± 0.04 (2), a: 3.59 (1)	[1971Hor]
calcite \parallel	(T in °C), T/λ , x: $0/4.00, 30/3.63, 50/3.40, 100/2.99, 150/2.73,$	[1940Bir ^a]
	$200/2.55, 250/2.41, 300/2.29, 350/2.20, 400/2.13$	
calcite \perp	(T in °C), T/λ , x: $0/3.48, 30/3.16, 50/3.00, 100/2.72, 150/2.52,$	[1940Bir ^a]
	$200/2.37, 250/2.25, 300/2.16, 350/2.09, 400/2.06$	
cerussite, PbCO_3	35 °C, a: 1.35 ± 0.02 (3)	[1988Dim]
dolomite, $\text{CaMg}[\text{CO}_3]_2$	25-35 °C, a: 4.85 ± 0.26 (73)	[1988Dim]
	? °C, λ_{11} : 4.7 (?), λ_{33} : 4.3 (?)	[1974Dre]
	? °C, a: 5.51 (1)	[1971Hor]

Pre-Print from:

Clauser, C., 2006. Geothermal Energy, In: K. Heinloth (ed), *Landolt-Börnstein, Group VIII: Advanced Materials and Technologies, Vol. 3: Energy Technologies, Subvol. C: Renewable Energies*, Springer Verlag, Heidelberg-Berlin, 493-604.

Mineral	T , state, λ , (n)	Source
	? °C, a: 5.97 ± 0.44 (2)	[1987Pop, 1999Pop ³]
magnesite, MgCO ₃	25-100 °C, \parallel : 7.86 ± 0.20 (4); \perp : 7.32 ± 0.36 (4) 34-35 °C, a: 8.18 ± 1.34 (5) ? °C, a: 5.84 (1)	[1988Dim] [1988Dim] [1971Hor]
siderite, FeCO ₃	35 °C, a: 2.99 ± 0.15 (3) ? °C, a: 3.01 (1)	[1988Dim] [1971Hor]
strontianite, SrCO ₃	35 °C, a: 1.38 ± 0.07 (4)	[1988Dim]
witherite, BaCO ₃	35 °C, a: 2.26 ± 0.02 (3)	[1988Dim]
phosphates		
apatite, Ca ₅ [PO ₄] ₃ (F,Cl,OH)	35 °C, a: 1.27 ± 0.02 (3) (hexagonal) ? °C, a: 1.38 ± 0.01 (2) ? °C, x: 1.58 ± 0.06 (3); 27 °C (100): 1.53 ± 0.07 (3), (010): 1.53 ± 0.07 (3), (001): 1.70 ± 0.07 (3)	[1988Dim] [1971Hor] [1987Pop, 1999Pop ³]
halides		
fluorite, CaF ₂ , iso	0-36 °C, x: 8.62 ± 1.11 (6) ? °C, λ_{11} : 10.1 (?) ? °C, a: 9.51 (1) ? °C, a: 8.64 (1)	[1988Dim] [1974Dre] [1971Hor] [1987Pop, 1999Pop ³]
halite, NaCl, iso (cubic)	0-35 °C, x: 5.55 ± 1.09 (8) ? °C, a: 6.1 (?) ? °C, a: 5.88 (1), λ_m : 5.90 (1); 27 °C (100): 5.89 ± 0.01 (2), (010): 5.89 ± 0.01 (2), (001): 5.89 ± 0.01 (2)	[1966Cla] [1974Dre] [1987Pop, 1999Pop ³]
halite, NaCl, iso	(T in °C), T/λ , x: 0/6.11 , 50/5.02 , 70/5.44 , 100/4.21 , 150/3.59 , 200/3.12 , 250/2.76 , 300/2.49 , 350/2.30 , 400/2.09	[1940Bir ³]
rock salt, NaCl, iso	27 °C, x: 6.05 ± 0.87 (5)	[1988Dim]
rock salt, NaCl, iso	(T in K), T/λ : 0.4/0.95 , 0.5/1.78 , 0.6/3.13 , 0.7/4.97 , 0.8/7.40 , 0.9/10.0 , 1/14.0 , 2/99.3 , 3/270 , 4/443 , 5/595 , 6/735 , 7/829 , 8/880 , 9/870 , 10/836 , 15/502 , 20/306 , 25/191 , 30/130 , 40/75.0 , 50/54.0 , 75/34.9 , 100/24.3 , 150/15.0 , 200/10.9 , 250/8.24 , 293/6.65 , 300/6.57 , 400/4.80 , 500/3.67 , 600/2.98 , 700/2.47 , 800/2.08 , 900/1.85 , 1000/1.67	[1981Yan]
sylvite, KCl, iso	0-12 °C, x: 6.74 ± 0.3 (2) ? °C, λ_{11} : 6.4 (?)	[1966Cla] [1974Dre]

Table 8.10. Thermal diffusivity κ ($10^{-6} \text{ m}^2 \text{ s}^{-1}$, upper number) and thermal conductivity λ ($\text{W m}^{-1} \text{ K}^{-1}$, lower number, *in italics*) at different temperatures for quartz, fused silica, olivine, and synthetic periclase; "x" denotes measurements of unknown orientation on single crystals, "a" on single-mineral aggregates; directions of anisotropy are specified either by the mineral's optical a-, b- or c-axes (100, 010, 001); Temperature conversion: $T(^{\circ}\text{C}) = T(\text{K}) - 273.15$; data: [1968Kan;].

mineral	300 K	400 K	500 K	600 K	700 K	800 K	900 K	1000 K	1100 K
quartz, (001)	7.14	3.57	2.38	1.69	1.37	1.14	1.41	1.54	1.64
	<i>13.93</i>	<i>8.20</i>	<i>6.24</i>	<i>4.81</i>	<i>3.91</i>	<i>3.56</i>	<i>3.87</i>	<i>4.56</i>	<i>5.15</i>
quartz, (010)	3.33	2.00	1.45	1.15	0.96	0.89	1.00	1.14	1.28
	<i>6.49</i>	<i>4.60</i>	<i>3.83</i>	<i>3.29</i>	<i>2.90</i>	<i>2.79</i>	<i>2.75</i>	<i>3.39</i>	<i>4.03</i>
fused silica	0.725	0.715	0.705	0.700	0.715	0.741	0.800	0.885	-
	<i>1.147</i>	<i>1.348</i>	<i>1.499</i>	<i>1.612</i>	<i>1.725</i>	<i>1.854</i>	<i>2.060</i>	<i>2.323</i>	-
olivine (Fo ₈₂ Fa ₁₈) (001)	1.85	1.49	1.22	1.08	1.03	1.04	1.09	1.2	1.35
	<i>5.07</i>	<i>4.73</i>	<i>4.23</i>	<i>3.89</i>	<i>3.86</i>	<i>3.98</i>	<i>4.23</i>	<i>4.77</i>	<i>5.44</i>
periclase (MgO) (001)	-	12.5	8.70	6.67	5.56	4.65	4.00	3.57	3.23
	-	<i>46.05</i>	<i>34.12</i>	<i>27.21</i>	<i>23.19</i>	<i>19.63</i>	<i>17.12</i>	<i>15.61</i>	<i>14.32</i>
jadeite (Na(Al,Fe)Si ₂ O ₆), a	1.54	1.28	1.11	0.97	0.88	0.84	0.83	0.89	0.96
garnet (mean of two), x	1.10	1.00	0.91	0.85	0.81	0.79	0.80	0.81	0.83
spinel (MgAl ₂ O ₄), x	-	-	3.45	3.13	2.86	2.56	2.44	2.25	2.13
	-	-	-	-	-	-	-	-	-
corundum (Al ₂ O ₃), x	-	6.06	4.55	3.45	2.86	2.50	2.13	1.85	1.64
	-	-	-	-	-	-	-	-	-
alkali feldspar (moonstone), x	7.09	6.67	6.49	6.71	6.99	7.30	7.81	8.33	8.93
	-	-	-	-	-	-	-	-	-

As for rocks, data on the temperature dependence of mineral thermal conductivity is not very abundant. Yang's temperature dependent data for rock salt [1981Yan] represent "recommended values" based on a great number of individual determinations and cover the temperature range 0.4 K – 1000 K. Table 8.10 lists thermal conductivity and thermal diffusivity as functions of temperature for some rock-forming minerals [1968Kan].

For single-mineral aggregates a linear relationship between temperature and thermal resistivity λ^{-1} discriminates between temperature-dependent contributions and other factors which are independent of temperature, such as micro-cracks, grain boundaries, shape and orientation of crystals and their fragments:

$$\frac{1}{\lambda(T)} = m + n T, \quad (8.31)$$

where λ is in $\text{W m}^{-1} \text{K}^{-1}$ and T is in K. By measuring thermal conductivity λ and plotting its inverse, thermal resistivity λ^{-1} , versus temperature m and n may be determined as intercept and slope of a linear regression. Table 8.11 provides values for the constants m and n in eq. (8.31) which may be used to infer the temperature dependence of thermal resistivity for some single-mineral aggregates [1969Cla].

Table 8.11 Values of m and n in eq. (8.31) for single-mineral aggregates; data: [1969Cla].

mineral	T (°C)	m ($10^{-3} \text{ W}^{-1} \text{ m K}$)	n ($10^{-3} \text{ W}^{-1} \text{ m}$)
halite, NaCl	0 – 400	-52.55	0.788
periclase, MgO	100 – 800	-21.50	0.127
corundum, Al ₂ O ₃	100 – 800	-28.66	0.155
quartz, SiO ₂ (*)	100 – 400	62.10	0.387
spinel, MgAl ₂ O ₄	100 – 1000	19.11	0.122
Zircon, ZrSiO ₄	100 – 800	131.37	0.093
forsterite, Mg ₂ SiO ₄ ,	100 – 600	85.98	0.282
enstatite, ferrosilite, (Mg ₂ ,Fe ₂)SiO ₃	100 – 300	200.63	0.222

(*): single SiO₂ crystal, heat flowing \perp to optical axis

According to eq. (8.15) thermal diffusivity can be expressed by thermal conductivity, density and isobaric specific heat capacity:

$$\kappa = \lambda / (\rho c). \quad (8.32)$$

Based on eq. (8.32), Robertson [1988Rob] converts the feldspar diffusivity data of Kanamori et al. [1968Kan] into conductivity, using a constant density of $\rho = 2600 \text{ kg m}^{-3}$ and a temperature dependent specific heat capacity. However, a comparison of this data set with results from temperature dependent measurements of feldspar conductivity performed by other authors yields a somewhat ambiguous result: Some measurements contradict the increase in conductivity with temperature displayed by Kanamori et al.'s [1968Kan] converted data while those performed by Birch and Clark [1940Bir^a; 1940Bir^b], seem to confirm it, at least in the temperature range 25 °C – 300 °C.

8.1.5.2 Thermal Conductivity of Rocks

For a large number of rocks thermal conductivity data are available and classified according to rock name and origin in several extensive compilations [1942Bir; 1966Cla; 1974Des; 1974Kap; 1981Roy; 1982Čer; 1988Rob; 1988Sun; 1996Sch]. However, it is important to realize that these compilations comprise rocks which are heterogeneous in important aspects, such as mineral composition, porosity, saturation, and experimental conditions. This is the reason for the great variability of thermal conductivity within each particular rock type. Indeed, rock type as such is a rather poor descriptor for thermal and most other

Pre-Print from:

Clauser, C., 2006. Geothermal Energy, In: K. Heinloth (ed), *Landolt-Börnstein, Group VIII: Advanced Materials and Technologies, Vol. 3: Energy Technologies, Subvol. C: Renewable Energies*, Springer Verlag, Heidelberg-Berlin, 493-604.

physical rock properties. This limits the usefulness of such tabulations, except for the rare instance when they comprise data for the exact location of particular interest. In all other cases, predictions based only on data collated according to general rock type may be seriously in error. For all practical applications it is therefore strongly recommended to obtain genuine, representative data of thermal conductivity, either by direct measurement (cf. section 8.1.5.1.1) or by inference from geophysical logs (cf. section 8.1.5.1.2).

Therefore, the complementary approach taken previously by Clauser and Huenges [1995Cla] is extended here with new data: Rather than arranging individual measurements of rock thermal conductivity in tables, data from earlier compilations [1940Bir^a; 1940Bir^b; 1966Cla; 1974Des; 1974Kap; 1981Roy; 1982Čer; 1988Rob] supplemented by a large amount of new data which have become available since [1988Sun; 1990Kob; 1995Pop; 1996Pop, 1998Pop^a; 1998Pop^b; 1999Pop^b; 1999Pop^c; 2002Pop; 2003Pop^a; 2005Rat; 2005Mot] is presented in a statistical way and arranged as in [1995Cla] according to the four basic rock types: sedimentary, volcanic, plutonic, and metamorphic.

Inspection of any of the available compilations shows that thermal conductivity varies by as much as a factor of two to three. This is due to the natural variation of rock mineral content as well as to several physical and diagenetic factors. All rocks are therefore arranged according to the conditions at the time of their formation as sedimentary, volcanic, plutonic or metamorphic rocks. Each group is described in a statistical way by histograms, median, mean, and standard deviation (Table 8.12). This illustrates the variation of thermal conductivity with those factors which have the most pronounced effect on each rock type. These are petrological aspects or petrophysical influences such as porosity (in sedimentary and volcanic rocks), the dominant mineral phase (in metamorphic and plutonic rocks), and anisotropy (in sedimentary and metamorphic rocks).

8.1.5.2.1 Thermal Conductivity of Sedimentary, Volcanic, Plutonic, and Metamorphic Rocks

Fig. 8.12 shows thermal conductivity histograms for the four basic rock types: sedimentary, volcanic, plutonic, and metamorphic. For *sediments*, a distinction is made between (1) chemical sediments comprising limestone, coal, dolomite, hematite, chert, anhydrite, gypsum, rock salt, and sylvinit; (2) low porosity (< 30 %) physical sediments comprising shale (dolomitic, pyritic, carbonaceous), marl, clayey marl, marlstone, conglomerate, tuff conglomerate, impact conglomerate, tuffite, breccia, quartz breccia, and sandstone (including limy and quartz sandstone); and (3) high porosity (> 80 %) physical sediments comprising ocean and lake-bottom sediments. For *volcanic rocks* a distinction is made between (1) high porosity rocks (lava, tuff, tuff breccia, and mod-ocean ridge basalt (MORB)); and (2) low porosity rocks (rhyolite, liparite, trachodolerite, andesite, and basalt, other than MORB). For *plutonic rocks* a distinction is made between (1) rocks with high feldspar content (> 60 %; syenite (including alkali and nepheline syenite), grano-syenite, syenite porphyry, and anorthosite); and (2) low feldspar content (< 60 %; granite (including alkali granite, plagiogranite, granodiorite, tonalite, quartz monzonite), quartz- and quartz-feldspar porphyry, diorite (including monzonite), gabbro (including quartz and olivine gabbro), porphyrite dykes (lamprophyre, diabase, quartz dolerite) and ultra mafic rocks (pyroxenite, peridotite, lherzolite, hypersthenite, bronzitite, dunite, olivinite, hornblendite, cumberlandite). For *metamorphic rocks* a distinction is made between (1) rocks with high quartz content (quartzites); and (2) low quartz content (quartz-mica schist, gneiss)

Influence of Porosity and the Dominant Mineral Phase: For *sedimentary rocks* the factors controlling thermal conductivity are porosity and sediment type (Fig. 8.12a): Both chemical sediments (formed mainly by precipitation of dissolved minerals or by compaction of organic material) and low porosity physical sediments ($\phi < 30\%$, formed by compaction and cementation of clastic material) have similar frequency distributions, means, medians, and first and third quartiles (Table 8.12). In contrast, the distribution of marine, high porosity ($\phi > 80\%$) physical sediments is skewed towards low conductivities, and mean and median are about half the size of those of the previous two distributions. Clearly, this is due to the low conductivity of the void filling fluid, either air or water.

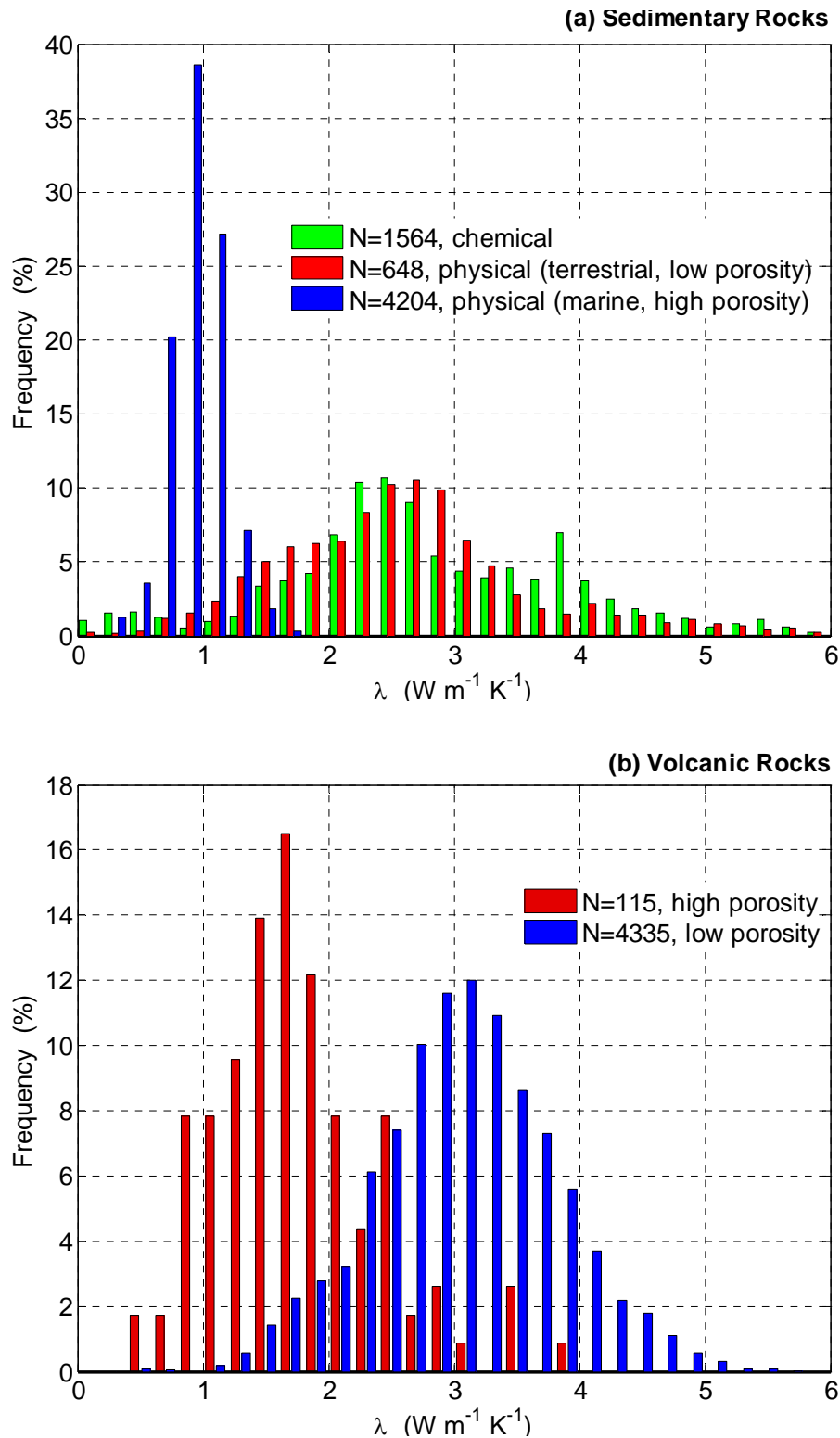


Fig. 8.12 Histograms of thermal conductivity for (a) sedimentary and (b) volcanic rocks (see text for details; plots by courtesy of Andreas Hartmann, RWTH Aachen University).

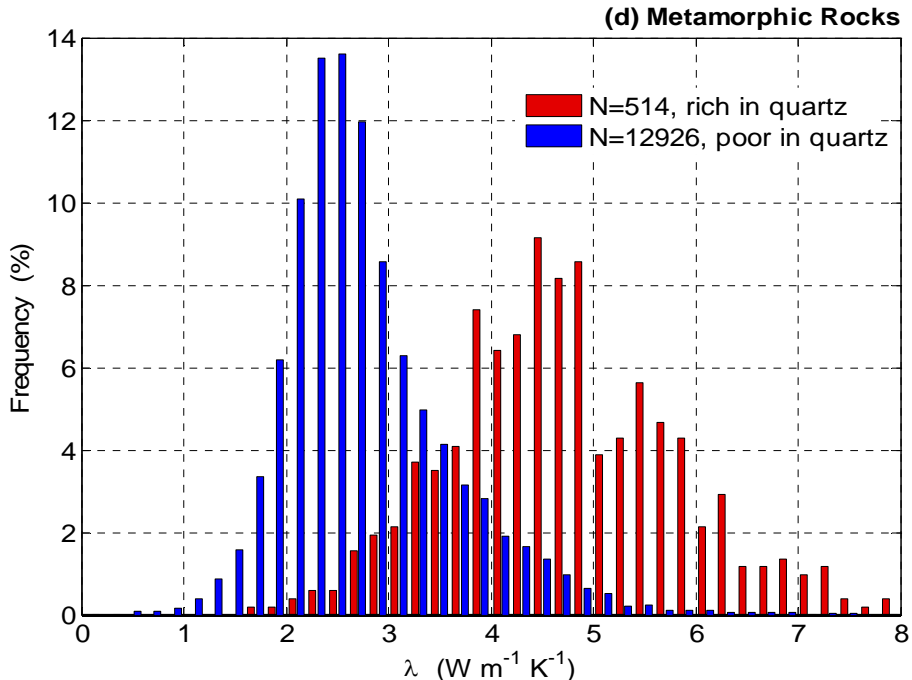
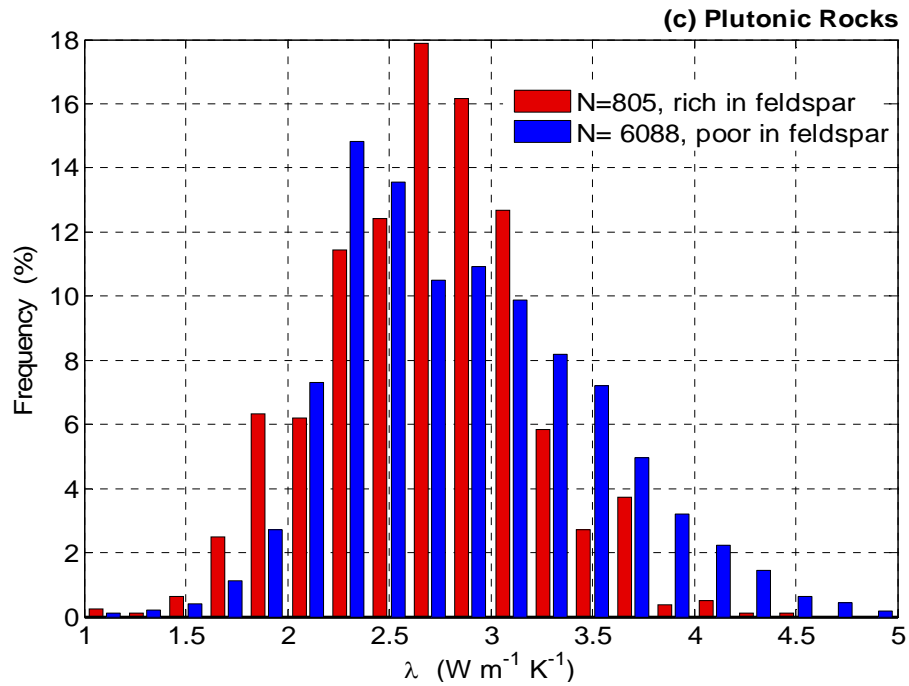


Fig. 8.12 (continued). Histograms of thermal conductivity of (c) plutonic and (d) metamorphic rocks (see text for details; plots by courtesy of Andreas Hartmann, RWTH Aachen University).

For *volcanic rocks* (Fig. 8.12b), spanning nearly the total possible range of porosity from 0 % – 100 %, porosity is clearly the controlling factor on thermal conductivity: mean and median of the high and low porosity histograms differ by nearly a factor of two, and the high porosity distribution is clearly skewed towards low conductivities (Table 8.12).

Plutonic and metamorphic rocks are generally much less porous. Here, the controlling factor is the dominant mineral phase. For *plutonic rocks* (Fig. 8.12c) the feldspar content determines the nature of the histogram: Rocks with a high feldspar content (i.e. > 60 %) show a nearly symmetrical conductivity distribution about a lower mean conductivity than rocks with low feldspar content. In spite of these differences, the means and medians for both distributions are nearly identical within the given standard deviation (Table 8.12).

For *metamorphic rocks* quartz content controls thermal conductivity (Fig. 8.12d). Mean and median of the distributions for high and low quartz content differ by nearly a factor of two. While the histogram for high quartz content rocks (mostly quartzites) is nearly symmetrical, that for low quartz content rocks is strongly skewed towards low conductivities (Table 8.12).

Table 8.12 Statistical moments of the histograms in Fig. 8.12: Number of measurements N; mean value μ ; standard deviation σ ; median M; and first and third quartile Q1 and Q3, respectively. Total number of data is 27230.

Rock Type		N	N_{total}	μ	σ	Q1	M	Q3
Sedimentary rocks	physical, marine ($\phi > 80\%$)	648	6416	0,94	0,21	0,80	0,94	1,06
	physical, terrestrial ($\phi < 30\%$)	4204		2,65	1,08	1,93	2,57	3,09
	chemical	1564		2,80	1,19	2,15	2,64	3,61
Volcanic rocks	high porosity	115	4450	1,75	0,64	1,31	1,66	2,10
	low porosity	4335		3,08	0,73	2,63	3,07	3,55
Plutonic rocks	rich in feldspar	805	6893	2,70	0,50	2,37	2,73	3,02
	poor in feldspar	6088		2,86	0,63	2,38	2,79	3,28
Metamorphic rocks	rich in quartz	514	13476	4,71	1,10	3,98	4,63	5,48
	poor in quartz	12962		2,70	0,82	2,20	2,54	3,00

Influence of Ambient Temperature: Thermal conductivity varies with temperature. This is primarily due to the decrease of lattice (or phonon) thermal conductivity with temperature and to a lesser extent to thermal cracking. Since the thermal expansion coefficient increases with temperature (but differently for all minerals) differential expansion may create contact resistances between mineral grains. This effect is less pronounced in water-saturated rocks than in dry rocks, the condition in which most rocks are tested at elevated temperatures. In contrast, the radiative contribution to thermal conductivity (cf. section 8.1.5.4) increases with the cube of temperature [see e.g. 1988Cla; 1999Hof]. Thus measurements of thermal conductivity as function of temperature generally first show a decrease with temperature, until – from about 1000 °C – 1200 °C onwards – the radiative component balances and sometimes even reverses this decreasing trend. Radiation is more important for rocks with a larger free mean path of radiation corresponding to smaller values of absorption coefficient and opacity (cf. section 8.1.5.4).

Fig. 8.13a illustrates the temperature variation of thermal conductivity for *sedimentary rocks*. Up to 300 °C there is a reduction by nearly a factor of two, both for physical and chemical sediments. Above 300 °C the decrease in thermal conductivity is less pronounced, for chemical still a little stronger than for physical sediments. However, there are very few data for this temperature range, which makes this last observation statistically weak. Above 300 °C, the mean thermal conductivity of sediments varies between $1.0 \text{ W m}^{-1} \text{ K}^{-1}$ – $1.5 \text{ W m}^{-1} \text{ K}^{-1}$.

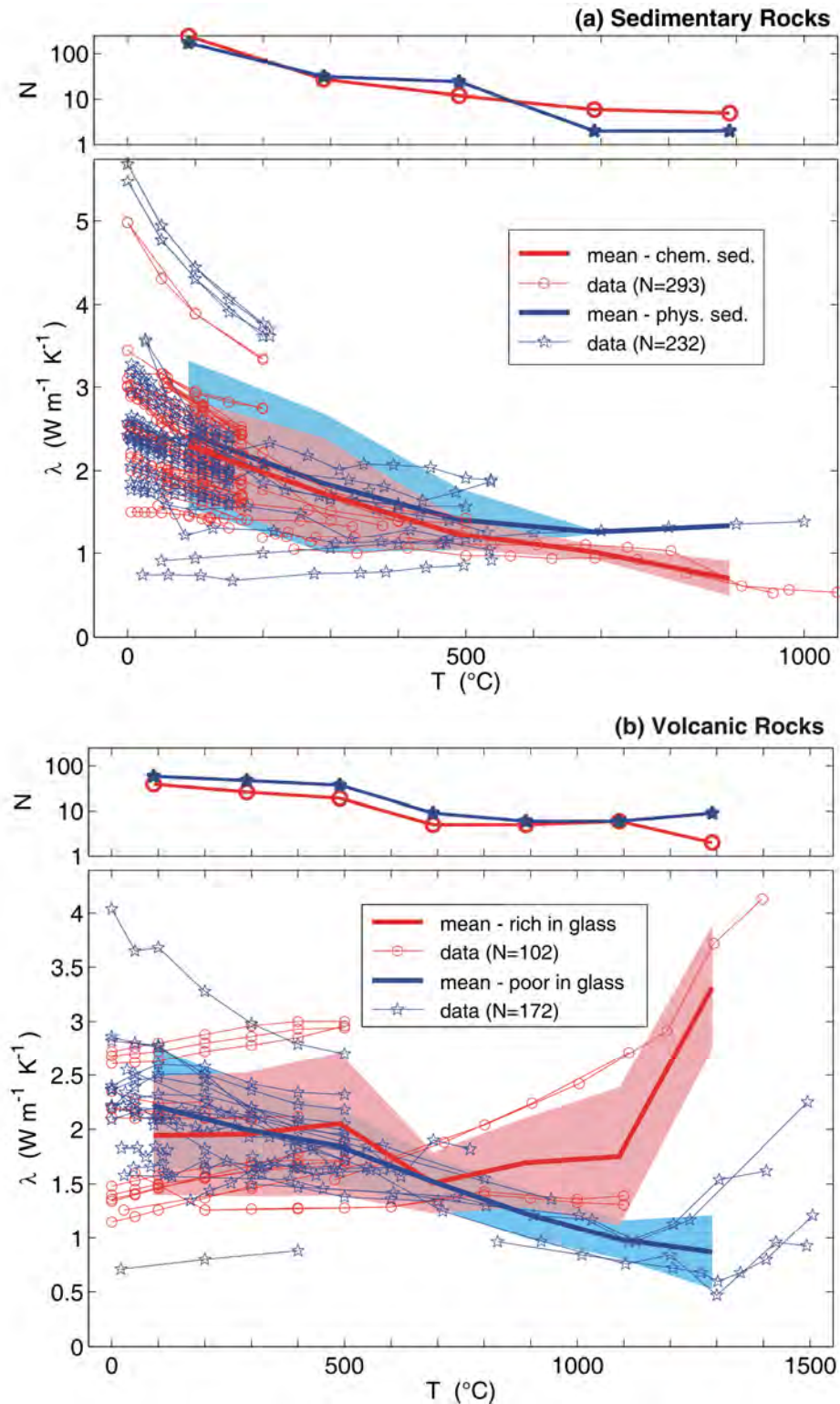


Fig. 8.13 Variation of thermal conductivity of (a) sedimentary and (b) volcanic rocks with temperature. Color shading indicates a range defined by plus and minus one standard deviation (see text for details; plots by courtesy of Andreas Hartmann, RWTH Aachen University).

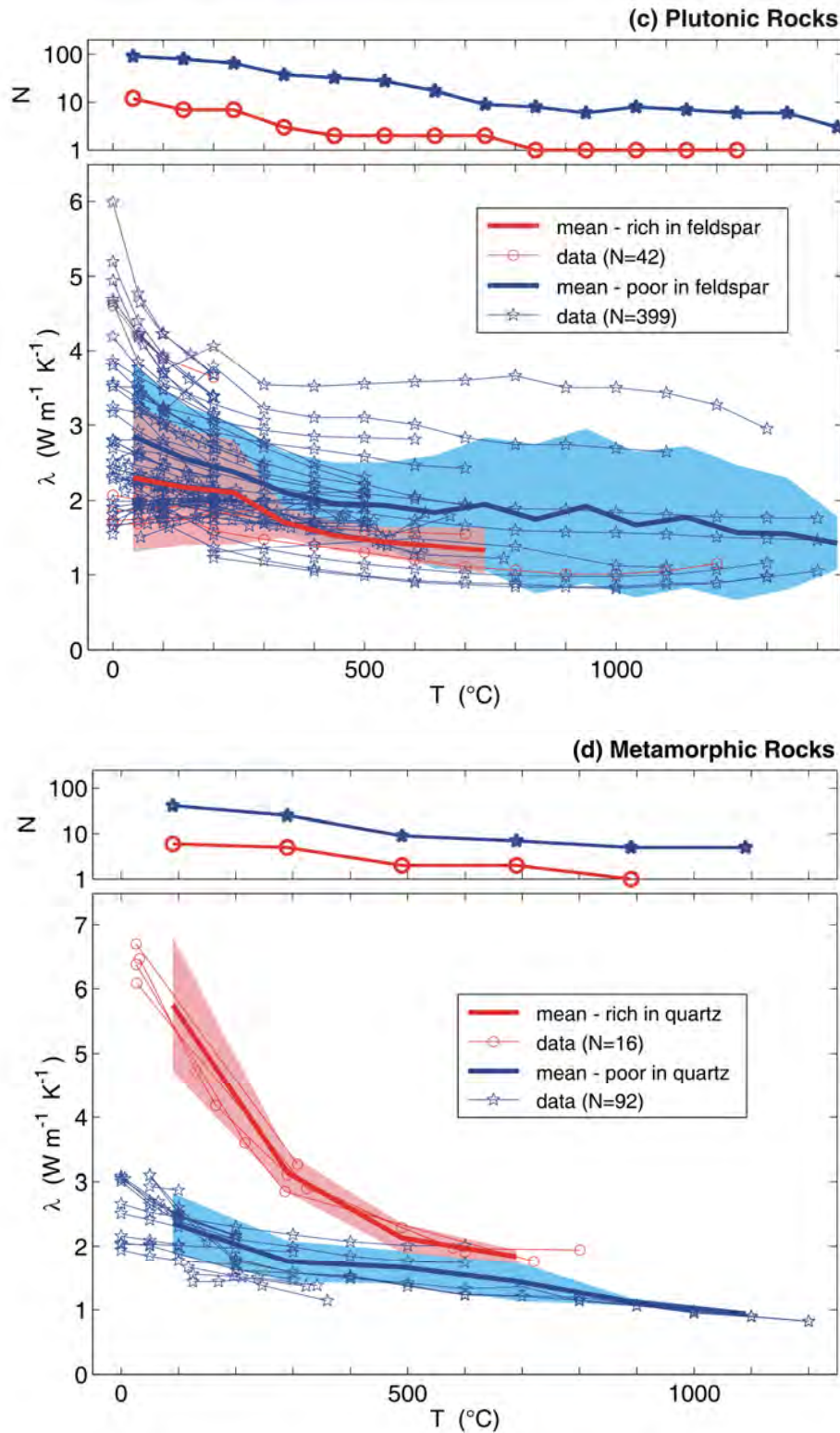


Fig. 8.13 (continued). Variation of thermal conductivity of (c) plutonic and (d) metamorphic rocks with temperature, Color shading indicates a range defined by plus and minus one standard deviation (see text for details; plots by courtesy of Andreas Hartmann, RWTH Aachen University).

Volcanic rocks (Fig. 8.13b) show a quite different behavior, depending on their opacity, i.e. on how well they transmit thermal energy by radiation. Due to this additional "radiative thermal conductivity", volcanic glasses and rocks with a small iron content experience an increase in thermal conductivity for temperatures above 800 °C – 1000 °C (cf. section 8.1.5.4 and e.g. [1988Cla] and [1999Hof]). In contrast, the thermal conductivity of conduction dominated rocks, such as volcanic glasses and rocks with high iron content, again decreases with temperature. An inversion of this trend is indicated by few available high-temperature measurements (above 1300 °C) but with too few measurements to calculate statistically meaningful means and standard deviations. At about 1000 °C thermal conductivity for these rocks is at about 50 % of the room-temperature value. Again, there are few data points above 700 °C.

In *plutonic rocks* there seems to be no strong radiative contribution (Fig. 8.13c). At temperatures above 600 °C thermal conductivity decreases only very little. However, the variation of thermal conductivity with temperature depends on the feldspar content of the rocks. For rocks enriched in feldspar, thermal conductivity decreases little up to 300 °C, while for those poor in feldspar the decrease is stronger, becoming more gentle above 300 °C, and spreading an additional 20 % over the next 1000 K. Interestingly, there is a large amount of data available for this high temperature range. The different behavior of rocks with high feldspar content is due to the increase in thermal conductivity with temperature of some plagioclase feldspars [1940Bir^a] which compensates the decrease in thermal conductivity with temperature observed for most other minerals and rocks. Other notable exceptions are fused silica as well as volcanic and silica glasses (see also discussion of empirical relationships below).

For *metamorphic rocks*, the decrease of thermal conductivity with temperature depends on the content in a dominant mineral phase, similar to plutonic rocks. For quartzites the decrease is rapid, by nearly a factor of three up to a temperature of about 500 °C. Above, there is only a very mild further decrease. For rocks that are poor in quartz the decrease in conductivity is not quite as dramatic, amounting to about one third of the room-temperature value up to 300 °C. Then it remains roughly constant up to 500 °C. Up to 750 °C, it decreases again to about one third of the room-temperature value.

Often data on thermal conductivity is available for room-temperature conditions only, even though it is required at elevated temperatures. For this purpose empirical relationships have been proposed based on measurements at elevated temperatures. With care, they can be used for extrapolation. It is strongly emphasized, however, that there is no real substitute for genuine measurements.

It has been long recognized that for moderate temperatures thermal conductivity, in general, varies with the inverse of temperature [1940Bir^b]. For this temperature range several approaches are available for inferring thermal conductivity at elevated temperatures. Based on the analysis of available tabulated data of thermal conductivity as function of temperature Zoth and Hänel [1988Zot] suggested the following relationship:

$$\lambda(T) = A + \frac{B}{350 + T}, \quad (8.33)$$

where λ is in $\text{W m}^{-1} \text{K}^{-1}$, T in °C, and the empirical constants A and B are determined from a least-squares fit versus temperature of data for different rock types (Table 8.12).

Linear relationships between temperature and thermal resistivity, such as eqs. (8.31) and (8.33), discriminate between temperature-dependent contributions and other factors, which are independent of temperature, such as micro-cracks, grain boundaries, pore volume, mineralogical composition, shape and orientation of crystals and their fragments. As discussed for minerals, the coefficients m and n in eq. (8.31) may be determined as intercept and slope of a linear regression of thermal resistivity versus temperature. Buntebarth [1991Bun] determined m and n from measurements on 113 samples of metamorphic rocks from the KTB research borehole in Germany (mostly gneisses and metabasites) in the temperature range 50 °C – 200 °C. The arithmetic means of 66 individual values determined for gneiss are

Table 8.13. Values for the constants A and B in eq. (8.33) for different rock types; data: [1988Zot].

rock type	T (°C)	A (W m ⁻¹ K ⁻¹)	B (W m ⁻¹)
(1) rock salt	-20 – 0	-2.11	2960
(2) limestones	0 – 500	0.13	1073
(3) metamorphic rocks	0 – 1200	0.75	705
(4) acid rocks	0 – 1400	0.64	807
(5) basic rocks	50 – 1100	1.18	474
(6) ultra-basic rocks	20 – 1400	0.73	1293
(7) rock types (2)-(5)	0 – 800	0.70	770

$\bar{m} = 0.16 \pm 0.03 \text{ m K W}^{-1}$ and $\bar{n} = (0.37 \pm 0.14) \times 10^{-3} \text{ m W}^{-1}$. The corresponding means determined on 36 metabasite samples are $\bar{m} = 0.33 \pm 0.03 \text{ m K W}^{-1}$ and $\bar{n} = (0.22 \pm 0.14) \times 10^{-3} \text{ m W}^{-1}$.

Sass et al. [1992Sas] and Vosteen and Schellschmidt [2003Vos] also distinguish between the effects of composition and temperature. They propose a general empirical relation for $\lambda(T)$, the thermal conductivity in $\text{W m}^{-1} \text{K}^{-1}$ at temperature T in °C, as a function of λ_0 , the thermal conductivity at 0 °C:

$$\lambda(T) = \frac{\lambda_0}{a + T(b - c/\lambda_0)} \quad \text{or} \quad \lambda_0/\lambda(T) = \underbrace{a}_{\text{intercept}} + \underbrace{(b - c/\lambda_0)}_{\text{slope}} T. \quad (8.34)$$

For different rock types, slopes and intercepts can be determined from linear regressions of eq. (8.34), yielding a mean intercept \bar{a} and its uncertainty Δa . Coefficients b and c and associated uncertainties σ_b and σ_c are determined from a second linear regression of the different slopes $(b - c/\lambda_0)$ as a function of $1/\lambda_0$ (Table 8.14).

Table 8.14. Coefficients \bar{a} , b, and c in eq. (8.34) and associated uncertainties Δa , and σ_b , σ_c ; Δa is the error of the mean intercept \bar{a} for all rock types of the linear regressions of the normalized thermal resistance $\lambda_0/\lambda(T)$ as a function of temperature T; σ_b and σ_c are the errors defined by the linear regression of the slopes $(b - c/\lambda_0)$ as a function of the thermal resistance $1/\lambda_0$ (see eq. (8.34)).

rock type	\bar{a} (–)	Δa (%)	b (K ⁻¹)	σ_b (K ⁻¹)	c (W m ⁻¹ K ⁻²)	σ_c (W m ⁻¹ K ⁻²)	T (°C)	Reference
Basement Rocks I (from felsic gneiss to amphibolite)	1.007	–	0.0036	–	0.0072	–	0-250	[1992Sas]
Basement Rocks II (magmatic and metamorphic)	0.99	1	0.0030	0.0015	0.0042	0.0006	0-500	[2003Vos]
Sediments	0.99	1	0.0034	0.0006	0.0039	0.0014	0-300	[2003Vos]

Since thermal conductivity is usually measured at room temperature, λ_0 is expressed as a function of λ_{25} , the room temperature thermal conductivity, by Sass et al. [1992Sas] for crystalline rocks (felsic gneiss to amphibolite) as:

$$\lambda_0 = \lambda_{25} \left[1.007 + 25 (0.0037 - 0.0074/\lambda_{25}) \right]. \quad (8.35)$$

Vosteen and Schellschmidt [2003Vos] find for magmatic and metamorphic rocks:

$$\lambda_0 = 0.53 \lambda_{25} + 0.5 \sqrt{1.13 \lambda_{25}^2 - 0.42 \lambda_{25}}, \quad (8.36)$$

and for sedimentary rocks:

$$\lambda_0 = 0.54 \lambda_{25} + 0.5 \sqrt{1.16 \lambda_{25}^2 - 0.39 \lambda_{25}}. \quad (8.37)$$

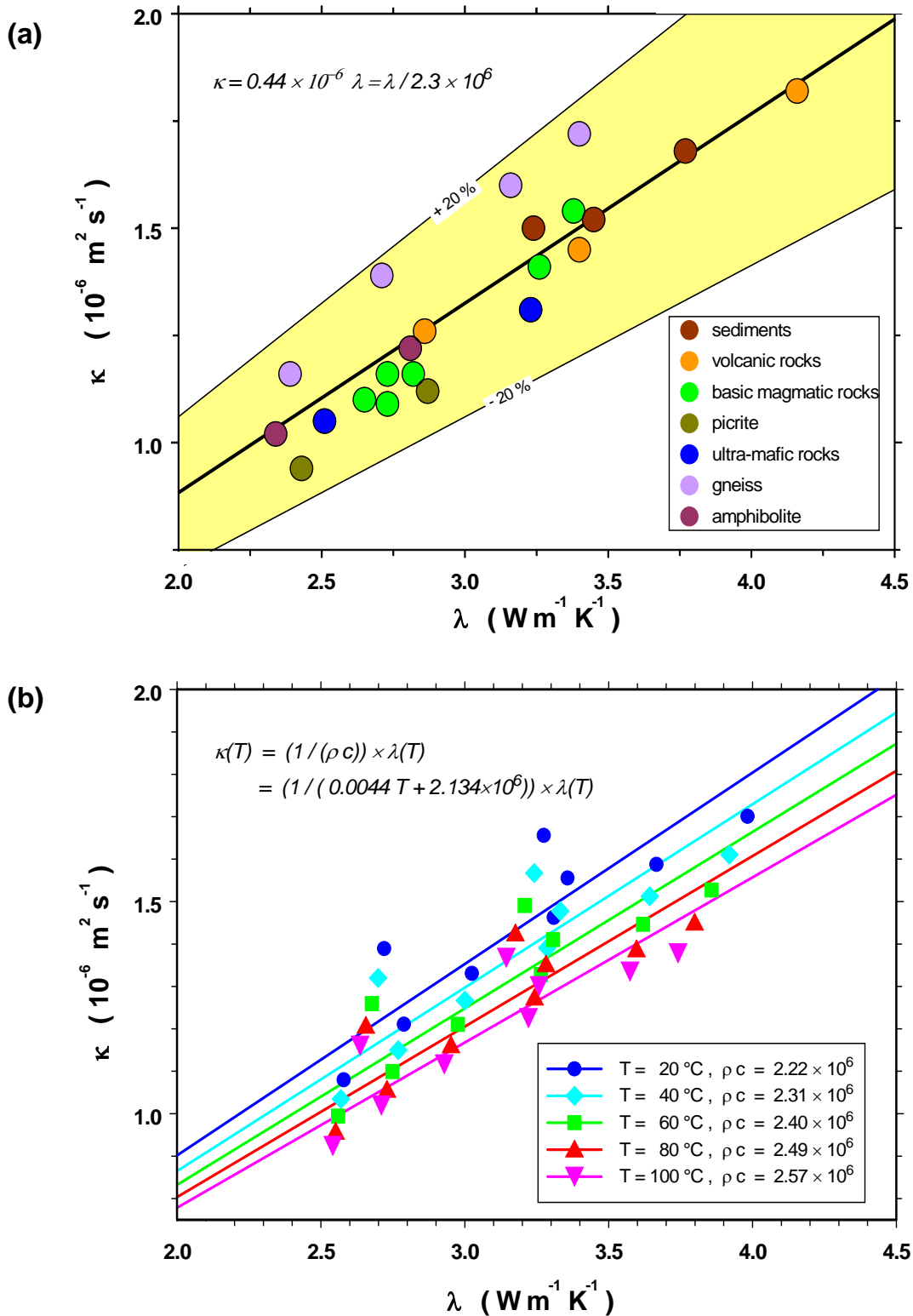


Fig. 8.14 Variation of thermal diffusivity κ with thermal conductivity λ for a suite of meta-sedimentary, volcanic, magmatic, and metamorphic rocks; (a) at room temperature; (b) as a function of temperature [2005Mot].

Sass et al. [1992Sas] derived eqs. (8.34) and (8.35) from thermal conductivity measured as function of temperature in the range 0 °C – 200 °C and higher on 38 samples from a large suite of materials including volcanic, metamorphic, plutonic, and sedimentary rocks [1940Bir^a; 1940Bir^b]. Their results for granites demonstrate the coupled effect of composition and temperature: The normalized thermal resistivity $\lambda_0/\lambda(T)$ is a linear function of temperature, while the slope increases with λ_0 . Sass et al. [1992Sas] tested eqs. (8.34) and (8.35) on an independent data set over a temperature range of 0 °C – 250 °C for rocks ranging in composition from felsic gneiss to amphibolite. In spite of some slight systematic differences, the deviations between measured and predicted values were well within the experimental error range. This suggests that eq. (8.35) yields useful estimates of the temperature dependence of thermal conductivity for crystalline rocks, independent of mineralogy, in the temperature interval 0 °C – 250 °C. Vosteen and Schellschmidt [2003Vos] used a similar approach to obtain thermal conductivity for different crystalline and sedimentary rocks from the Eastern Alps in the temperature range 0 °C – 500 °C and 0 °C – 300 °C, respectively.

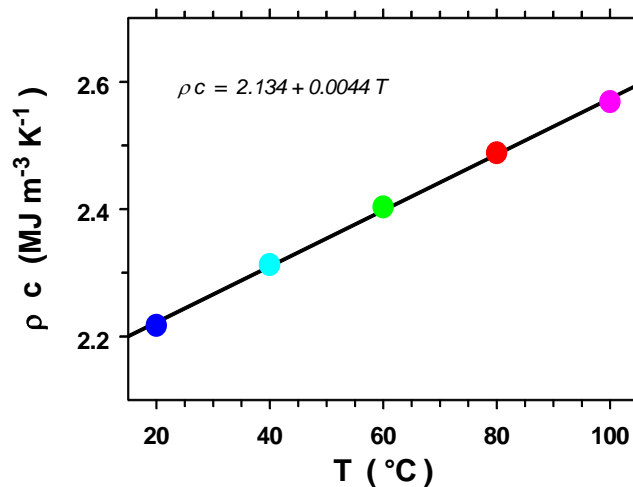


Fig. 8.15 Variation of thermal capacity ρc with temperature (after [2005Mot]); color code: as in Fig. 8.14.

For crystalline rocks up to a temperature of 100 °C, predictions based on the coefficients of Sass et al. [1992Sas] and Vosteen and Schellschmidt [2003Vos] yield comparable results with errors of $\pm 15\%$. From 100 °C – 500 °C predictions based on the coefficients of Vosteen and Schellschmidt [2003Vos] remain within this error range, while those based on the coefficients of Sass et al. [1992Sas] show a systematic increase and shift of the error range with temperature from $+5\% - -30\%$ at 200 °C to $-10\% - -55\%$ at 500 °C [2003Vos].

For sedimentary rocks up to a temperature of 80 °C, predictions based on the coefficients of Sass et al. [1992Sas] and Vosteen and Schellschmidt [2003Vos] yield comparable results with errors ranging from $+5\% - -18\%$. From 80 °C – 300 °C the errors of the predictions based on the coefficients of Vosteen and Schellschmidt [2003Vos] range from $+8\% - -34\%$, while those based on the coefficients of Sass et al. [1992Sas] systematically increase and vary in the range of $-5\% - -60\%$ [2003Vos]. Thus predictions based on the coefficients of Vosteen and Schellschmidt [2003Vos] appear to be more accurate at higher temperature and, in particular, for sedimentary rocks.

Thermal diffusivity of rocks varies even more strongly with temperature than thermal conductivity. This is caused by the opposite behavior of thermal conductivity and thermal capacity (ρc) with respect to temperature: While thermal conductivity decreases by $4\% - 7\%$ in the range 1 °C – 100 °C, thermal diffusivity decreases by $18\% - 22\%$. Fig. 8.14a shows the variation of thermal diffusivity with thermal conductivity at ambient temperature for a suite of meta-sedimentary, volcanic, magmatic, and metamorphic rocks [2005Mot]. A linear regression through the origin yields:

$$\kappa = \frac{\lambda}{\rho c} = 0.44 \times 10^{-6} \lambda = \frac{\lambda}{2.3 \times 10^6} \quad (8.38)$$

Because of several self-compensating factors, thermal capacity (ρc) with few exceptions generally varies within $\pm 20\%$ of $2.3 \text{ MJ m}^{-3} \text{ K}^{-3}$ for the great majority of minerals and rocks [1988Bec]. Fig. 8.14b shows the variation of thermal diffusivity for the previous rock suite [2005Mot] with thermal conductivity at

temperatures up to 100 °C. Thermal capacity (ρc) is the inverse slope of each of these linear regressions and varies linearly with temperature, too (Fig. 8.15). A linear regression of thermal capacity as a function of temperature again yields a linear relationship from which the variation of thermal diffusivity $\kappa(T)$ with temperature can be derived from the variation of thermal conductivity $\lambda(T)$ with temperature:

$$\kappa(T) = \frac{\lambda(T)}{2.134 \times 10^6 + 0.0044 T} \quad (8.39)$$

Similar relationships have been reported by Kukkonen and Suppala [1999Kuk] and Vosteen and Schell-schmidt [2003Vos].

8.1.5.2.2 Influence of Various Factors on Thermal Conductivity

Apart from temperature, thermal conductivity also varies with pressure, saturation, pore fluid, dominant mineral phase, and anisotropy of different rock types.

Pressure: The effect of overburden pressure is twofold, different for two distinct pressure ranges. First, fractures and micro-cracks (developed during stress release, when samples are brought to the surface) begin to close with increasing pressure. This reduces thermal contact resistance as well as porosity, which is usually filled with a low conductivity fluid. When an overburden pressure of about 15 MPa is reached, this process comes to an end. A compilation of measurements on various sedimentary, volcanic, plutonic and metamorphic rocks [1995Cla] indicates that this effect accounts for an increase of about 20 % relative to thermal conductivity at ambient conditions. A further pressure increase to 40 MPa does not affect thermal conductivity significantly. If pressure is increased further, however, a second process becomes effective, the reduction of intrinsic porosity, i.e. voids which are not created by stress release. For granite and for metamorphic rocks data indicate a corresponding increase of thermal conductivity on the order of 10 % over the pressure range 50 MPa – 500 MPa.

Porosity and Saturating Fluid: For large porosities (i.e. $\phi \gg 1$ %) the thermal conductivity of the saturating fluid affects significantly the bulk rock thermal conductivity. The influence varies with the thermal conductivity of the saturating fluids: water, oil, natural gas or air (cf. Table 8.7). The resulting bulk thermal conductivity can be estimated from a suitable mixing model (e.g. eqs. 8.23 – 8.26; see also Fig. 8.10). This effect is illustrated in Fig. 8.16 for data obtained by Robertson and Peck [1974Rob] from Hawaiian marine basalt saturated by air and water. This data set is remarkable as it comprises nearly the total possible range of porosity from 0 % – 100 %.

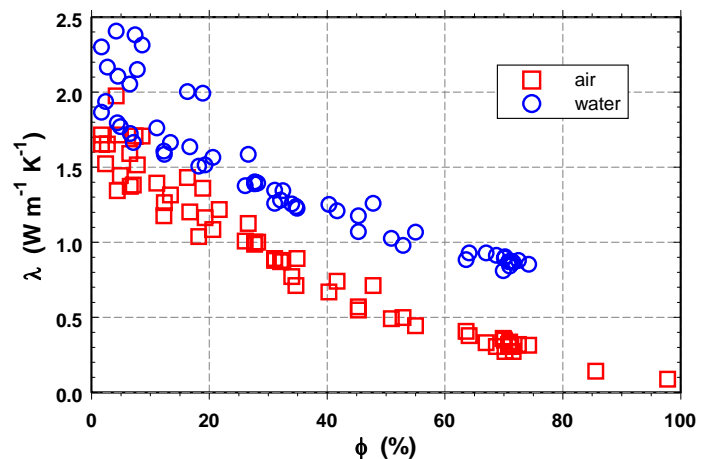


Fig. 8.16 Variation of thermal conductivity λ with porosity ϕ for Hawaiian basalt [1974Rob], measured dry (air) and saturated with water.

Partial Saturation: The effect of partial saturation is different for porous or fractured rocks. Porosity in porous rocks consists of the bulk pore space and bottlenecks in between formed by the contact between individual grains. Dry bottlenecks act as thermal contact resistances between grains, while the bulk pore volume contributes proportionally to the effective rock thermal conductivity. In fractured rocks, in con-

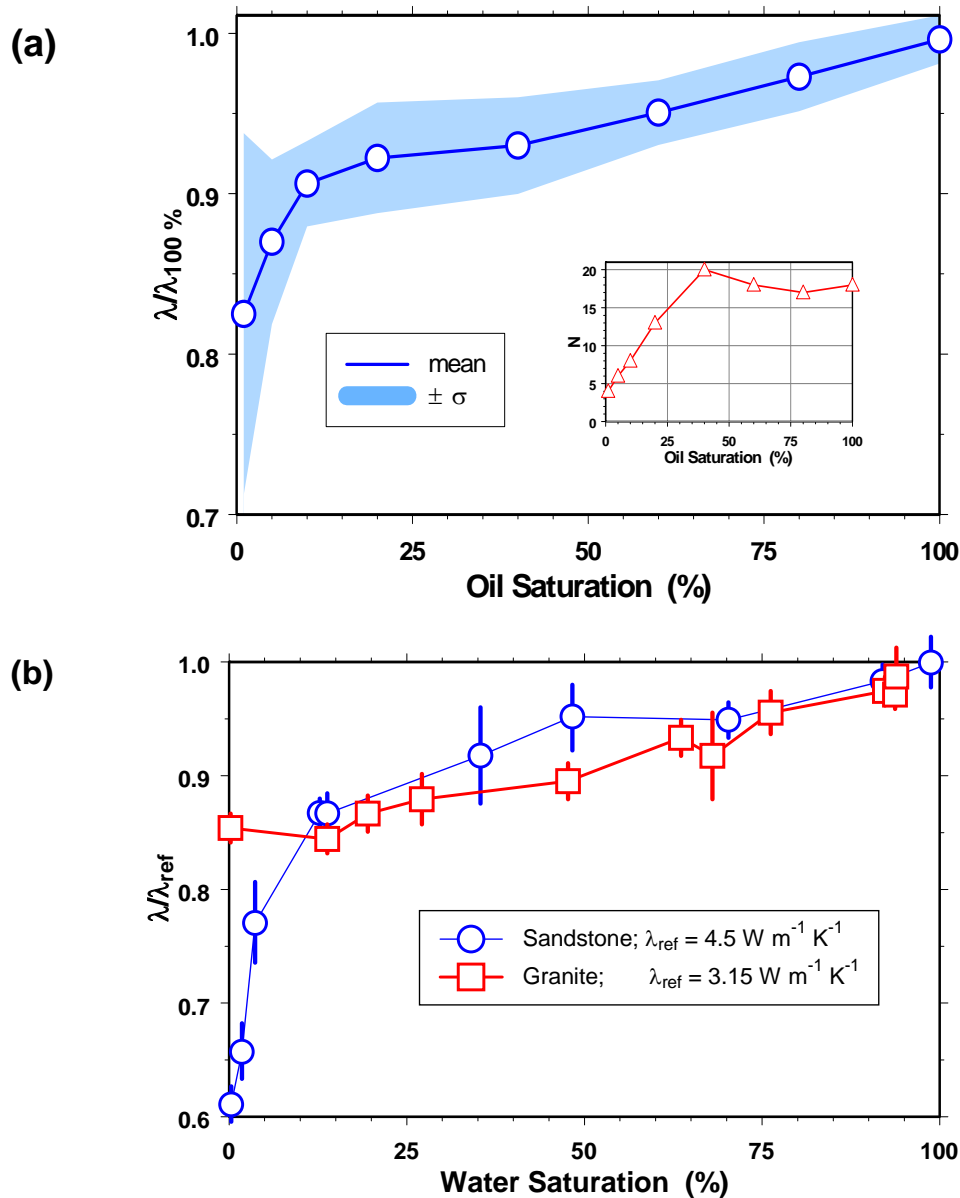


Fig. 8.17 Variation of thermal conductivity with partial saturation. (a) Sandstones ($3\% \leq \phi \leq 30\%$) saturated with oil; values normalized by thermal conductivity at full saturation (circles); data: [1965Mes; 1974Des]; (b) Sandstone ($\phi = 18\%$) (circles) and granite ($\phi = 1\%$) (squares) saturated with water and standard deviations (bars); values normalized by reference thermal conductivities shown in legend; data: [1991Rei].

trast, there are no bottlenecks between grains as in porous rocks, and the small void volume in the fractures corresponds to the bulk pores space of porous rocks.

Saturating these two basic types of voids results in a completely different variation of thermal conductivity with saturation. Fig. 8.17a illustrates the variation of thermal conductivity with the degree of oil saturation in sandstones of low- to medium-porosity. Initially, there is a rapid increase in conductivity with saturation: Starting from completely unsaturated conditions (where conductivity is only about 80 %

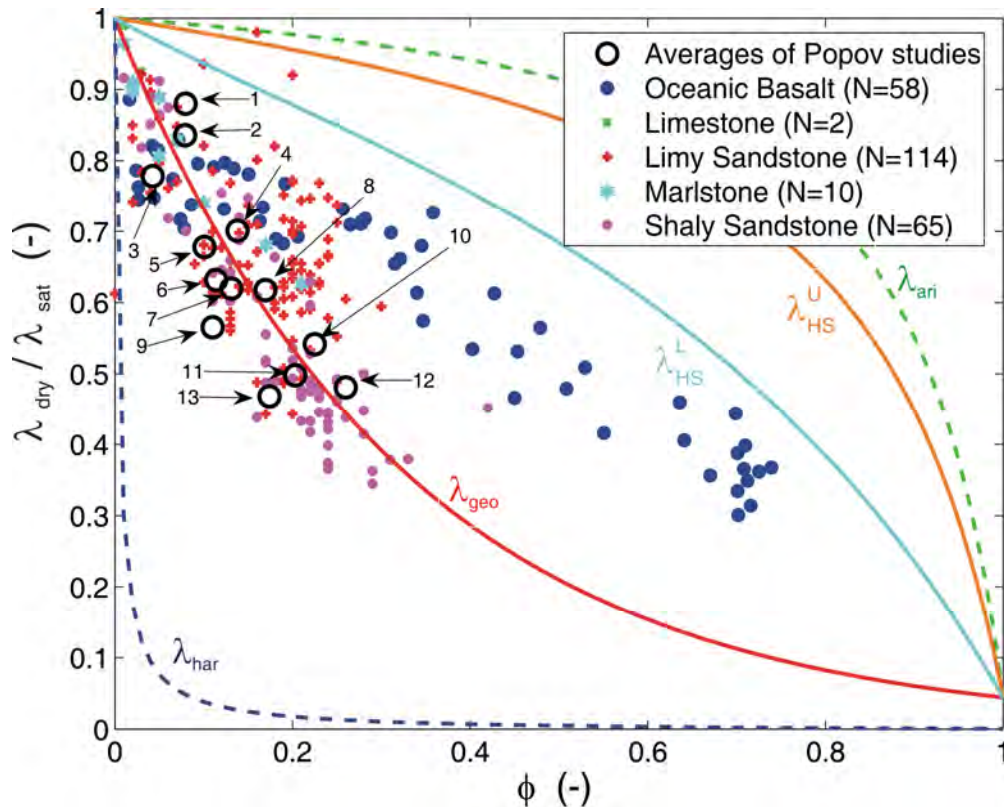


Fig. 8.18. Variation of thermal conductivity ratio $\lambda_{\text{dry}}/\lambda_{\text{sat}}$ (dry and saturated measurements) with porosity ϕ for different rock types. Open circles represent mean values of Popov's measurements on sedimentary rocks [1990Kob; 1995Pop; 1996Pop; 1998Pop^b; 1999Pop^b; 2002Pop]: (1) 21 limestones (North Khasedayu); (2) 54 limestones (Kaliningrad); (3) 13 quartz sandstones (Talinskoe); (4) 44 quartz siltstones (Povkhovskoe, Vat-Eganskoe); (5) 35 conglomerates (Talinskoe); (6) 141 quartz sandstones (Samotlorskoe); (7) 33 claystones (Samotlorskoe); (8) 99 polymictic sandstones (Orenburgskoe); (9) 30 quartz sandstones (East European platform); (10) 22 claystones (Povkhovskoe, Vat-Eganskoe); (11) 65 quartz siltstones (EM-Egovskoe); (12) 99 quartz siltstones (EM-Egovskoe); (13) 241 quartz siltstones (Samotlorskoe); curves labeled λ_{ari} , $\lambda_{\text{HS}}^{\text{U}}$, $\lambda_{\text{HS}}^{\text{L}}$, λ_{geo} , and λ_{har} correspond to the arithmetic, upper and lower Hashin-Shtrikman bound, geometric and harmonic mixing laws, λ_{ari} , $\lambda_{\text{HS}}^{\text{U}}$, $\lambda_{\text{HS}}^{\text{L}}$, λ_{geo} , and λ_{har} , respectively (eq. 8.23); plots by courtesy of Andreas Hartmann, RWTH Aachen University.

of the saturated value), a level of 90 % is reached at about 10 % saturation. The 10 % conductivity residual is spread almost linearly over the remaining 90 % of saturation. Fig. 8.17b illustrates these two effects for the case of water-saturation and a medium-porosity sandstone. The behavior is quite similar to the preceding case: Starting from a completely unsaturated conductivity of only about 60 % of the saturated value, a level of 85 % is reached again at about 10 % saturation. The 15 % conductivity residual is again spread almost linearly over the remaining 90 % of saturation. Physically this observation indicates that the filling of inter-granular bottlenecks, which accounts for only about 10 % – 15 % of the total porosity, significantly reduces the contact resistances between the individual grains. The replacement of low conductivity air by a more conductive fluid in the major part of the pore volume accounts for the second effect. If only fractures contribute to the total porosity, such as in crystalline rock, there are no bottlenecks and we observe only the second effect. This is shown in Fig. 8.17b for granite with a porosity of 1 %. Starting from completely unsaturated conditions at a level of only about 85 % of the saturated conductivity, there is a quasi linear increase until the 100 % level is reached for complete saturation. Obviously, porous rocks whose pore volume comprises many bottlenecks experience this

linear conductivity increase only after the contact resistances due to the bottlenecks have been overcome within the first 10 % – 15 % of saturation.

Fig. 8.18 compares the variation of the conductivity ratio $\lambda_{\text{dry}}/\lambda_{\text{sat}}$ of dry and saturated measurements on a total of 1088 sedimentary rock samples with curves corresponding to the arithmetic, upper and lower Hashin-Shtrikman bound, geometric, and harmonic mixing laws (λ_{ari} , $\lambda_{\text{HS}}^{\text{U}}$, $\lambda_{\text{HS}}^{\text{L}}$, λ_{geo} , and λ_{har} , respectively in eq. 8.23). With the exception of oceanic basalt and the greater part of the limy sandstones, the overwhelming part of the data seems to follow the geometric mixing law within an acceptable variation.

Anisotropy: Thermal conductivity of sedimentary and metamorphic rocks is often anisotropic due to the conditions of their formation. Fig. 8.19 illustrates this effect with measurements performed parallel (λ_{\parallel}) and perpendicular (λ_{\perp}) to the apparent direction of layering or foliation. Notwithstanding the relatively low number of measurements it can be seen that the histograms in Fig. 8.19 are skewed and do not follow a normal distribution. The factor of anisotropy, the ratio $\lambda_{\parallel} / \lambda_{\perp}$, is generally between 1 – 2. In Fig. 8.19 the 54 and 29 individual values are plotted for sedimentary and metamorphic rocks, respectively. While for sedimentary rocks there is a general trend of decreasing λ_{\perp} with factor of anisotropy $\lambda_{\parallel} / \lambda_{\perp}$, the data indicate no such trend for metamorphic rocks.

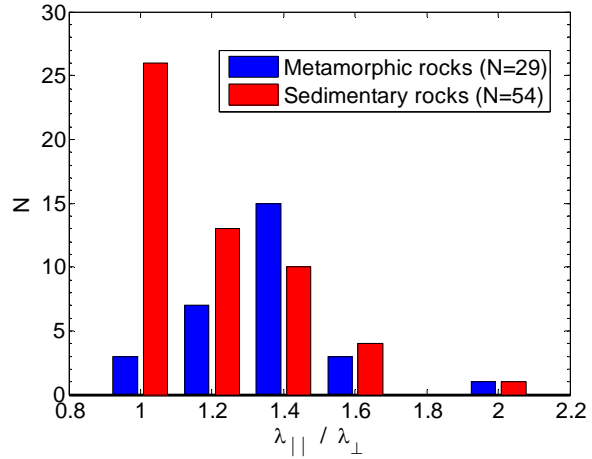


Fig. 8.19 Coefficient of anisotropy $\lambda_{\parallel} / \lambda_{\perp}$ for a suite of metamorphic and sedimentary rocks (plot by courtesy of Andreas Hartmann, RWTH Aachen University).

Robertson [1988Rob] discusses an empirical approach which permits to account for the combined effects of porosity ϕ , saturating fluid, and dominant mineral phase. Plotting measured thermal conductivities of various rocks versus $(1-\phi)^2$, the square of solidity, he finds linear relationships whose slopes vary with the percent content in a specific mineral (e.g. quartz, olivine, etc). He proposes an interpolation formula that accounts for the effects of both water- or air-filled porosity and variable mineral content:

$$\lambda = \lambda_f + (1-\phi)^2 ([\lambda_s + pS] - \lambda_f), \quad (8.40)$$

where λ_f is pore the fluid thermal conductivity intercept at $(1-\phi)^2 = 0$, λ_s the solid rock thermal conductivity intercept at $(1-\phi)^2 = 1$ for zero percent specific mineral content, p the actual percentage of the specific mineral, and S a slope constant equal to the change of λ with the specific mineral content, determined from intercept values obtained from experimental data at $(1-\phi)^2 = 1$.

Table 8.15a-c lists some of the data reported by Robertson [1988Rob] which may be inserted into eq. (8.40) to obtain estimates of thermal conductivity as function of porosity, pore-fluid, and mineral content for mafic and felsic igneous rocks, and for sandstones (note that variations in air and water thermal conductivity in Table 8.15a-c result from linear interpolations of different data sets).

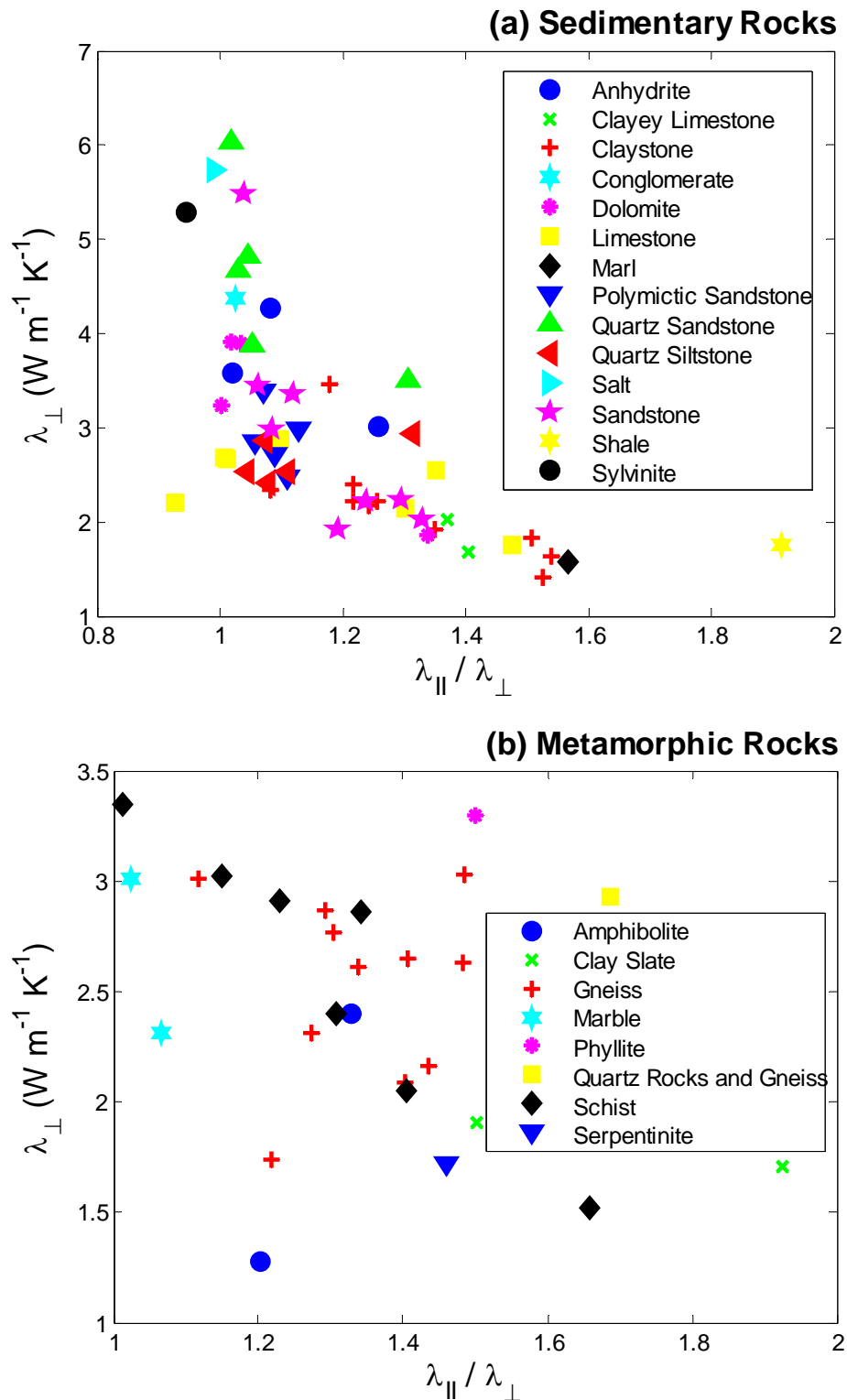


Fig. 8.20 Variation of thermal conductivity normal to bedding of foliation, λ_{\perp} , with factor of anisotropy $\lambda_{\parallel} / \lambda_{\perp}$ for (a) sedimentary and (b) metamorphic rocks (plots by courtesy of Andreas Hartmann, RWTH Aachen University).

Table 8.15a. Constants λ_f , λ_s , and S from eq. (8.40) for mafic igneous rocks (after [1988Rob]; determined on tholeiitic basalt samples with 0 % – 40 % olivine content; data: [1974Rob]).

solidity (1- ϕ) (-)	pore fluid	olivine content p (%)	λ (W m ⁻¹ K ⁻¹)	S (W m ⁻¹ K ⁻¹ % ⁻¹)
0	air	0	$\lambda_f = 0.188$	
1	air	0	$\lambda_s = 1.51$	
1	air	30	$\lambda_s = 1.96$	0.015
0	water	0	$\lambda_f = 0.75$	
1	water	0	$\lambda_s = 1.84$	
1	water	30	$\lambda_s = 2.60$	0.025

Table 8.15b. Constants λ_f , λ_s , and S from eq. (8.40) for felsic igneous rocks (after [1988Rob]; determined on samples with 0 % – 45 % quartz content; data: [1940Bir^a; 1940Bir^b; 1958Bec]).

solidity (1- ϕ) (-)	pore fluid	quartz content p (%)	λ (W m ⁻¹ K ⁻¹)	S (W m ⁻¹ K ⁻¹ % ⁻¹)
0	air	0	$\lambda_f = 0.026$	
1	air	0	$\lambda_s = 1.47$	
1	air	100	$\lambda_s = 5.23$	0.038

Table 8.15c. Constants λ_f , λ_s , and S from eq. (8.40) for sandstone (after [1988Rob]; determined on samples with 0 % – 100 % quartz content; data: [1939Bul; 1940Bir^a; 1940Bir^b; 1941Cla; 1951Bul; 1955Asa; 1956Zie; 1968Hut; 1961Kun; 1961Sug; 1961Woo; 1962Sug; 1970Suk; 1973Ana]).

solidity (1- ϕ) (-)	pore fluid	quartz content p (%)	λ (W m ⁻¹ K ⁻¹)	S (W m ⁻¹ K ⁻¹ % ⁻¹)
0	air	0	$\lambda_f = 0.026$	
1	air	0	$\lambda_s = 1.47$	
1	air	100	$\lambda_s = 5.23$	0.038
0	water	0	$\lambda_f = 0.62$	
1	water	0	$\lambda_s = 1.52$	
1	water	100	$\lambda_s = 8.10$	0.038

Pre-Print from:

Clauser, C., 2006. Geothermal Energy, In: K. Heinloth (ed), *Landolt-Börnstein, Group VIII: Advanced Materials and Technologies, Vol. 3: Energy Technologies, Subvol. C: Renewable Energies*, Springer Verlag, Heidelberg-Berlin, 493-604.

8.1.5.3 Heat Advection

Non-isothermal flow is always associated with advective heat transport. For laminar flow in a porous medium, Darcy's equation [1856Dar] describes the linear relationship between the specific fluid discharge \mathbf{v} and the pressure gradient ∇P over a wide range of pressure gradients:

$$\mathbf{v} = -\frac{\mathbf{k}}{\mu}(\nabla P + \rho_f \mathbf{g} \nabla z) \quad (8.41)$$

where ρ_f and μ are the density and dynamic viscosity of the water and \mathbf{g} is gravity. The relationship between pressure gradient and Darcy velocity is described by the hydraulic permeability tensor \mathbf{k} . The first term accounts for hydrostatic pressure P and the second one for the weight of the water column. The equation of continuity follows from the law of mass conservation:

$$0 = \frac{\partial(\rho_f \phi)}{\partial t} + \nabla(\rho_f \mathbf{v}) + \rho^* W \quad (8.42)$$

where W is a source or sink term and ρ^* the corresponding fluid density. The transient flow equation is then obtained by rewriting the first term on the right side [see e.g. 1986Mar] and substituting for \mathbf{v} :

$$\rho_f(\alpha + \beta \phi) \frac{\partial P}{\partial t} = \nabla \left(\frac{\rho_f \mathbf{k}}{\mu} (\nabla P + \rho_f \mathbf{g} \nabla z) \right) + \rho^* W. \quad (8.43)$$

Here, α and β are the compressibilities of rock and fluid (i.e. the reciprocals of their elastic bulk moduli). An alternative form of the flow equation can be obtained by the following substitutions:

$$\rho_f = \rho_0 \left(1 + \underbrace{(\rho_f - \rho_0)/\rho_0}_{\rho_r} \right) = \rho_0(1 + \rho_r) \quad \text{and} \quad h_0 = z + \frac{P}{\rho_0 \mathbf{g}}, \quad (8.44)$$

where h_0 is a constant density hydraulic head at reference conditions with respect to temperature T , pressure P , and solute concentration C (i.e., $\rho(T_0, P_0, C_0) = \rho_0$), and $\rho_r = (\rho_f - \rho_0)/\rho_0$ is relative fluid density. With

$$\nabla P = \rho_0 \mathbf{g} (\nabla h_0 - \nabla z) \quad \text{and} \quad \frac{\partial P}{\partial t} = \rho_0 \mathbf{g} \frac{\partial h_0}{\partial t} \quad (8.45)$$

Darcy's equation (8.41) finally reads:

$$\mathbf{v} = -\frac{\rho_f \mathbf{g} \mathbf{k}}{\mu} (\nabla h_0 + \rho_r \nabla z). \quad (8.46)$$

Then the flow equation (8.43) becomes:

$$S_s \frac{\partial h_0}{\partial t} = \nabla \left(\frac{\rho_f \mathbf{g} \mathbf{k}}{\mu} (\nabla h_0 + \rho_r \nabla z) \right) + \frac{\rho^*}{\rho_0} W, \quad (8.47)$$

where $S_s = \rho_f \mathbf{g} (\alpha + \beta \phi)$ is the specific storage coefficient. In this form, the terms on the right side of eq. (8.47) correspond to the different driving forces for fluid flow (from left to right): (1) forced convection due to hydraulic gradients; (2) free convection resulting from differences in density; (3) sources/sinks.

The equation for heat transport in a porous medium follows, in an analogous way as the flow equation, from the law of conservation of energy. It is obtained from the thermal energy balance in a unit volume:

$$\frac{\partial(\rho c T)}{\partial t} = \nabla(\lambda \nabla T - (\rho c)_f T \mathbf{v}) + A, \quad (8.48)$$

where A is a heat generation rate, and ρc and $(\rho c)_f$ are the thermal capacities of the saturated medium and the fluid, respectively. The terms on the right side of the heat transport equation (8.48) can again be

correlated with the different heat transport mechanisms (from left to right): diffusion resulting from a temperature gradient (corresponding to conduction in the steady state), advection of heat in a flow field, and sources and sinks.

The Darcy equation (8.41), the flow equation (8.43), and the heat transport equation (8.48) are the basis for numerical modeling of fluid flow and heat transport [e.g. 2003Cla^a]. To fully describe the interdependence of these equations, equations of state are required for the rock and fluid properties as a function of temperature, pressure, and solute concentration.

Heat advection does not require large flow velocities to become as efficient or even dominate steady-state heat conduction or transient heat diffusion. The non-dimensional Péclet and Nusselt numbers, Pe and Nu , quantify the efficiency of advective heat transport versus heat conduction. For instance, for flow over a distance L across a temperature difference $T_1 - T_0$ one obtains:

$$Pe = \frac{(\rho c)_f v L}{\lambda} = \frac{(\rho c)_f v (T_1 - T_0)}{\lambda (T_1 - T_0)/L} = \frac{q_{\text{advection}}}{q_{\text{conduction}}} = \frac{q_{\text{advection}} + q_{\text{conduction}}}{q_{\text{conduction}}} - \frac{q_{\text{conduction}}}{q_{\text{conduction}}} = Nu - 1. \quad (8.49)$$

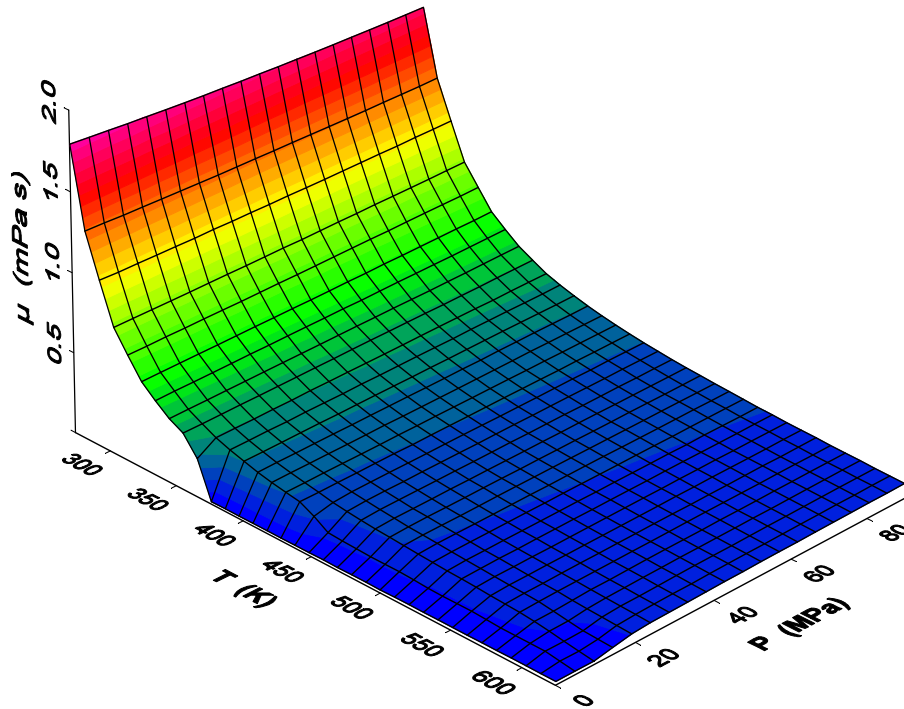


Fig. 8.21 Variation of water dynamic viscosity μ with pressure P and temperature T ; data: [1998Wag].

In almost all heat production technologies heat advection is the principal transport mechanism: It forms the base in hydrothermal heat production and can improve the efficiency of Earth heat exchangers significantly. Thus, insight into coupled flow and heat transport processes is important for most heat production strategies. In many cases this requires numerical simulation. A more detailed treatment of this topic is well beyond the scope of this review. Interested readers are encouraged to consult the pertinent literature [e.g. 1986Mar; 1998Ing; 2002Kol; 2003Cla^a]. As heat advection scales linearly with the specific discharge rate v (eq. (8.46)), it varies linearly with permeability and relative fluid density and inversely with fluid viscosity. Fig. 8.21 and Fig. 8.22 illustrate the variation of the dynamic viscosity and relative density of (pure) water with pressure and temperature.

Pre-Print from:

Clauser, C., 2006. Geothermal Energy, In: K. Heinloth (ed), *Landolt-Börnstein, Group VIII: Advanced Materials and Technologies, Vol. 3: Energy Technologies, Subvol. C: Renewable Energies*, Springer Verlag, Heidelberg-Berlin, 493-604.

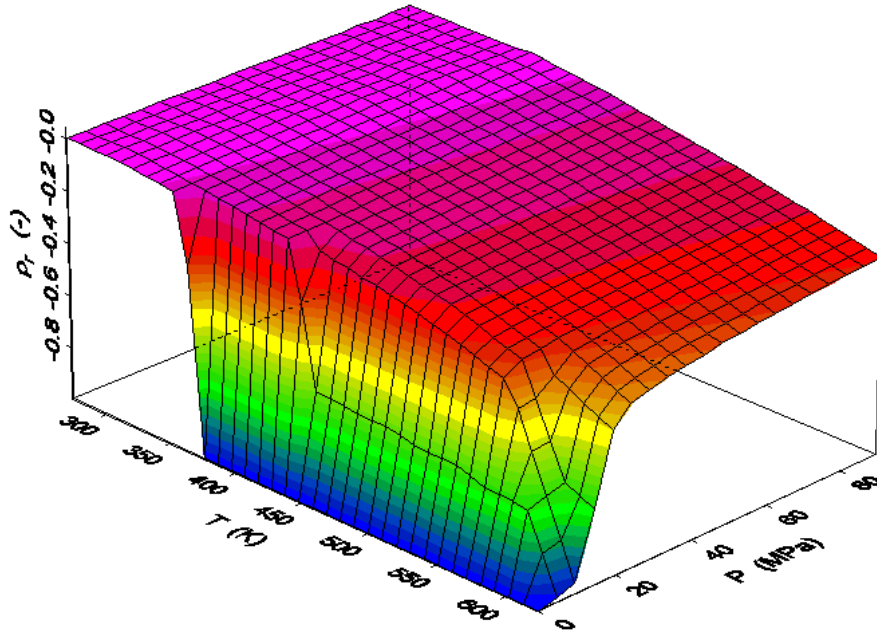


Fig. 8.22 Variation of relative water density ρ_r (eq. (8.44)) (with respect to $P=0.1$ MPa and $T=293.15$ K= 20 °C) with pressure P and temperature T ; data: [1998Wag].

In contrast, the variation of permeability is much larger and much less well defined. For any given type of rock, permeability varies within several orders of magnitude. Actually, rock type defines permeability rather poorly. In fact, it depends on porosity but also on the rock's diagenesis in a highly non-linear way. Therefore it varies also with the internal surface area of the rock's void spaces and the tortuosity of the network of pores and fractures.

For unconsolidated and sedimentary rocks a number of empirical relationships allow to derive permeability from porosity and other quantities, such as specific surface, average or median pore and grain size, and shale content [1972Bea; 1986Mar; 2003Cla^a]. The best known of these relationships, the Kozeny-Carman equation, relates permeability to porosity and specific surface S_0 , the surface area exposed to the fluid per unit volume of solid material (given in m^{-1}) [1972Bea; 1986Mar]:

$$k = c_0 \frac{\phi^3}{S_0^2 (1-\phi)^2}. \quad (8.50)$$

Values used for the constant c_0 vary between $1/6 \leq c_0 \leq 1/2$ [1972Bea], the most frequently used values being $c_0=1/5$ [1972Bea; 1986Mar] and $c_0=1/2$ [e.g. 1999Pap]. If the mean grain radius r_g is given by $r_g=3/S_0$ [1972Bea] and $c_0=1/5$, eq. (8.50) can be expressed by:

$$k = \frac{r_g^2}{45} \frac{\phi^3}{(1-\phi)^2}. \quad (8.51)$$

For unconsolidated sediments permeability may be expressed in terms of the particle size distribution. With $d_{10}=2r_{10}$, the "effective grain diameter" which is larger or smaller for 10 or 90 weight % of a sample, respectively, permeability can be expressed by [1986Mar]:

$$k = d_{10}^2/1000 = r_{10}^2/250. \quad (8.52)$$

For unconsolidated sand Bretjinski's formula [1986Mar] gives hydraulic conductivity $K = \rho_f g k/\mu$ as

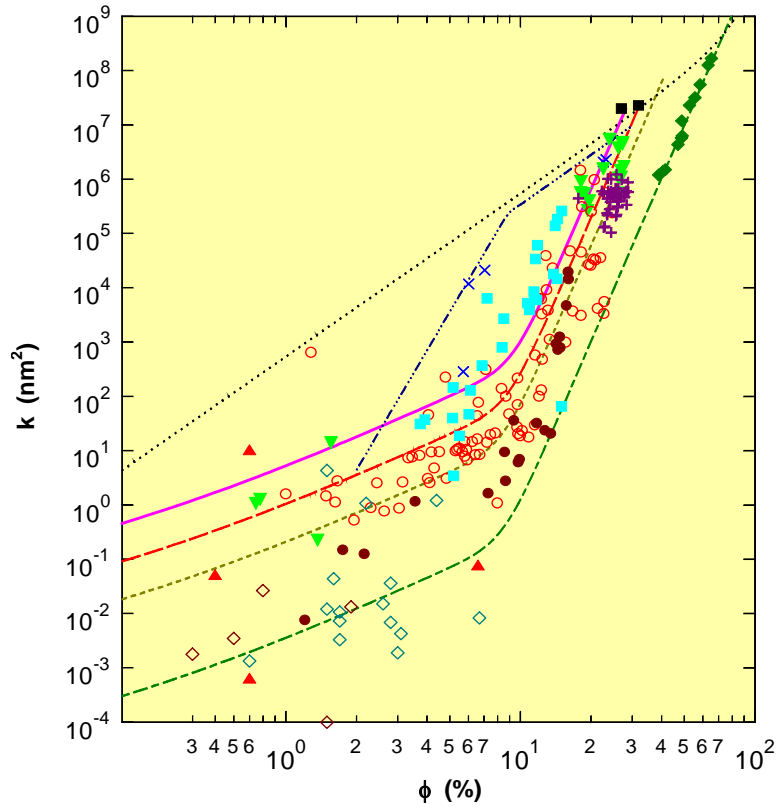


Fig. 8.23 Log-log plot of permeability k versus porosity ϕ for different consolidated and unconsolidated clean and shaly sandstones from the Northern German sedimentary basin. The colored curves, calibrated by several hundred data points, correspond to different clean to shaly sandstones (top to bottom), and are validated by independent data (symbols); details: see [2003Cla^a]. The broken red line corresponds to average North German sandstone (eq. (8.55)), the straight dotted line to the frequently employed cubic relationship between permeability and porosity, and the bent, straight line characterizes French Fontainebleau sandstone [1985Bou].

$$K=3.332 \times 10^6 \phi^7 \quad (K \text{ in m d}^{-1}) \quad \text{or:} \quad K=38.564 \phi^7 \quad (K \text{ in m s}^{-1}). \quad (8.53)$$

For consolidated porous and fractured rocks Pape et al. [1999Pap; 2000Pap; 2005Pap] derived a three-term power series in porosity ϕ for permeability k from a petrophysical model in which the internal surface's roughness is expressed by its fractal dimension which defines the different exponents:

$$k=A\phi^{\text{exp}_1} + B\phi^{\text{exp}_2} + C(10\phi^{\text{exp}_3}). \quad (8.54)$$

The coefficients A , B , and C and the exponents exp_1 , exp_2 , and exp_3 need to be calibrated for each type of (clean to shaly) sandstone. They express the different types of compaction and cementation sandstones may have experienced during diagenesis. For average sandstone from the Northern German sedimentary basin Pape et al. [1999Pap] derived the following coefficients and exponents:

$$k=31\phi + 7463\phi^2 + 191(10\phi^{10}). \quad (8.55)$$

Fig. 8.23 gives an example for shaly to clean sandstones which illustrates the strong non-linearity, involving exponents of porosity as large as 10.

8.1.5.4 Heat Radiation and Thermal Conductivity in the Earth's Mantle

In the Earth, heat radiation becomes a relevant heat transfer mechanism only for temperatures above about 600 °C (see [1988Cla] for a review). Thus, in the context of this review, it may become relevant only in exceptional cases involving temperatures which are unusually high for crustal conditions. Examples might involve, for instance, lava lakes, underground fires in coal seams, and burning coal and waste piles.

In an absorbing and scattering medium the radiative contribution to the total heat transport is due to repeated absorption and re-emission of energy. If the mean free path of radiation is small compared to the distance to material discontinuities (such as grain boundaries) and for moderate temperature gradients (no large anisotropy in the intensity of radiation), the total specific heat flow propagated through the medium can be approximated by:

$$q_i = - \underbrace{(\lambda_{p,ij} + \lambda_{r,ij})}_{\lambda_{ij}} \frac{\partial T}{\partial x_j} \quad (8.56)$$

In eq. (8.56) the radiative contribution is expressed by a “radiative” thermal conductivity λ_r , much in the same way as the diffusive contribution is expressed by the phonon thermal conductivity λ_p in Fourier’s law, eq. (8.22). Various expressions can be given for λ_r under different assumptions. The transmitted intensity I , is related to the incident intensity I_0 , the radiation path, x , and the opacity, ε : $I = I_0 \exp(-\varepsilon x)$. Opacity is defined as $\varepsilon = 1/\ell$, with ℓ the mean free path of radiation (i.e. the average distance a photon travels until it interacts with matter). The so-called gray body approximation requires a medium’s opacity to be finite, constant, and independent of the radiation’s wavelength while, in general, opacity is a function of the radiation wavelength. Opacity in an absorbing and scattering medium is the sum of contributions from these two processes: $\varepsilon = \chi + \varsigma$, where χ and ς are the absorption and scattering coefficients, respectively.

All materials have a complex index of refraction m defined by:

$$m = n - i K, \quad (8.57)$$

where $n=c_0/c$ (the ratio of the speed of light in vacuum and in the substance) is the real part of the index of refraction and K is its imaginary part, sometimes also called extinction coefficient. The absorption coefficient χ is related to the complex index of refraction K by:

$$\chi = 4 \pi K / \Lambda, \quad (8.58)$$

where Λ is the wavelength of radiation [see e.g. 1970Aro].

If the real part of the index of refraction and the spectral radiance are also independent of wavelength and temperature T , λ_r can be expressed by [1952Van; 1988Cla]:

$$\lambda_r = \frac{16 \sigma n^2}{3 \varepsilon} T^3, \quad (8.59)$$

where $\sigma = 5,6704 \times 10^{-8} \text{ W m}^{-2} \text{ K}^{-4}$ is the Stefan-Boltzmann constant. As an example of magnitude, when opacity is identified with the absorption coefficient (neglecting contributions from scattering) and taking typical silicate values of $n = 1.7$ (Table 8.16) and values of the olivine ($\text{Fo}_{92}\text{Fa}_{08}$) absorption coefficient at 1700 K of $1000 \text{ m}^{-1} \leq \chi \leq 1500 \text{ m}^{-1}$ [1979Sha], this yields a range for radiative thermal conductivity at 1700 K of $2.86 \text{ W m}^{-1} \text{ K}^{-1} \leq \lambda_r \leq 4.29 \text{ W m}^{-1} \text{ K}^{-1}$.

Phonon and radiative conductivity jointly form the effective thermal conductivity (eq. (8.56)). Effective thermal conductivity is the property measured in experiments at elevated temperatures. Thus, with the exception of some low-opacity minerals, such as obsidian, and particularly at temperatures below about 600 °C, λ_r need not be accounted for separately.

Table 8.16 Index of refraction n of some substances

substance	$n=c_0/c$
air	1.000272
water	1.333
rock salt (NaCl)	1.544
glass	1.5 – 1.6
carbon disulfide (CS ₂)	1.628
silicates	1.7
diamond	2.417

A more detailed analysis of heat transport based on an analysis of phonon lifetimes obtained from infrared reflectivity has been provided by Hofmeister [1999Hof]. It accounts for the variation of the phonon contribution λ_p to thermal conductivity with both temperature and pressure as well as for the pressure dependent radiative contribution λ_r to thermal conductivity. It replicates experimental data at ambient conditions and is therefore particularly attractive for calculating mantle geotherms. Under the following

assumptions thermal conductivity can be approximated for mantle conditions: (1) K'_0 , the pressure derivative of the isothermal bulk modulus K_T , is constant: $K'_0=dK_T/dP=const$; (2) the variations of the bulk modulus as a function of temperature and pressure are mutually independent; (3) the pressure derivative of the thermodynamic Grüneisen parameter γ (cf. section 8.1.1) is constant: $d\gamma/dP=f$. For mantle substances, γ varies from 1 – 1.4, K'_0 from 4 – 5, and the constant vanishes approximately, $f \approx 0$ [1999Hof]. Within the uncertainty of these parameters, thermal conductivity under mantle condition is given by Hofmeister [1999Hof] as:

$$\lambda(T, P) = \lambda_{298 K, 1 atm} \left(\frac{298}{T} \right)^a \exp \left[- (4\gamma + 1/3) \int_{298}^T \alpha(\theta) d\theta \right] \left(1 + \frac{K'_0 P}{K_T} \right) + \lambda_r, \quad (8.60)$$

where $\lambda_{298 K, 1 atm}$ is the thermal conductivity at ambient conditions, $\alpha(T)$ the volume coefficient of thermal expansion as a function of temperature, and a is a fitting parameter. The radiative contribution λ_r may be approximated by eq. (8.59). Alternatively, Hofmeister [1999Hof] provides expressions for λ_r (in $W m^{-1} K^{-1}$) for ferrous minerals or dense silicates and oxides (Fig. 8.24):

$$\begin{aligned} \lambda_r &= 0.01753 - 1.0365 \times 10^{-4} T + 2.2451 \times 10^{-7} T^2 - 3.407 \times 10^{-11} T^3 \quad (\text{ferrous minerals}) \\ \lambda_r &= 8.5 \times 10^{-11} T^3 \quad (\text{dense silicates and oxides}). \end{aligned} \quad (8.61)$$

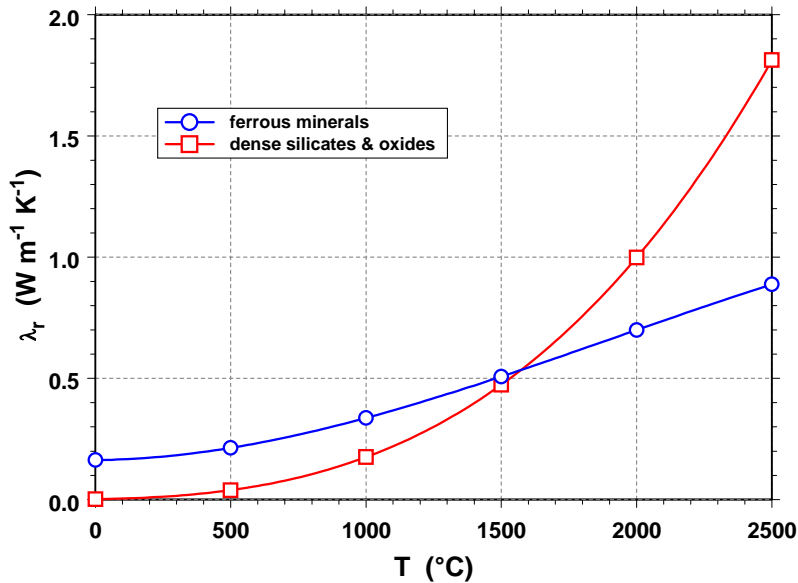


Fig. 8.24 Variation of radiative thermal conductivity λ_r of ferrous minerals, dense silicates, and oxides with temperature according to eq. (8.61) [1999Hof].

8.2 Geothermal Energy Resources

Geothermal energy is generally defined as the heat stored in the Earth (and its internal fluids) [e.g. 2000Ano; 2000Rog]. This comprises the heat stored both in the solid rock and in the fluids of its voids, and distinguishes it from heat stored in surface water bodies such as rivers, lakes and oceans. This definition disregards whether the heat stored in the Earth is generated by internal or external sources. While such a distinction is sometimes proposed for various reasons (mostly with regard to solar heat stored at shallow depth), the origin of the geothermal resource is of no importance at all to its use: It is where the heat is stored which defines how it can be mined and used. Apart from this, the overwhelming part of geothermal heat is of internal origin anyway, as discussed in section 8.1.2.

Four types of geothermal resources are usually distinguished [1997Moc; 2000Rog]:

- *hydrothermal*: hot water or steam at moderate depth (i. e. 1 km – 4 km) with temperatures of up to 350 °C in a permeable region of porous rock with active free or forced convection systems;
- *geopressed*: hot, high-pressure reservoir brines containing dissolved natural gas (methane). Their energy content is about 58 % thermal, 32 % hydrocarbon chemical, and 10 % hydraulic, at best;
- *hot dry rock (HDR)*: systems where fluids are not produced spontaneously. Therefore these systems require stimulation before energy can be extracted. They may occur within or at the margins of active hydrothermal reservoirs or may be associated only with an elevated heat flow in a conduction-dominated geologic setting. The term *hot wet rock* was suggested for cases where significant porosity and natural water are present in open fractures or permeable rock. More recently the term *enhanced geothermal systems (EGS)* was introduced to describe all different types of low-permeability reservoirs which require permeability enhancement prior to heat production;
- *magma*: molten rock at temperatures of 700 °C – 1200 °C at accessible depth (about < 7 km).

It is customary to classify energy resources according to the scheme proposed initially by McKelvey [1967McK] for mineral resources (Fig. 8.25). It accounts for the varying degrees of geological assurance and economic feasibility (or time prior to a commercial production).

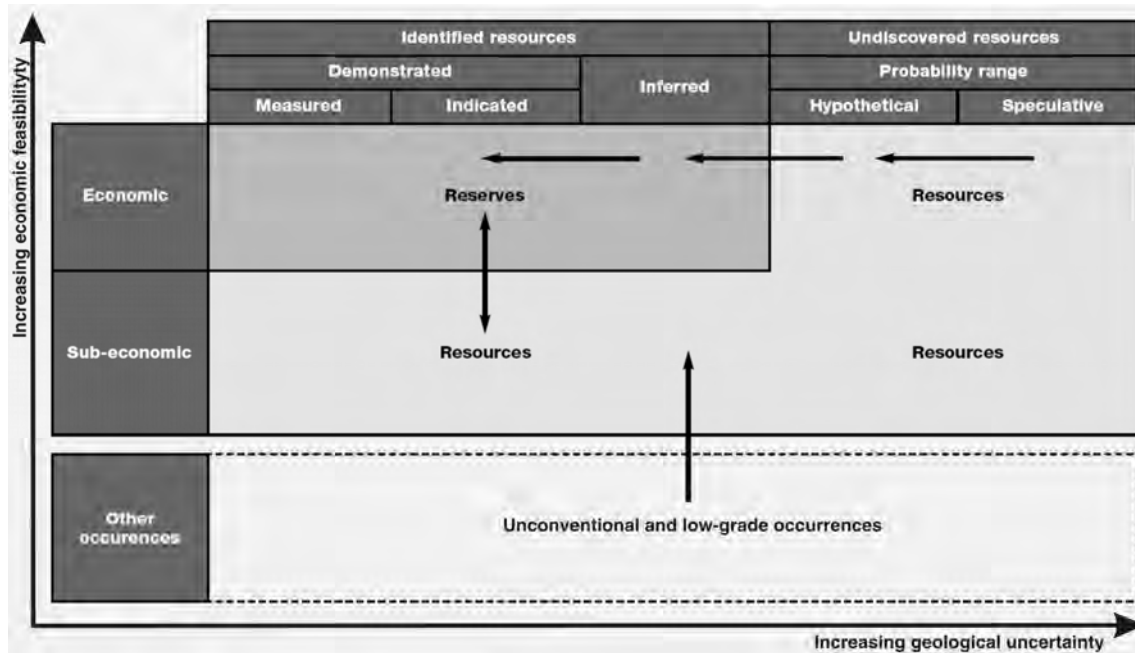


Fig. 8.25 McKelvey-diagram [1967McK] for classifying resources (modified after [2000Rog]).

Thus, geothermal *resources* are defined as the fraction of the accessible resource base or “heat in place” which could be produced at a price which will become competitive with other types of energy within a reasonable period of time [1978Muf]. Geothermal *reserves*, in contrast, are the fraction of the resources which will become economical in a much nearer future. Table 8.17 shows a classification of geothermal resources and an estimate of their global potential.

Table 8.17 Definition of geothermal resource categories and their estimated global potential (after [2000Rog]).

Resource category	Energy (EJ)
<i>Accessible resource base</i> (heat in place: amount of heat which can be produced theoretically from the topmost 5 km)	140,000,000
<i>Useful accessible resource base</i>	600,000
<i>Resources</i> (fraction of the accessible resource base which is expected to become economical within 40-50 years)	5,000
<i>Reserves</i> (fraction of the accessible resource base which is expected to become economical within 10-20 years)	500

Different recent estimates of the accessible geothermal resource base vary between 140,000,000 EJ [2000Rog] and about 117,000,000 EJ [1997Moc], i.e. by less than 20 %. Table 8.18 shows that it is available world-wide. Only about 4 ‰ of this huge resource base is considered as useful and accessible, and of this again only about 1 % are considered as resources. Finally, 10 % of the resources, i.e. their most accessible part, are considered as reserves. Tiny as this might appear, this amount exceeds the global annual primary energy consumption of 420 EJ in the year 2001 [2003IEA]. Therefore, and for its widespread availability on our planet at any time of the day and the year, “the technological ability to use geothermal energy, not its quantity, will determine its future share” [2000Rog].

Table 8.18 Accessible geothermal resource base by region (after [2000Rog]).

Region	Energy (EJ)	Percentage of world total
North America	26,000,000	18.6
Latin America and Caribbean	26,000,000	18.6
Western Europe	7,000,000	5.0
Eastern Europe and former Soviet Union	23,000,000	16.4
Middle East and North Africa	6,000,000	4.2
Sub-Saharan Africa	17,000,000	12.1
Pacific Asia (excl. China)	11,000,000	7.9
China	11,000,000	7.9
Central and South Asia	13,000,000	9.3
<i>Total</i>	<i>140,000,000</i>	<i>100.0</i>

Pre-Print from:

Clauser, C., 2006. Geothermal Energy, In: K. Heinloth (ed), *Landolt-Börnstein, Group VIII: Advanced Materials and Technologies, Vol. 3: Energy Technologies, Subvol. C: Renewable Energies*, Springer Verlag, Heidelberg-Berlin, 493-604.

8.3 Types of Geothermal Energy Use

Geothermal energy can be used directly, i. e. without any further conversion, as heat. The direct application of geothermal heat is referred to as *direct use*. Alternatively, geothermal heat can be converted into other types of energy at the expense of some energy for the conversion. *Electric power generation* requires conversion into electricity. Direct use exploits the resource more efficiently than power generation as no energy is lost during conversion of heat into electricity. However, heat cannot be transmitted over distances of more than some kilometers at most without a notable reduction of efficiency due to inevitable heat losses. There has been a long tradition of direct use of geothermal heat in various human cultures over several millennia, mostly associated with (but not restricted to) hot springs. Although there is no exact starting date for the direct use of geothermal heat, it is well known when geothermal heat was supplied to a large-scale municipal district heating system for the first time: in Iceland in the year 1930 [2001Fri]. Since then, Iceland has become independent of fossil fuels for heating, eliminating the serious prior pollution problems related to the burning of black coal in winter. In contrast to direct use, it is exactly known where and when geothermal heat was first converted into electric power: in Lardarello, Italy, in the year 1904, a century ago when the engineer Count Piero Ginori Conti succeeded in producing sufficient electricity from geothermal steam to power five electric light bulbs.

Different technologies are used to produce geothermal heat. They are based on either heat conduction or advection: (1) In conductive heat production, heat diffuses into an isolated underground heat exchange system without any exchange of substance (see sections 8.3.1.1.1 and 8.4.1.1). This technique is employed in direct use, predominantly for shallow heat production systems. (2) Advective heat production is based on the production of hot fluids, mostly brines, from underground reservoirs at appropriate depths (see sections 8.3.1.1.2 and 8.3.2). This technique is used both for direct use (see section 8.4.1.2) and power generation in low enthalpy¹ and medium or high enthalpy fields (see section 8.4.2.1), respectively, depending on the temperature of the produced fluids (Table 8.19).

Table 8.19 Classification of geothermal reservoirs (after [2002Bar]).

Type	Resource	Temperature range (°C)	Energy content
Water dominated	Warm water	< 100	Low enthalpy
	Wet steam	100 - 150	Medium enthalpy
Vapor dominated	Dry steam	> 150	High enthalpy

Of approximately 100 hydrothermal systems studied worldwide, less than 10 % are vapor dominated dry steam fields, 60 % are water dominated wet steam fields, and 30 % produce hot water [2002Bar].

8.3.1 Direct Use

In direct use geothermal energy is employed directly as heat without further conversion in other types of energy. By the year 2005, the global annual production of direct use geothermal energy amounted to 72,622 GW h or 261 PJ [2005Lun]. Large as this figure may appear, it amounts to just about one percent of the primary energy consumption of 14,319 PJ in a medium sized, developed industrial country like Germany in the year 2002 [2004BMW]. Fig. 8.26 shows, on a logarithmic scale, the contribution of the top 55 countries to the global production of direct use geothermal heat. As direct use is most attractive in moderate to cold climates, the territory of most of these countries lies in this region, at least in part. It is notable that the Peoples Republic of China, a developing and emerging industrial country, is the top producer ahead of the USA, Iceland (where nationwide heat production is almost exclusively geothermal), and a dynamically developing Turkey. More than half of the global direct geothermal heat in the year 2000 was produced in these four countries alone.

¹ Enthalpy $H = E + PV$, where E is internal energy, P pressure and V volume, see Sect. 8.1.4.

The extent to which the available installed geothermal capacity is being used to its full potential is expressed by the capacity factor, the ratio of energy produced per year versus maximum possible annual production. With regard to this capacity factor Fig. 8.26 and Table 8.20 illustrate that the top five producers of direct use geothermal heat, the People’s Republic of China, Sweden, the USA, Iceland, and Turkey used between just 13 % and 53 % of the capacity installed in the year 2005. These numbers suggest that an increase in direct use would be possible here without installation of any new capacity. Whether this can be really implemented, however, cannot be predicted without a detailed analysis of the reasons for the comparatively low capacity factors. However, as these five countries comprise 60 % of the global direct geothermal heat production, an increased use of their installed capacity would increase the

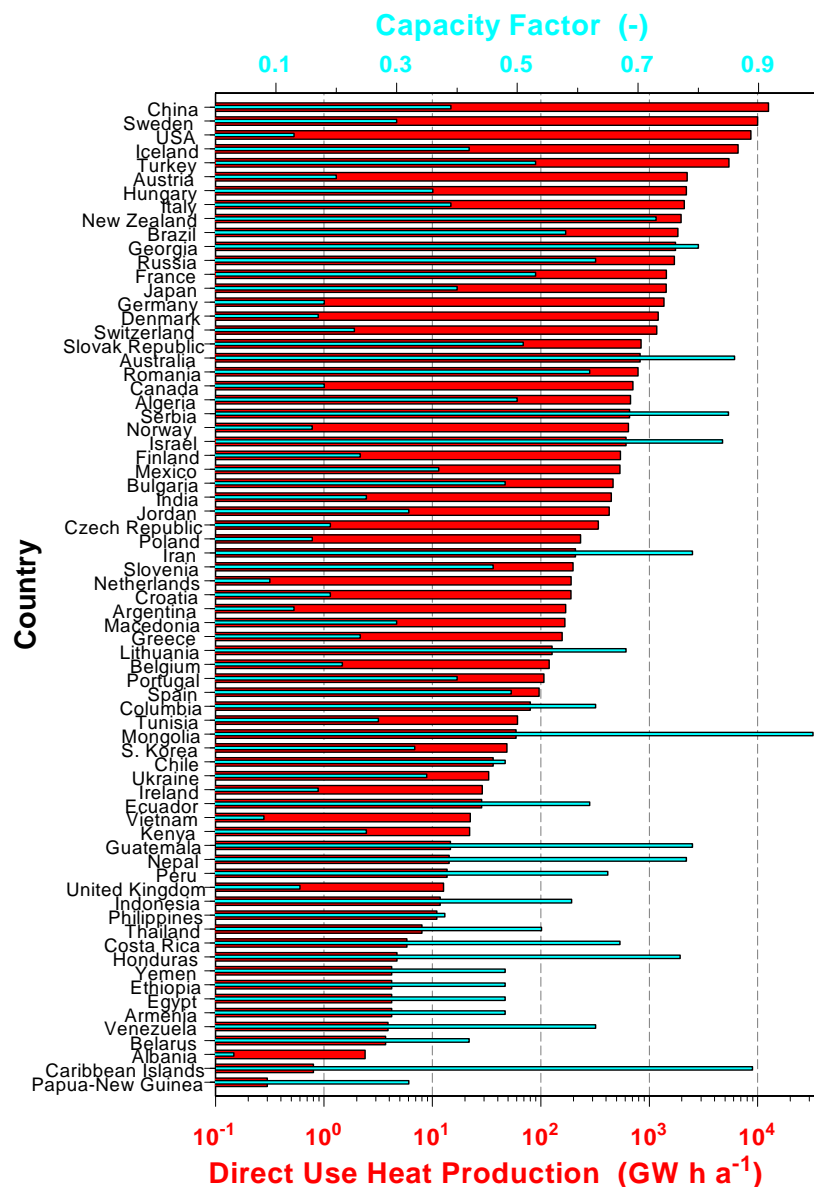


Fig. 8.26 National contributions to the global annual production of about 261 PJ (72.6 TW h) of direct use geothermal heat (big red bars) and capacity factors (energy produced vs. year-round energy production at full capacity; slim blue bars) by the year 2005 (data: see

Table 8.20).

Table 8.20 Installed capacity and direct use geothermal heat production in 71 countries (data: [2005Lun]; for Germany: [2005Sch] and own calculations, see Table 8.21).

Country	Capacity (MW _t)	Direct Use Heat production		Capacity Factor (-)
		(TJ a ⁻¹)	(GW h a ⁻¹)	
Albania	9.6	8.5	2.4	0.03
Algeria	152.3	2,417.0	671.4	0.50
Argentina	149.9	609.1	169.2	0.13
Armenia	1.0	15.0	4.2	0.48
Australia	109.5	2,968.0	824.5	0.86
Austria	352.0	352.0	2,229.9	0.20
Belarus	1.0	13.3	3.7	0.42
Belgium	63.9	431.2	119.8	0.21
Brazil	360.1	6,622.4	1,839.7	0.58
Bulgaria	109.6	1,671.5	464.3	0.48
Canada	461.0	2,546.0	707.3	0.18
Caribbean Islands	0.1	2.8	0.8	0.89
Chile	8.7	131.1	36.4	0.48
China	3,687.0	45,373.0	12,604.6	0.39
Columbia	14.4	287.0	79.7	0.63
Costa Rica	1.0	21.0	5.8	0.67
Croatia	114.0	681.7	189.4	0.19
Czech Republic	204.5	1,220.0	338.9	0.19
Denmark	821.2	4,360.0	1,211.2	0.17
Ecuador	5.2	102.4	28.4	0.62
Egypt	1.0	15.0	4.2	0.48
Ethiopia	1.0	15.0	4.2	0.48
Finland	260.0	1,950.0	541.7	0.24
France	308.0	5,195.7	1,443.4	0.53
Georgia	250.0	6,307.0	1,752.1	0.80
Germany	884.6	4,922.0	1,368.3	0.18
Greece	74.8	567.2	157.6	0.24
Guatemala	2.1	52.5	14.6	0.79
Honduras	0.7	17.0	4.7	0.77
Hungary	694.2	7,939.8	2,205.7	0.36
Iceland	1,791.0	23,813.0	6,615.3	0.42
India	203.0	1,606.3	446.2	0.25
Indonesia	2.3	42.6	11.8	0.59
Iran	30.1	752.3	209.0	0.79
Ireland	20.0	104.1	28.9	0.17
Israel	82.4	2,193.0	609.2	0.84
Italy	606.6	7,554.0	2,098.5	0.39
Japan	413.4	5,161.1	1,433.8	0.40
Jordan	153.3	1,540.0	427.8	0.32
Kenya	10.0	79.1	22.0	0.25
S. Korea	16.9	175.2	48.7	0.33
Lithuania	21.3	458.0	127.2	0.68
Macedonia	62.3	598.6	166.3	0.30
Mexico	164.7	1,931.8	536.7	0.37
Mongolia	6.8	213.2	59.2	0.99
Nepal	2.1	51.4	14.3	0.78
Netherlands	253.5	685.0	190.3	0.09
New Zealand	308.1	7,086.0	1,968.5	0.73
Norway	450.0	2,314.0	642.8	0.16
Papua-New Guinea	0.1	1.0	0.3	0.32
Peru	2.4	49.0	13.6	0.65
Philippines	3.3	39.5	11.0	0.38
Poland	170.9	838.3	232.9	0.16
Portugal	30.6	385.3	107.0	0.40
Romania	145.1	2,841.0	789.2	0.62
Russia	308.2	6,143.5	1,706.7	0.63

Country	Capacity (MW _t)	Direct Use Heat production		Capacity Factor (-)
		(TJ a ⁻¹)	(GW h a ⁻¹)	
Serbia	88.8	2,375.0	659.8	0.85
Slovak Republic	187.7	3,034.0	842.8	0.51
Slovenia	48.6	712.5	197.9	0.46
Spain	22.3	347.2	96.5	0.49
Sweden	3,840.0	36,000.0	10,000.8	0.30
Switzerland	581.6	4,229.3	1,174.9	0.23
Thailand	1.7	28.7	8.0	0.54
Tunisia	25.4	219.1	60.9	0.27
Turkey	1,177.0	19,623.1	5,451.3	0.53
Ukraine	10.9	118.8	33.0	0.35
United Kingdom	10.2	45.6	12.7	0.14
USA	7,817.4	31,239.0	8,678.2	0.13
Venezuela	0.7	14.0	3.9	0.63
Vietnam	30.7	80.5	22.4	0.08
Yemen	1.0	15.0	4.2	0.48
TOTAL	27,824.8	261,418.0	72,621.9	0.30

global production significantly. In contrast, in countries with comparatively large capacity factors, a significant increase in direct use geothermal heat production requires new facilities.

8.3.1.1 Space Heating

In moderate and cold climates most of the national final energy is consumed as heat. As an example, we find that in Germany in the year 2002 about 58 % of the national final energy was consumed for space heating, process heat, and hot water (Fig. 8.27). Thus it appears that a huge market should be available for direct use geothermal heat. However, two main obstacles may prevent the use of geothermal heat: (1) In many places heat is available as abundant waste heat, e.g. from thermal power stations. This limits the price that can be obtained on the market. Also, market penetration for geothermal heat may be difficult if the current demand is already satisfied by existing sources. (2) Heat cannot be transported over long distances from the point of production to the end-user, unless a grid of well insulated pipelines is in place

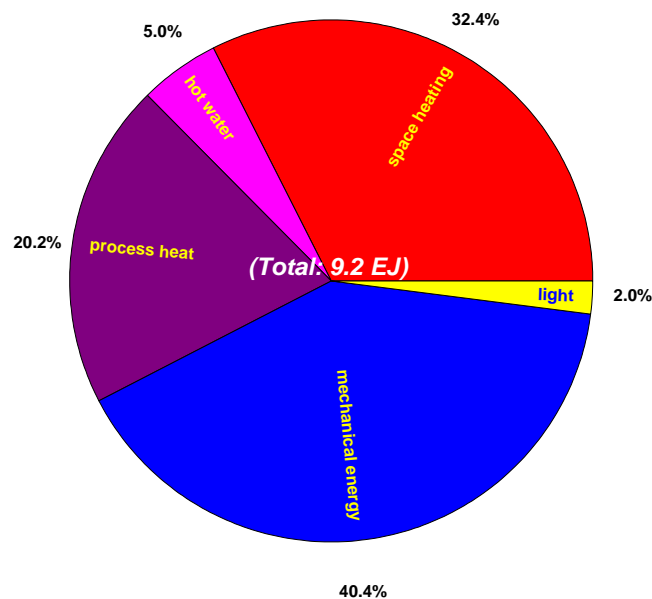


Fig. 8.27 Consumption of final energy in Germany in 2002; Data: [2003VDE; 2004BMW].

which can be fed with geothermal heat. Installing a grid exclusively for direct use geothermal heat often turns out to be prohibitively expensive. If, in contrast, heat supply systems are planned for new buildings they can be optimized for direct geothermal use. In these cases geothermal heat may be supplied at a competitive price based on proven and reliable technology: ground-source heat pumps, used primarily for heating (and cooling) of individual buildings, and hydrothermal heating plants for providing heat to municipal district heating systems.

8.3.1.1.1 Earth Coupled Heat Extraction Systems

There is variety of different Earth coupled heat extraction systems. All have in common that they extract heat by diffusion only – there is no need to produce groundwater or fluids from deeper reservoirs. There are shallow and deep systems of this kind, consisting of one or several shallow or deep pipe systems in which a heat exchange fluid is circulated which is not in direct contact with the ground or rock. Heat diffuses into these systems across the pipe system from the outside ground or rock [2001Dic; 2003Lun^a].

Horizontal Earth coupled heat exchangers (Fig. 8.28) are pipe systems buried in the ground below the freezing depth. They can be used wherever there is sufficient surface area available for their installation. Therefore they are more rarely installed for space heating and cooling of buildings than vertical borehole heat exchangers.

Shallow borehole heat exchangers (Fig. 8.29) commonly consist of one or several U-pipes (Fig. 8.30) installed and backfilled in a borehole, the most frequent configuration consisting of two U-pipes arranged at an angle of 90°. Alternatively, coaxial pipe arrangements are also used, but more frequently for deeper boreholes (Fig. 8.30). Shallow borehole heat exchangers are installed in boreholes with depths varying between about 50 m – 250 m. In all shallow systems, heat exchangers extract heat from the isolated primary circulation within the U-pipes or horizontal pipe systems and transmit it into a secondary circuit. As a rule, shallow systems additionally require a heat pump to obtain suitable input temperatures. Depending on the type of domestic heating system, input temperatures vary between about 40 °C – 70 °C for surface heating elements (floor, wall, ceiling) or conventional radiators, respectively. Per unit length, shallow borehole heat exchangers typically possess a specific power of about 40 W m⁻¹ – 55 W m⁻¹ ± 16 W m⁻¹ [1999Kal; 2001Ano^a; 2003Cla^b].



Fig. 8.28 Horizontal Earth coupled heat exchanger system (after [1999Ano^a]; yellow box in building basement: heat pump).



Fig. 8.29 Vertical borehole heat exchanger system (after [1999Ano^a; yellow box in building basement: heat pump).

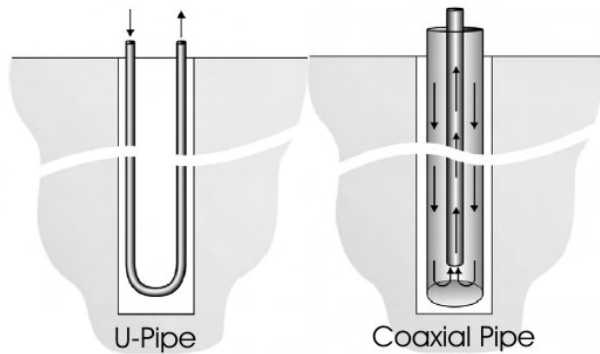


Fig. 8.30 Two common basic pipe arrangements used in borehole heat exchangers (after [2002Geh]).

performance of the system may be significantly improved. At the same time, the underground geothermal regime can recover more quickly during the warm season when no heating is required. Heating and cooling with Earth coupled heat pumps requires appropriate large-surface heat distribution systems in the buildings or structures because of the low supply temperature level. Although shallow borehole heat exchangers can be installed in nearly any type of subsurface, soft (sedimentary) rocks are generally more easy (and less expensive) to drill than hard (basement) rocks, from a technical point of view. Also, in porous and fractured rocks heat may flow to the borehole not only by diffusion but also by advection in a regional groundwater flow field. This can improve the thermal yield of a ground-source heat pump significantly.

Since they do not require any particular thermal anomaly, ground-source heat pumps represent a geothermal heat production technology which is suitable even for regions with altogether ordinary geothermal conditions. This is illustrated by the examples of Sweden, Switzerland, and Austria, three countries without significant geothermal anomalies in cold to moderate climate, but with an impressive annual per capita heat production from ground-source heat pumps (Table 8.21). The corresponding installed thermal power puts Sweden, after Iceland, on rank 2 in the list of per capita installed direct use geothermal power, and Switzerland, Austria, and Germany on ranks 4, 5, and 9.

Table 8.21 Top producers of geothermal heat by ground-source heat pumps (data: [2003Lun^a; 2004Sig^b; 2004BWP] and own calculations).

Country, population (10 ⁶)	Number of ground-source heat pumps	Annual heat production (TJ)	Installed power (MW _{th})	Per capita annual heat production (MJ)
Sweden, 9	200,000	28,800	2,000	3200
USA, 294	500,000	13,392	3,720	46
Germany, 82	51,000	4,212	780	51
Canada, 32	36,000	1,080	435	34
Switzerland, 7	27,500	2,268	420	324
Austria, 8	23,000	1,332	275	167

Heat exchanger piles (Fig. 8.31) are relatively recent developments: Heat exchanger pipe systems integrated directly into the concrete foundations of buildings and other constructions for heating and cooling. If properly designed and integrated into a combined heating and cooling system right from the beginning, these systems can be a useful part of modern low-energy, low CO₂-emission buildings and constructions. Depending on the size of the buildings or structures, the installed power may range from 10 kW – 800 kW for small houses and large industrial buildings, respectively [2002Vua^a]. These integrated systems are usually connected to a heat pump. Like for other Earth coupled heat exchangers, their specific power de-

The uncertainty of $\pm 30\%$ is primarily due to the natural variability of thermal rock properties, mainly of thermal conductivity or diffusivity. Since these systems are coupled to a heat pump, they can be used for both heating and cooling of buildings, depending on whether the Earth or the building is the heat source. Cooling buildings with ground-source heat pumps in the summer, while heating the same building with the same systems in winter is becoming increasingly attractive. This can be achieved if heat from the building can be fed into the cooler subsurface during the warm season, i.e. if the underground temperature is lower than that of the fluid circulation. This way, the economical perfor-

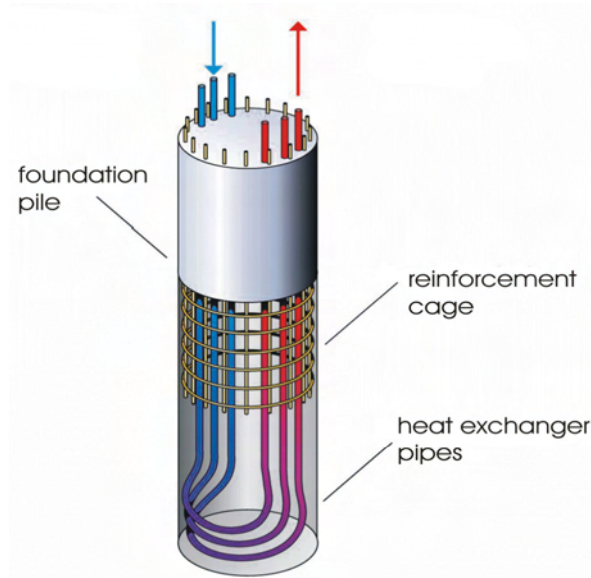


Fig. 8.31 Heat exchanger piles: Earth coupled heat exchanger pipe systems integrated in building foundation piles (after [2004Von^b]).

Zürich is heated in winter and cooled in summer using heat exchanger piles integrated in 315 foundation pillars of 30 m length and diameters of 0.9 m – 1.5 m. The associated heating and cooling energy is 470 MW h and 1,100 MW h, respectively.

While statistical data on this type of direct use is scarce – for instance 7 MW of installed power are reported for Switzerland by the year 2004 [2004Sig^b] – its potential is significant. By the end of the year 2002, more than 380 such systems were reported to have been in operation in Austria, Germany, and Switzerland [2002Vua^a]. Many more applications are conceivable for all kinds of buildings with deep foundations, in particular high-rise buildings and towers, bridges etc.. Obviously, an intensified use of these integrated systems for modern low-energy, low-carbon dioxide emission buildings requires both an increased awareness of the available technological options on the part of planners, architects, and developers, and a close cooperation between construction companies and specialists in space heating and cooling systems on the one hand and in Earth coupled heat production systems on the other hand.

Deep borehole heat exchangers have been installed to depths of about 1500 m – 3000 m and maximum temperatures of about 60 °C – 110 °C [e.g. 1999Wet; 2002Koh]. In contrast to shallow borehole heat exchangers, U-pipes cannot be used here anymore due to the much greater depth of the boreholes. Instead, these systems consist of a coaxial arrangement of an inner production pipe inserted into an outer borehole casing. Water flows down the annulus of this coaxial system and up again in a central production pipe. In order to minimize heat losses, the production pipe needs to be insulated where the production temperature exceeds the ambient rock temperature. The available operational data from the small number of currently operating deep borehole heat exchangers indicate a specific power of about 20 W m⁻¹ – 54 W m⁻¹, similar to that of shallow systems [1999Wet; 2002Koh]. However, recent studies suggest that currently operating deep borehole heat exchangers may be under-exploiting the available resource significantly [2002Koh]: Based on detailed numerical simulations calibrated on operational data from an existing system they conclude that a specific power of at least 85 W m⁻¹ can be reached for a system with a depth of 2300 m, corresponding to an installed power of about 200 kW.

depends on the flow rate, the temperature difference between inflow and outflow of the heat exchange fluid (a function of the flow rate as well), the thermal properties of the ground, and the amount of heat advection due to groundwater flow. Depending on local conditions and pile diameters, values reported for specific power per meter of foundation pile range between 20 W m⁻¹ – 75 W m⁻¹ [2004Von^b].

Similar types of heat exchangers can also be integrated in other concrete constructions, such as concrete floors, ceilings and walls. A combined use of these different types of heat exchangers was recently realized in Vienna for heating and cooling of the “Schottenring” subway station [2004Von^a] where they were integrated in concrete floors and foundation piles. Here, the maximum specific power per square meter of heat exchange surface of all systems exceeds 40 W m⁻². The annual average specific power of about 13 W m⁻² is accordingly lower than this maximum value, corresponding to an average annual heating and cooling energy of about 170 MW h and 120 MW h, respectively.

A large new terminal building of the airport in

As with shallow systems, the heat of the primary circulation within the deep borehole is transferred to a secondary circuit by a heat exchanger. Deep systems often do not require a heat pump due to their higher output temperature. Heat can be fed directly into the building's space heating system or into a local heat distribution system via the heat exchanger. Sometimes, however, a heat pump is used additionally. Without additional shallow boreholes, cooling cannot be provided by most deep borehole heat exchangers: Their elevated production temperatures preclude their use for space cooling.

8.3.1.1.2 Hydrothermal Heating Systems

Hydrothermal heating systems consist of one or several, usually deep, boreholes for producing (and injecting) water from aquifers or deep reservoirs. Shallow systems are referred to as *groundwater heat pumps* (Fig. 8.32), deep systems as *hydrothermal heating plants* (Fig. 8.33). While there is a variety of different configurations for hydrothermal heating plants, all have in common that hot water or brine is produced and cooled at the surface. Unless it can be further used or discharged into surface waters, the cooled water is injected back into a subsurface reservoir or aquifer. In some countries there are legal thresholds with respect to the permitted heating of the affected aquifer. In the surface unit, heat is extracted from the produced hot water or brine in a heat exchanger and fed into a secondary distribution circuit. Sometimes a heat pump is also switched into the secondary circuit at an appropriate position. In groundwater heat pump installations this is the rule. There are systems which use one single well for fluid production and injection from a deep and into a shallower reservoir, respectively, but most are doublet installations consisting of two boreholes, one for production and one for injection (Fig. 8.32, Fig. 8.33). A sufficient minimum offset between the two well bottoms prevents a thermal short circuit during the installation's life time, commonly 20 – 30 years. For hydrothermal heating plants, this offset is often on the order of 10^3 m. Frequently the two wellheads are equally offset. However, sometimes it may be attractive or even necessary to drill both boreholes from the same platform and deviate one or both of them.

In contrast to conductive heat production by ground-source heat pumps, advective heat production by hydrothermal heating systems requires producing large volumes of hot fluid. Therefore, the most critical properties are hydraulic permeability, reservoir porosity and thickness (see sections 8.1.5.3 and 8.4.1.2;

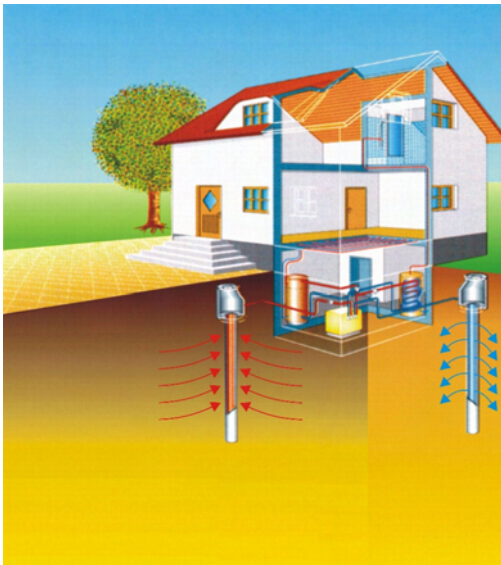


Fig. 8.32 Groundwater heat pump system (after [1999Ano^a]; yellow box in building basement: heat pump).

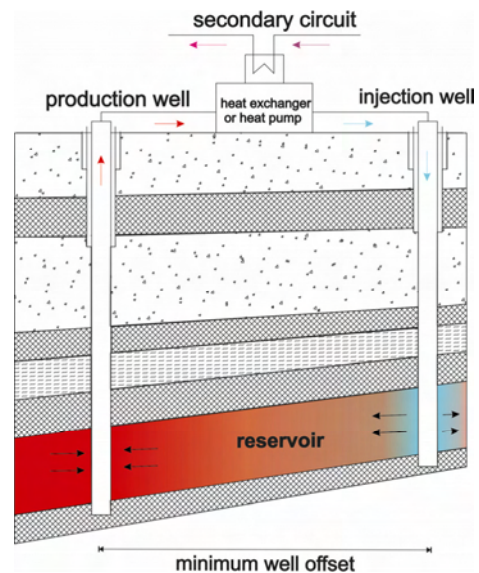


Fig. 8.33 Hydrothermal heating plant (doublet installation; after Geothermie Neubrandenburg GmbH).

sometimes transmissivity, the product of reservoir thickness and hydraulic conductivity, is used as a lumped property to characterize reservoirs). Accordingly, almost all hydrothermal heating systems are placed in sedimentary rocks, often in sedimentary basins. Sedimentary basins, such as the Pannonian and Paris basins or the Rhine Graben in Europe, frequently display geothermal anomalies (see e.g. [2002Hur]). Placing these systems into geothermal anomalies can help to reduce drilling depth to the desired temperature. This ranges usually from about 60 °C – 100 °C for these low enthalpy heat production systems (cf. Table 8.19). A reduced drilling depth can be crucial for the economic feasibility of hydrothermal heating plants as drilling cost amounts to at least half of the final turnkey investment cost [1999Kay] (see also section 8.4.1.2).

8.3.1.2 Commercial and Industrial Applications

Direct use geothermal energy may be both cost effective and reliable in industrial applications. Some industries use steam or superheated water, while agriculture and aquaculture require lower temperature geothermal fluids. At present, the largest industrial applications are in pulp, paper and wood processing. Examples include timber processing in New Zealand, a diatomaceous earth plant in Iceland, a vegetable dehydration plant in the United States, and industrial water in Romania [2004Wor]. Other applications currently operating or studied for feasibility include [1992Ste^a; 2000Rag; 2001Fri; 2001Lun; 2002Bar; 2003Lie; 2003Lun^b; 2003Raf^b; 2004Wor]:

- Hydrogen production by high-temperature steam hydrolysis operating at 800 °C – 1000 °C;
- hot-dip galvanizing of metals (a chemical process used to coat steel or iron with zinc by passing the steel through a molten bath of zinc at a temperature of around 450 °C);
- diatomite (kieselguhr) production (requiring steam for heating and drying);
- salt production from seawater (requiring steam for evaporation and drying);
- timber drying;
- seaweed and kelp processing (requiring hot water at about 110 °C);
- fat-liquoring and drying in the tanning process of leather; fat-liquoring is introducing oil into the skin prior to drying to replace the natural oils lost during processing (usually performed at temperatures of 60 °C – 66 °C);
- thermal distillation desalination driven by low enthalpy (52°C – 76 °C) geothermal resources;
- geothermal water (48 °C – 79 °C) used for washing in wool mills and for dyeing cloth;
- production of chemicals as a by-product of heat production from geothermal brines.

Next to process heat, direct use geothermal heat is also successfully used for [2003Pop^b; 2003Raf^a]:

- heating of swimming pools;
- heating of greenhouses;
- heating of fish and turtle aquaculture pools to increase productivity;
- melting of snow and ice on sports fields, bridges, and roads;
- air conditioning and refrigeration by absorption or adsorption cooling.

Table 8.22 summarizes a variety of geothermal direct use applications and the associated temperatures. In applications which require high conversion efficiencies to reach economic feasibility, the concept of cascaded use has been introduced, i. e. the serial connection of several direct use applications on successively lower temperature levels. This way the resource can be exploited much more effectively and therefore the efficiency can be increased significantly.

To what extent these commercial and industrial applications can contribute to the national energy supply may be illustrated using the example of Iceland. There geothermal energy provides 50 % of the country's annual primary energy consumption of about 120 PJ, corresponding to 434 GJ per capita – higher than in any other country [2000Rag]. A total of 20 PJ, nearly 17 % of this energy, is provided by direct use geo-

thermal heat. While about $\frac{3}{4}$ of this are consumed for space heating, the remaining $\frac{1}{4}$ is used in industrial and commercial applications. Traditionally, their energy demand would have been satisfied by fossil fuels. Therefore, substituting these with direct use geothermal heat helps not only to reduce the need to import hydrocarbons, but also to reduce the emission of the greenhouse gas carbon dioxide to the atmosphere.

Table 8.22 Commercial and industrial applications of geothermal direct use and associated temperatures (after [2002Bar; 2004Wor]).

T (°C)	Process
180	evaporation of highly concentrated solutions refrigeration by ammonia absorption digestion in paper pulp
170	heavy water via hydrogen sulfide process drying of diatomaceous earth digestion of paper pulp
160	drying of fish meal drying of timber
150	alumina via Bayer's process
140	drying farm products at high rates canning of food
130	evaporation in sugar refining extraction of salts by evaporation and crystallization fresh water by distillation
120	most multi-effect evaporation concentration of saline solution
110	drying and curing of light aggregate cement slabs
100	drying of organic materials (seaweed, grass, vegetables, etc.) washing and drying of wool
90	drying of stock fish intense de-icing operations
80	space-heating (buildings and greenhouses)
70	refrigeration (lower temperature limit)
60	animal husbandry greenhouses by combined space and hotbed heating
50	mushroom growing balneology
40	soil warming swimming pools, biodegradation, fermentations warm water for year-round mining in cold climates
30	de-icing hatching of fish or turtles
20	fish farming

8.3.2 Power Generation

Geothermal power generation requires vapor to drive turbines. It can be derived as either wet or dry steam from natural reservoirs. In absence of natural steam reservoirs, steam can be also generated in hot dry rock (HDR) or enhanced geothermal systems (EGS) engineered in the subsurface. At a lower temperature level, vapor for driving turbines can be obtained alternatively by evaporating fluids with a lower boiling point than water. This process is known as Organic Rankine Cycle (ORC) because initially it involved organic compounds, such as toluol (C_7H_8), pentane (C_5H_{12}), propane (C_3H_8) or halogenated hydrocarbons. More recently, the so-called Kalina Cycle technology [1984Kal; 1989Wal] improves the efficiency of this process further by evaporating a mixture of water and ammonia (NH_3) over a finite temperature range rather than a pure fluid at a definite boiling point (see also section 8.4.2.2).

Wet and dry steam reservoirs are water and vapor dominated, respectively (Table 8.19). Wet steam fields contain pressurized water at temperatures above 100 °C and a smaller amount of steam in the shallower, lower-pressure parts of the reservoir. Hot, pressurized water is the dominant phase inside the reservoir. Vapor dominated, dry steam fields produce dry saturated or slightly super-heated steam at pressures above atmospheric. This steam has the highest enthalpy (energy content), generally close to 2.8 MJ kg^{-1} . Dry steam fields are less common than wet steam fields, but about half of the geothermal electric energy produced worldwide is generated in the six vapor dominated fields at Lardarello and Monte Amiata in *Italy*; The Geysers (California) in the *USA*; Matsukawa in *Japan*; and Kamojang and Darajat in *Indonesia* [2002Bar].

Examples of electric power producing wet steam fields are: Cerro Prieto, Los Azufres, and Los Humeros in *Mexico*; Momotombo in *Nicaragua*; Ahuachapán-Chipilapa in *El Salvador*; Miravalles in *Costa Rica*; Zunil in *Guatemala*; Wairakei, Ohaki, and Kawerau in *New Zealand*; Salton Sea, Coso, and Casa Diablo (California), Puna (Hawaii), Soda Lake, Steamboat Springs and Brady Hot Springs (Nevada), Cove Fort (Utah) in the *USA*; Dieng and Salak in *Indonesia*; Mak-Ban, Tiwi, Tongonan, Palinpinon, and Bac Man in the *Philippines*; Pauzhetskaya and Mutnovsky in *Russia*; Fang in *Thailand*; Kakkonda, Hatchobaru, and Mori in *Japan*; Olkaria in *Kenya*; Krafla in *Iceland*; Azores in *Portugal*; Kizildere in *Turkey*; Latera in *Italy*; Milos in *Greece*.

While geothermal power has been produced for a century, its development has been rather slow in the first half of this period: The first geothermal power plant was commissioned in 1913 in Lardarello, Italy with an installed capacity of 250 kW_e. Only about half a century later the next geothermal power plants were commissioned at Wairakei, New Zealand in 1958, an experimental plant at Pathe, Mexico in 1959, and The Geysers in the USA in 1960. Today, the Tuscan region around Lardarello is still the center of the Italian geothermal power production with an installed capacity of about 790 MW_e and a production of 5340 GW h_e in the year 2003 [2005Ber]. But new centers have emerged since, in particular in Asia and Central America (Table 8.23), so that by the year 2005 the total global installed capacity for geothermal electric energy production had reached a level of 8912 MW_e [2005Ber]. While this is just about the equivalent of 9 – 15 nuclear or large thermal power stations, the growth of geothermal power has been steady over the last decade at an impressive rate of 24 % or roughly 2 ½ % per year. Fig. 8.34 shows the capacity for geothermal electric energy production installed in 24 countries world-wide. The top two countries in this list, the USA and the Philippines, represent already half of the total installed capacity, the next three, Mexico, Indonesia, and Italy, another 29 % (see also Table 8.23).

In contrast to direct use, electric power production is not concentrated in countries of moderate to cold climates, but follows the availability of natural steam reservoirs. The next six countries on this list, Japan, New Zealand, Iceland, Costa Rica, El Salvador, and Kenya, contribute another 17 % to the global total installed capacity. The following 13 countries with less than 100 MW_e installed capacity each make up the remaining 4 %. However, Fig. 8.34 clearly shows that geothermal power production will become ever important both in some of the most important emerging economies, such as the Philippines, Mexico, and Indonesia, and in developing countries such as El Salvador, Costa Rica, Nicaragua, and Kenya. In

developed countries as well, such as Iceland, New Zealand, Italy, and the USA, geothermal production of electric energy has reached and maintained a level between 16 % – 0.5 % relative to the total national production (Fig. 8.35 and Table 8.23). Remarkable increases of 244 % and 182 % have been achieved since the year 2000 in Russia and Kenya, respectively, if only from an admittedly low level [2005Ber].

In emerging economies and developing countries geothermal electric power production is boosting the industrial development already today. Fig. 8.35 shows the geothermal contributions to the production of electric energy and the installed capacity for electric energy production [2005Ber] by the year 2005 for the same 24 countries as in Fig. 8.34: Here, Iceland is the only developed country among the top five with respect to both criteria, the others being developing or emerging economies. In these five countries, more than 10 % of the produced electricity is geothermal. It cannot be over-estimated how beneficial an increased independence from imported hydrocarbons is on the national budgets of developing or emerging economies in countries which are in general not among the oil or gas producers. Additionally, due to low emission of greenhouse gases during geothermal energy production, geothermal electric energy is a serious alternative to consider with respect to a reduction of greenhouse-gas emissions to the atmosphere (see section 8.4.2.4.3 for more details).

Table 8.23 Geothermal electric capacity and energy production in 24 countries, as well as corresponding fractions of the total national capacity and energy production, and the world geothermal electric capacity and energy production of 8912 MW_e and 56.8 TW h (204.5 PJ), respectively, in the year 2005 (data: [2005Ber]); highlighted in color: major contributions to national (green) and world (blue) capacity and energy.

Country	Installed Capacity (MW)	Running Capacity (MW)	Energy Produced (GW h a ⁻¹)	Number of Units	% Natl. Capacity	% World Capacity	% Natl. Energy	% World Energy
Australia	0.2	0.1	0.5	1	negligible	negligible	negligible	0.001
Austria	1	1	3.2	2	negligible	negligible	negligible	0.006
China (Tibet)	28	19	95.7	13	30.0	0.314	30.0	0.168
Costa Rica	163	163	1145.0	5	8.4	1.829	15.0	2.016
El Salvador	151	119	967.0	5	14.0	1.694	24.0	1.703
Ethiopia	7	7	–	1	1.0	0.078	–	–
France (Guadeloupe isl.)	15	15	102.0	2	9.0	0.168	9.0	0.180
Germany	0.2	0.2	1.5	1	negligible	negligible	negligible	0.003
Guatemala	33	29	212.0	8	1.7	0.370	3.0	0.373
Iceland	202	202	1406.0	19	13.7	2.267	16.0	2.475
Indonesia	797	838	6085.0	15	2.2	8.943	6.7	10.713
Italy	790	699	5340.0	32	1.0	8.864	1.9	9.402
Japan	535	530	3467.0	19	0.2	6.003	0.3	6.104
Kenya	127	127	1088.0	8	11.2	1.425	19.0	1.916
Mexico	953	953	6282.0	36	2.2	10.693	3.1	11.060
New Zealand	435	403	2774.0	33	5.5	4.881	7.1	4.884
Nicaragua	77	38	270.7	3	11.2	0.864	9.8	0.477
Papua-New Guinea (Lihir isl.)	6	6	17.0	1	10.9	0.067	–	0.0299
Philippines	1931	1838	9419.0	57	12.7	21.667	19.1	16.58
Portugal (San Miguel isl.)	16	13	90.0	5	25.0	0.179	–	0.158
Russia	79	79	85.0	11	negligible	0.886	negligible	0.150
Thailand	0.3	0.3	1.8	1	negligible	0.003	negligible	0.003
Turkey	20	18	105.0	1	negligible	0.224	negligible	0.185
USA	2544	1914	17840.0	189	0.3	28.546	0.5	31.410
TOTAL	8912	8010	56798.0	468	–	100.000	–	100.000

The HDR technology has been developed since the early 1970s in the US, Japan, France, Germany, the UK, and Sweden [1999Abe]. While current HDR research projects in Europe and Japan are being transformed into commercial demonstration installations, commercial projects are under way in Australia. In contrast to preceding scientific experimentation and demonstration installations, this new phase involves local and international power producers at a significant level. Although at present no HDR-

produced electricity is marketed yet, several commercial HDR installations are currently being planned and drilled, for instance in the Central European Rhine Graben and in Australia. They are expected to start producing electric power with an installed capacity of 3 MW – 15 MW within the period 2005 – 2010 [1999Ano^b; 2002Vua^b; 2003Ano^a; 2003Ano^c]. If successful, this technology has a great potential for producing geothermal electric energy in regions without natural steam reservoirs.

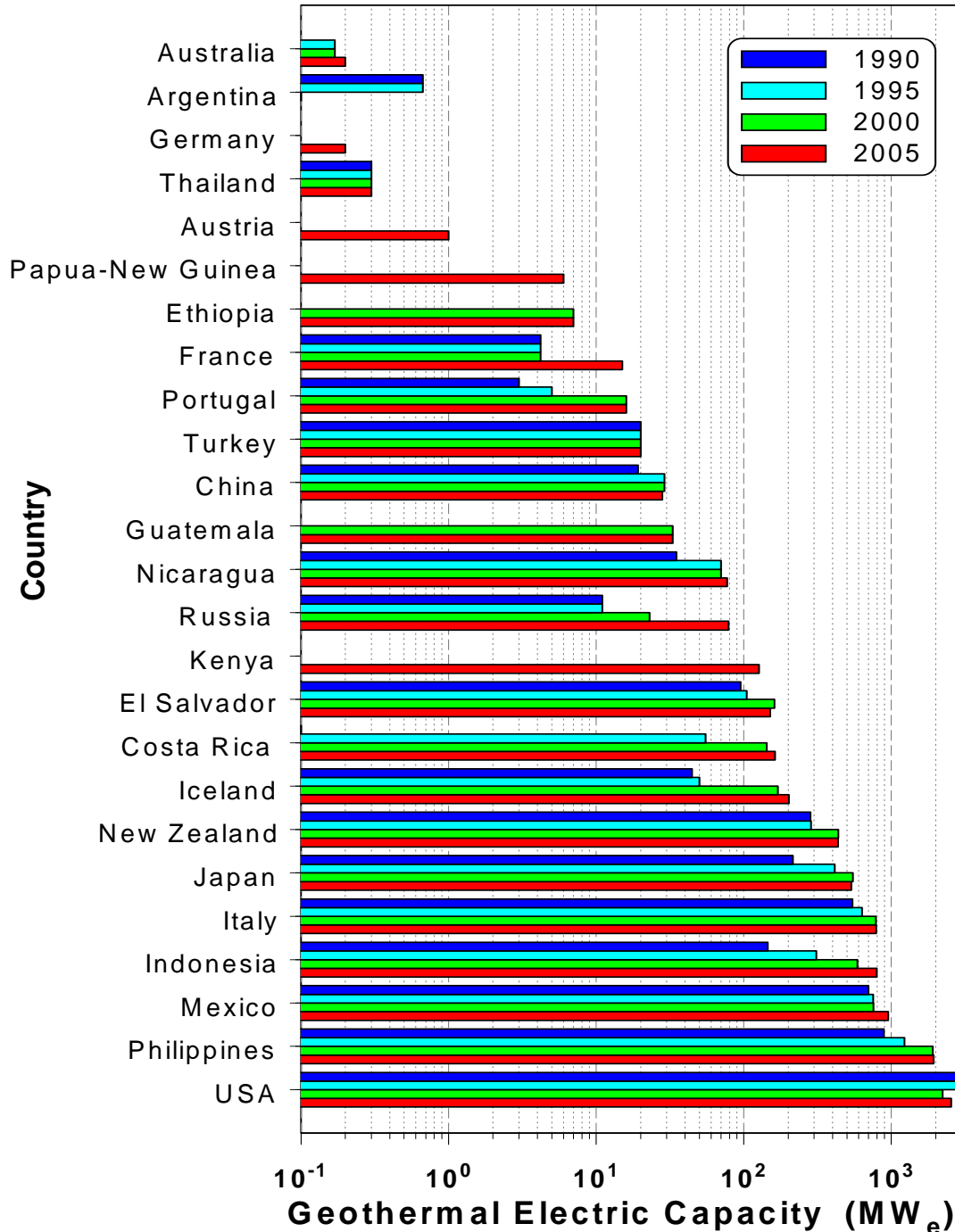


Fig. 8.34 Geothermal electric capacity installed worldwide in the years 1990 – 2005 (see also Table 8.23; data: [2005Ber]).

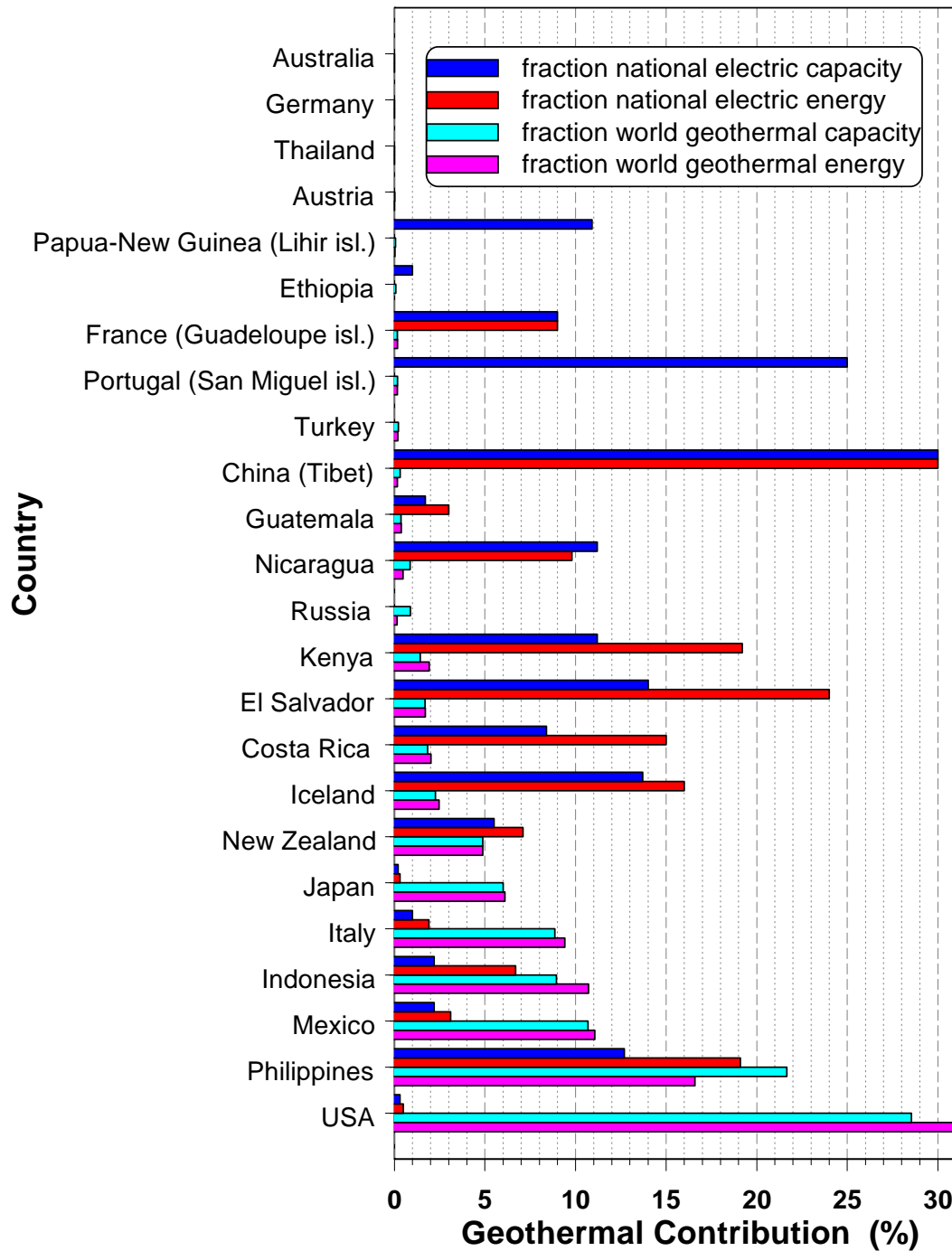


Fig. 8.35 Geothermal contribution to the national electric capacity (blue) and the electric energy production (red) of 24 countries; National contributions to the world geothermal electric capacity of 8912 MW_e (cyan) and the world geothermal energy production of 56800 MW h (magenta) by the year 2005 (see also Table 8.23; data: [2005Ber]).

Pre-Print from:
 Clauser, C., 2006. Geothermal Energy, In: K. Heinloth (ed), *Landolt-Börnstein, Group VIII: Advanced Materials and Technologies, Vol. 3: Energy Technologies, Subvol. C: Renewable Energies*, Springer Verlag, Heidelberg-Berlin, 493-604.

8.4 Technological and Economical Aspects of Geothermal Energy

Geothermal energy, like other types of non-fossil, low carbon dioxide, renewable energies, will supply a greater and even more significant share of the future global electric power and heat demand only if it can be offered at a reasonable, if not competitive price. As a rule, competitiveness is defined with respect to the energy prices based on fossil fuels, i. e. oil, gas, and coal, but commonly the price of oil is used as a reference. This is an extremely volatile quantity. It adjusts itself not to demand and supply in a free market but is determined also by political boundary conditions. Over the past 35 years it has fluctuated to a great extent, by more than 120 % around its 35-year average of 18.95 US \$ (Fig. 8.36). As a consequence, the competitiveness of geothermal energy varied accordingly, becoming more or less attractive in times of high or low oil prices, respectively.

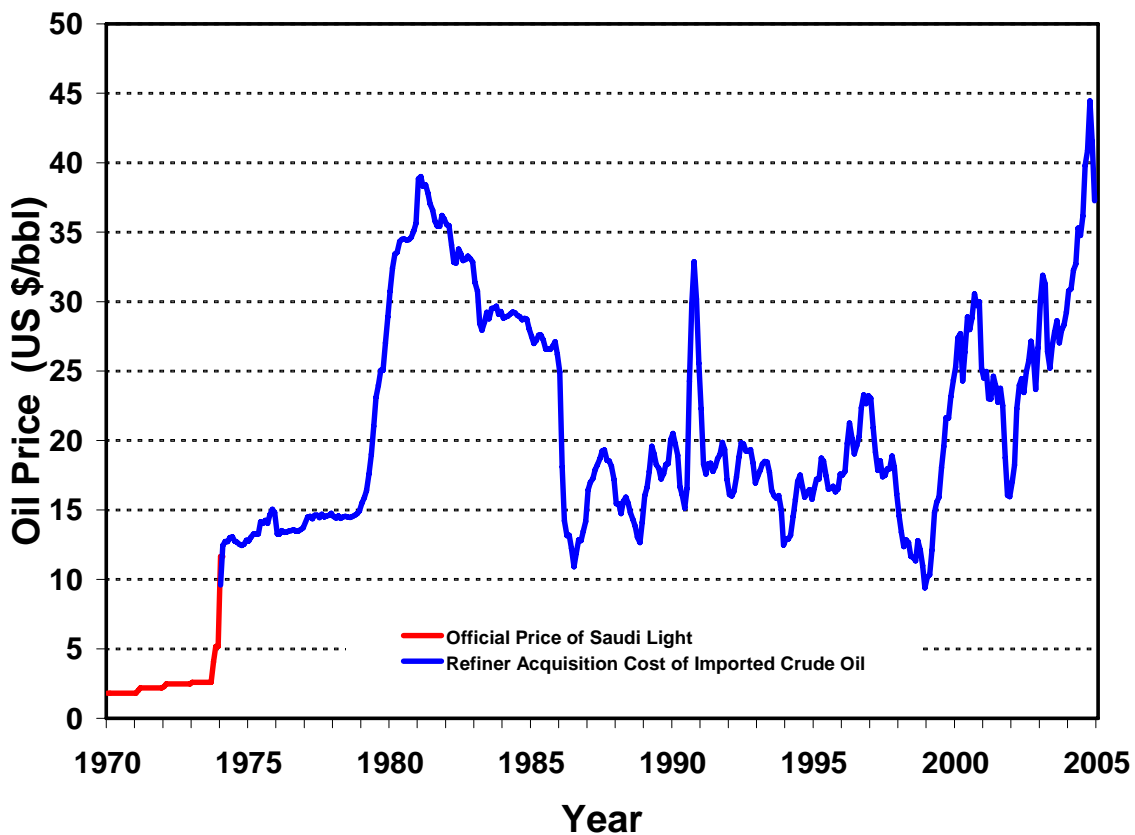


Fig. 8.36 Variation of the monthly average price of a barrel of crude oil in the period 1970 – 2004 (data: U.S. Energy Information Administration (EIA) [2004EIA] and International Energy Agency (IEA) [2005IEA]).

In spite and independently of these external circumstances, geothermal energy has experienced considerable growth in these 35 years (c.f. section 8.3). This is due to its attractive features:

- it is available everywhere;
- unlike some other forms of renewable energy, its supply does not vary with weather conditions, season or time of the day and is more or less constant over a long period of time, provided the resource is managed reasonably;
- it can be used for heat and power supply, depending on the subsurface geothermal conditions.

Its use is likely to increase further when new technologies for developing, production, and transformation of geothermal energy presently being developed and tested will become available commercially. These will contribute to a further increase in efficiency and cost reduction.

8.4.1 Direct Use

Direct geothermal heat use of some sort is possible almost anywhere on the continents, with few exceptions. Requirements with respect to temperature or physical rock properties are less stringent than for electric power generation. However, different technological and economical aspects apply to the different types of direct geothermal energy use, i.e. shallow ground-source heat pump systems, deep borehole heat exchangers, and hydrothermal heating systems. This is owed to the fact that the corresponding heat production installations differ significantly in type, size, and both technological and economic expenditure. Various aspects of space and district heating with regard to building types, pipe systems, equipment and economics are discussed in Eliasson et al. [2003Eli].

8.4.1.1 Earth Coupled Heat Extraction Systems

A great number of Earth coupled heat extraction systems are currently in operation worldwide, more than 800.000 at minimum (Table 8.21). Many of these systems have been operating for one or even several decades. Most of them are shallow borehole heat exchangers coupled to a heat pump. Therefore the following discussion is focused on shallow borehole heat exchangers. With the exception of the underground pipe system, most aspects also apply to horizontal Earth coupled heat exchangers. Deep borehole heat exchangers are discussed separately.

Ground-source heat pump systems consist of surface and subsurface installations (Fig. 8.28, Fig. 8.29). The surface installation consists of a heat pump which is connected at one end to the heat distribution system and on the other end to the sub-surface installation, i.e. the Earth coupled heat exchanger. The sub-surface installation consists of a horizontal heat exchanger (Fig. 8.28) or one or several borehole heat exchangers (Fig. 8.29). The components of the surface installation, i. e. heat pump and heat distribution system, are industry standard. The same components are used for geothermal heat production as for other heat pump and heat distribution applications. The effectiveness of heat pumps is characterized by their coefficients of performance (COP) and efficiency η . The COP is defined as the ratio of output energy (heat) to input energy (for instance electricity for the compressor). The COP of a heat pump is different in the heating and cooling modes (COP_h and COP_c, respectively). In the heating mode the total heating power is composed of the geothermal power and the electric power of the compressor. In the cooling mode, in contrast, the cooling power is simply the cooling power of the heat pump, and the electric heating of the compressor goes to waste. In the cooling mode, the coefficient of performance is accordingly lower. Thus, in general we have COP_h > COP_c. The maximum efficiencies $\eta_{h,max}$ or $\eta_{c,max}$ of a heat pump in heating or cooling modes, respectively, is defined as the ratio of heating or cooling power, respectively, and input power (commonly electric). It decreases in general with the temperature difference ΔT between output temperature T_{warm} and input temperature T_{cold} (Fig. 8.37):

$$\eta_{h,max} = T_{warm}/\Delta T = 1/\eta_{Carnot} ; \quad \eta_{c,max} = T_{cold}/\Delta T ; \quad \Delta T = T_{warm} - T_{cold} \quad (T \text{ in K}), \quad (8.62)$$

where $\eta_{Carnot} = \Delta T/T_{warm}$ is the efficiency of an ideal thermodynamic Carnot process. In practice, however, heat pumps - like thermal power stations - cannot operate at maximum theoretical thermodynamic efficiency. This is inevitable and due to various factors, such as heat losses, energy required to drive the pumps for the primary circulation, to name just a few. Therefore, the effective efficiency η_h or η_c of a heat pump in heating or cooling modes, respectively, is determined by the theoretical maximum efficiency $\eta_{h,max}$ or $\eta_{c,max}$ diminished by the so-called exergy factor ε :

$$\eta_h = \varepsilon \eta_{h,max} \quad (\eta_c = \varepsilon \eta_{c,max}); \quad \text{with } 0.4 \leq \varepsilon = X/E \leq 0.5, \quad (8.63)$$

where exergy $X = E - A$ is the fraction of energy E which can be freely converted into other forms of energy. This follows directly from the second law of thermodynamics which states that not all available heat energy can be converted into useful work. The fraction A of the energy E which cannot be converted into useful work is sometimes called anergy. Fig. 8.37 shows the variation of the effective efficiency η_h with the temperature difference ΔT for an exergy factor of $\varepsilon = 0.5$.

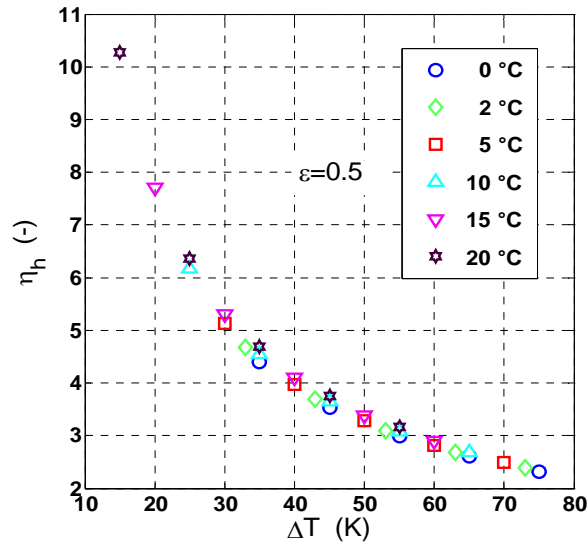


Fig. 8.37 Variation of heat pump efficiency η_h with temperature difference ΔT between input and output temperatures T_{cold} (see legend) and T_{warm} , respectively (cf. eqs. (8.62) and (8.63)); ε : exergy factor).

Heat pumps differ with respect to the fluids in the primary and secondary circuits. Groundwater heat pumps usually use water in both circuits. Thus their input temperature T_{cold} equals about 10 °C in moderate latitudes; in lower or higher latitudes T_{cold} will be accordingly higher or lower, respectively. In contrast, heat pumps coupled to *borehole heat exchangers* usually are brine-water heat pumps which use some sort of brine in the primary, ground-coupled circuit, and water in the secondary one. Often the input temperature T_{cold} is chosen at or slightly above the freezing temperature of pure water. In this situation the use of brines instead of water in the primary circuit prevents the freezing of the borehole heat extraction system. Since the output temperature T_{warm} of the secondary circuit is defined by the requirements of the specific application, for instance the domestic space or water heating system, the efficiency η^{ww} of water-water heat pumps is therefore always superior to that of brine-water heat pumps, η^{bw} , at the same output temperature T_{warm} (cf. Fig. 8.37).

In the heating and cooling modes, the maximum coefficients of performance of modern brine-water heat pumps vary between $4 < \text{COP}_h < 5$ and $3 < \text{COP}_c < 4$, respectively. For water-water heat pumps the corresponding ranges are $5 < \text{COP}_h < 6$ and $4 < \text{COP}_c < 5$. This means that more primary energy is produced than used as input, given a thermodynamic efficiency η between $0.3 \leq \eta \leq 0.4$ (e.g. [1997Die]) for the conversion of primary energy (e.g. coal, hydrocarbons) into electricity. The greater the efficiency, the greater is also the COP. An optimization, however, cannot be performed with respect to efficiency and COP alone, as some data cannot be chosen freely, such as the output temperature. This is generally defined by the requirements of the application. For groundwater heat pumps the input temperature T_{cold} is equal to the local groundwater temperature and more or less constant. With borehole heat exchangers, in contrast, T_{cold} must be optimized with respect to both COP and maximum heat extraction from the subsurface: While the COP decreases with temperature difference ΔT , the heat extraction increases with ΔT . The efficiency of the heat transfer between the sub-surface and the primary circuit in the borehole is governed mainly by the thermal properties of the subsurface, groundwater flow in the subsurface, and the volume flow rate in the primary circuit. Important rock thermal properties are both thermal conductivity and thermal diffusivity, since ground-source heat exchangers are commonly operated in a strongly transient fashion with respect to daily and seasonal operation cycles.

The effect of various rock properties and technical parameters on mean thermal power and output temperature can be studied comprehensively by detailed numerical simulations of the borehole heat exchanger system using appropriate software (e.g. [2002Koh; 2003Cla^a; 2003Cla^b]). As an illustration, Fig. 8.38

shows the effect of thermal conductivity on the mean thermal power of a shallow coaxial borehole heat exchanger: A 50 % increase in thermal conductivity in the range $2 \text{ W m}^{-1} \text{ K}^{-1} - 3 \text{ W m}^{-1} \text{ K}^{-1}$ corresponds to an equal increase in mean thermal power. This illustrates the importance of good control of the thermal rock properties for an adequate design and dimensioning of ground-source heat pump systems (see section 8.1.5.2). In contrast, if thermal properties are unknown or can only be estimated from literature data, this uncertainty is usually accommodated by the use of safety margins. A common result of this is an over-sizing of the system, i.e. the borehole is drilled to an unnecessarily great depth. As a consequence, the system will be unnecessarily expensive. The most critical technical parameter which can be optimized is the volume flow rate: Its variation affects both the mean thermal power and the mean output temperature of the borehole heat exchanger, but in opposite direction (Fig. 8.39). Thus an optimum flow rate can be defined for obtaining the required output temperature at an optimum thermal power.

The average thermal conductivity $\bar{\lambda}$ from the surface to the maximum depth of the borehole heat exchanger can be estimated from a *thermal response test*, a long-term in situ heat extraction or injection experiment involving the borehole heat exchanger (Fig. 8.40). Different analytical and numerical methods are available for the analysis of response test data (see e.g. [2002Geh] for a discussion).

The infinite line source is one popular model for approximating the heat source (or sink) of a borehole heat exchanger with a constant cooling (or heating) rate Q (in W m^{-1}) as a function of time t and radius r from the line source. For long times, i.e. for large ratios $\kappa t/r^2$, the temperature at the borehole wall ($r=r_b$) can be approximated by [1959Car]:

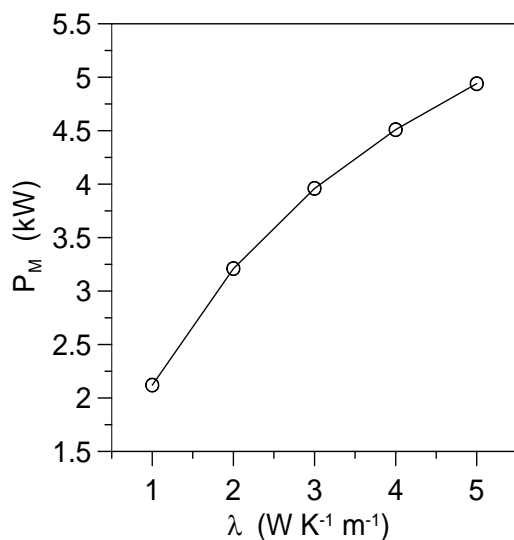


Fig. 8.38 Variation of the mean thermal power P_m (\circ) of a coaxial borehole heat exchanger (at a given volume flow rate of $1.8 \text{ m}^3 \text{ h}^{-1}$ at a constant inflow temperature of $0 \text{ }^\circ\text{C}$) with rock thermal conductivity λ (length: 100 m; operation over 10 years: 12 h per day for 6 months – recovery during the following 6 months; after Geophysica Beratungsgesellschaft mbH, Stolberg).

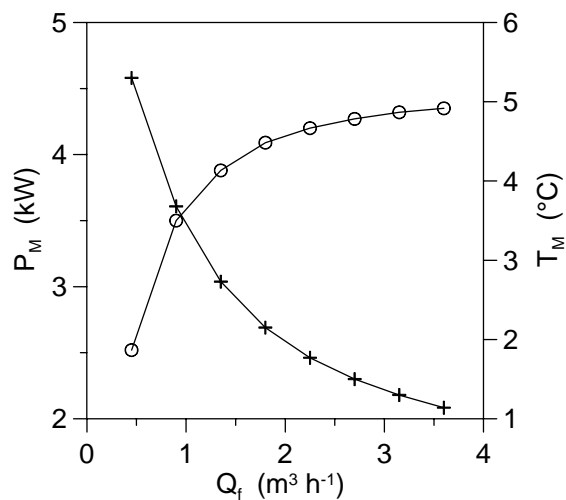


Fig. 8.39 Variation of the mean thermal power P_m (\circ) and mean output temperature T_m ($+$) of a coaxial borehole heat exchanger with volume flow rate Q_f (length: 100 m; rock thermal conductivity $\lambda = 2 \text{ W m}^{-1} \text{ K}^{-1}$; inflow temperature: $0 \text{ }^\circ\text{C}$; operation over 10 years: 12 h per day for 6 months – thermal recovery during the following 6 months; source: see Fig. 8.38).

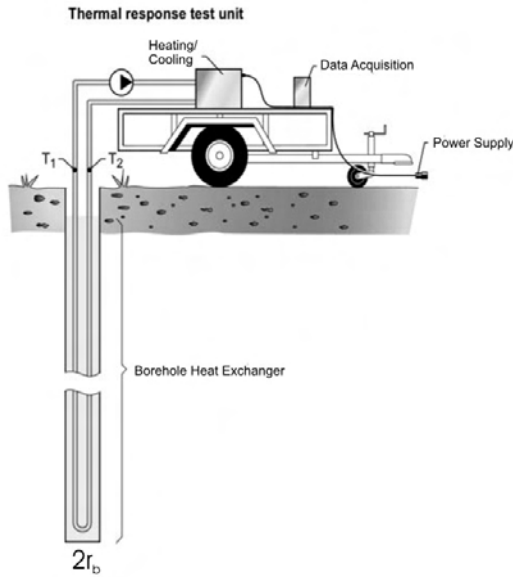


Fig. 8.40 Typical experimental set-up for a thermal response test in a borehole heat exchanger (after [2002Geh]).

linear regression of \bar{T} versus the logarithm of time t . With $\bar{\lambda}$ known, the thermal resistance R_b can be calculated from the intercept value b , provided the thermal diffusivity is known independently. In the quasi steady-state regime described by equation (8.65), the storage effect of thermal capacity included in thermal diffusivity κ is not felt any more. Therefore, thermal conductivity and thermal capacity (and hence thermal diffusivity) cannot be determined simultaneously from this type of experiment.

Several factors must be considered when interpreting the results of thermal response tests [see e.g. 2002Koh; 2002Geh; 2003Cla^b; 2004Sig^a]:

- $\bar{\lambda}$ is an average for the entire depth of the borehole and cannot account for contrasts in thermal conductivity, for instance due to layering;
- The analytical line- and cylindrical-source solutions cannot account for groundwater driven advective heat transport to and from borehole heat exchangers. This, however, is frequently observed with respect to both natural flow systems and free convection around the borehole induced by the test itself [cf. 2002Geh for a discussion]. This yields unrealistically high values for thermal conductivity, if not accounted for properly. Thermal response tests run in the cooling mode seem to be less influenced by free convection induced due to the test itself than those in the heating mode;
- The thermal resistance of borehole heat exchangers depends critically on the technical quality of the backfilling and the thermal properties of the backfill material [see e.g. 2001Pah];
- Heat losses between the heating or cooling unit and the borehole (cf. Fig. 8.40) may lead to significant errors in the analysis.

A number of technical recommendations are available for the design and layout of ground-source heat pump systems and borehole heat exchangers in particular [e.g. 1996Ano^a; 1997Hub; 2001Ano^a; 2001Ano^c; 2004Ano^a], heat storage systems [2001Ano^b], and direct uses [2004Ano^b]. Also, commercial software is available for the planning of heat pump systems (e.g. *TRNSYS*², *YUM* [1989Afj], *WPcalc* [1994Nan]), the layout of systems consisting of one or several borehole heat exchangers (e.g. *EED*³, *EWS*⁴) or heat exchanger piles (*PILESIM*⁵ [1999Pah]). As these codes are based on different simplifying

² <http://sel.me.wisc.edu/trnsys/default.htm>

³ <http://www.buildingphysics.com/index.htm>

⁴ <http://www.igjzh.com/huber/index.htm>

⁵ daniel.pahud@geothermal-energy.ch

$$T(r_b, t) \approx \frac{Q}{4\pi\bar{\lambda}} \left[\ln(4\kappa t/r_b^2) - \gamma \right] + Q R_b + T_0, \quad (8.64)$$

where κ is the thermal rock diffusivity, R_b the borehole thermal resistance, T_0 the undisturbed temperature, and $\gamma \approx 0.5772$ Euler's constant. The maximum error of eq. (8.64) is 2.5 % and 10 % for $\kappa t/r_b^2 \geq 20$ and 5, respectively. Expanding the logarithm's argument in (8.64) by t^*/t^* (t^* : time unit) and collecting terms, this yields an expression for the average fluid temperature \bar{T} :

$$\bar{T}(t) = a \ln(t/t^*) + b, \quad \text{where } a = \frac{Q}{4\pi\bar{\lambda}}, \quad \text{and} \quad (8.65)$$

$$b = Q \left(R_b + \frac{\ln(4\kappa t^*/r_b^2) - \gamma}{4\pi\bar{\lambda}} \right) + T_0.$$

The temperatures recorded in a thermal response test follow the linear relation of eq. (8.65) in the steady-state approximation, i.e. for long times, commonly several hours. The average thermal conductivity $\bar{\lambda}$ can then be calculated from the slope of a

assumptions (e.g. constant temperature gradient, constant thermal properties, etc.) they must be applied with appropriate care. While they can be very useful for the layout and design of individual and groups of shallow borehole heat exchangers, they should not, as a rule, be applied to deep borehole heat exchangers. Ground-source heat pump systems for heating or combined heating and cooling are a mature technology. Designed, laid-out, and installed properly, they have a proven life time equal to comparable investment goods, on the order of 30 years and more. With COP values between 4-5, modern brine-water heat pumps deliver between $4/3 - 5/3$ more heat than primary energy used for generating the electric energy (at a thermodynamic efficiency of $\eta=1/3$) required as input. This relation becomes even better if gas heat pumps are used instead of electric heat pumps. Except for the pollution associated with the generation of electric energy by burning of fossil fuels, ground-source heat pumps do not generate any pollution, unless their isolated circuits are damaged. Once they are installed, however, this is not very likely.

The cost of a ground-source heat pump system depends on its size. For a typical single-family home in Germany the investment for a borehole heat exchanger in soft or hard rock, is about 13.000 € roughly 1.000 € or 4.000 € more than what is required for a conventional oil or gas furnace, respectively. This relation will vary from country to country, but indicates an extra cost on the order of 10 % – 40 %. However, unlike ground-source heat pumps, oil and gas furnaces cannot provide any cooling during the warm season. Depending on summer temperatures, this option for cooling alone may well be worth the extra investment. Moreover, the higher investment cost for a ground-source heat pump system is balanced within a few years by the much lower annual cost (energy consumption, maintenance, and mortgage) compared to an oil furnace. An example based on German year 2004 prices illustrates that electrical ground-source heat pumps start saving money already after three years of operation compared to an oil furnace. At current German gas prices, however, the difference in annual cost of about 26 € between a gas furnace and an electrical ground-source heat pump is insufficient to offset the difference in investment cost within reasonable time (Fig. 8.41). This difference, however, is only about 1 % of the total cost of a house. And beyond doubt, oil and gas prices will increase further in coming years. Therefore it can be expected that this relation will become even more favorable for ground-source heat pumps in the future.

In the long run, i.e. with respect to 20 years of operation in the example calculation of (Fig. 8.41), ground-source heat pumps may help to cut down heating cost significantly, by about 15.000 € compared to an oil furnace. This is as much as the initial hardware investment for a ground-source heat pump system.

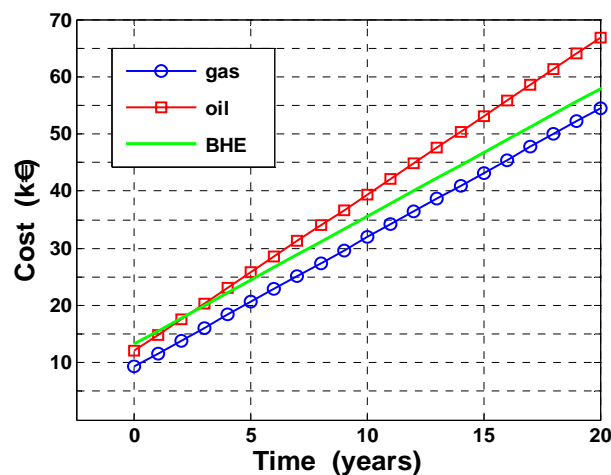


Fig. 8.41 Example for heating cost comparison of a typical single family home (150 m²) based on oil and gas furnaces or borehole heat exchangers (BHE) in hard or soft rock (German year 2004 prices; data courtesy of ECOS Umwelt GmbH, Aachen).

Deep borehole heat exchangers can be designed for direct heat exchange in combination with a heat pump or without. The extracted heat can be used for space heating or, if used to drive adsorption or

absorption cooling systems, for space cooling. Roughly speaking, temperatures below or above 75 °C are best suited to drive adsorption or absorption cooling systems, respectively [e.g. 2002Gas; 2003Raf^a; 2004Ano^f].

The cost of deep borehole heat exchangers is dominated by the drilling cost. While drilling costs vary from country to country, a detailed recent cost analysis based on German prices [2002Sch^{a,b}] provides some general orientation. In this analysis drilling cost amounted to about 47 % of the total investment for a borehole heat exchanger system to a depth of 2500 m (Fig. 8.42). Depending on different cases considered this corresponds to a specific cost for the borehole heat exchanger (excluding engineering, measurement and control systems, and heat pump) of between 550 €m⁻¹ – 700 €m⁻¹ drilling depth. The associated gas heat pump accounts for another 34 %. In this study, specific drilling cost did not vary extremely up to a depth of 2500 m. A significant increase occurs for greater depths which require hydrocarbon special deep drilling technology. A total of four different scenarios was considered in this study [2002Sch^{a,b}], with different boundary condition with respect to depth (2500 m – 2800 m), rock thermal conductivity (3.0 W m⁻¹ K⁻¹ – 4.5 W m⁻¹ K⁻¹), temperature gradient (30 K km⁻¹ – 35 K km⁻¹), bottom hole temperature (85 °C – 108 °C), and thermal power of the installed gas heat pump (310 kW_t – 790 kW_t). The resulting average heat cost and its variation is shown in Fig. 8.43. This demonstrates that deep borehole heat exchangers, even if operated almost year round (i.e. at 6000 h a⁻¹ – 8000 h a⁻¹), deliver heat at a cost equal to or above the cost of a corresponding gas heating furnace. For instance, at the end of the year 2004 the corresponding gas price for the required amount varies in Germany between 34 € – 39 € per MW h, depending on location. However, economic feasibility will be reached as gas prices increase with an increasing oil price and if the heat produced can be used during the summer as driving power for adsorption or adsorption space cooling systems.

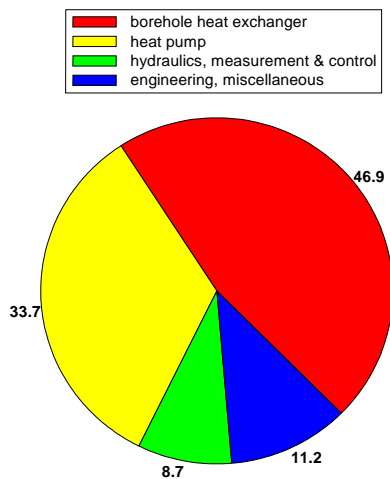


Fig. 8.42 Relative cost factors for deep borehole heat exchanger systems (depth 2500 m, German year 2002 prices; (after [2002Sch^a])).

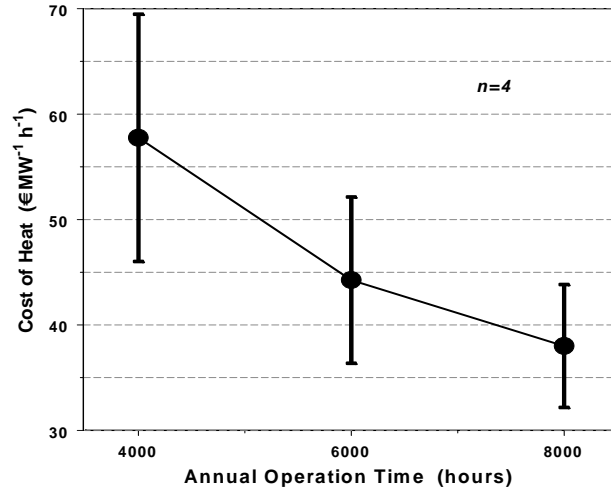


Fig. 8.43 Mean and standard deviations of average cost for deep borehole heat exchanger systems based on German year 2002 prices and four different scenarios considered (after [2002Sch^a])).

Additionally, present and anticipated future financial incentives for CO₂ reductions will further increase the economic feasibility of deep borehole heat exchangers systems. For instance, since the end of the year

2004, the European Energy Exchange AG (EEX)⁶ is publishing with its European Carbon Index a daily market price for CO₂ emission allowances. Since the official beginning of trading of EU allowances on 17 December 2004, prices rose from initial 8.45 € per ton of CO₂ to 23 € per ton of CO₂ on 26 June 2005 (Fig. 8.44a).

The range of installed thermal power of 310 kW_t – 790 kW_t and annual operation times of 6000 h a⁻¹ – 8000 h a⁻¹ considered in the scenarios of this study [2002Sch^{a,b}] corresponds to maximum ranges of annual CO₂ reductions on the order of 250 t – 1260 t if geothermal heat replaces a gas furnace, and of 350 t – 1770 t if geothermal heat replaces an oil furnace. Based on the above price of 23 € per ton of CO₂ this corresponds to a financial bonus of about 5700 € – 29000 € if geothermal heat replaces a gas furnace, and about 8000 € – 40100 € if geothermal heat replaces an oil furnace.

8.4.1.2 Hydrothermal Heating Systems

Unlike local, Earth coupled heat extraction systems, hydrothermal heating systems are large installations with two or more boreholes deeper than 1000 m. While there are cases where they provide process heat mainly to one client, more often their heat is distributed to a large number of end users through a distribution grid. New grids require an additional major investment while existing grids already have a provider of heat, often excess heat from fossil power production. Therefore, market access is difficult for hydrothermal heat and often requires crowding out current heat providers. This will only occur if geothermal heat use is more attractive.

One clear advantage of geothermal heat is its unlimited availability, regardless of weather, time of day or time of year. This makes it an excellent choice for providing large base loads and less attractive for more transient systems requiring high peak loads (Fig. 8.44b). Therefore, geothermal heat becomes economically more attractive if, additional to space heating of apartments and houses, it can be used to provide a significant thermal base load, such as 2000 h – 4000 h per year, to major customers of space heating or commercial and industrial process heat (cf. section 8.3.1.2).

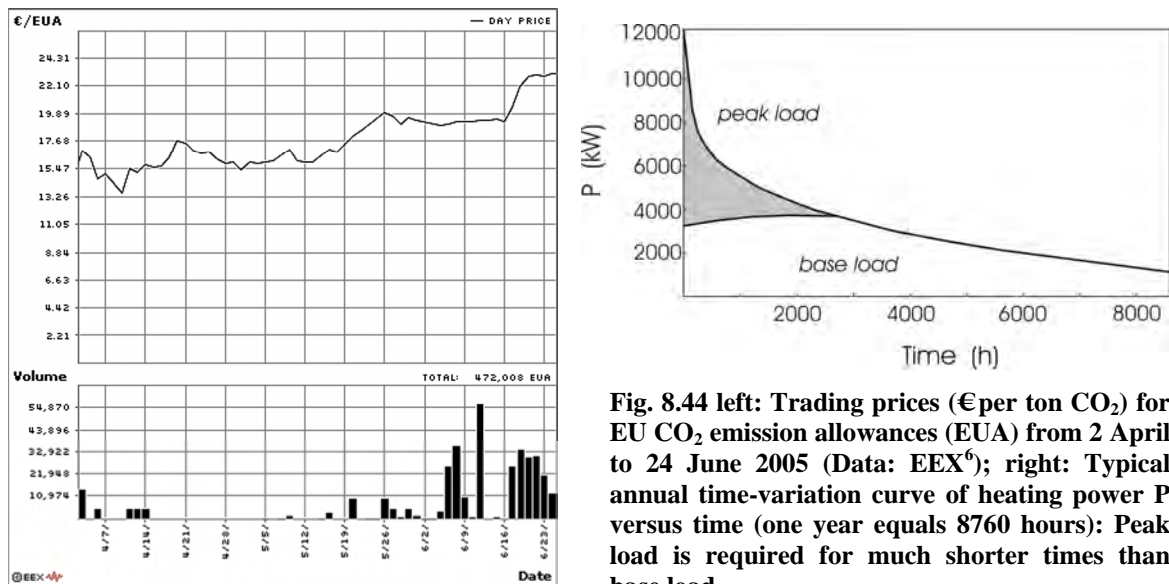


Fig. 8.44 left: Trading prices (€ per ton CO₂) for EU CO₂ emission allowances (EUA) from 2 April to 24 June 2005 (Data: EEX⁶); right: Typical annual time-variation curve of heating power P versus time (one year equals 8760 hours): Peak load is required for much shorter times than base load.

⁶ <http://www.eex.de>

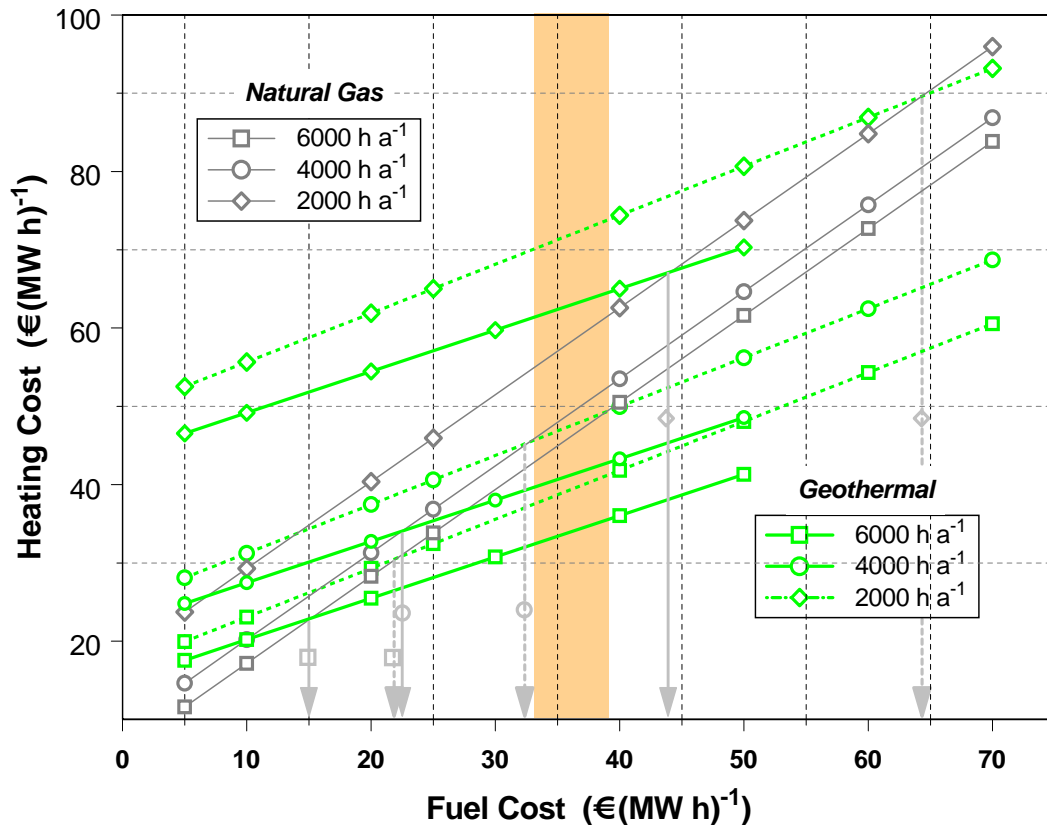


Fig. 8.45 Cost comparison for heating plants using natural gas (11.2 MW_t ; dark gray lines) and geothermal heat with heat pumps of 11.2 MW_t and 11.4 MW_t with and without direct heat exchange of 2.1 MW_t (full and broken green lines, respectively) (data: [2002Sch^a])⁷. Solid and broken light gray arrows indicate break-even cost for geothermal heat with respect to fossil fuel for heat pumps with and without direct heat exchange, respectively. Brown shading indicates German year 2004 large-consumer price range for natural gas. Symbols correspond to different annual cumulative heating times (one year equals 8760 hours).

Crowding-out of current heat providers usually requires a financial reward, i.e. geothermal heat must be less expensive. In existing, well developed heat markets, such as in the industrial world, cheap excess heat is often available from fossil and nuclear power production. In such an economic environment selling of geothermal heat is difficult and depends strongly on fuel prices, in particular for oil and gas. Therefore, conditions may vary between countries and even regions. As an example based on conditions in Germany, Fig. 8.45 shows results of a recent heat cost comparison for stations using natural gas and geothermal heat [2002Sch^a; 2002Sch^b]. The stations considered have an installed power of 11.4 MW_t , either based on burning natural gas or by producing geothermal heat using a gas motor heat pump or, in a second scenario, by an additional direct heat exchange providing an additional power of 2.1 MW_t .

It is evident that cumulative heating times of 4000 h a^{-1} and more are required for geothermal heat to become competitive if geothermal heat is produced by a gas motor heat pump alone. With the additional direct heat exchange the break even cost is considerably lower, making geothermal heat attractive for cumulative heating times as low as about 3000 h a^{-1} . This conclusion is based on Germany year 2004 large-consumer gas prices. In the past, the price of natural gas generally varied parallel to the oil price (see Fig. 8.36) which increased on average over the years with large fluctuations. When a detailed study based on German prices [2002Sch^a; 2002Sch^b] was prepared in May 2002, the price of natural gas was

⁷ Not shown: Heating cost for a 13.5 MW_t natural gas plant which is only slightly more than for a 11.2 MW_t plant.

about 20 €/per MW h. In contrast, it varies between 34 €– 39 €/per MW h in November 2004. As a result, geothermal heat was too expensive in 2002, while at the end of 2004 it does appear attractive. There is a clear long-term trend of increasing oil and gas prices (Fig. 8.36), and both financial incentives for CO₂ reductions and additional taxation of CO₂ producing technologies can be anticipated in several industrial countries for the near future. In view of this it may be expected that, in the long run, the cost advantage of geothermal heat produced in hydrothermal plants will become stable or even larger. However, extending this conclusion based on German year 2005 conditions to other countries requires an appraisal of the local cost, mainly of drilling and natural gas. Since German energy prices are neither extremely high nor low it may be expected that results will be similar for a number of countries, and favor geothermal heat even more wherever fossil fuels are more expensive or the burning of fossil fuels is discouraged.

Burning of natural gas produces about 200 kg CO₂ per thermal MW h_t. At 4000 h a⁻¹ cumulative heating time, the 11.4 MW fossil fuel heating plant discussed above ([2002Sch^a; 2002Sch^b]; Fig. 8.45) produces approximately 53,000 MW h heat per year. This corresponds to an emission of about 10.6 kt of CO₂. Based on a cumulative heating time of 4000 h a⁻¹ and a thermal COP_h = 1.6 for the gas fired adsorption heat pump, 28000 MW h a⁻¹ are required to drive the gas motor heat pump. This corresponds to an emission of 5.6 kt of CO₂. Replacing gas by geothermal heat thus saves about half of the CO₂ emissions of a natural gas heating plant. Even for one single heating plant of 11.2 MW_t this amounts to 5 kt of CO₂ which are prevented from being emitted into the atmosphere. Based on the aforementioned allowance of 23 €/per ton of CO₂ emission fixed at the European Energy Exchange AG (EEX)⁶ in June 2005, this corresponds to a financial bonus of about 115000 €/per year if geothermal heat replaces a gas furnace.

8.4.2 Power Generation

Vapor is required to drive turbines for generating electric power. In general, this is natural dry or wet, medium to high enthalpy steam at temperatures above 150 °C (cf. Table 8.19). For some time, binary systems employing substances with a lower boiling point than water in a secondary circuit have been used to generate vapor for driving turbines at a lower temperature level. This process is known as Organic Rankine Cycle (ORC) or Kalina Cycle (see sections 8.3.2 and 8.4.2.2). Binary systems are used in combination with low to moderate temperature, water dominated reservoirs. In absence of natural steam or hot water reservoirs or in case of insufficiently permeable reservoirs, hydraulic fracturing provides additional permeability in engineered hot dry rock (HDR) or enhanced geothermal systems (EGS). Geothermal power production has more stringent requirements with respect to temperature or physical rock properties than direct use. However, different technological and economical aspects apply to the different types of geothermal power production, depending on whether they are natural or engineered systems, involve dry or wet steam or ORC or Kalina Cycle technology. One of the advantages of geothermal power plants is that they can be built economically in much smaller units than e.g. hydropower stations. Geothermal power plant units range from less than 1 MW_e up to 30 MW_e. Thus, the capacity of geothermal power plants can be adjusted more easily to the growing demand for electric power in developing countries with their relatively small electricity markets than hydropower plants which come in units of 100 MW_e – 200 MW_e (Fig. 8.46). Geothermal power plants are very reliable: Both the annual load and availability factors are commonly around 90 %. Additionally, geothermal fields are little affected by external factors, such as seasonal variations in rainfall, since meteoric water has a long residence time in geothermal reservoirs [2002Bar].

8.4.2.1 Natural Steam Power Plants

Dry Steam Power Plants use dry saturated or superheated steam at pressures above atmospheric from vapor dominated reservoirs, an excellent resource that can be fed directly into turbines for electric power production. Permeability is generally lower in dry than in wet steam fields, and the reservoir requires a tight cap rock. Steam is the predominant continuous phase in control of reservoir pressure which is practic-

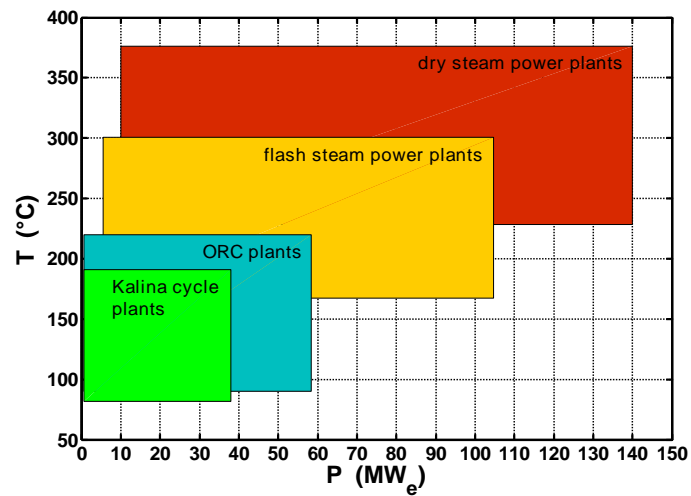


Fig. 8.46 Power range and characteristic reservoir temperatures for generation of electric power by direct-intake dry steam plants, single or multiple flash wet steam plants, ORC and Kalina cycle hot water plants (modified after [2004Len^a]).



Fig. 8.47 Dry steam geothermal power plants (top left to bottom right): Lardarello, Italy; The Geysers, USA; Matsukawa, Japan; Kamojang, Indonesia (source: [2001Ano^d; 2003Sat; 2004Lun^a; 2004Wor]).

ally constant throughout the reservoir [2002Bar]. On the surface, these fields may be indicated by boiling springs and geysers. In general, the produced steam is superheated, containing only small quantities of other gases, mainly CO_2 and H_2S . Superheating in dry steam reservoirs is caused by a transient heat transfer between the reservoir rock and the steam phase: When production begins in a well penetrating

such a reservoir, a low-pressure zone forms around the well screen, and nearby liquid water starts boiling and evaporates. This creates a zone void of liquid water through which steam flows towards the well. In this dry region the steam expands into the voids and cools. However, heat originally stored in the reservoir rock maintains a steam temperature above the local evaporation point, thus generating superheated steam. Superheating of up to 100 K results, for instance, for steam production temperatures hotter than 200 °C and well head pressures of 0.5 MPa – 1 MPa [2002Bar]. Thus, superheating allows mining more heat from dry than from wet steam reservoirs. As a consequence, about half the global geothermal electric energy is produced from only six dry steam power plants: Lardarello (since 1904) and Monte Amiata in Italy; The Geysers, the only source of geothermal dry steam in the USA (since 1960); Matsukawa in Japan (since 1966); Kamojang (since 1983) and Darajat in Indonesia (see Fig. 8.47). With less than 10 %, however, vapor dominated reservoirs are much less frequent than water dominated reservoirs which make up 60 %, while the remaining 30 % produce hot water [2002Bar].

In power plants exploiting dry steam fields, steam can be fed directly from the production wells into the turbine and exhausted to the atmosphere. This *direct non-condensing cycle* is the simplest and cheapest option for generating geothermal electricity. Steam from the geothermal well is simply passed through a turbine and exhausted to the atmosphere: there are no condensers at the outlet of the turbine (Fig. 8.48). Direct non-condensing cycle plants require about 15 kg – 25 kg of steam per kW_e generated electricity [2002Bar]. Non-condensing systems must be used if the steam contains more than 50 weight % of non-condensable gases. They are generally preferred over condensing cycles if the steam contains more than 15 weight % non-condensable gases, because their removal from the condenser consumes power and reduces plant efficiency.



Fig. 8.48 Direct-intake, non-condensing single flash geothermal power plant at Pico Vermelho (São Miguel Island, Azores) exhausting steam to the atmosphere. (source: [2004Lun^b]).

In *condensing plants* steam is condensed at the outlet of the turbine and cooled in conventional cooling towers (Fig. 8.49). Condensing the steam at the turbine exhaust creates a vacuum of about 150 hPa (less than 15 % atmospheric pressure), thus maximizing the pressure drop across the turbine and hence the power output [2004Lun^b]. Thus, condensing plants require substantially (i.e. about 50 %) less steam than non-condensing ones, only 6 kg – 10 kg of steam per kW_e generated. However, the steam may not contain more than 15 % of non-condensable gases. The specific steam consumption of these units largely depends on the turbine inlet pressure: At pressures of 1.5 MPa – 2.0 MPa the consumption is close to 6 kg of steam per kW_e; at 0.5 MPa – 1.5 MPa it is 9 kg – 7 kg of steam per kW_e, and for even lower pressures it becomes much larger [2002Bar]. In power plants based on a *direct-intake condensing cycle*, dry or superheated steam is piped directly from the wells into the steam turbine. This is a well developed, commercially available technology. Capacities of typical turbine units range between 20 MW_e and 120 MW_e, but modular standard generating units of 20 MW_e are also available [2002Bar].

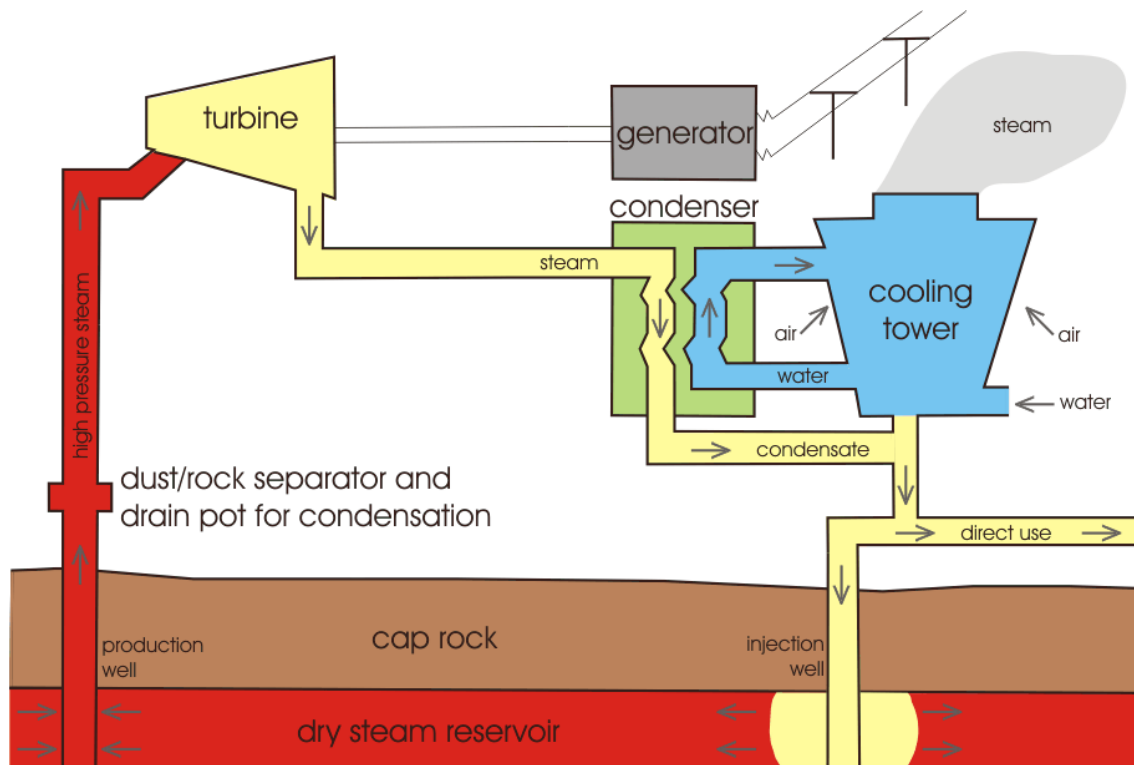


Fig. 8.49 Direct-intake, condensing power plant for heat production from dry steam fields (modified after [2004Tri]).

Flash Steam Power Plants exploit water dominated, wet steam reservoirs in which most of the high-temperature geothermal resource is provided by pressurized water. These fields are much more common than vapor dominated ones. On the surface, they are often indicated by boiling springs and geysers.

When a well penetrates into such a reservoir, the pressurized water flows into the well because well pressure, in general, is lower than reservoir pressure. As a result of the pressure drop, a certain fraction of the liquid water evaporates and the well co-produces hot water and steam, with water as the dominant phase. Therefore, these fields are also called wet steam fields. The actual water-steam ratio varies from field to field and even among wells within the same field. The heat source is large, generally of magmatic origin, forming a resource of the hydrothermal type (see section 8.2). The water produced often contains a large load of dissolved minerals ($10^{-3} - 10^{-1} \text{ kg}_{\text{mineral}} \text{ per kg}_{\text{fluid}}$, in some fields up to 0.35 kg kg^{-1}), mainly chlorides, bicarbonates, sulfates, borates, fluorides, and silica [2002Bar]. This can cause severe scaling in pipelines and plants. An important economic aspect in exploiting wet steam fields is the large quantity of brines produced with the steam (e.g. 6600 t h^{-1} at Cerro Prieto, Mexico): Owing to their large load of dissolved minerals, they need to be reinjected, preferably at the margins of the reservoir [2002Bar].

Wet steam cannot be fed to standard turbines without risk of damage to the turbine blades. Therefore, separators are used in all installations exploiting wet steam reservoirs for separating steam from water. Single or multiple flash steam plants are used to produce energy from these fields by evaporating depressurized liquid water into steam in one or several separators at the surface. Single, double-, and triple flash systems are used (Fig. 8.50). Commercially available turbo-generator units are commonly in the range $10 \text{ MW}_e - 55 \text{ MW}_e$, but modular standard generating units of 20 MW_e are also used [2002Bar]. Examples for triple and dual flash cycle wet steam geothermal power plants are, among many others, Wairakei, New Zealand, and Imperial Valley, USA, respectively (Fig. 8.51).

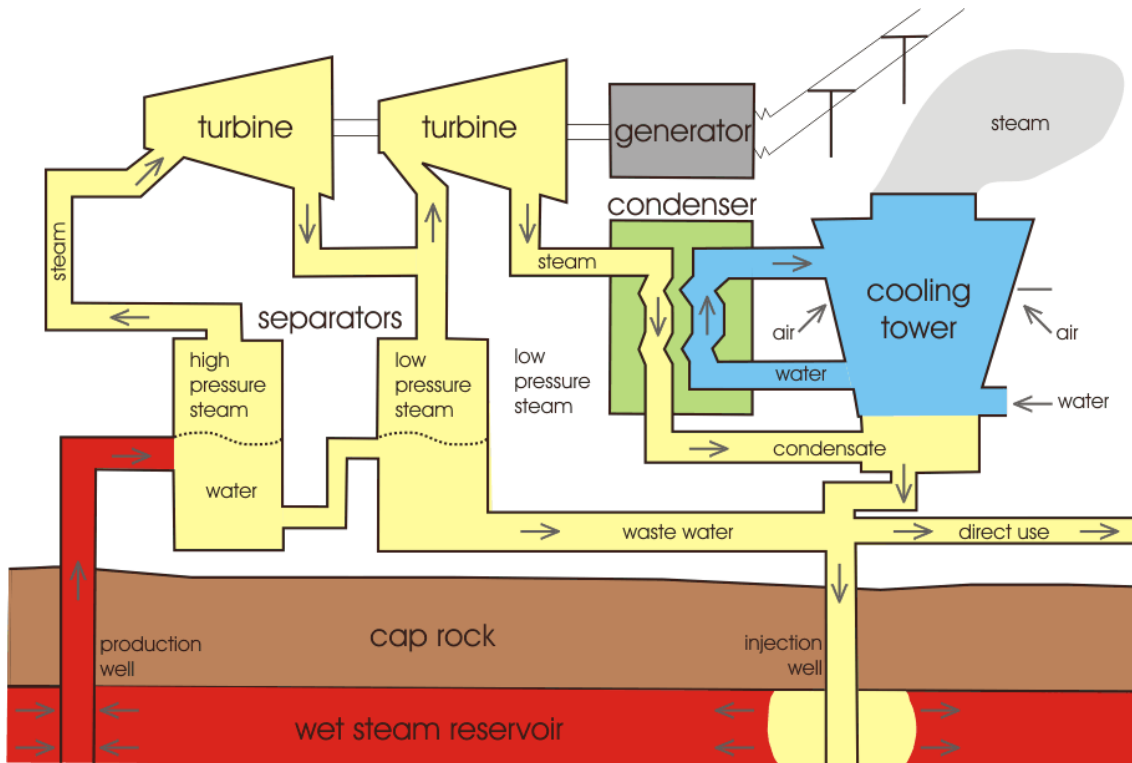


Fig. 8.50 Double flash, condensing power plant for heat production from wet steam fields (modified after [2004Tri]).



Fig. 8.51 Wet steam geothermal power plants with triple and dual flash cycles (left to right): Wairakei, New Zealand (with prawn pond in foreground) and Imperial Valley, USA, respectively (source: [2001Ano^d; 2002Ano]).

8.4.2.2 Binary Power Plants

Binary power plants allow converting geothermal heat from low enthalpy, water dominated hot water reservoirs into electricity, provided reservoir temperatures exceed 85 °C. In addition to hot water reservoirs, this technology is also well suited to exploit medium enthalpy wet steam resources with high water-to-steam ratios at temperatures lower than practical for flash steam systems. Binary plants convert medium-temperature resources into electricity more efficiently than other technologies.

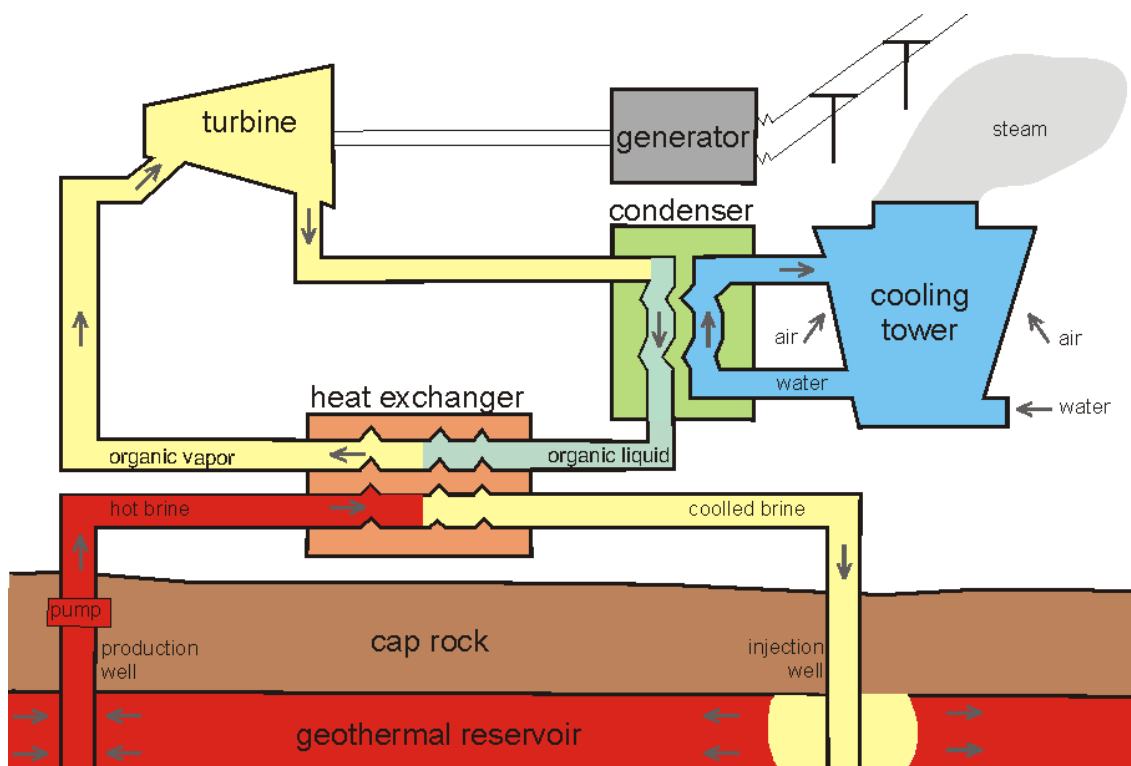


Fig. 8.52 Binary power plant (water-cooled) for heat production from hot water or low enthalpy wet steam fields (modified after [2004Tri]).

In binary plants a heat exchanger transfers heat from the produced hot brine in a primary loop to a low boiling-point working fluid in a secondary loop, such as halogenated hydrocarbons (e.g. Freon™, Frigen™), propane (C_3H_8), isobutane (C_4H_{10}), pentane (C_5H_{12}), ammonia (NH_3). This thermodynamic cycle is known as Organic Rankine Cycle (ORC) because initially organic compounds were used as working fluid. The working fluid in the secondary loop is evaporated in the vaporizer by the geothermal heat provided in the primary loop. The vapor expands as it passes through the organic vapor turbine which is coupled to the generator. The exhaust vapor is condensed in a water-cooled condenser or air cooler and is recycled to the vaporizer by the motive fluid cycle pump (Fig. 8.52). Binary cycle plants require $400 \text{ kg kW}^{-1} \text{ h}^{-1}$ of hot water from low-to-medium enthalpy resources ($85 \text{ }^\circ\text{C} - 150 \text{ }^\circ\text{C}$) [2002Bar]. The cooled brine can be discharged or reinjected into the reservoir without flashing, which minimizes scaling problems. A typical unit size is $1 \text{ MW}_e - 3 \text{ MW}_e$. However, the binary power plant technology has emerged as the most cost-effective and reliable way to convert large amounts of low temperature geothermal resources into electricity, and it is now well known that large low-temperature reservoirs exist at accessible depths almost anywhere in the world. The power rating of geothermal turbine/generator units tends to be smaller than in conventional thermal power stations. The most common unit capacities are 55, 30, 15, 5 MW_e or smaller [2002Bar].

ORC systems have been installed in significant numbers within the past 30 years because binary plants convert low enthalpy geothermal resources more efficiently into electricity than other technologies. This widens the spectrum of locations suitable for geothermal power production significantly. It makes decentralized geothermal power production feasible with unit sizes varying on the order of $0.1 \text{ MW}_e - 100 \text{ MW}_e$ (Fig. 8.53) and economically attractive in many remote or less developed regions of the world, but also in low enthalpy regions of developed countries where financial incentives promote low

™ registered trade marks of DuPont and Hoechst

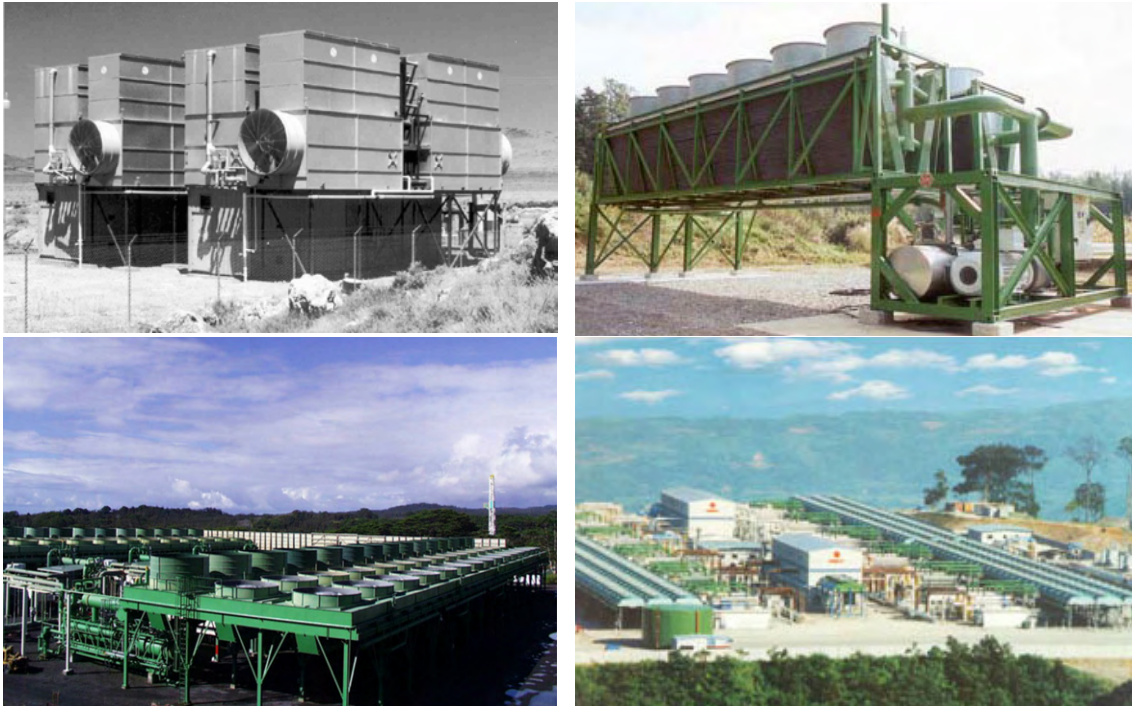


Fig. 8.53 Binary (top) and combined cycle (bottom) geothermal power plants (top left to bottom right): Wendel Hot Springs CA., USA (700 kW_e); Bad Blumau, Austria (250 kW_e); Puna District, Big Island HI, USA (30 MW_e); Leyte, The Philippines (125 MW_e), both the largest air-cooled and largest combined cycle power plant in the world (source: [1999Nic; 2001Ano^d; 2004Ano^c]).

CO₂-emission energy production technologies. For instance, as a result of Germany's renewable energy act [2004Ano^d], which requires grid operators to feed geothermal electric energy into their grids at a certified price of up to 0.15 €kW⁻¹ h⁻¹, low- to medium-enthalpy hot water resources are being developed in this country which is lacking natural steam reservoirs. As a result, the first geothermal power production in Germany went into commercial operation at Neustadt-Glewe in the North-German Sedimentary Basin in November 2003 (0.2 MW_e, 98 °C [2003Ano^b]). More projects are being developed in the upper Rhine Graben in France, Germany, and Switzerland, and the pre-Alpine Molasse Basin in Austria (the first installation went into operation in Altheim in 2000 with 0.7 MW_e at 106 °C [2002Per]) and Germany with projected capacities of up to 5 MW_e.

Recently, the efficiency of binary power plants is further improved by the Kalina Cycle technology [1984Kal; 1989Wal]. Here, a mixture of water and ammonia (NH₃) is evaporated over a finite temperature range (Fig. 8.54), producing a two-component vapor (70 % ammonia and 30 % water) in contrast to the ORC process which is based on pure fluids evaporating at specific boiling temperatures. The main thermodynamic advantage of the Kalina over the Organic Rankine cycle is owed to the fact that the water-ammonia mixture, unlike pure fluids, boils at a variable temperature (Fig. 8.55). Therefore the working fluid temperature remains closer to that of the hot brine in the primary circuit which improves the exergy efficiency by 10 % – 20 % [1989Wal].

While this fact has been known for some time, it is the Kalina cycle which, for the first time, provides a practical and efficient way to condense the mixture back to the liquid state for recycling. In particular, in the Kalina cycle the working fluid is circulated in different parts of the cycle at different compositions: A low ammonia concentration (40 % ammonia and 60 % water) is used during condensation (stages 1-3 in Fig. 8.55), while evaporation (stages 4-5 in Fig. 8.55) occurs at higher ammonia concentrations (70 % ammonia and 30 % water) for optimum cycle performance [2004Ano^c]. This provides an improved effi-

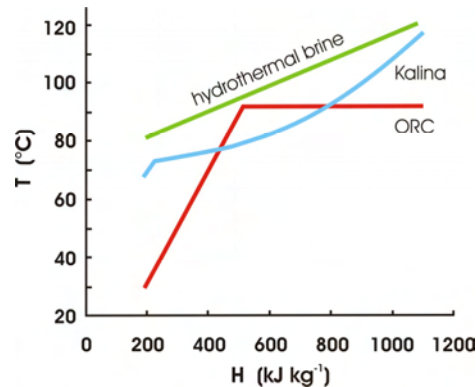


Fig. 8.54 Evaporation curves of working fluids in ORC and Kalina cycles, and hydrothermal brines showing temperature T versus enthalpy H (modified after [2004Len^a]).

schematic diagram

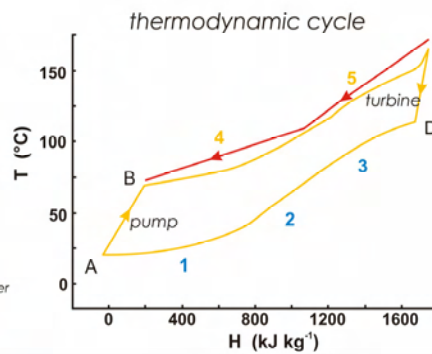
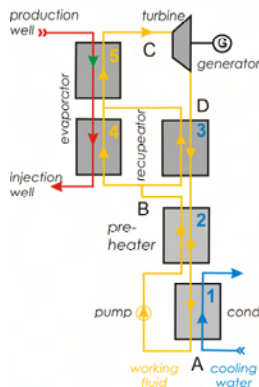


Fig. 8.55 Schematic diagram (left) and thermodynamic cycle of the Kalina process (right) showing temperature T versus enthalpy H (modified after [2004Len^a]). The temperature range in this example is 150 K, from 21 °C at point A to 171 °C at point C.

ciency of at least 10 % of the Kalina cycle over the conventional Organic Rankine Cycle [1989Wal]. At present, however, there is just one geothermal Kalina cycle power plant in operation in Husavik, Iceland and available for comparisons [2004DiP]; several more are under construction. In contrast, the ORC is a mature technology with hundreds of megawatts of various kinds of cycles installed throughout the world. A recent comparison based on simulated identical conditions observed a difference in performance of about 3 % in favor of the Kalina cycle [2004DiP].

8.4.2.3 Power Plants for Hot Dry Rock or Enhanced Geothermal Systems

Hot dry rock (HDR) or enhanced geothermal reservoirs are engineered systems in contrast to natural geothermal hot or wet steam reservoirs. While natural systems are restricted to regions with geodynamic activity (plate boundaries, mid-ocean ridges, subduction zones, active volcanoes), engineered systems are not limited in distribution: In principle, they can be established in all places with sufficiently high rock temperature because lacking or insufficient hydraulic permeability is created artificially by hydraulic fracturing of the rock at depth. This way, any convenient volume of hot dry rock in the Earth's crust, at accessible (and affordable) depth, may become an engineered HDR or enhanced geothermal reservoir.

A number of wells, usually 2 – 3, are drilled into the rock, terminating several hundred meters apart. Water is circulated down the injection well(s) and through the HDR reservoir, which acts as a heat exchanger. The fluid then returns to the surface through the production well, and thus transfers heat to the surface as steam or hot water. Various concepts for generating different kinds of sub-surface heat exchangers have been proposed and studied, and various combinations of these three basic types are possible as well:

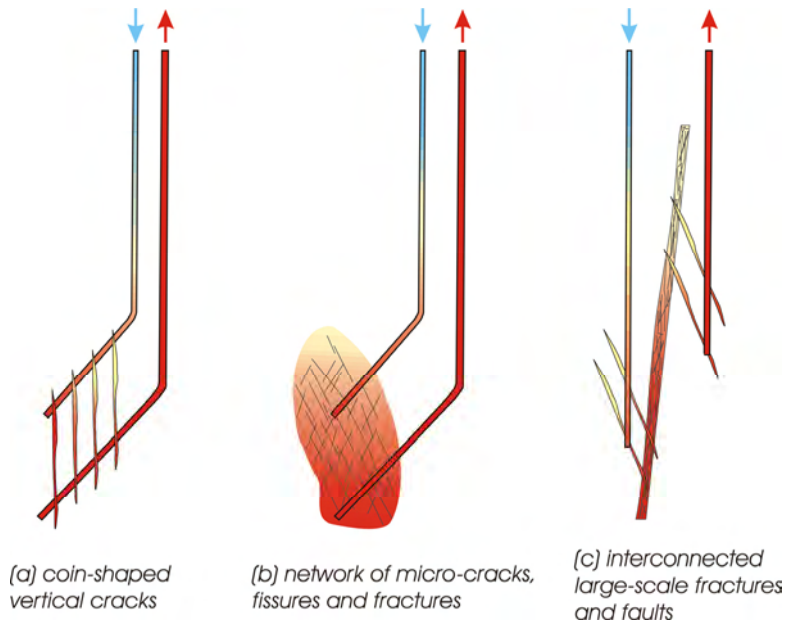


Fig. 8.56 Different kinds of sub-surface heat exchanger systems in HDR and enhanced geothermal systems (after [2003Jun]).

- single and multiple coin-shaped, vertical cracks, such as the first HDR system at Fenton Hill, NM [1999Bro] or the system created at Falkenberg, Germany [1989Jun] (Fig. 8.56a);
- networks of micro-cracks, fissures and fractures, such as the systems at Rosemanowes, UK [1999Par], Hijiori, Japan [1999Kur], and Ogachi, Japan [1999Hor] (Fig. 8.56b);
- systems of reactivated, interconnected large-scale fractures and faults, such as Soultz-sous-Forêts, France [1992Bre; 1999Bar], and Fjällbacka, Sweden [1999Wal] (Fig. 8.56c).

At present, a number of commercial projects based on the different approaches for engineering HDR systems (Fig. 8.56 or modifications and combinations of these types) are under way in countries without natural steam reservoirs, such as Australia [1998Nar] and Germany [2003Ano^b]. Systems such as the one shown in Fig. 8.56c, sometimes referred to as “hot wet rock”, fall in between a closed HDR system (Fig. 8.56a) and open, permeable hydrothermal systems [1999Abe]. These enhanced geothermal systems are engineered in high-temperature, low-permeability fracture systems or on the margins of productive geothermal fields. They are currently the new frontier and may offer a way for economic geothermal power generation in places where heat is provided by nature not jointly with permeable reservoirs and sufficient suitable fluids.

Stimulation is generally related to rock permeability and well connectivity and aimed at creating highly conductive fractures. Stimulation techniques developed for HDR creating heat exchangers draw on experience from the hydrocarbon industry for enhancing reservoir permeability. The most common stimulation techniques are:

- *hydraulic fracturing*: massive fluid injection ($10 \text{ L s}^{-1} - 100 \text{ L s}^{-1}$) at pressures of up to 100 MPa;
- *chemical stimulation*: both *fracture acidizing* and *matrix acidizing*;
- *explosive fracturing*: controlled underground explosions.

However, there are important differences between HDR systems and hydrocarbon reservoirs, the most significant ones being due to the different kinds of rock. While hydrocarbon reservoirs are mostly sandstones and limestones, HDR systems are often placed in basement or plutonic rocks, such as granite, gneiss, and basalt. These rocks differ significantly in their mechanical properties. Hydraulic fracturing in hydrocarbon reservoirs may create new fractures of several hundred meters in length. In contrast, new fractures in basement rock seem to be created more rarely, while existing and ancient, closed fractures are more often found to be widened and reactivated, respectively. Additionally, HDR systems require much larger fracture areas for heat exchange than required in hydrocarbon applications.

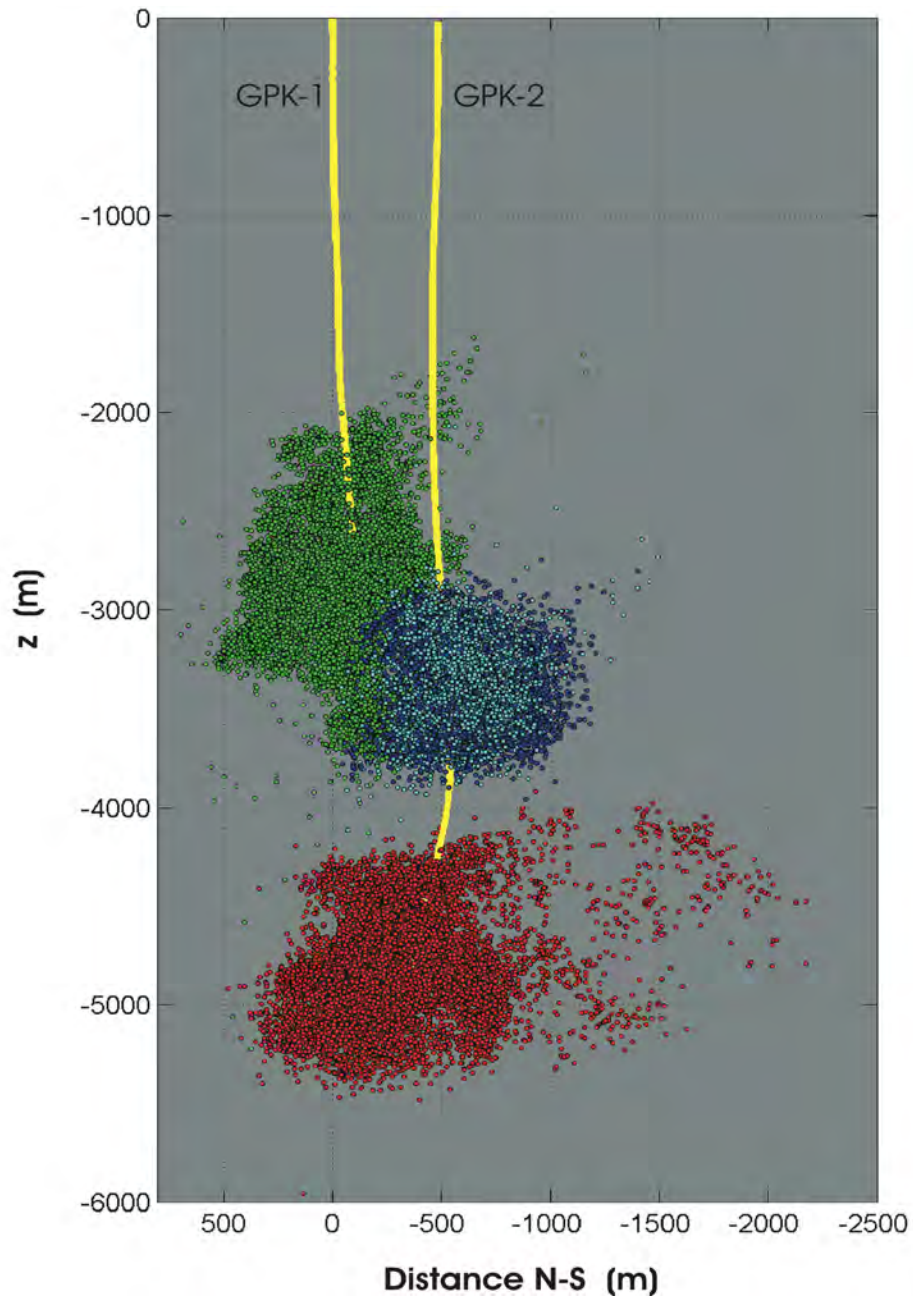


Fig. 8.57 Hypocenters of micro-seismicity generated by four massive hydraulic stimulations in 1993 (green), 1995 (blue), 1996 (cyan), and 2000 (red) in the boreholes GPK-1 and GPK-2 (yellow lines) of the European HDR experimental site at Soutz-sous-Forêts, France (modified after [2002Wei]).

For the key parameters of a HDR installation, Barbier [2002Bar] and Jung et al. [2003Jun] specify the following minimum requirements for a commercial success:

- production flow rate: $50 \text{ L s}^{-1} - 100 \text{ L s}^{-1}$;
- flow losses: $< 10 \%$ of injection flow or $< 10 \text{ L s}^{-1}$;
- flow resistance, i.e.: (injection pressure - production pressure)/ production flow rate: $< 100 \text{ kPa s L}^{-1}$;
- effective heat exchange surface: $> 5 \text{ km}^2 - 10 \text{ km}^2$;
- rock volume accessed: $> 0.2 \text{ km}^3$.

Systems with these characteristics, developed by two 5 km deep boreholes about 1 km apart, aim for a thermal power of $50 \text{ MW}_t - 100 \text{ MW}_t$ corresponding to an electric power of $5 \text{ MW}_e - 10 \text{ MW}_e$ delivered over an operation time of 20 years at minimum [2003Jun].

The creation of a sufficiently large and permeable underground heat exchanger can be verified by either active seismic tomography or passive monitoring of micro-seismicity. Results of the last method are illustrated in Fig. 8.57 which shows the effect of hydraulic fracturing performed at the European HDR experimental site at Soultz-sous-Forêts, France on four different occasions. Hydraulic overpressure causes the rock to crack at many places, indicated by the corresponding micro-seismic hypocenters. Connectivity between boreholes is indicated by a corresponding overlap of hypocenter locations. At Soultz-sous-Forêts, the stimulations do not result in a system as in Fig. 8.56b, but rather in one as in Fig. 8.56c, because ancient, large-scale fractures were reactivated by the hydraulic fracturing. Once created, these fractures and new pathways are prevented from closing again by the natural displacement of the fracture walls with respect to each other due to the natural stress field or, additionally, by injecting proppants. In enhanced geothermal systems, increasing the productivity of dry wells on the margins of existing productive geothermal fields by stimulation may turn these fields more profitable. It is assumed that dry wells exist where flow-paths are restricted and permeability k is on the order of 10^{-15} m^2 or less [2002Bar].

8.4.2.4 Technical, Economic, and Ecological Aspects of Geothermal Power Production

Efficiency, life time, and pollution all differ among the technologies used for converting geothermal heat into electric energy. Hudson [2003Hud] discusses technical features of various plant options as well as economic aspects of well-head generating units, Bloomquist and Knapp [2003Blo] economic and financial aspects, and Brown and Webster-Brown [2003Bro] environmental impacts and mitigation. Case studies of various geothermal projects are discussed by Grant [1996Gra] as an illustration for the methodology used from the exploration of the resource to the building of the surface installations. In particular, Grant's study [1996Gra] includes an appraisal of the trade-offs between additional information and corresponding cost, aspects of field management, and guidelines – a spectrum well beyond this text but of great practical value.

8.4.2.4.1 Efficiency

Geothermal steam from natural and HDR systems is converted into electric energy with a thermal efficiency, the ratio of net electric power output to heat input rate, ranging from 10 % – 17 %, depending on the type of steam and its temperature [1999Del; 2002Bar; 2003Jun]. This may appear low, by about a factor of three, compared to the efficiency of nuclear or fossil power plants, but is the result of the comparatively low temperature of geothermal steam, generally less than $250 \text{ }^\circ\text{C}$. In addition, geothermal steam has a chemical composition different from pure water steam, containing, in general, the non-condensable gases CO_2 , H_2S , NH_3 , CH_4 , N_2 and H_2 in concentrations varying from 1 g – 50 g per kg of fluid. Extracting these aggressive gases from the condensers of power plants additionally reduces the efficiency of electricity generation [2002Bar]. However, geothermal steam power plants possess quite impressive utilization efficiencies, the ratio of net electric power output to exergy input rate (exergy: see section 8.4.1.1), ranging from about 40 % – 65 % [1997DiP]. This demonstrates that particularly direct steam power plants typically convert the bulk of the maximum available thermodynamic work into electric energy.

In general, the efficiency of binary cycle power plants is lower than that of steam power plants. It varies with the resource temperature: values reported for installations commissioned within the last decade range from about 5 % – 14 % (Fig. 8.58). Again, the utilization efficiency is larger, ranging from about 16 % – 54 % [1997DiP; 2004DiP].

Frequently, binary units are also combined with direct steam, single- or multiple flash systems in order to improve the use of the available resource. Then the additional efficiency provided by the binary units helps to raise the overall efficiency of the combined system. The binary ORC and Kalina cycle technologies have emerged as the most cost-effective and reliable way to convert large amounts of low temperature geothermal resources into electricity. In spite of the low efficiency and in view of the attractive pollution balance, this technology appears to be on the threshold to be used on a larger scale for the conversion into electric energy in particular of the large low- to medium-enthalpy reservoirs abundant at accessible depth at numerous locations in the world.

The same considerations as for natural systems apply to the efficiency of engineered HDR systems as far as the surface installations are concerned. As for natural steam reservoirs, the thermal efficiency of HDR systems critically depends on the temperature and flow rates to be realized over a long period of operation. Thus the main challenge in engineering these systems lies not in the energy conversion efficiency of the surface installations, but in creating an adequately sized reservoir with sufficient permeability for sustaining sufficient flow rates at a high temperature.

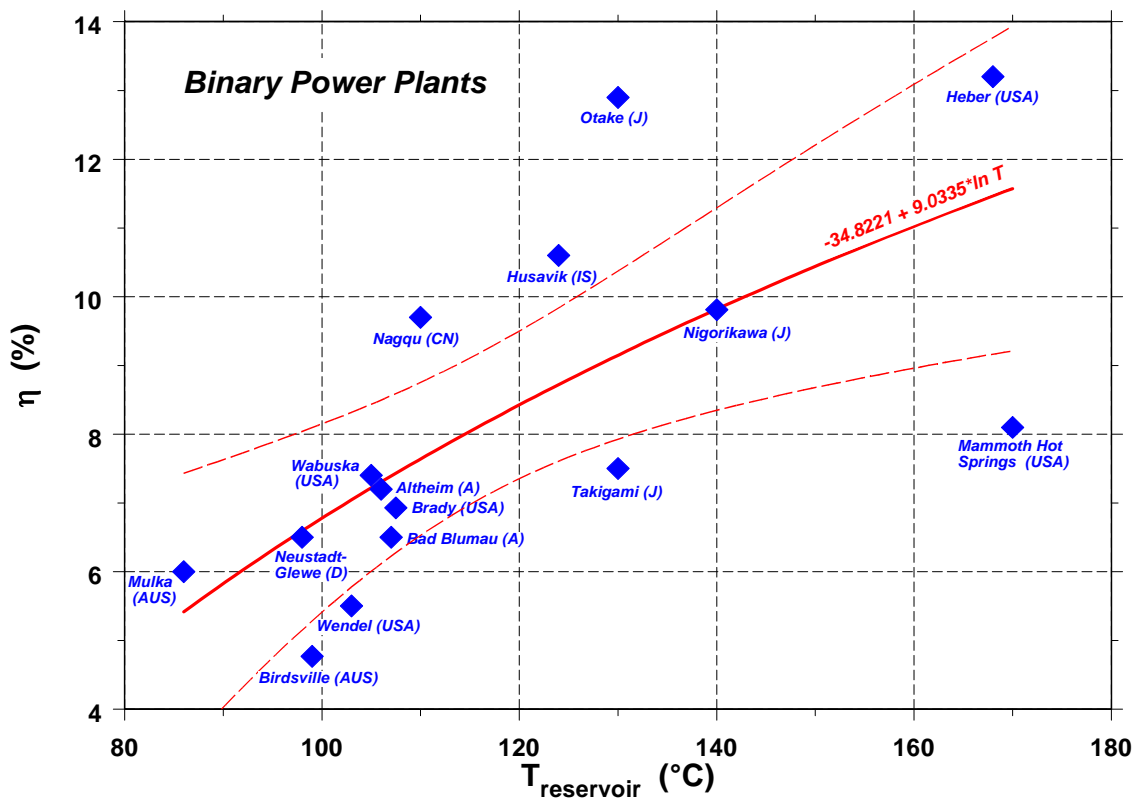


Fig. 8.58 Net thermal efficiency η (i. e. the ratio of output electric power to input thermal power) versus input reservoir temperature for various binary power plants (Husavik: Kalina cycle, all others: ORC). Full red line indicates a possible, logarithmic trend defined by the associated nonlinear regression; broken red lines indicate 95 % confidence limits, notwithstanding the low number of data points (A: Austria, AUS: Australia, CN: People's Republic of China, D: Germany, IS: Iceland, J: Japan; data: [1986Cul; 1997DiP; 2000Bur; 2000Low; 2000Ura; 2002Per; 2003Ano^b; 2003Jun; 2004DiP]).

8.4.2.4.2 Cost and Life Time

Among the renewables, geothermal energy has a remarkably long and proven record of reliability, both for direct use and electric energy production, dating back over 100 years. Indeed, the oldest geothermal field for generation of electric energy, at Lardarello (Italy), is looking back today on a continuous operation of over a century. Other fields, such as at The Geysers (USA) and Wairakei (New Zealand), have been operating for more than seven and five decades, respectively. Experience thus proves that geothermal fields, both vapor and water dominated, can be operated economically over a century. Prudent reinjection of spent fluids will help to constrain the decline of reservoir pressure and thus flow rate and the associated land subsidence.

Accordingly, substantial investments have been made for developing geothermal fields, but unfortunately the last survey of investments made in the main geothermal countries in the world in the period 1973 – 1992 dates back already 10 years [1994Fri]. It indicated a total investment of around 22,000 million US \$. Of these, 7,600 M\$ were invested between 1973 – 1982 and 14,300 M\$ between 1983 – 1992. This corresponds to an increase in total investments of 89 % in the second decade analyzed. In detail, 17,600 M\$ (80%) were invested in industrialized countries, 3,500 M\$ (16%) in developing countries, and 800 M\$ (4 %) in Eastern European countries.

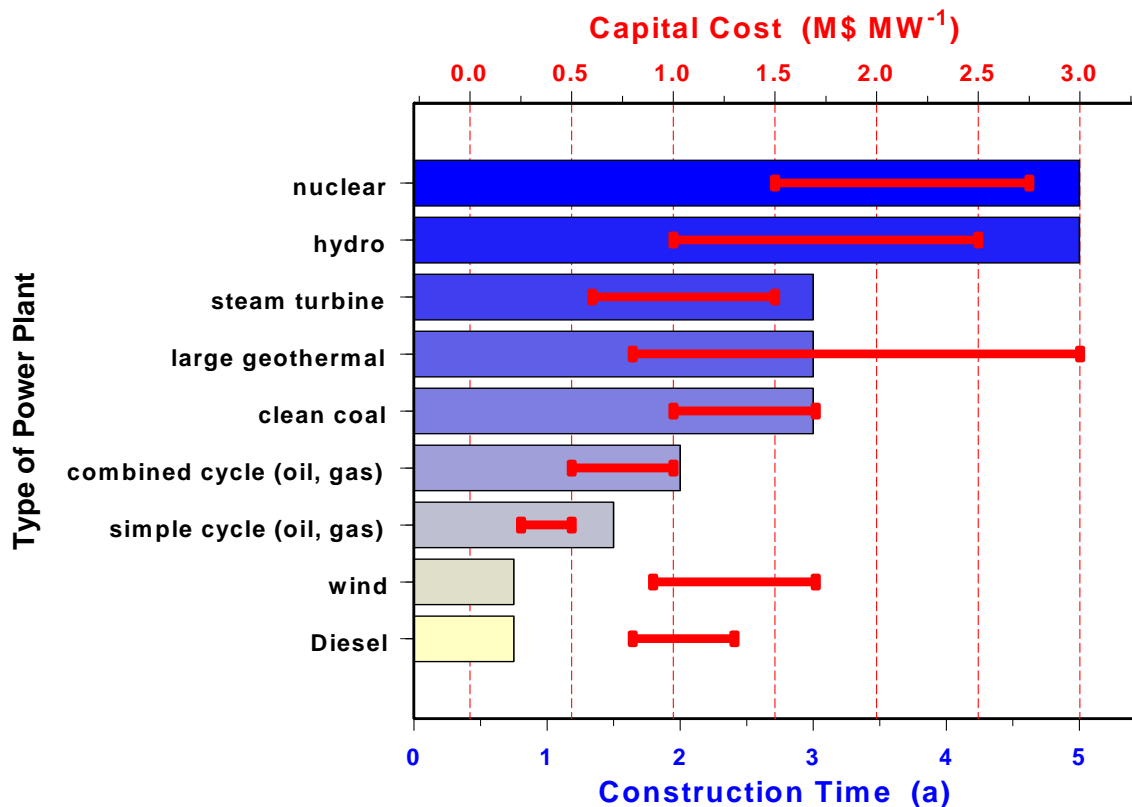


Fig. 8.59 Turnkey investment in US \$ (red bars) and average time required for power plant construction (blue bars) based on various kinds of conventional and renewable energy (data: [1996Ano^b; 2000Tur]).

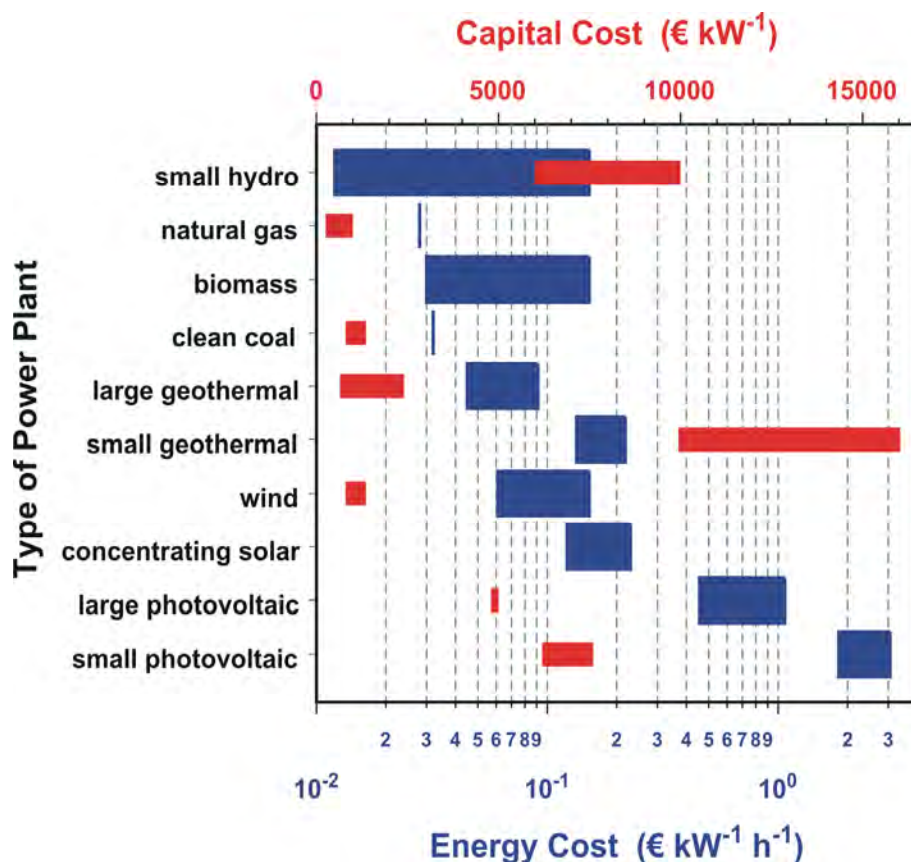


Fig. 8.60 Cost range for electricity produced from various fossil and renewable sources of energy (blue bars) and specific investment cost range for various fossil and renewable power plants (red bars) (data: [1996Ano^b; 1999Del; 2003Jun; 2003Kal; 2003Pas]). “Large geothermal” and “small geothermal” refers to steam power plants exploiting natural fields and HDR or enhanced geothermal systems with binary power plants, respectively.

As for oil and gas, much of this money is spent for technological research and development, geothermal exploration based on geological, geophysical, and geochemical surveys, drilling, field development, and surface installations for power generation or direct uses. However, geothermal projects are more closely linked to the specific site than oil and gas projects since geothermal fluids are normally used at or near the producing field. This is due to the cost of insulation for minimizing heat losses from pipelines which makes pumping fluids over long distances uneconomical. This is also reflected in the more than ten-fold larger enthalpy of oil (41,800 kJ kg⁻¹) compared to that of high-enthalpy geothermal steam (3000 kJ kg⁻¹) or hot water (209 kJ kg⁻¹) for a production and injection temperature of 80 °C and 30 °C, respectively [2002Bar].

Natural steam systems:

A time of about 3 years is required to develop new geothermal dry or wet steam fields and to install corresponding power plants [1996Ano^b; 1996Gra; 2002Ste]. This is reasonably short and in keeping with the construction times of power stations based on other fuels ([1996Ano^b; 2000Tur]; Fig. 8.59). Available numbers for the specific investment required for large geothermal steam power plants vary little and are consistently on the order of 1 million US \$ per installed MW (Fig. 8.59) or 1 million € per installed MW [1996Ano^b; 1999Del; 2003Kal; 2003Pas] (Fig. 8.60). Depending on plant type and size, costs range from 0.8 M\$ MW⁻¹ – 3.0 M\$ MW⁻¹ [1996Ano^b; 2000Tur] and 0.6 M€ MW⁻¹ – 2.4 M€ MW⁻¹ [1999Del; 2003Kal; 2003Pas]. Corresponding production costs of 0.045 €kW⁻¹ h⁻¹ – 0.091 €kW⁻¹ h⁻¹ [1996Ano^b;

[1999Del] are not too far above the energy price of a clean coal power plant and competitive compared to other sources of renewable energy, i.e. comparable to biomass and wind, and one or two orders of magnitude below concentrating solar or photovoltaic, respectively (Fig. 8.60).

In a comparison based on five geothermal power plants built in Iceland between 1994 –1999, Stefansson [2002Ste] reports that, on average, surface installations contribute about $977 \pm 215 \text{ \$ kW}^{-1}$ to the capital cost. Notwithstanding the small number of data points he finds a good correlation ($R^2=0.97$) for a linear trend between surface cost and installed capacity:

$$\text{surface cost (M\$)} = -0.9 \pm 4.6 + (1.0 \pm 0.1) \times \text{capacity (MW)}. \quad (8.66)$$

He combines this with results of an earlier survey of data from 31 geothermal steam fields world-wide (Table 8.24) and arrives at an expression for the total capital cost for a known geothermal field:

$$\text{cost (M\$)} = -0.9 \pm 4.6 + (1.29 + 0.31/-0.19) \times \text{capacity (MW)}. \quad (8.67)$$

Assuming that exploration in an unknown field requires an additional 50 % of the average number of wells (9.3 ± 6.1 , Table 8.24), i.e. 4.6 ± 3.0 at a cost of 1.5 M\$ each corresponding to an additional cost of $6.9 \pm 4.5 \text{ M\$}$, Stefansson [2002Ste] arrives at an expression for the total capital cost for an unknown geothermal field:

$$\text{cost (M\$)} = 6.0 \pm 9.1 + (1.29 + 0.31/-0.19) \times \text{capacity (MW)}. \quad (8.68)$$

Table 8.24 Characteristics of steam fields (data: [1992Ste^b]).

Average yield (MW _e) per well	Average yield (MW _e) per drilled km	Average number of wells for achieving maximum yield
4.2 ± 2.2	3.4 ± 1.4	9.3 ± 6.1

HDR and enhanced systems: HDR or enhanced geothermal systems differ from conventional reservoirs in so far as they require additional hydraulic stimulation of the reservoir's permeability to obtain the required flow rate of $50 \text{ L s}^{-1} - 100 \text{ L s}^{-1}$. In general, stimulation is accomplished by hydraulic fracturing of the rock at depth. This involves injection of large quantities of fluid, typically several hundred cubic meters of water, at flow rates between $10 \text{ L s}^{-1} - 100 \text{ L s}^{-1}$ and high pressures of up to 100 MPa. This operation requires large powerful pumps, a drill rig, and miscellaneous surface installations on site which involve an additional cost.

A pioneer HDR project at Los Alamos (USA) reached the threshold of economic feasibility at a cost of 175 million US \$ in 1993 [2002Bar]. However, this sum comprises much research and “learning-by-doing” in this prototype installation. Current cost can be expected to be an order of magnitude less as two recent studies conducted for Central European conditions demonstrate:

Jung et al. [2003Jun] calculate the cost for two such installations in Germany consisting of two boreholes each, 2.2 km and 4.6 km deep, located in the Upper Rhine Graben and in the North German Sedimentary Basin, respectively, a production temperature of 150 °C at a volume flow rate of 100 L s^{-1} , with a binary power plant at the surface; they arrive at total costs of roughly 8.5 M€ and 13.6 M€ respectively (cf. Fig. 8.60, “small geothermal”). The 60 % difference is mostly due to the larger borehole depth required in the second case to secure the desired production temperature of 150 °C .

For a similar system of three 5.5 km deep boreholes in the Upper Rhine Graben and a production temperature of 200 °C at 70 kg s^{-1} mass flow rate, Delacroix [1999Del] discusses three cases: The first one corresponds to verified costs in the past, the second one to current costs, and the third one to costs which can be expected for the near future, given the decrease in cost between the two previous cases and future technical improvements. For this “optimistic but nevertheless not unrealistic” [1999Del] scenario,

Delacroix [1999Del] arrives at a total cost of 27.5 M€ Considering the additional cost for the third borehole and the greater borehole depth, this estimate is in reasonable agreement with that of Jung et al. [2003Jun], particularly when considering the period of four years between these two studies.

In summary, while experience is still lacking for commercial geothermal HDR power plants, it appears that this technology is on the verge of becoming economical. This development can certainly be supported and accelerated by national legislation, as for instance in Germany, by allowing geothermal electric energy to be fed into the grid at a certified price (cf. Table 8.26). If successful, this technology will make it possible to generate electric energy from geothermal heat nearly everywhere, even in lack of geothermal anomalies and natural steam reservoirs.

8.4.2.4.3 Pollution

Large volumes of steam (or steam and water) need to be produced in the process of generating electric energy from geothermal heat. For instance 8000 t h⁻¹ are required at The Geysers in California, with a current capacity of 1036 MWe, and 3000 t h⁻¹ at Larderello in Italy, with an installed capacity of 547 MWe. These geothermal fluids vary in chemical composition depending on the reservoir rocks. The major environmental impact of geothermal power production therefore corresponds to the discharge of various gases dissolved in the geothermal fluids into the atmosphere and of water into bodies of surface water, such as rivers and lakes. Minor environmental impacts are connected to land subsidence, induced seismicity, and noise. In his review on “Geothermal Energy Technology and Current Status”, Barbier [2002Bar] discusses all these aspects in detail. Where not stated differently, the following discussion in this paragraph summarizes his synopsis. Further aspects are discussed in [1998Ren], [2000Hun], and [2003Dic].

Air pollution

Steam from major geothermal fields contains an amount of non-condensable gases, CO₂, H₂S, NH₃, CH₄, N₂, and H₂, ranging from 1.0 g – 50 g per kg of steam. Carbon dioxide is the major component, but much less is discharged into the atmosphere per kW h generated from geothermal power plants than from gas-, oil- or coal-fired ones (Fig. 8.61). Even with respect to natural gas, most existing geothermal power plants discharge significantly less CO₂ into the atmosphere. Based on a price for European Emission Allowances of 23 €/per ton of CO₂ traded at the European Energy Exchange⁶, regulations within European Union member states with respect to permissible emissions for various industries provide significant incentives for CO₂ reduction and for low CO₂ energy production and emission. Geothermal emissions of carbon dioxide are in the range of 0.010 kg kW⁻¹ h⁻¹ – 0.380 kg kW⁻¹ h⁻¹ with the exception of one plant on the Azores islands where the geodynamic setting is responsible for a large CO₂ content in the produced steam [1997Bar; 1998Ren; 2002Bar]. In fact, most existing plants emit clearly less than 0.200 kg kW⁻¹ h⁻¹ of CO₂ (Fig. 8.61). This is significantly less than the CO₂ emissions of power plants based on fossil fuels which are in the range of 0.450 kg kW⁻¹ h⁻¹ – 1.040 kg kW⁻¹ h⁻¹. Thus replacing existing oil, gas or coal fired plants by geothermal plants will result in a reduction on the order of 0.250 kg kW⁻¹ h⁻¹, 0.700 kg kW⁻¹ h⁻¹ or 0.850 kg kW⁻¹ h⁻¹, respectively. Based on the number of 23 €/per ton of CO₂ traded at the European Energy Exchange (EEX)⁶ on 24 June 2005, this corresponds to minimum incentives of 0.006 €/kW⁻¹ h⁻¹, 0.016 €/kW⁻¹ h⁻¹ or 0.02 €/kW⁻¹ h⁻¹, if natural gas, oil or coal is replaced.

Apart from the greenhouse gas carbon dioxide, hydrogen sulfide is an air pollutant of major concern in geothermal development. Its emissions are in the range 0.03 g kW⁻¹ h⁻¹ – 6.4 g kW⁻¹ h⁻¹. H₂S is oxidized to sulfur dioxide and then to sulfuric acid, the major source of acid rain. Without extraction, the specific emissions of sulfur from geothermal power plants are about half of those from coal-fired plants (Fig. 8.61). There are no emissions of toxic nitrogen oxides from geothermal power plants, in contrast to fossil fuel plants. However gases in geothermal steam may also contain ammonia (NH₃), traces of mercury (Hg), boron vapors (B), hydrocarbons such as methane (CH₄), and radon (Rn). Boron, ammonia, and – to a smaller amount – mercury are leached from the atmosphere by rain and may contaminate soil and vegetation. Boron, in particular, can have a serious impact on vegetation. Salt water spray from well test-

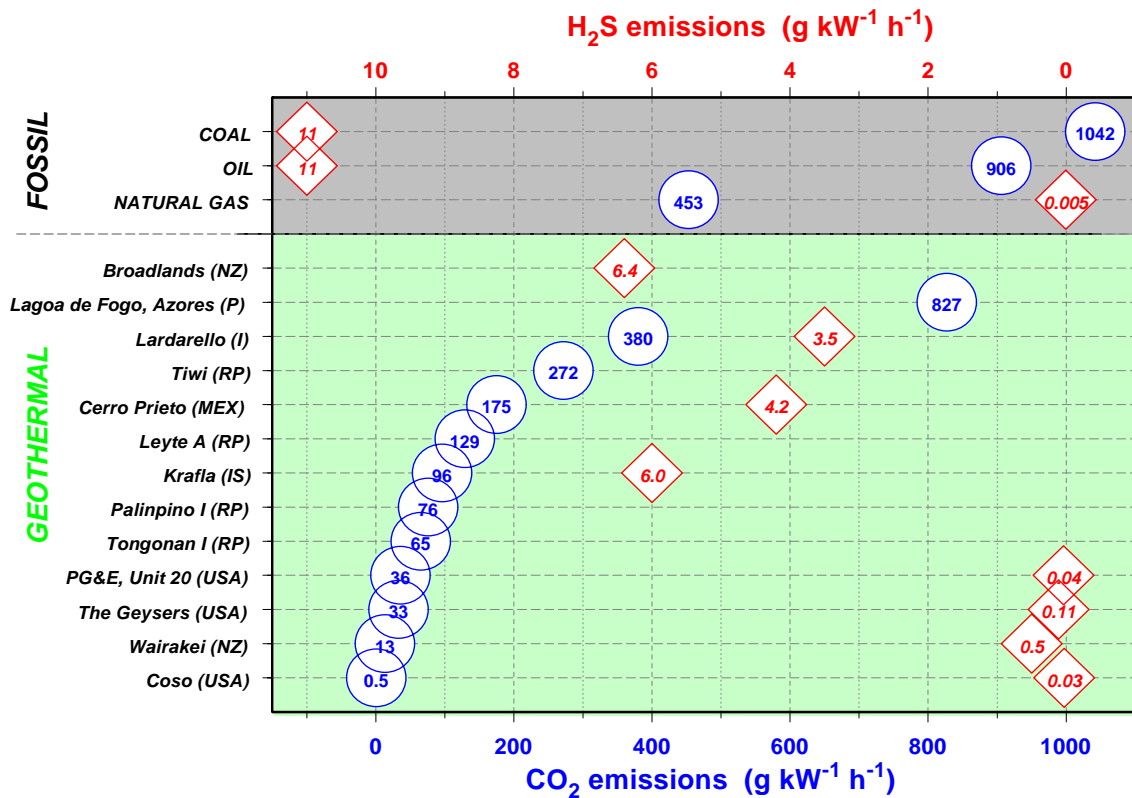


Fig. 8.61 Emission of carbon dioxide (CO₂) and hydrogen sulfide (H₂S) per kW h produced electric energy reported for geothermal power plants in Asia, Europe, North America and typical fossil power plants (I: Italy, IS: Iceland, MEX: Mexico, NZ: New Zealand, P: Portugal, RP: The Philippines; data: [1997Bar; 1998Ren; 2002Bar]).

Table 8.25 Emission limitations or reduction commitments under the Kyoto protocol^{8,9}.

Country	Percentage of emissions by the year 2012 relative to the level of 1990 (or the base period)	Country	Percentage of emissions by the year 2012 relative to the level of 1990 (or the base period)
Austria	87.0	Liechtenstein	92.0
Belgium	92.5	Lithuania	92.0
Bulgaria	92.0	Luxembourg	72.0
Canada	94.0	Netherlands	94.0
Czech Republic	92.0	New Zealand	100.0
Denmark	79.0	Norway	101.0
Estonia	92.0	Poland	94.0
Finland	100.0	Portugal	127.0
France	100.0	Romania	92.0
Germany	79.0	Russia	100.0
Greece	125.0	Slovakia	92.0
Hungary	94.0	Slovenia	92.0
Iceland	110.0	Spain	115.0
Ireland	113.0	Sweden	104.0
Italy	93.5	Switzerland	92.0
Japan	94.0	Ukraine	100.0
Latvia	92.0		

⁸ http://unfccc.int/essential_background/kyoto_protocol/background/items/1351.php

⁹ http://www.bmu.de/files/pdfs/allgemein/application/pdf/kyoto_denkschr.pdf

ing is also reported as a significant source of plant damage within about 50 m – 350 m from the well heads [2005Tuy]. These contaminants may also affect surface waters with a corresponding negative impact on aquatic life. Geothermal literature reports that mercury emissions from geothermal power plants range between $45 \mu\text{g kW}^{-1} \text{h}^{-1}$ – $900 \mu\text{g kW}^{-1} \text{h}^{-1}$, comparable to those from coal-fired power plants. Ammonia is discharged into the atmosphere in concentrations between $57 \text{ mg kW}^{-1} \text{h}^{-1}$ – $1,938 \text{ mg kW}^{-1} \text{h}^{-1}$, but atmospheric circulation leads to rapid dispersion and dilution. Radon (^{222}Rn), a radioactive gas isotope which occurs naturally in the Earth's crust, is contained in geothermal steam and discharged into the atmosphere in concentrations of $3,700 \text{ Bq kW}^{-1} \text{h}^{-1}$ – $78,000 \text{ Bq kW}^{-1} \text{h}^{-1}$. The radon concentration in air at ground level is 5.5 Bq m^{-3} at Larderello (Italy), and varies from mere traces up to 6.0 Bq m^{-3} at The Geysers (USA). By comparison, average levels of radon in air elsewhere are around 3 Bq m^{-3} . Although its levels should be monitored, there is little evidence that radon concentrations are raised above background level by geothermal emissions.

With respect to air and water pollution it merits mention that closed-loop installations, such as binary plants, in which the geothermal fluid is passed through a heat exchanger and reinjected without contact with the atmosphere, will discharge neither gas nor fluid to the environment during normal operation.

Much as stated before with respect to the direct use of geothermal energy, the economics of geothermal power production is ultimately defined by the cost of energy from other, mainly fossil sources, in particular by the price for oil and gas. As a result of the Kyoto protocol^{8,9}, many countries accepted obligations for reducing their CO_2 emissions to the atmosphere, on average, to a level of 92 % of their emissions in the year 1990 (Table 8.25). The Kyoto protocol went into effect by 25 February 2005 after having been ratified by 55 countries which are responsible for at least 55 % of the global CO_2 emissions in 1990. The protocol specifies no limitations for the CO_2 emissions of the People's Republic of China and other developing countries. By 25 February 2004, the Kyoto protocol had been ratified by 141 countries representing 85 % of the world population and 62 % of the current CO_2 emissions; notable exceptions are Australia, Croatia, Monaco, and the USA.

Corresponding policies of other member states of the European Union consist in a combination of penalties and incentives for the production and reduction of CO_2 emissions to the atmosphere, respectively. In combination with the long-term trend of increasing prices for hydrocarbon fuels (Fig. 8.36), this will make geothermal power production increasingly competitive. Additional national legislation can support this process. For instance, in Germany grid operators are required to feed geothermal electric energy into their grids at a certified price of up to $0.15 \text{ €kW}^{-1} \text{h}^{-1}$ until the end of 2009 (Table 8.26); from 2010 onwards this reimbursement is diminished annually by one percent relative to the preceding year's compensation.

Table 8.26 Reimbursement for geothermal electric energy according to the German Renewable Energy Act (2004Ano^d)

Installed capacity (MW)	Reimbursement ($\text{€kW}^{-1} \text{h}^{-1}$)
0 – 5	0.1500
5 – 10	0.1400
10 – 20	0.0895
> 20	0.0716

Pollution is not considered a cost factor as long as its impact on the environment is small and can be neglected. Today, this is generally no longer the case, and national legislation regularly both requires provisions for limiting the environmental burden and provides incentives for the use of environmentally more benign technologies. The effect of both factors is to make low emission technologies more economical.

In this context, the interrelation between pollution and cost has been analyzed using the so-called “eco-efficiency analysis” [2000Kic]. Developed by BASF, the world's largest producer of base chemicals, for analyzing jointly the economic and ecologic characteristics of products and industrial procedures, it has recently been applied by Siemens, a leading producer of equipment for generating electric energy from a variety of different sources of primary energy, to determine which among the renewable energies appear most attractive with respect to both ecology and economy [2004Len^b]. The result summarized in Fig. 8.62 illustrates that geothermal energy is attractive in both respects and well ahead of all kinds of fossil and nu-

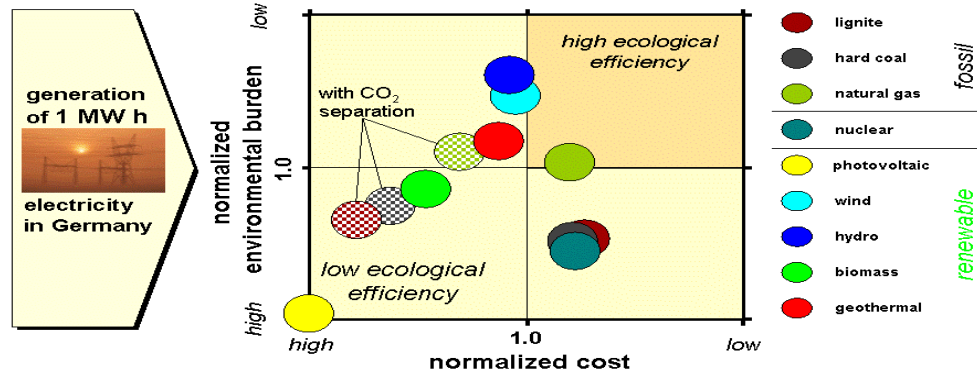


Fig. 8.62 Environmental burden vs. cost associated with the generation of electric energy in Germany based on different sources of fossil and renewable primary energy (modified after [2004Len^b]; wind: 5.5 m s⁻¹ at 50 m above land surface; biomass: wood).

clear energy. Among the renewables it is surpassed in this particular analysis only by hydro and wind energy, and clearly ahead of biomass and photovoltaic energy. Needless to say that analysis requires values to be assigned for various parameters, and Fig. 8.62 does not make their choice transparent. Still, this is an interesting result for two reasons:

- It demonstrates that even today and even under less than optimum premises for the generation of electric energy – in a developed economy such as Germany without natural steam reservoirs, but with many competitors among well developed and well established technologies for energy production – geothermal energy is attractive and competitive with respect to fossil and nuclear as well as other renewable sources of primary energy;
- While hydro and wind energy appear more attractive at present, both have already reached or are close to their maximum development: At least in Germany (and certainly in many other countries) there are few or no sites for new hydropower dams, and similarly, all of the optimum locations for wind turbines are already used. New development appears possible only off-shore, where an additional price must be paid for enforced structures, additional grid lines and ecological safeguarding. In contrast, geothermal energy in countries without natural steam reservoirs is just at the beginning of its development.

Water pollution

As a rule, the discharge of geothermal fluids into surface waters leads to pollution of rivers and lakes and is a potential hazard associated with geothermal electric energy production [2005Sim]. In vapor dominated reservoirs most of the pollutants are in the vapor state, and pollution of surface waters is controlled easier than in water dominated reservoirs. There, waste steam condensate (20 % of the steam supply) must be added to the waste water. The water and the condensate generally carry a variety of toxic chemicals in suspension and solution: arsenic, mercury, lead, zinc, boron and sulfur, together with significant amounts of carbonates, silica, sulfates and chlorides (see e.g. [2005Mro] for a field example). In water dominated and in hot water reservoirs, water and steam (if present) are separated at the surface. The steam is used for generating electric energy, and the volume of water to be disposed of can be as much as 70 kg kW⁻¹ h⁻¹, more than four times the steam supply, and up to 400 kg kW⁻¹ h⁻¹ in binary cycle plants. Often this water contains large amounts of dissolved salts, even above 300 g per kg of extracted fluid. ReInjection into the reservoir is the most common method of disposal. This also helps to control

Pre-Print from:

Clauser, C., 2006. Geothermal Energy, In: K. Heinloth (ed), *Landolt-Börnstein, Group VIII: Advanced Materials and Technologies, Vol. 3: Energy Technologies, Subvol. C: Renewable Energies*, Springer Verlag, Heidelberg-Berlin, 493-604.

reservoir pressure (in order to prevent an unwanted, premature pressure decline) and to extract additional heat from the rock, thus helping to extend the useful life of the resource. At first sight, reinjection might seem expensive, as it requires additional wells, surface piping, and continuous pumping. But in the long run it is very helpful and, calculated over the entire lifetime of a geothermal project, normally helps to save cost compared to a scenario without reinjection.

Land subsidence

As fluids are produced from a reservoir, pore pressure declines causing the ground to subside. Less subsidence occurs for harder than for softer reservoir rocks. The order at which geothermal fluids are produced is comparable to that in large groundwater production for agriculture where land subsidence has been a problem in some cases. Water dominated fields subside more than vapor dominated fields. For example, the Wairakei (New Zealand) water dominated geothermal field (currently at 220 MW_e running capacity) experienced a localized subsidence of 4.5 m in the period 1964 – 1974 (corresponding to a production of 622 Mt of fluid) and a total subsidence of 14 m at maximum in the period 1950 – 1998 [2000All]. In contrast, The Geysers (USA) vapor dominated field (currently at 888 MW_e running capacity) subsided only by 14 cm in the period 1973 – 1977, and Larderello (Italy) – also a vapor dominated field (currently at 473 MW_e running capacity) – subsided by 1.7 m in the period 1923 – 1986. Subsidence can be controlled or prevented by the reinjection of spent fluids. On the other hand, reinjection may give rise to micro-seismicity.

Induced seismicity

Many geothermal reservoirs, in particular at high temperature, are located in geologically active zones of the Earth's crust. These are characterized by volcanic activity, deep earthquakes, and a heat flow larger than average resulting in a natural seismicity which is more frequent than elsewhere. In such a geodynamic framework, water injection into a reservoir may create additional seismicity by increasing pore pressure, reducing rock stress, thus triggering the release of accumulated tectonic stress. A study of the correlation between seismicity and water injection into wells of the Larderello (Italy) geothermal area suggested an increase of low-magnitude events but not an increase in the maximum value of the event magnitudes. Reinjection of waste fluids may therefore have even a positive effect, triggering a higher number of low intensity shocks, but favoring the progressive, non instantaneous release of the stress accumulated in the rocks. This has been known also for some time from experience in fluid injection in oil fields in regimes of tectonic stress and from experiments at the Rocky Mountain Arsenal, near Denver (USA) [1968Hea; 1981Her]. Although this has not yet emerged as a technology by which seismic risk can be managed actively, it deserves greater attention and systematic, focused research in the context of creating and managing HDR or enhanced geothermal reservoirs. While ambitious programs are being discussed in some countries aiming to use this technique massively for developing geothermal energy for electric energy production, the public acceptance of an increasing number of these systems depends critically on whether associated safety concerns of the public can be addressed adequately.

Noise

During drilling or maintenance, a noise level of 90 dBA¹⁰ – 122 dBA or 75 dBA – 90 dBA is associated with wells at free discharge or through silencers, respectively. Well testing is associated with noise levels of 70 dBA – 110 dBA (if silencers are used), and Diesel engines for driving drill rigs with 45 dBA – 55 dBA (if suitable muffling is used). The pain threshold lies at 120 dBA in the frequency range 2000 Hz – 4000 Hz. By comparison, at a distance of 60 m a jet takeoff corresponds to a noise level of 125 dBA, a noisy urban environment to 80 dBA – 90 dBA, and a quiet suburban residence to 50 dBA. On a drill site itself the noise level can be kept below 60 dBA during normal operation. At a distance of one kilometer it should be practically indistinguishable from other background noises [1998Ren].

¹⁰ dBA: unit of sound intensity, exactly like the decibel (dB) except that prior to a measurement sounds of high and low frequencies, heard poorly or not at all by the human ear, have been filtered out. The letter A refers to one of two customary filtering methods.

8.5 Summary

Geothermal heat flows to the surface of the Earth from great depth. In order to use this source for providing heat and electric energy, the governing processes must be understood and the associated physical properties must be known. This chapter hopefully provides a sound starting point for more detailed study and work on this subject

Geothermal energy can be used in a variety of ways: directly as industrial process heat or for space heating (and even cooling). This chapter introduced the most important current concepts in geothermal energy use. However, those wishing to pursue this topic further are advised to consult the special literature much of which is referenced in this text (without claiming completeness).

Sometimes questions are raised whether geothermal is a truly renewable source of energy or whether much of the heat stored in the Earth is not absorbed from solar radiation. While these questions have been addressed earlier in this chapter so much only in this summary: On a human time scale, the produced heat is normally not replaced. In general, replenishing the heat takes longer than producing it. This is why the term “heat mining” is frequently used. However, on a geological scale the produced heat is indeed replenished. This is why geothermal is a truly renewable form of primary energy. On a cosmological time scale all forms of life on earth as we know it today – and thus also all forms of energy production – are limited by the life span of our solar system. What may come after the time when the sun will have become a white giant and subsequently a black dwarf is fortunately beyond our imagination. It certainly poses a limit to the concept of something being renewable.

The advantages and disadvantages of geothermal energy in our present life can be summarized as follows:

- + very small CO₂ output;
- + comparatively small environmental burdens involved;
- + very little land use: production facilities below the Earth’s surface;
- + installations inconspicuous for direct use and comparable to conventional installations with respect to power production;
- + well suited to provide thermal and electric base loads; does not suffer from large peaks which require buffering when fed into grids.
- generation of electric energy currently restricted basically to regions with natural steam reservoirs;
- HDR and enhanced geothermal technology not yet industry standard; further research in generating and localizing fractures required;
- competitiveness of direct use heat hampered by existing sources of (waste) heat with associated difficulty in crowding out and market penetration;
- larger use in regions lacking natural steam reservoirs often hampered by inadequate information on thermal and hydraulic rock properties.

Already today, geothermal energy is an important source of electric energy in many countries. It is particularly valuable for many developing and emerging national economies as it is an indigenous source of energy providing a degree of independence from the variability of the price of hydrocarbons. Even in some of the developed economies it contributes on the order of 0.5 % - 16 % to the national production of electric energy. In countries without natural steam reservoirs it is just at the beginning of its development. The years to come will show whether the existing potential can be put to an economic use. Direct use of geothermal heat is more ubiquitous. Rather than on geological and economic conditions, its use depends on market access, penetration and, in part, crowding out of other sources of available heat. Some countries have made considerable progress in direct use of geothermal heat, both in developed and emerging economies. Similar to the conversion into electric energy, direct use of geothermal heat will benefit from an increase in the price of fossil fuels, in particular hydrocarbons, which can be anticipated for the future based on the historical development and the natural limitation of the resource base.

In summary, geothermal energy appears an attractive, promising, clean, and renewable source of energy.

Pre-Print from:

Clauser, C., 2006. Geothermal Energy, In: K. Heinloth (ed), *Landolt-Börnstein, Group VIII: Advanced Materials and Technologies, Vol. 3: Energy Technologies, Subvol. C: Renewable Energies*, Springer Verlag, Heidelberg-Berlin, 493-604.

Acknowledgements

Klaus Heinloth (Bonn University) for entrusting this chapter to me and for his kind encouragement and patience until its completion; Enrico Barbier (Institute of Geosciences and Earth Resources CNR, Pisa); Michael Baumann (Landesinitiative Zukunftsenergien NRW, Düsseldorf); Ingvar B. Fridleiffson and Valgardur Stefansson (Orkustofnun, Reykjavik); Darrell L. Gallup (Unocal Geothermal Technology & Services, Santa Rosa, CA); Andreas Hartmann (Angewandte Geophysik, RWTH Aachen University); Ernst Huenges (Geoforschungszentrum, Potsdam); Thomas Kohl (Geowatt AG, Zürich), Edgar Laube and Thomas Mathews (ECOS Umwelt GmbH, Aachen); Uwe Lenk (Siemens AG, Erlangen); John Lund and Tonya Boyd (GeoHeat Center, Klamath Falls); Renate Pechnig and Roland Wagner (Geophysica Beratungsgesellschaft mbH, Stolberg); Yuri Popov (Moscow State Geological Prospecting Academy); Gunter Schaumann and Christian Pohl (Transferstelle für rationelle und regenerative Energienutzung, FH Bingen); Rüdiger Schellschmidt (Leibniz Institute for Applied Geosciences, Hannover) for active support and sharing of published and unpublished information and data with me; Jörn Bartels (Geothermie Neubrandenburg GmbH), Daniel Pribnow (Shell Research, Rijswijk), Heiner Villinger (Universität Bremen) for critical reading of the manuscript; and finally, but certainly not least, my wife Karin and my children Johanna and Simon for their kind support and willingness to do without me on countless weekends while this manuscript was written.

References

- 1999Abe Abé, H., Niitsuma, H., Baria, R. (Eds): *Hot Dry Rock/Hot Wet Rock Academic Review, Geothermics* **28(4/5)** (1999)
- 1989Afj Afjei, T.: YUM - A Yearly Utilisation Model for Calculating the Seasonal Performance Factor of Electric Driven Heat Pump Heating Systems, Technical Form, IET-LES, ETH Zürich,; Zürich (1989).
- 2000All Allis, R.G.: *Geothermics* **29(4/5)** (2000) 455-478
- 1973Ana Anand, J., Somerton, W.H., Gomaa, E.: *Soc. Petrol. Eng. J.* **13** (1973) 267-273
- 1996Ano^a Anonymous: *Anforderungen an Wärmepumpenanlagen für die Nutzung von Wärme aus Grundwasser, Oberflächenwasser, Erdwärmesonden, Erdregister*, Wasser- und Energiewirtschaftsamt & Amt für Gewässerschutz und Abfallwirtschaft des Kantons Bern, Bern.
- 1996Ano^b Anonymous: *Electricity Generation Today*, ABB Asea Brown Boveri Ltd, Zürich (1996)
- 1998Ano Anonymous: *Geothermal Atlas of Azerbaijan*, Geology Institute, Azerbaijan National Academy of Sciences, <http://www.gia.az/html/production/atlases/a1.html> (1998)
- 1999Ano^a Anonymous: *Planen mit der Sonne*, 2nd ed, IWP-00-126, Initiativkreis Wärmepumpe (IWO), München (1999)
- 1999Ano^b Anonymous: *Europäisches Geothermieprojekt Soultz-sous-Forêts*, Projektinfo 06/99, <http://www.bine.info/pdf/publikation/bi0699.pdf>, BINE Informationsdienst, Karlsruhe (1999)
- 2000Ano Anonymous: *Thermal use of the underground; Part 1: Fundamentals, approvals, environmental aspects*, VDI-Richtlinien VDI 4640/I, Verein deutscher Ingenieure (VDI), Düsseldorf (2000)
- 2001Ano^a Anonymous: *Thermal use of the underground; Part 2: Ground source heat pump systems*, VDI-Richtlinien VDI 4640/II, Verein deutscher Ingenieure (VDI), Düsseldorf (2001)
- 2001Ano^b Anonymous: *Utilization of the subsurface for thermal purposes; Part 3: Underground thermal energy storage*, VDI-Richtlinien VDI 4640/III, Verein deutscher Ingenieure (VDI), Düsseldorf (2001)
- 2001Ano^c Anonymous: *Leitfaden zur Nutzung von Erdwärme mit Erdwärmesonden*, 3rd ed, Ministerium für Umwelt und Verkehr Baden-Württemberg, Stuttgart (2001)
- 2001Ano^d Anonymous: *Geothermal Energy Slide Show*, <http://geothermal.marin.org/GEOpresentation/>, Geothermal Education Office, Tiburon USA (2001)
- 2002Ano *Aniwanina* **19** <http://www.niwascience.co.nz/pubs/an/19/waikato> (2002)
- 2003Ano^a Anonymous: *European Deep Geothermal Energy Programme*, <http://www.soultz.net/> (2003)
- 2003Ano^b Anonymous: *Geothermal Electricity Generation in Neustadt-Glewe*, Projekt-Info 9/03, <http://www.bine.info/pdf/publikation/bi0903eninternetx.pdf>, BINE Informationsdienst, Karlsruhe (2003)
- 2003Ano^c Anonymous: *Geodynamics Business Plan*, www.geodynamics.com.au/ (2003)
- 2004Ano^a Anonymous: *Geothermie – Daten zur Nutzung des oberflächennahen geothermischen Potenzials*, Geologischer Dienst Nordrhein-Westfalen, Krefeld (2004) CD-ROM, http://www.gla.nrw.de/g_details.php?id=1700
- 2004Ano^b Anonymous: *Thermal use of the underground; Part 4: Direct uses*, VDI-Richtlinien VDI 4640/IV, Verein deutscher Ingenieure (VDI), Düsseldorf (2004)
- 2004Ano^c Anonymous: *Selected Geothermal Power Plants*, ORMAT Technologies Inc., Sparks NV, USA, http://www.ormat.com/index_projects.htm (2004)
- 2004Ano^d Anonymous: *Gesetz zur Neuregelung des Rechts des Erneuerbaren Energien im Strombereich*, Bundesgesetzblatt, Teil I, Nr. 40, 1918, <http://217.160.60.235/BGBL/bgb11f/bgb1104s1918.pdf>, Bonn (2004)
- 2004Ano^e Anonymous: *Heat Engines*, U.S. Dept. of Energy, Washington, <http://www.eere.energy.gov/consumerinfo/factsheets/ba9.html> (2004)
- 2004Ano^f Anonymous: *Absorption Cooling*, U.S. Dept. of Energy, Washington, <http://www.eere.energy.gov/buildings/info/components/hvac/cooling/absorption.html>

Pre-Print from:

Clauser, C., 2006. Geothermal Energy, In: K. Heinloth (ed), *Landolt-Börnstein, Group VIII: Advanced Materials and Technologies, Vol. 3: Energy Technologies, Subvol. C: Renewable Energies*, Springer Verlag, Heidelberg-Berlin, 493-604.

- 1970Aro Aronsson, J.R., Bellotti, L.H., Eckroad, S.W., Emslie, A.G., McConnell, R.K., von Thüna, P.C.: *J. Geophys. Res.* **75(17)** (1970) 34433456
- 1955Asa Asaad, Y.: *A Study on the Thermal Conductivity of Fluid-Bearing Rocks*, Doctoral Dissertation, Univ. of California, Berkeley (1955)
- 1997Bar Barbier, E.: *Renewable and Sustainable Energy Rev.* **1(1/2)** (1997) 1-69
- 1999Bar Baria, R., Baumgärtner, J., Gérard, A., Jung, R., Garnish, J.: *Geothermics* **28(4/5)** (1999) 655-669
- 2002Bar Barbier, E.: *Renewable and Sustainable Energy Rev.* **6** (2002) 3-65
- 1972Bea Bear, J.: *Dynamics of Fluids in Porous Media*, Elsevier, New York (1972); reprinted by Dover, Mineola N.Y. (1988)
- 2001Bea Beardsmore, G.R., Cull, J.P.: *Crustal Heat Flow*, Cambridge University Press, Cambridge (2001)
- 1958Bec Beck, A.E., Beck, J.M.: *Trans. Am. Geophys. Union* **39** (1958) 1111-1123
- 1965Bec Beck, A.E., in: Lee, W.H.K. (Ed), *Terrestrial Heat Flow*, Am. Geophys. Union, Washington D.C. (1965) 24-57
- 1988Bec Beck, A.E., in: Hänel, R., Rybach, L., Stegena, L. (Eds), *Handbook of Terrestrial Heat Flow Density Determination*, Kluwer Academic Publishers, Dordrecht (1988) 87-124
- 1995Ber Berryman, J.G., in: Arens, T.J. (Ed), *Rock Physics and Phase Relations – A Handbook of Physical Constants, AGU Reference Shelf 3*, Am. Geophys. Union, Washington D.C. (1995) 205-228
- 2005Ber Bertani, R.: World Geothermal Generation 2001-2005: State of the Art, in: Horne, R.N., Okandan, E. (Eds), *Proc. World Geothermal Congress 2005 (CD)*, Intl. Geothermal Association, Paper 0008, Reykjavik (2005)
- 1940Bir^a Birch, F., Clark, H.: *Am. J. Sci.* **238(8)** (1940) 529-558
- 1940Bir^b Birch, F., Clark, H.: *Am. J. Sci.* **238(9)** (1940) 613-635
- 1942Bir Birch, F., in: Birch, F., Schairer, J.F., Spicer, H.C. (Eds), *Handbook of Physical Constants*, Special Paper 36, Geol. Soc. of America, New York, (1942) 243-266
- 1954Bir Birch, F.: *Am. J. Sci.*, **252(1)** (1954) 1-25
- 1966Bir Birch, F., in: Clark Jr., S.P. (Ed), *Handbook of Physical Constants, rev. ed.*, Memoir 97, Geol. Soc. of America (1966) 97-173
- 1989Bla Blackwell, D.D., in: Naser, N.D., McCulloh, T.H. (Eds), *Thermal History of Sedimentary Basins*, Springer, Berlin (1989) 13-36
- 1992Bla Blackwell D.D., Steele J.L.: *Geothermal Map of North America*, Geol. Soc. of America, Boulder, CO (1992)
- 2003Blo Bloomquist, R.G., Knapp, G., in: Dickson, M.H., Fanelli, M. (Eds): *Geothermal Energy: Utilization and Technology*, UNESCO, Paris (2003) 175-201
- 2004BMW Bundesministerium für Wirtschaft und Arbeit (BMWA): *Energie Daten 2003*, BMWA, Berlin (2004) (recent statistics see: <http://www.bmwi.de/BMWi/Navigation/Energie/Energiestatistiken/energieDaten.html>)
- 1985Bou Bourbie T., Zinsner, B.: *J. Geophys. Res.* **90(B13)** (1985) 11524-11532
- 1992Bre Breese, J.C. (Ed.): *The Soutz Hot Dry Rock Project*, Gordon and Breach, Philadelphia (1992)
- 1990Bri Brigaud, F., Chapman, D. S., Le Douran, S.: *AAPG Bulletin* **74(9)** (1990) 1459-1477
- 1981Bro Brown, G.C., in: Smith, D.G. (Ed), *Cambridge Encyclopedia of Earth Sciences*, Prentice-Hall, Scarborough (1981) 141-161
- 1993Bro Brown, G.C.: *The Inaccessible Earth, 2nd ed*, Chapman and Hall, London (1993)
- 1999Bro Brown, D. W., Duchane, R. H.: *Geothermics* **28(4/5)** (1999) 591-601
- 2001Bro Brown, M.E.: *Introduction to Thermal Analysis: Techniques and Applications (Hot Topics in Thermal Analysis and Calorimetry)*, Kluwer Academic Publishers, Dordrecht (2001)
- 2003Bro Brown, K., Webster-Brown, J., in: Dickson, M.H., Fanelli, M. (Eds): *Geothermal Energy: Utilization and Technology*, UNESCO, Paris (2003) 155-173
- 1935Bru Brugeman, D.A.G.: *Ann. d. Physik*, **24** (1935) 636-679
- 1939Bul Bullard, E.C.: *Proc. Roy. Soc. London, Series A* **173** (1939) 474-502

- 1951Bul Bullard, E.C., Niblett, E.R.: *Monthly Notices Roy. Astr. Soc. London, Geophys. Suppl.* **6** (1951) 222-238
- 1991Bun Buntebarth, G.: *Scientific Drilling* **2** (1991) 73-80
- 2002Buf Buffett, B.A.: *Geophys. Res. Lett.* **29(3)**, 1566 (2002) doi: 10.1029/2001GL014649
- 2003Buf Buffett, B.A.: *Science* **299** (2003) 1675-1677
- 2000Bur Burns, K.L., Weber, C., Perry, J., Harrington, H.J., in: E. Iglesias, D. Blackwell, T. Hunt, J. Lund, S. Tamanyu, K. Kimbara (Eds), *Proc. World Geothermal Congress 2000*, Intl. Geothermal Association, Auckland (2000) 99-108
- 2004BWP Bundesverband Wärmepumpe e.V.: *BWP-inform* **1** (2004)
- 2000Can Canup R. M., Righter, K. (Eds): *Origin of the Earth and Moon*, University of Arizona Press, Tucson AZ (2000)
- 1959Car Carlsaw, H. S., Jaeger, J. C.: *Conduction of Heat in Solids*, 2nd ed, Clarendon, Oxford.
- 1982Čer Čermák, V., Rybach, L., in: Angenheister, G. (Ed), *Landolt-Börnstein: Numerical Data and Functional Relationships in Science and Technology*, New Series, V(1a), Springer, Berlin (1982) 305-343
- 2004Chr Christensen, U., Tilgner, A.: *Nature* **429** (2004) 169-171
- 1941Cla Clark, H.: *Trans. Am. Geophys. Union* **22(II)** (1941) 543-544
- 1966Cla Clark Jr., S.P., in: Clark Jr., S.P. (Ed), *Handbook of Physical Constants*, Memoir 97, Geol. Soc. of America, New York (1966) 459-482
- 1969Cla Clark Jr., S.P., in: Hart, P.J. (Ed), *The Earth's Crust and Upper Mantle*, Geophysical Monograph 13, Am. Geophys. Union, Washington D.C. (1969) 622-626
- 1988Cla Clauser, C., in: Hänel, R., Rybach, L., Stegena, L. (Eds), *Handbook of Terrestrial Heat Flow Density Determination*, Kluwer Academic Publishers, Dordrecht (1988) 143-165
- 1992Cla Clauser, C.: *EOS Trans. Am. Geophys. Union* **73(21)** (1992) 233, 237
- 1995Cla Clauser, C., Huenges, E. in: Ahrens, T.J. (Ed), *Rock Physics and Phase Relations - a Handbook of Physical Constants*, AGU Reference Shelf 3, Am. Geophys. Union, Washington D.C. (1995) 105-126
- 2001Cla Clauser, C.: *Update of the permeability of crystalline rocks*, <http://www.rwth-aachen.de/geop/Forschung/Petrophysik/rocks/perm.htm>, RWTH Aachen University, Aachen (2001)
- 2002Cla Clauser, C., Griesshaber, E., Neugebauer, H.J.: *J. Geophys. Res.* **107(B11)** (2002) doi: 10.1029/2001JB000675
- 2003Cla^a Clauser, C. (Ed): *Numerical Simulation of Reactive Flow in hot Aquifers using SHEMAT/-Processing Shemat*, Springer, Berlin (2003)
- 2003Cla^b Clauser, C., Kleiner, S., Wagner, R., Mathews, T.: *Brennstoff, Wärme, Kraft (BWK)* **55(9)** (2003) 29-30
- 1947Cos Coster, H.P.: *Monthly Notices Roy. Astr. Soc., Geophys. Suppl.* **5(5)** (1947) 131-145
- 1986Cra Crain, E.R.: *The Log Analysis Handbook*, Quantitative Log Analysis Methods Series, Vol. 1, Pennwell Publishing, Tulsa, OK (1986)
- 1986Cul Culver, G.: *Performance Evaluation of the ORMAT Generator at Wabuska, Nevada*, Geo Heat Center, Oregon Institute of Technology, Klamath Falls, OR, <http://geoheat.oit.edu/pdf/be1.pdf> (1986)
- 1856Dar Darcy, H.: *Les fontaines publiques de la ville de Dijon*, Dalmont, Paris (1856)
- 1988Dav Davis, E.E., in: Hänel, R., Rybach, L., Stegena, L. (Eds), *Handbook of Terrestrial Heat Flow Density Determination*, Kluwer Academic Publishers, Dordrecht (1988) 223-260
- 1999Del Delacroix, S.: *Les Cahiers du CLIP*, **10** http://www.iddri.org/iddri/telecharge/cahier-du-clip/clip_10 (1999) 29-63
- 1991Dem Demongodin, L., Pinoteau, B., Vasseur, G., Gable, R.: *Geophys. J. Int.* **105** (1991) 675-691
- 1974Des Desai, P.D., Navarro, R.A., Hasan, S.E., Ho, C.Y., DeWitt, D.P., West, T.R.: *Thermophysical Properties of Selected Rocks*, CINDAS Report 23, Center for Information and Numerical Data Analysis and Synthesis (CINDAS), Purdue Univ., West Lafayette, IN (1974)
- 2001Dic Dickson, M., Fanelli, M.: *Renewable Energy World* **4** (July-August) (2001) 211-217
- 2003Dic Dickson, M.H., Fanelli, M. (Eds): *Geothermal Energy: Utilization and Technology*, UNESCO, Paris (2003)
- 1997Die Diekmann, B., Heinloth, K.: *Energie*, 2nd ed, B. G. Teubner, Stuttgart (1997)

- 1988Dim Diment, W.H., Pratt, H.R.: *Thermal Conductivity of Some Rock-Forming Minerals: a Tabulation*, Open File Report 88-690, U.S. Geol. Survey, Denver CO (1988)
- 1997DiP DiPippo, R. in: Elliott, T.C., Chen, K., Swanekamp, R.C. (Eds), *Standard Handbook of Powerplant Engineering, 2nd ed*, McGraw-Hill, New York (1997) 8.27-8.60
- 2004DiP DiPippo, R.: *Geothermics* **33(5)** (2004) 565-586
- 1974Dre Dreyer, W.: *Materialverhalten anisotroper Festkörper: Thermische und elektrische Eigenschaften*, Springer, Wien (1974)
- 1981Dzi Dziewonski, A.M., Anderson, D.L.: *Phys. Earth Planet. Int.* **25** (1981) 297-356
- 1997Edw Edwards, J.D.: *American Association of Petroleum Geologists Bulletin* **81** (1997) 1292-1305
- 2003Elf Elíasson, E.T., Ármansson, H., Thórhallsson, S., Gunnarsdóttir, M.J., Björnsson, O.B., Karlsson, T., in: Dickson, M.H., Fanelli, M. (Eds): *Geothermal Energy: Utilization and Technology*, UNESCO, Paris (2003) 53-79
- 2004EIA U.S. Energy Information Administration (EIA): *World Oil Market and Oil Price Chronologies 1970-2003*, EIA, Washington, D.C., <http://www.eia.doe.gov/emeu/cabs/chron.html> (2004)
- 1983Eth Etheridge, M.A., Wall, V.J., Vernon, R.H.: *J. Metamorph. Geol.* **1** (1983) 205-226
- 1995Fei Fei, Y. in: Arens, T.J. (Ed), *Mineral Physics and Crystallography – A Handbook of Physical Constants, AGU Reference Shelf 2*, Am. Geophys. Union, Washington D.C. (1995) 29-44
- 1994Fri Fridleifsson, I.B., Freeston, D.H.: *Geothermics* **23** (1994) 175-214
- 2001Fri Fridleifsson, I.B.: *Renewable Sustainable Energy Rev.* **5** (2001) 299-312
- 1998Gal Gallagher, P.K. (Ed): *Handbook of Thermal Analysis and Calorimetry*, Elsevier, Amsterdam (1998)
- 2002Gas Gassel, A.: *Erneuerbare Energie*, **2** (2002) 23 http://www.energytech.at/pdf/ee_gassel.pdf
- 2002Geh Gehlin, S.: *Thermal response test – Method development and evaluation*, Doctoral Dissertation, Luleå University of Technology, Department of Environmental Engineering, Luleå (2000)
- 1991Gho Ghosh, S., Dasgupta, S.: *Geothermal Atlas of India*, Special Publication 19, Geol. Survey of India, Calcutta, <http://www.gsi.gov.in/splpub.htm> (1991)
- 1942Gor Goranson, R.W., in: Birch, F., Schairer, J.F., Spicer, H.C. (Eds): *Handbook of Physical Constants*, Special Paper 36, Geological Society of America, New York NY (1942)
- 1996Gra Grant, M.A.: *Geothermal Resource Management*, Geothermal Energy New Zealand Ltd (GENZL), Auckland (1996)
- 1990Gri Grigull, U., Sandner, H., *Wärmeleitung, 2nd ed*, Springer, Berlin (1990)
- 1995Gup Gupta, M.L., Yamano, M. (Eds): *Terrestrial Heat Flow and Geothermal Energy in Asia*, A. A. Balkema, Rotterdam (1995)
- 1980Hän Hänel R. (Ed): *Atlas of Subsurface Temperatures in the European Community*, Th. Schäfer, Hannover (1980)
- 1988Hän Hänel R., Staroste E. (Eds): *Atlas of Geothermal Resources in the European Community*, Th. Schäfer, Hannover (1988)
- 2002Hai Haines, P. (Ed): *Principles of Thermal Analysis and Calorimetry*, Royal Soc. Chem., London (2002)
- 1996Ham Hamza, V.M., Muñoz, M.: *Geothermics* **25(6)** (1996) 599-621
- 2005Har Hartmann, A., Rath, A., Clauser, C.: Thermal Conductivity from Core and Well log Data, *Int. J. Rock Mech. Mining Sci.* **42** (2005) 1042-1055, doi:10.1016/j.ijrmms.2005.05.015
- 1962Has Hashin, Z., Shtrikman, S.: *J. Appl. Phys.* **33(10)** (1962) 3125-3131
- 1968Hea Healy, J.H., Rubey, W.W., Griggs, D.T., Raleigh, C.B.: *Science*, **161** (1968) 1301-1310
- 1984Hem Hemminger, W.F., Höhne, G.W.: *Calorimetry – Fundamentals and Practice*, Verlag Chemie, Weinheim (1984)
- 1989Hem Hemminger, W.F., Cammenga, H.K.: *Methoden der thermischen Analyse*, Springer, Berlin (1989)
- 1981Her Herrmann, R.B., Park, S.K., Wang, C.Y.: *Bull. Seism. Soc. Am.*, **71** (1981) 731-745
- 1997Höh Höhne, G.W.H., Hemminger, W., Flammersheim, H.-J.: *Differential Scanning Calorimetry*, Springer, Berlin (1997)
- 1999Hof Hofmeister, A.M.: *Science*, **283** (1999) 1699-1706.

- 1969Hor Horai, K., Simmons, G.: *Earth and Planet. Sci. Lett.* **6** (1969) 359-368
- 1971Hor Horai, K.: *J. Geophys. Res.* **76(5)** (1971) 1278-1308
- 1972Hor Horai, K., Baldrige, S.: *Phys. Earth Planet. Interiors* **5** (1972) 157-166
- 1991Hor Horai, K.: *J. Geophys. Res.* **96(B3)** (1991) 4125-4132
- 1999Hor Hori, Y., Kitano, K., Kaieda, H., Kiho, K.: *Geothermics* **28(4/5)** (1999) 637-645
- 1997Hub Huber, A., Schuler O.: *Berechnungsmodul für Erdwärmesonden*, Bundesamt für Energie-wirtschaft, Bern. ENET Nr. 9658807
- 2003Hud Hudson, R.B., in: Dickson, M.H., Fanelli, M. (Eds): *Geothermal Energy: Utilization and Technology*, UNESCO, Paris (2003) 29-52
- 2000Hun Hunt, T. (Ed): *Environmental Aspects of Geothermal Development*, *Geothermics* **29(4/5)** (2000)
- 1992Hur Hurtig E., Čermák V., Hänel R., Zui V. (Eds): *Geothermal Atlas of Europe*, Geographisch-Kartographische Anstalt J. Perthes, Gotha (1992)
- 2002Hur Hurter, S.J., Hänel R. (Eds): *Atlas of Geothermal Resources in Europe*, Publication No. EUR 17811, European Commission Office for Official Publications of the European Communities, Luxemburg (2002)
- 1968Hut Hutt, J.R., Berg Jr., J.: *Geophysics* **33** (1968) 489-500
- 1998Ing Ingebritsen, S.E., Sanford, W.E.: *Groundwater in Geologic Processes*, Cambridge University Press, Cambridge (1998)
- 2002IEA International Energy Agency (IEA): *World Energy Outlook 2002*, International Energy Agency (IEA), Paris, (2002) 58; (recent statistics: see: <http://library.iea.org/Textbase/publications/index.asp>).
- 2003IEA International Energy Agency (IEA): *Key World Energy Statistics*, International Energy Agency (IEA), Paris, (2003) 6 (recent statistics see: <http://www.iea.org/dbtw-wpd/Textbase/publications/index.asp>)
- 2005IEA International Energy Agency (IEA): *End-User Petroleum Product Prices And Average Crude Oil Import Costs*, IEA, Paris <http://www.iea.org/Textbase/stats/surveys/mps.pdf> (2004)
- 1989Jun Jung, R.: *Int. J. Rock Mech. Min. Sci. Geomech. Abstr.* **26(3/4)** (1989) 301-308
- 2003Jun Jung, R., Kabus, F., Kaltschmitt, M., Nill, M., Schröder, G., Rogge, S. in: Kaltschmitt, M., Wiese, A., Streicher, W. (Eds), *Erneuerbare Energien*, Springer, Berlin (2003) 489-517
- 1984Kal Kalina, A. L.: *ASME J. of Engineering for Gas Turbines and Power* **106(4)** (1984) 737-742.
- 1999Kal Kaltschmitt, M., Huenges, E., Wolff, H. (Eds): *Energie aus Erdwärme*, Deutscher Verlag für Grundstoffindustrie, Stuttgart (1999)
- 2003Kal Kaltschmitt, M., Streicher, W., in: Kaltschmitt, M., Wiese, A., Streicher, W. (Eds), *Erneuerbare Energien*, Springer, Berlin (2003) 519-574
- 1968Kan Kanamori, H., Fujii, N., Mizutani, H.: *J. Geophys. Res.* **73(2)** (1968) 595-605
- 1974Kap Kappelmeyer, O., Hänel, R. *Geothermics with Special Reference to Application*, Gebrüder Bornträger, Berlin-Stuttgart (1974)
- 1999Kay Kayser, M., Kaltschmitt, M., in: Kaltschmitt, M., Huenges, E., Wolff, H. (Eds), *Energie aus Erdwärme*, Deutscher Verlag für Grundstoffindustrie, Stuttgart (1999) 189-210
- 1960Kel Kelley, K.: *Contributions to the data on theoretical metallurgy: XIII High-Temperature Heat-Content, Heat-Capacity, and Entropy data for the Elements and Inorganic Compounds*, U.S. Bureau of Mines Bull. 584, U.S. Government Printing Office, Washington D.C. (1960)
- 1995Ken Kennett B.L.N., Engdahl E.R. Buland R.: *Geophys. J. Int.* **122** (1995) 108-124
- 2000Kic Kicherer, A., Pfisterer, H.E., Staudacher, R.: *The BASF Ecoefficiency Analysis*, BASF in Dialogue, November 2000, http://www.basf.de/basf/img/position/effizienz_e.pdf?id=6FPP-Y6SI6bsf39c, Ludwigshafen (2000)
- 1990Kob Kobolev, V.P., Kutas, R.I., Popov, Y.A.: *Geophysical Journal* **12(4)** Naukova Dumka, Kiev (1990) 29-37 (in Ukrainian).
- 2002Koh Kohl, T., Brenni, R., Eugster, W.: *Geothermics* **31(6)** (2002) 687-708
- 2002Kol Kolditz, O.: *Computational Methods in Environmental Fluid Mechanics* Springer, Berlin (2002)
- 1999Kuk Kukkonen, I., Suppala, I.: *Measurements of thermal conductivity and diffusivity in situ: literature survey and theoretical modelling of measurements*, report POSIVA 99-1, Geological Survey of Finland, Espoo (1999)

- 1961Kun Kunii, D., Smith, J.M.: *Soc. Petrol. Eng. J.* **1(1)** (1961) 37-42
- 1999Kur Kuriyagawa, M., Tenma, N.: *Geothermics* **28(4/5)** (1999) 627-636
- 1999Kyl Kyle, L.: *Total Solar Irradiance*, http://daac.gsfc.nasa.gov/CAMPAIGN_DOCS/FTP_SITE/INT_DIS/readmes/sol_irrad.html, NASA Goddard Space Flight Center, Greenbelt, MD. (1999)
- 2004Len^a Lenk, U.: *Umwandlung geothermischer Energie in Strom mit dem Kalina Cycle*, RENEXPO 2004, http://www.muc.zae-bayern.de/zae/a4/deutsch/pub/renexpo/Geothermie_Renexpo_21-10-2004-2_Lenk-U_Kalina-Cycle.pdf Augsburg (2004)
- 2004Len^b Lenk, U.: *Welche Technologien nutzen die Kraftwerke der Zukunft?* 42. Fachtagung der Österreichischen Gesellschaft für Energietechnik, <http://www.ove.at/veranstaltungen/OGE2004/ppt/Lenk.pdf> Graz (2004)
- 2000Lid Lide, D.R. (Ed): *CRC Handbook of Chemistry and Physics, 81st ed*, CRC Press, Boca Raton (2000) 6-7; 6-21; 6-187; 14-2
- 2003Lie Lienau, P.J., in: Dickson, M.H., Fanelli, M. (Eds): *Geothermal Energy: Utilization and Technology*, UNESCO, Paris (2003) 129-154
- 1997Low Lowrie, W.: *Fundamentals of Geophysics*, Cambridge University Press, Cambridge (1997)
- 2000Low Low, P., Morris, G., in: E. Iglesias, D. Blackwell, T. Hunt, J. Lund, S. Tamanyu, K. Kimbara (Eds), *Proc. World Geothermal Congress 2000*, Intl. Geothermal Association, Auckland (2000) 3217-3222
- 2001Lun Lund, J.W., Freeston, D.H.: *Geothermics* **30(1)** (2001) 29-68
- 2003Lun^a Lund, J.W., Sanner, B., Rybach, L., Curtis, R., Hellström, G.: *Renewable Energy World* **4** (July-August) (2003) 218-227
- 2003Lun^b Lund, J. W., in: Dickson, M.H., Fanelli, M. (Eds): *Geothermal Energy: Utilization and Technology*, UNESCO, Paris (2003) 113-120
- 2004Lun^a Lund, J.W.: *Renewable Energy World* **7(4)** (2004) 218-227
- 2004Lun^b Lund, J.W., Dipippo, R., Boyd, T. L.: *The Basics Of Geothermal Power Conversion*, Geo-Heat Center, Oregon Institute Of Technology, Klamath Falls, http://www.bgr.de/veranstaltungen/renewables_2004/presentations_DGP/Block1Introduction_pdf/3_Lund.pdf (2004)
- 2005Lun Lund, J.W., Freeston, D.H., Boyd, T.I.: *World-Wide Direct Uses of Geothermal Energy 2005*, in: Horne, R.N., Okandan, E. (Eds), *Proc. World Geothermal Congress 2005 (CD)*, Paper 0007, Intl. Geothermal Association, Reykjavik (2005)
- 1999Man Manning, C.E., Ingebritsen, S.E.: *Rev. Geophys.* **37(1)** (1999) 127-150
- 1986Mar Marsily, G. de: *Quantitative Hydrogeology*, Academic Press, Orlando (1986).
- 1967McK McKelvey, V.E.: *Am. Scientist* **60** (1967) 32-40
- 1990Mel Melosh, H. J.: *Giant impacts and the thermal state of the early Earth*, in: Newsom, H. E., Jones, J. H. (Eds), *Origin of the Earth*, Oxford University Press, New York NY (1990) 69-83
- 1965Mes Mesmer, J.H., in: *Proceedings of the Fifth Conference on Thermal Conductivity, Vol. 1*, University of Denver, Denver (1965) 1-29
- 2002Mes Meschede, D.: *Gerthsen Physik, 21st ed*, Springer, Berlin (2002)
- 1982Mil Miller, H., in: Angenheister, G. (Ed), *Landolt-Börnstein – Numerical Data and Functional Relationships in Science and Technology*, New Series, V(1b), Springer, Berlin (1982) 482-507
- 1997Moc Mock, J.E., Tester, J.W., Wright, P.M.: *Ann. Rev. Energy Environment* **22** (1979) 305-356
- 1995Mon Montagner J.P., Kennett B.L.N.: *Geophys. J. Int.* **125** (1995) 229-248
- 2005Mot Mottaghy, D.C., Schellschmidt, R., Popov, Y.A., Clauser, C., Kukkonen, I.T., Nover, G., Milanovsky, S., Romushkevich, R.A.: *Tectonophysics* **401/1-2** (2005) 119-142, doi: 10.1016/j.tecto.2005.03.005.
- 2005Mro Mroczek, E.K., in: Hunt, T. (Ed), *Environmental Aspects of Geothermal Energy*, *Geothermics* **34(2)** (2005) 218-233
- 1978Muf Muffler, L. J. P., Cataldi, R.: *Geothermics* **7** (1978) 53-89
- 1997Nak Nakićenović, N., Grubler, A., McDonald, A. (Eds): *Global Energy Perspectives*, Cambridge University Press, Cambridge (1998)

- 2000Nak Nakićenović, N. in: Goldemberg, J., Baker, J.W., Ba-N'Daw, S., Khatib, H., Popescu, A., Viray, F.L. (Eds): *World Energy Assessment*, United Nations Development Programme, New York NY (2000) 333-366 (<http://www.undp.org/energy/activities/wea/drafts-frame.html>)
- 1994Nan Nani, M., Stalder, M., Schweizer, A., Baumgartner, T.: *WPcalc. Rechenprogramm zur Auslegung von WP-Anlagen*, Bundesamt für Energiewirtschaft, Bern (1994)
- 1998Nar Narayan, S. P., Dumbrell, R. Rahman, S. S.: *Geothermische Energie* **22/23(2/3)** ([http://www.geothermie.de/gte/gte22-23/artikel 5/artikel 5.htm](http://www.geothermie.de/gte/gte22-23/artikel%205/artikel%205.htm)) (1998)
- 2002NGD National Geophysical Data Center (NGDC): *Daily total solar irradiance*, <http://www.ngdc.noaa.gov/stp/SOLAR/IRRADIANCE/irrad.html>, National Oceanographic and Atmospheric Administration (NOAA), Boulder CO (2002)
- 1999Nic Nichols, K.: *Case histories Barber-Nichols small geothermal power plants*, Barber Nichols, Arvada CO, USA (<http://www.barber-nichols.com/graphics/techpapers/geothermal.pdf>) (1999)
- 1999Pah Pahud, D., Fromentin, M., Hibbuch, M.: *Heat Exchanger Pile System of the Dock Midfield at the Zürich Airport – Detailed Simulation and Optimisation of the Installation*, Final Report, Swiss Federal Office of Energy, Bern, Switzerland (<http://www.energieforschung.ch/ENET/Project?ReadForm&proj=23966>) (1999)
- 2001Pah Pahud, D., Matthey, B.: *Energy and Buildings*, **33** (1999) 503-507
- 1986Pal Palciauskas, V.V, in: Burrus, J. (Ed), *Thermal Modeling in Sedimentary Basins*, Edition Technip, Paris (1986) 323-336
- 1999Pap Pape, H., Clauser, C., Iffland, J.: *Geophysics* **64(5)** (1999) 1447-1460
- 2000Pap Pape, H., Clauser, C., Iffland, J.: *Pure Appl. Geophys.* **15** (2000) 603-619
- 2005Pap Pape, H., Clauser, C., Iffland, J., Krug, R., Wagner, R.: *Int. J. Rock Mech. Min. Sci.* **42** (2005) 1056-1069, doi:10.1016/j.ijrmm.2005.05.00
- 1999Par Parker, R.: *Geothermics* **28(4/5)** (1999) 603-615
- 2003Pas Paschen, H., Oertel, D., Grünwald, R.: *Möglichkeiten geothermischer Stromerzeugung in Deutschland*, Büro für Technikfolgenabschätzung beim Deutschen Bundestag, Arbeitsbericht Nr. 84, (<http://www.tab.fzk.de/de/projekt/zusammenfassung/ab84.pdf>) (2003)
- 2002Per Pernecker, G.: *Geothermische Energie* **36/37(3/4)**, (http://www.geothermie.de/gte/gte36-37/altheim_pernecker.htm), (2002)
- 1993Pol Pollack, H.N., Hurter, S.J., Johnson, J.R.: *Rev. Geophys.* **31(3)** (1993) 267-280
- 1987Pop Popov, Y.A., Berezin, V.V., Solov'yev, G.A., Romushkevich, R.A., Korostelev, V.M., Kostyrin, A.A., and Kulikov, I.V., *Izvestia, Physics of the Solid Earth*, **23(3)** (1987) 245-253
- 1995Pop Popov, Y.A., Pevzner, L.A., Romushkevich, R.A., Korostelev, V.M., Vorob'ev, M.G.: *Izvestiya (Physics of the Solid Earth)* **30(9)** (1995) 778-789
- 1996Pop Popov, Y.A., Romushkevich, R.A., Popov, E.Y., in: Mazur, V.B. (Ed), *The Tymen superdeep well*, Nedra, Perm (1996) 163-175 (in Russian)
- 1998Pop^a Popov, Y., Pimenov, V., Pevzner, L., Romushkevich, R. , Popov, E., *Tectonophysics* **291** (1998) 205-213
- 1998Pop^b Popov, Y.A., Pevzner, S.L., Pimenov, V.P., Romushkevich, R.A., Pevzner L.A., in Orlov, V.P. , Laverov, N.P. (Eds), *Kola superdeep. Scientific Results and Research Experience*, Technoneftegaz, Moscow (1998) 176-184 (in Russian)
- 1999Pop^a Popov, Y.A., Pribnow, D., Sass, J.H., Williams, C.F., Burkhardt, H.: *Geothermics* **28(2)** (1999) 253-276
- 1999Pop^b Popov, Y.A., Romushkevich, R.A., Popov, E.Y., Bashta, K.G., in: Khakhaev, B.N., Morozov, A.E. (Eds), *Results of drilling and investigation of Ural superdeep well, Vol. 5*, Nedra, Yaroslavl, (1999) 77-88 (in Russian),
- 1999Pop^c Popov, Y.A., Pevzner, L.A., Romushkevich, R.A., Pimenov, V.P., Shlafstein, E.E., in: Masaitis V.L., Pevzner, L.A., (Eds), *Deep drilling in the Puchezh-Katunki impact structure*, VSEGEI Press, St. Petersburg (1999)136-144 (in Russian)
- 2002Pop Popov, Y.A, Romushkevich, R.A., in: Popov, Y., Khutorskoy, M., Korobkov, D. (Eds), *The Earth's thermal field and related research methods*, Proc. Intl. Conference, June 13-17, 2002, Moscow, Moscow State Geological Prospecting University (2002) 219-223
- 2003Pop^a Popov, Y., Pohl, J., Romushkevich, R., Tertychnyi, V., Soffel, H. *Geophys. J. Int.* **154(2)** (2003) 355-378

- 2003Pop^b Popovski, K., in: Dickson, M.H., Fanelli, M. (Eds): *Geothermal Energy: Utilization and Technology*, UNESCO, Paris (2003) 91-112
- 1993Prib Pribnow, D., Williams, C.F., Burkhardt, H.: *Geophys. Res. Lett.* **20(12)** (1993) 1155-1158
- 2003Raf^a Rafferty, K. D., in: Dickson, M.H., Fanelli, M. (Eds): *Geothermal Energy: Utilization and Technology*, UNESCO, Paris (2003) 81-90
- 2003Raf^b Rafferty, K. D., in: Dickson, M.H., Fanelli, M. (Eds): *Geothermal Energy: Utilization and Technology*, UNESCO, Paris (2003) 121-128
- 2000Rag Ragnarsson, Á.: *Geothermal development in Iceland 1995-1999*, http://www.os.is/obd/wgc2000/country_update_files/frame.htm (2000)
- 2003Ral Ralph, J.: *Mindat.org mineral data base*, <http://www.mindat.org/> (2003)
- 1959Rat Ratcliffe, E. H.: *Brit. J. Appl. Phys.* **10** (1959) 22-25
- 2000Rat Rath, V.: *Fluidsysteme in der Kruste: Modellrechnungen zur Entstehung impermeabler Barrieren*, Doctoral Dissertation, Freie Universität Berlin, Fachbereich Geowissenschaften, Berlin (2000)
- 2005Rat Rath, V., Clauser, C.: *Erkennen und Quantifizieren von Strömung: Eine geothermische Rasteranalyse zur Klassifizierung des tiefen Untergrundes in Deutschland hinsichtlich seiner Eignung zur Endlagerung radioaktiver Stoffe*, Bericht zum Auftrag 9WS0009-8497-2 an das Bundesamt für Strahlenschutz, Salzgitter, Geophysica Beratungsgesellschaft mbH, Stolberg
- 1991Rei Reibelt, M.: *Study on the influence of surface structure and fluid saturation of rocks on the determination of thermal conductivity by a half-space line source*, Diploma thesis (unpublished), Inst. F. Angew. Geophysik, Tech. Univ. Berlin (1991) (in German)
- 1998Ren Renewable Energy Working Party: *Benign Energy : The Environmental Implications of Renewables- Appendix G: Geothermal*, <http://spider.iea.org/pubs/studies/files/benign/index.htm>, International Energy Agency (IEA), Paris (1998)
- 1974Rob Robertson, E.C., Peck, D.L.: *J. Geophys. Res.* **79(32)** (1974) 4875-4888
- 1988Rob Robertson, E.C.: *Thermal Properties of Rocks*, Open File Report 88-441, U.S. Geol. Survey, Reston, VA (1988)
- 2003Rob Roberts, P.H., Jones, C.A., Calderwood, A. R., in: Jones, C.A., Soward, A., Zhang, K. (Eds), *Earth's Core and Lower Mantle*, Fluid mechanics of Astrophysics and Geophysics, Vol. 11, Taylor & Francis, London (2003) 100-129
- 2000Rog Rogner, H.-H., in: Goldemberg, J., Baker, J.W., Ba-N'Daw, S., Khatib, H., Popescu, A., Viray, F.L. (Eds), *World Energy Assessment*, U. N. Development Programme, Bureau for Development Policy, <http://www.undp.org/seed/eap/activities/wea/>, New York (2000) 135-171
- 1970Ros Rosen, B.W., Hashin, Z.: *Int. J. Engng. Sci.* **8** (1970) 157-173
- 1981Roy Roy, R.F., Beck, A.E., Touloukian, Y.S., in: Touloukian, Y.S., Judd, W.R., Roy, R.F. (Eds), *Physical Properties of Rocks and Minerals*, McGraw-Hill/CINDAS Data Series on Material Properties, Vol. II-2, McGraw-Hill, New York (1981) 409-502
- 1965Sas Sass, J. H.: *J. Geophys. Res.* **70(16)** (1965) 4064-4065
- 1971Sas Sass, J. H., Lachenbruch, A.H., Monroe, R.J.: *J. Geophys. Res.* **76(14)** (1971) 3391-3401
- 1992Sas Sass, J.H., Lachenbruch, A.H., Moses Jr, T. H.: *J. Geophys. Res.* **97(B4)** (1992) 5017-5030
- 2003Sat Satoshi, M.: *Nipponia* **26** <http://web-japan.org/nipponia/nipponia26/en/feature/feature08.html> (2003)
- 1996Sch Schön, J.H.: *Physical Properties of Rocks – Fundamentals and Principles of Petrophysics*, Pergamon, Oxford (1996)
- 2001Sch Schärli, U., Rybach, L.: *Geothermics* **30(1)** (2001) 93-110
- 2002Sch^a Schaumann, G.: *Untersuchung der Wirtschaftlichkeit der geothermischen Wärmegewinnung in Deutschland im Vergleich zu konventionellen Verfahren sowie die Beurteilung der Erfolgsaussichten für die Geothermie bei heutigen Energiepreisen*, Abschlussbericht zum Forschungsvorhaben 0327114, http://www.tsb-energie.de/service/publikationen/2002/tsb_geobericht.pdf, Transferstelle für rationelle und regenerative Energienutzung (TSB), Bingen (2002)
- 2002Sch^b Schaumann, G.: *Brennstoff, Wärme, Kraft (BWK)* **54(10)** (2002) 53-58

- 2005Sch Schellschmidt, R., Sanner, B., Jung, R., Schulz, R.: Geothermal Energy Use in Germany, in: Horne, R.N., Okandan, E. (Eds), *Proc. World Geothermal Congress 2005 (CD)*, Paper 0150, Intl. Geothermal Association, Reykjavik (2005)
- 1979Sha Shankland, T.J., Nitsan, U., Duba, A.G.: *J. Geophys. Res.* **84(B4)** (1979) 1603-1610
- 2004Sig^a Signorelli, S.: *Geoscientific Investigations for the Use of Shallow Low-Enthalpy Systems* Doctoral Dissertation, Swiss Federal Institute of Technology (ETH), Zürich, (2004)
- 2004Sig^b Signorelli, S., Andenmatten-Berthoud, N., Kohl, T., Rybach, L.: *Statistik geothermische Nutzung der Schweiz für die Jahre 2002 und 2003*, Schlussbericht 2004, Bundesamt für Energie, Bern (2004)
- 2005Şim Şimşek, Ş., Yildirim, N., Gülgör, A., in: Hunt, T. (Ed), *Environmental Aspects of Geothermal Energy, Geothermics* **34(2)** (2005) 234-251
- 1966Ski Skinner, B.J., in: Clark Jr., S.P. (Ed), *Handbook of Physical Constants, rev. ed.*, Memoir 97, Geol. Soc. of America (1966) 76-96
- 1992Som Somerton, W.H.: *Thermal Properties and Temperature Related Behavior of Rock/Fluid Systems*, Elsevier, Amsterdam (1992)
- 1992Sta Stacey, F.D.: *Physics of the Earth, 2nd ed.*, Brookfield Press, Brisbane (1992)
- 1992Ste^a Steingrímsson, B., Elíasson, E. T., Línal, B., Pálmasson, G. (Eds): *Industrial Uses of Geothermal Energy, Geothermics* **21(5/6)** (1992)
- 1992Ste^b Stefánsson, V.: *Geothermics* **21(5/6)** (1992) 823-834
- 1995Ste Stein, C., in: Ahrens, T.J. (Ed), *Global Earth Physics – A Handbook of Physical Constants, AGU Reference Shelf 1*, Am. Geophys. Union, Washington D.C. (1995) 144-158
- 2002Ste Stefánsson, V.: *Geothermics* **31(2)** (2002) 263-272
- 1961Sug Sugarawa, A., Yoshizawa, Y.: *Austral. J. Phys.* **14(4)** (1961) 469-480
- 1962Sug Sugarawa, A., Yoshizawa, Y.: *J. Appl. Phys.* **33** (1962) 3135-3138
- 1970Suk Sukharev, G.M., Sterlenko, Z.V.: *Doklady Akademija Nauk, SSSR* **194** (1970) 683-685 (in Russian)
- 1988Sun Sundberg, J.: *Thermal Properties of Soils and Rocks*, SGI Report 35, Swedish Geotechnical Institute (SGI), Linköping (1988)
- 1991Tip Tipler, P.A.: *Physics for Scientists and Engineers: Extended Version*, Worth Publishers, New York (1991)
- 1990Tor Torgersen, T.: *EOS Trans. Am. Geophys. Union* **71(1)** (1990) 1,4,13
- 2004Tri Trinnaman, J., Clarke, A. (Eds): *Survey of Energy Resources*, World Energy Council, <http://www.worldenergy.org/wec-geis/publications/reports/ser/foreword.asp>, London (2004)
- 2000Tur Turkenburg, W.C., in: Goldemberg, J., Baker, J.W., Ba-N'Daw, S., Khatib, H., Popescu, A., Viray, F.L. (Eds): *World Energy Assessment*, <http://www.undp.org/seed/eap/activities/wea/-drafts-frame.html>, United Nations Development Programme, New York NY (2000) 219-272
- 2005Tuy Tuyor, J.B., de Jesus, A.C., Medrano, R.S., Garcia, J.R.D., Salinio, S.M., Santos, L.S., in: Hunt, T. (Ed), *Environmental Aspects of Geothermal Energy, Geothermics* **34(2)** (2005) 252-265
- 1969Tye Tye, R.P. (Ed.), *Thermal Conductivity, Vol. 1 & 2*, Academic Press, London (1969)
- 2000Ura Ura, K., Saitou, S., in: E. Iglesias, D. Blackwell, T. Hunt, J. Lund, S. Tamanyu, K. Kimbara (Eds), *Proc. World Geothermal Congress 2000*, Intl. Geothermal Association, Auckland (2000) 3327-3333
- 1952Van van der held, E.F.M.: *Appl. Sci. Res.* **A3** (1952) 237-247
- 1995Van van Schmus, W.R., in: Ahrens, T.J. (Ed), *Global Earth Physics – a Handbook of Physical Constants, AGU Reference Shelf 1*, Am. Geophys. Union, Washington D.C. (1995) 283-291
- 1991Vac Vacquier, V.: *Geophys. J. Int.* **106(1)** (1991) 199-202
- 1992Vac Vacquier, V.: *Geophys. J. Int.* **111(3)** (1992) 637-638
- 2003VDE VDEW-Projektgruppe „Nutzenergiebilanzen“, Arbeitsgemeinschaft Energiebilanzen: *Endenergieverbrauch in Deutschland 2002*, VDE-Materialien, VDEW M-19/2003, Verband der Elektrizitätswirtschaft e.V. (VDEW), Frankfurt (2003)
- 1980Ver Verhoogen, J.: *Energetics of the Earth*, Natl. Acad. Sciences, Washington, D.C. (1980)
- 2004Von^a von der Hude, N., Völkner, R.: *bbr – Fachmagazin für Brunnen- und Leitungsbau*, **6** (2004) 36-41

- 2004Von^b von der Hude, N., Wend, R.: *Energie-, Wasser-Praxis* **9** (2004) 12-17
- 2003Vos Vosteen, H.-D., Schellschmidt, R.: *Physics and Chemistry of the Earth* **28(9-11)** (2003) 499-509
- 2002Vua^a Vuataz, F.-D. (Ed): *Technische Notiz*, **3**, Schweizerische Vereinigung für Geothermie (SVG), <http://www.geothermie.de/oberflaechennahe/Notiz3.pdf> (2002)
- 2002Vua^b Vuataz, F.-D. (Ed): *Info-Geothermie* **2/2002**, Schweizerische Vereinigung für Geothermie (SVG), http://www.geothermie.de/geothermieartikel/basisartikel/IG2_DE.pdf (2002)
- 1998Wag Wagner, W., Kruse, A.: *Properties of Water and Steam - The Industrial Standard IAPWS-IF97*, Springer, Berlin (1998)
- 1989Wal Wall, G., Chuang, C.-C., Ishida, M., in: Bajura, R. A., von Spakovsky, M. R., Geskin E. S. (Eds), *Analysis and Design of Energy Systems: Analysis of Industrial Processes*, AES-Vol. 10-3, Am. Soc. Mech. Engrs. (ASME) (1989) 73-77
- 1999Wal Wallroth, T., Eliasson, T., Sundquist, U.: *Geothermics* **28(4/5)** (1999) 617-6625
- 1996Wan Wang, J. (Ed): *Geothermics in China*, Seismological Press, Beijing (1996)
- 2002Wei Weidler, R., Gerard, A., Baria, R., Baumgaertner, J., Jung, R.: Hydraulic and Micro-Seismic Results of a Massive Stimulation Test at 5 km Depth at the European Hot-Dry-Rock Test Site Soultz, France. *Proc. 27th Workshop on Geothermal Reservoir Engineering*, Stanford University, CA, <http://geothermal.stanford.edu/pdf/SGW/2002/Weidler.pdf> (2002)
- 1999Wet Wetzal, H., Stutzke, R.: Geothermal Energy – Prenzlau (Germany) <http://www.agores.org/Publications/CityRES/English/Prenzlau-DE-english.pdf> (1999)
- 1990Wil Williams, C.F., Anderson, R.A.: *J. Geophys. Res.* **95(B6)** (1990) 9209-9236
- 1961Woo Woodside, W., Messmer, J.H.: *J. Appl. Phys.* **32** (1961) 1688-1706
- 2004Wor World Bank: *Geothermal Energy*, <http://www.worldbank.org/html/fpd/energy/geothermal/applications.htm> (2004)
- 1981Yan Yang, J.M., in: Gevantman, L.H. (Ed), *Physical Properties Data for Rock Salt*, Monograph 167, National Bureau of Standards, Washington, D.C. (1981) 205-221
- 1956Zie Zierfuss, H., van der Vliet, G.: *Bull. Am. Assoc. Petrol. Geol.* **40** (1956) 2475-2488
- 1984Zim Zimmerman, R. W.: *The effect of pore structure on the pore and bulk compressibilities of consolidated sandstones*, Ph.D. thesis, University of California, Berkeley, Ca. (1984)
- 1989Zim Zimmerman, R. W.: *J. Petrol. Sci. Eng.* **3(3)** (1989) 219–227
- 1988Zot Zoth, G., Hänel, R.: in: Hänel, R., Rybach, L., Stegena, L. (Eds), *Handbook of Terrestrial Heat Flow Density Determination*, Kluwer Academic Publishers, Dordrecht (1988) 449-466